RETARDATION OF BREACH GROWTH UNDER HIGH FLOW VELOCITIES

Applicability of a bentonite-additive

Msc thesis

TU Delft — Delft University of Technology
NUS — National University of Singapore
ARCADIS — Design & Consultancy for natural and built assets

B. (Björn) Foortse
February, 2016

Front cover: Early state of the breaching process, artist impression.

Retardation of breach growth under high flow velocities

by

B.(Björn) Foortse

in partial fulfillment of the requirements for the degree of

Master of Science
in Civil Engineering

at the Delft University of Technology and the National University of Singapore
to be presented publicly on February 29th, 2016.

Thesis committee:

Prof. dr. ir. C. Van Rhee	Delft University of Technology, Department of Maritime Transport Technology, Section Offshore and Dredging Engineering
Dr. ir. P.J. Visser	Delft University of Technology, Department of Hydraulic Engineering
Ir. F. Bisschop	Delft University of Technology, Department of Maritime Transport Technology, Section Offshore and Dredging Engineering and Arcadis
Dr. Jing Yuan	National University of Singapore, Department of Civil and Environmental Engineering

An electronic version of this dissertation is available at http://repository.tudelft.nl/.

Acknowledgements

This Msc Thesis is written as final fulfillment for the completion of the double degree Master of Science programme Hydraulic Engineering and Water Resources Management of Delft University of Technology (track Hydraulic Engineering of the Msc in Civil Engineering) and National University of Singapore (Department of Civil and Environmental Engineering). The work of this thesis was partially conducted in the Laboratory for Fluid Mechanics and the Laboratory of Geoscience and Engineering at the Delft University of Technology and was in collaboration with Arcadis.

First of all, my thesis project would not have been a success without the full support of my graduation committee. I am most grateful for the positive feedback, guidance and ever present enthusiasm of my direct supervisors Paul Visser and Rik Bisschop. They continuously triggered me to think critically about the next phases and most of all the accuracy of the experiments. Furthermore I would like to express my thanks to Jing Yuan and Cees van Rhee for their critical and most useful comments and insights.

In preparing the experiments, I was aided by numerous people, to whom I want to sincerely express my gratitude. The guidance and assistance given by the staff of the Laboratory for Fluid Mechanics and the Laboratory of Geoscience and Engineering of the Technical University of Delft were of paramount importance. A special thanks is in order for Arno Mulder, Sander de Vree and Jaap van Duin.

A significant role in this research was taken by Dennis Lemmens, my predecessor, who provided the preliminary insights into the applicability of bentonite as a retardation option in breach growth. Next to his inspiring Msc Thesis I am very grateful for his feedback and offered support.

Continuing thanks also to Jeroen Stam from Cebo Holland B.V., whom provided 200kg Sealfix bentonite for my erosion tests, free of charge.

Björn Foortse
Delft, February 2016

Summary

People all around the world live and work in low-lying areas. Low-lying areas have to be protected against high water levels in rivers and at sea by a water protection system (e.g. by dunes, dikes and barriers). Dikes are an important component within water protection systems. Generally, dikes are described as elongated naturally occurring or artificially constructed (earthen) structures, which prevent flooding of the hinterland. Dikes are mainly found along seas, estuaries, rivers, canals, lakes and water courses. Many dikes contain sand cores, which are covered by a protection layer (e.g. clay, asphalt etc.) to prevent erosion of the core. Unfortunately, there are times that one of the many known failure mechanisms of a dike causes (local) dike failure, exposing the sand core to the water (Rijkswaterstaat, 2006). A so-called initial breach is formed. Once the sand core is no longer fully covered by a protection layer, the sand core start to erode and the core is prone to fast breaching (Visser, 1998).

The water flowing through the breach is eroding the sandy sediment and the breach keeps growing, which can have significant economical consequences and can also lead to loss of human life and animal life. Several options to retard the breaching process have been investigated by Lemmens (2014). Based on laboratory experiments, especially a mixture of sand and bentonite (in the core of the dike) seems to significantly slow down the breaching process. Thus far, this theory has only been tested for relatively low flow conditions in the order of 1 m/s. However, during the breaching process high flow conditions in the order of 2-10 m/s can be reached (Visser, 1998)) and under high flow conditions dilatant behaviour of the sediment is going to play a role (Van Rhee, 2010). As a result an inward directed hydraulic gradient will hinder the erosion and is expected to have a significant impact on the breaching process. The aim of this Msc Thesis project is to find an answer to the following main question:

“How does bentonite reduce the erosion velocity of sand under high flow velocity conditions?"

A literature review has resulted in an understanding that at high flow velocities (>2 m/s) the erosion velocity depends on the properties of the soil mass and not only on the properties of a particle. Important parameters of the soil mass are the permeability and dilatancy. From the erosion experiments it can be concluded that the effect of dilatancy, which plays a role at higher flow velocities, indeed hinders erosion and thus reduces the erosion velocity at higher flow velocities. This effect is caused by a volume change, as a result of shearing of the bed. The volume change generally leads to a drop in pore pressure in the top of the sand bed. This pressure drop introduces a hydraulic gradient and thus an inflow of water that hinders the entrainment of sediment. The permeability also significantly influences the erosion behaviour. Falling head tests were executed to determine the effectiveness of adding bentonite to the core of a dike. Adding a certain amount of bentonite to sand certainly yields a high decrease in permeability. This is the result of the swelling potential of the bentonite, which is assumed to fill the empty space between the sand particles. It appears that the most significant decrease in permeability happens with bentonite contents up to 6% of the volume. Adding more bentonite still reduces the permeability, but the overall effect is starting to flatten out for bentonite contents higher than 8%. Overall, the approximate decrease in permeability is almost three orders of magnitude (from 10^{-4} to 10^{-7}) with bentonite volume percentages up to 10%.

Results from the direct shear tests show no significant differences between sand mixtures and sand-bentonite mixtures with a bentonite content up to 10%. The apparent cohesion is not changing drastically by adding more bentonite (< 3kPa) and the friction angle is also not significantly decreasing for higher bentonite contents. Hence, sand-bentonite mixtures with a bentonite volume content up to 10% still show sand-like behaviour. This indirectly indicates that the strength characteristics of a dike core will not be altered.

Erosion experiments were carried out in a tilting flume with a length of about 14 m, an effective height of 0.40 m, a constricted width of 0.145 m and a maximum discharge of about 0.025 m^3/s. Thirteen different test runs were executed. In these tests, the volume percentage of bentonite additive, the diameter of the sand and the mean flow velocity were varied. All erosion experiments were performed under supercritical flow conditions. As a consequence of this flow regime, the preferred equilibrium flow velocities (1 and 2 m/s) were hard to regulate. In order to objectively calculate the effectiveness of a bentonite additive, the erosion velocity of the bed of a sand-bentonite mixture was compared with the erosion velocity of a sand mixture at the same mean flow velocity. This procedure was applied to two different methods. The first one related the erosion velocities to the mean flow velocities squared U^2 and the second related the erosion velocities to the corrected bed shear stresses. Both methods show a similar trend. Significant reductions in erosion velocity are obtained by adding bentonite to a sand mixture. A 2% sand-bentonite mixture already reduces the original erosion velocity by about 50%, a 3% or 4% mixture by 50 to 65%

and a 6% mixture by at least 90%. It has to be added that the reproducibility of the tests has been confirmed to be reasonably well.

A literature study concerning the erosion behaviour of sand-bentonite mixtures, has resulted in the conclusion that very few data are available. At higher flow velocities these are even non-existent. A comparison of the data that is currently present clearly indicates that it is very difficult to predict and verify the absolute reduction in erosion velocities for different bentonite mixtures. Only relative reductions in erosion velocities for different sand-bentonite mixtures make it possible to compare data from different data sets.

The observed behaviour in the experiments enhances the development of an adapted erosion function. The erosion function of Van Rhee (2010) - including the effect of dilatancy and the permeability - has been adapted to the experimental data of the erosion tests to get reasonable accurate model results. This study also discusses some possible causes of the discrepancies between the experimental data and the results predicted by the erosion function of Van Rhee (2010). The adapted erosion function includes the effect of the bentonite content on the erosion velocity. This effect is indirectly taken into account by adapting the permeability in the erosion function. The adapted erosion function has been implemented in the BRES-Visser model. The BRES-Visser model - which decomposes the breaching process in five different phases as proposed by Visser (1998) - calibrated with data from the Zwin'94 experiment, has been used to model the performance of the bentonite additives. The data from the Zwin'94 experiment has also been used as a reference scenario for a dike with a sand core. The effects of the retardant sand-bentonite mixtures have been compared to this reference scenario. The comparison is based on breach width, flow through the breach, the inundation velocity and duration of the breaching process. Significant reductions of these parameters have been realized with increasing bentonite percentages. By reducing the inundation velocity below a threshold value of 0.5 m/h, the mortality and the LIR (Localized Individual Risk), can theoretically be decreased by a factor 10. A sand-bentonite mixture with a bentonite content of 6.3% would be necessary to reduce the inundation velocity to a value below 0.5 m/h for the fictitious case of the Zwin'94 experiment. The effectiveness of the bentonite measure has also been tested in the Borssele case study.

To conclude, sand-bentonite mixtures are able to significantly reduce the erosion velocity. The effects of dilatancy and a decrease in permeability have a large impact on the erosion velocity. This is already noticeable at very low percentages of added bentonite. A sand-bentonite mixture with a bentonite volume content of 6% substantially reduces the erosion velocity (also at high flow velocities) and the mixture generally has a reasonably good homogeneity. With lower percentages of added bentonite the homogeneity is less reliable, which might be a considerable practical limitation. Sand-bentonite mixtures with a bentonite content up to 6% still show sand-like behaviour, indicating that the strength characteristics of a dike will not alter. Finally, case studies with the BRES model indicate that an increase in safety level by a factor of 10 can be achieved using sand-bentonite mixtures in the core of a dike and that the polder area has a big influence on the inundation velocity and the polder water levels. In both the Van Citterspolder I and the Van Citterspolder II the safety increases with a factor 2.5 to 10 when a 2% sand-bentonite mixture is added to the core. Higher percentages of bentonite additive increase the safety even more and in some cases even completely stop the breach growth, because the outside water level drops faster than the breach grows vertically. In the Zwin'94 case study a 6.3% sand-bentonite mixture increases the safety by a factor 10.

Contents

Acknowledgements **i**

Summary **iii**

Nomenclature **viii**

List of Figures **xiv**

List of Tables **xviii**

1 Introduction **1**
1.1 Background . . . 1
1.2 Relevance of the research . . . 1
1.3 Problem description . . . 2
1.4 Research questions . . . 2
1.5 Approach . . . 2
1.6 Structure of the thesis . . . 3

2 Theoretical Background **4**
2.1 Sediment transport and sediment transport modes . . . 4
2.2 Concept of initiation of motion . . . 5
2.3 Concept of hindered erosion . . . 6
2.4 The breaching process . . . 6
2.5 Modeling of the retardation of breach growth . . . 8
2.6 Erosion functions in the BRES model . . . 8
2.7 The Zwin'94 experiment . . . 10

3 Retardation of the breaching process **12**
3.1 Alteration of the shape of the dike . . . 12
3.2 Changing the characteristics of the soil . . . 13
3.3 Addition of erosion resistant components to the dike . . . 15
3.4 Alternative approaches . . . 16

4 Hypotheses **17**
4.1 Hypotheses regarding the physical behaviour of erosion . . . 17
4.2 Hypotheses regarding the modeling of breach growth . . . 17
4.3 Research method . . . 17

5 The experimental setup **19**
5.1 Experimental setup of the erosion tests . . . 19
5.1.1 Preparation of the erosion test . . . 20
5.1.2 Measuring equipment . . . 23
5.2 The permeability tests . . . 25
5.2.1 Experimental setup of the permeability tests . . . 25
5.2.2 Preparation of the permeability test samples . . . 26
5.2.3 Run plan permeability tests . . . 26
5.3 The direct shear tests . . . 28
5.3.1 Experimental setup of the direct shear tests . . . 28
5.3.2 Run plan direct shear tests . . . 29
5.4 Sediment properties . . . 31
5.4.1 The sand . . . 31
5.4.2 The bentonite . . . 33
5.4.3 Preparation of the mixtures . . . 34
5.4.4 Classification of the mixtures . . . 34

6 The experimental results **36**
6.1 Results erosion test . . . 36
6.2 Results permeability tests . . . 49
6.3 Results direct shear tests . . . 51

7 Discussion of the experimental tests **54**
7.1 The directs shear tests . . . 54
7.2 The erosion tests . . . 54
7.3 The permeability tests . . . 59
7.4 General remarks . . . 60

8 Modelling the performance of the bentonite additive **62**
8.1 The critical Shields parameter . . . 62
8.2 The erosion function . . . 62
8.3 The adapted erosion function . . . 65
8.4 Inclusion of the effect of the bentonite content on the erosion velocity . . . 66
8.5 Calibration of the erosion function and the performance of the bentonite additive in the core of a dike 67
8.6 Effect of bentonite mixtures on the mortality . . . 69

9 Case study Borssele **71**
9.1 Assumptions . . . 71
9.2 Model setup . . . 72
9.3 Run plan . . . 75
9.4 Results . . . 76

10 Conclusions & Recommendations **79**
10.1 Conclusions . . . 79
10.2 Recommendations . . . 81

References **84**

Appendices **87**

A Data Direct Shear Tests **88**

B Specifics of the Cebogel Sealfix bentonite (Dutch) **101**

C Results Permeability Tests **103**

D Results Erosion Tests **105**

E Clear water tests **119**

F Data analyses **123**

G Additional data case study Borssele **128**

H Estimation of the near bed concentration **139**

Nomenclature

A	A tune parameter, which is equal to 3/4 for a single particle and approximately 1.7 for a continuum	[-]
A	Cross-sectional area of a soil sample	[m^2]
A_C	Corrected sample area	[m^2]
a	Cross-section of the tube of the falling head test device	[m]
a	Regression coefficient	[-]
B	Width of a stretch	[m]
B	Width of a breach	[m]
$B\%$	Percentage of added bentonite	[-]
b	Initial breach width	[m]
b	Width of the flume	[m]
C	Apparent cohesion	[N/m^2]
C_u	Dimensionless coefficient of uniformity	[-]
C_c	Dimensionless coefficient of curvature	[-]
c	A fitting coefficient	[-]
c_b	Near bed concentration	[-]
c_{bed}	Initial bed concentration	[-]
c_a	Sediment concentration at 'a' meters above the bottom	[-]
c_f	Dimensionless friction coefficient	[-]
c_z	Sediment concentration at 'z' meters above the bottom	[-]
D	Sediment particle size	[m]
D_{50}	Median diameter of the sediment	[m]
D_i	Particle size such that $i\%$ of the volume particles of the sediment has a diameter smaller than D_i	[m]

D_*	Dimensionless particle diameter	[-]
d	Water depth	[m]
e_b	Measure for the efficiency of the bed load transport	[-]
e_s	Measure for the efficiency of the suspended load transport	[-]
F	Dimensionless form factor	[-]
F_D	Drag force	[N]
F_g	Gravity force	[N]
F_L	Lift force	[N]
Fr	Froude number	[-]
f, f_B, f_s	Effectiveness ratio, effectiveness ratio of a sand-bentonite mixture and the effectiveness of a pure sand mixture	[-]
f_b	Bed friction factor	[-]
fk, fu^2, f_τ	Effectiveness ratio based on permeability data (subscript k), mean flow velocity squared data (subscript u^2) and the corrected bed shear stress data (subscript τ)	[-]
f_D	Darcy-Weisbach friction factor	[-]
f_{evac}	Fraction of the inhabitants that is evacuated	[-]
f_w	Wall friction factor	[-]
g	Gravitational acceleration	[m/s^2]
H_d	Height of the crest of the dike above NAP (reference level in the Netherlands at about mean sea level)	[m]
H_p	Initial polder water level above NAP (reference level in the Netherlands at about mean sea level)	[m]
h	Water depth	[m]
h_0	Initial water level or average water level	[m]
h_a	First order tidal amplitude	[m]

h_b	Height of the bed	[m]
h_t	Water level after t seconds	[m]
h_w	The surface water level	[m]
k	In-situ permeability	[m/s]
k_l	the permeability given a loose soil packing	[m/s]
k_s	Particle roughness height	[m]
k_{sand}, $k_{\boldsymbol{B}}$	the permeability of the originally chosen sand and the permeability of a sand-bentonite mixture	[m/s]
L	Height of the soil sample	[m]
LIR	Localized Individual Risk of loss of life due to a flood event	[-]
M	Mortality rate	[-]
M	Mass	[kg]
M_L	Mortality, number of casualties as a fraction of the inhabitants left in the zone of flooding	[-]
$M_{mixture}$	Total mass of a sand-bentonite mixture	[kg]
$M_{additive}$	Mass of the bentonite additive	[kg]
n	Porosity	[-]
n	Manning roughness coefficient	[$s/m^{1/3}$]
n_b, n_w	Bed-related Manning roughness coefficient and the wall-related Manning roughness coefficient	[$s/m^{1/3}$]
n_0	Porosity prior to erosion (in-situ porosity)	[-]
n_l	Porosity in the sheared zone (loose packing)	[-]
$n_{mixture}$	Porosity of a sand-bentonite mixture	[-]
P_f	Probability of inundation	[-]
Q	Discharge	[m^3/s]
Q_{br}	Water flow through a breach	[m^3/s]
R	Hydraulic radius	[m]

RD	Relative density	[-]
Re	Reynolds number	[-]
R_w	Wall related hydraulic radius	[m]
S	Energy slope gradient	[m/m]
S_x, S_y	Sediment transport in a x or y direction	[$m^3/m/s$]
s_s	Suspended load transport capacity	[$m^3/m/s$]
s_b	Bed load transport capacity	[$m^3/m/s$]
s_t	Total load transport capacity	[$m^3/m/s$]
T	Dimensionless transport parameter	[-]
T	Temperature	[$°C$]
T_a	Standard duration of the astronomical tide	[hr]
T_s	Typical storm duration	[hr]
t	Time	[s]
U	Depth-averaged or mean flow velocity	[m/s]
U_{cr}	Critical flow velocity	[m/s]
u_*	Bed shear velocity	[m/s]
V	Change of volume between time t_0 and time t	
V_{bed}	Total volume of the sand bed	[m^3]
v_e	Erosion velocity	[m/s]
$v_{e,sand}$, $v_{e,mixture}$	Erosion velocity of pure sand of a sand-bentonite mixture	[m/s]
V_i	Inundation velocity	[m/s]
W_d	Crest width of the dike	[m]
w_s	Hindered settling velocity	[m/s]

Z_{br}	Bottom of the breach above NAP (reference level in the Netherlands at about mean sea level)	[m]
Z_p	Bottom level of the polder above NAP (reference level in the Netherlands at about mean sea level)	[m]
Z_w	Bottom level of the sea above NAP (reference level in the Netherlands at about mean sea level)	[m]
z	Vertical axis coordinate	[m]
z_a	Reference level of the reference concentration	[m]
z_b	Bed level	[m]
α	Outer slope angle	[deg]
β	Angle of the slope	[deg]
γ	Side slope angle	[deg]
γ_0	Dimensionless constant	[-]
δ	Dilatancy factor	[-]
δ	Relative displacement between the upper and lower halves of a square box in the direct shear test	[m]
Δ	Relative density	[-]
Δ	Difference operator	[-]
θ	Shields parameter	[-]
$\theta_{b,i}$	Shields parameter according to the Flow-depth method (subscript h), Hydraulic radius method (R), Vanoni & Brooks method (v) and Einstein method (e)	[-]
θ_{cr}	Critical Shields parameter	[-]
$\theta^1{}_{cr}$	Adapted critical Shields parameter	[-]
κ	Von Karman coefficient	[-]
μ	Ripple factor	[-]
ν	Kinematic viscosity	[m^2/s]
ρ, ρ_w	Density of water	[kg/m^3]

$\rho_{in\ situ}$	In situ density	$[kg/m^3]$
ρ_s	Particle density	$[kg/m^3]$
ρ_{sand}	Dry bulk density of sand	$[kg/m^3]$
ρ_{min}	Minimum density limit of a soil	$[kg/m^3]$
ρ_{max}	Maximum density limit of a soil	$[kg/m^3]$
$\rho_{mixture}$	Density of a sand-bentonite mixture	$[kg/m^3]$
σ	Normal stress	$[N/m^2]$
τ	Soil shear strength	$[N/m^2]$
τ_b	Bed shear stress	$[N/m^2]$
$\tau_{b,i}$	Corrected bed shear stress according to the Flow-depth method (subscript h), Hydraulic radius method (R), Vanoni & Brooks method (v) and Einstein method (e)	$[N/m^2]$
τ_w	Wall shear stress	$[N/m^2]$
$\tau_{b,cr}$	Critical bed shear stress	$[N/m^2]$
ϕ	Angle of internal repose	$[deg]$
Φ_p	Dimensionless pick-up flux	[-]

List of Figures

1 The sediment transport modes, from De Vet (2014). 4
2 Initiation of motion as proposed by Shields, from De Vet (2014). 5
3 Increase of volume due to shearing from De Vet (2014); original figure from Van Rhee (2010). 6
4 Several failure modes of dikes from Tonneijck and Weijers (2008). 7
5 The five stage breaching process from De Vet (2014), original figure from Visser (1998). 7
6 SWOT analysis from Peeters et al. (2011). 8
7 Comparison BRES-model output and Zwin'94 dataset, from Foortse (2013). 10
8 Cross-section Zwin dike from De Vet (2014). 10
9 Observed breach with in time and the end on each subsequent phase from Visser (1998). 11
10 Retardation of the breaching process by decreasing the inner slope angle from Smolders (2010). 12
11 Retardation of the breaching process by increasing the crest width from Smolders (2010). 13
12 Development of the breaching process in a sand dike experiment from Zhu (2006). 13
13 Development of the breaching process in a clay dike experiment from Zhu (2006). 14
14 Retardation of the breaching process with bentonite under low flow velocities from Lemmens (2014). 14
15 Retardation with bentonite and fibers under low flow conditions, from Lemmens (2014). 15
16 Reduction in lateral breach width for different sill heights from Van Gerven (2004). 16
17 Rise in water level of the polder for different sill heights from Van Gerven (2004). 16
18 Side and top view of the flume. 19
19 Experimental setup 1 of the erosion test: top view (above) and side view (bottom) with measures in meters. 21
20 Experimental setup 2 of the erosion test: top view (above) and side view (bottom) with measures in meters. 22
21 (a) Flowmeter display and (b) Acoustic flow meter attached to the inflow pipe. 23
22 (a) Setup of the camera and (b) Grid on the glass wall in the area of interest. 24
23 (a) Device falling head test and (b) Sample positioning. 25
24 Conceptual sketch of the falling head test, from Barends and Uffink (2011). 26
25 Device direct shear test, from Lemmens (2014). 28
26 Setup direct shear test, from Mulder and Verwaal (2006). 28
27 Upper and lower rigid ring containing the sample, from Mulder and Verwaal (2006). 29
28 Gradation curve sand with a D_{50} of 0.256 mm 31
29 Gradation curve sand with a D_{50} of 0.150 mm 32
30 In situ density related to the minimum and maximum densities, from Price (2009). 33
31 The green-greyish fine bentonite particles. 34
32 Best attempt to determine the plastic limit of a 6% mixure. 35
33 Erosion velocity versus mean flow velocity squared for (a) sand with a D_{50} of 0.256 mm and (b) sand with a D_{50} of 0.150 mm. 37
34 Reduction coefficient f as function of the bentonite content from mean flow velocities squared. 38
35 Prediction of bed shear stresses using different theories versus velocity squared for (a) sand with a D_{50} of 0.256 mm and (b) sand with a D_{50} of 0.150 mm. 42
36 Erosion velocity versus bed shear stress for (a) sand with a D_{50} of 0.256 mm and (b) sand with a D_{50} of 0.150 mm. 43
37 Reduction coefficient f as function of the bentonite content from corrected bed shear stresses. 44
38 Erosion velocity versus bed shear stress for sands with a different D_{50}. 44
39 Bed shear stress versus velocity squared with data from Lemmens (2014), Foortse and theoretical predictions. 45
40 Reduction of the erosion velocity and permeability as function of the bentonite content (a) from depth-averaged flow velocities squared (b) from bed shear stresses. 47
41 Results of the permeability coefficients for different sand diameters. 49
42 Reduction of the permeability coefficients as functions of the volume percentage of bentonite. 50
43 Visualization of the sample area correction, adapted from Bardet (1997). 51
44 Results direct shear tests of sand with a D_{50} of 0.256 mm. 52
45 Results direct shear tests of sand with a D_{50} of 0.150 mm. 52
46 No formation of a scour hole and appearance of bedforms. 54
47 (a) Local weak spot in a 1 m/s test (b) Local weak sport in a 1 m/s test, 10 seconds later. 55

48 Local inhomogeneous erosion of a soil lump. 56
49 Formation of a hydraulic jump. 56
50 Part of the bed has still not been in contact with water after 24 hours. 57
51 Topview of the bed after an erosion test. 57
52 Inhomogeneous mass erosion of a 6% mixture. 58
53 (a) Softening of the soil bed with a 6% mixture (b) Softening of the soil bed with a 6% mixture, 10 seconds later. 58
54 (a) Horizontal erosion as a result of downstream effects. (b) Horizontal erosion as a result of downstream effects, a few seconds later. 59
55 The appearance of cracks for a mixture with 8% bentonite. 60
56 Comparison between the results of the erosion tests and the unadapted erosion function of Van Rhee for (a) sand only (b) a 2% mixture (c) a 4% mixture and (d) a 6% mixture sand with a D_{50} of 0.256 mm. 63
57 Comparison between the results of the erosion tests and the unadapted erosion function of Van Rhee for (a) sand only (b) a 3% mixture (c) a 6% mixture sand with a D_{50} of 0.150 mm. 64
58 Comparison between the results of the erosion tests and the adapted erosion function of Van Rhee for (a) sand only (b) a 2% mixture (c) a 4% mixture and (d) a 6% mixture of sand with a D_{50} of 0.256 mm. 66
59 Comparison between the results of the erosion tests and the adapted erosion function of Van Rhee for (a) sand only (b) a 3% mixture (c) a 6% mixture of sand with a D_{50} of 0.150 mm. 66
60 Comparison of the effectiveness of different bentonite mixtures in reducing the breach width, flow through the breach, the inundation velocity and duration of the breaching process. 68
61 Exponential relationship between the reduction in inundation velocity and the volume bentonite percentage. 68
62 Breach width, flow through the breach, the inundation velocity and duration of the breaching process for a 6.3% mixture. 69
63 The Van Cittersspolder I and II are located in the province of Zeeland in the Netherlands, partly adapted from Rijkswaterstaat (2014) 71
64 The water level signal (right) is composed of a tidal effect (middle) and a surge effect (left). 73
65 Schematization of the system including a cross-section of the dike as proposed by Visser (1998). 73
66 (a) The development of the breach width in time and (b) the development of the breach bottom in time for several sand-bentonite mixtures in the Van Citterspolder I. 77
67 (a) The development of the breach width in time and (b) the development of the breach bottom in time for several sand-bentonite mixtures in the Van Citterspolder II. 78
A1 Results direct shear test of sand with a D_{50} of 0.256 mm. 88
A2 Shear stress versus horizontal displacement of sand with a D_{50} of 0.256 mm. 88
A3 Results direct shear test of a 2% mixture with a D_{50} of 0.256 mm. 89
A4 Shear stress versus horizontal displacement of a 2% mixture with a D_{50} of 0.256 mm. 89
A5 Results direct shear test of a 4% mixture with a D_{50} of 0.256 mm. 90
A6 Shear stress versus horizontal displacement of a 4% mixture with a D_{50} of 0.256 mm. 90
A7 Results direct shear test of a 6% mixture with a D_{50} of 0.256 mm. 91
A8 Shear stress versus horizontal displacement of a 6% mixture with a D_{50} of 0.256 mm. 91
A9 Results direct shear test of a 8% mixture with a D_{50} of 0.256 mm. 92
A10 Shear stress versus horizontal displacement of a 8% mixture with a D_{50} of 0.256 mm. 92
A11 Results direct shear test of a 10% mixture with a D_{50} of 0.256 mm. 93
A12 Shear stress versus horizontal displacement of a 8% mixture with a D_{50} of 0.256 mm. 93
A13 Results direct shear test of sand with a D_{50} of 0.150 mm. 94
A14 Shear stress versus horizontal displacement of sand with a D_{50} of 0.150 mm. 94
A15 Results direct shear test of a 2% mixture with a D_{50} of 0.150 mm. 95
A16 Shear stress versus horizontal displacement of a 2% mixture with a D_{50} of 0.150 mm. 95
A17 Results direct shear test of a 4% mixture with a D_{50} of 0.150 mm. 96
A18 Shear stress versus horizontal displacement of a 4% mixture with a D_{50} of 0.150 mm. 96
A19 Results direct shear test of a 6% mixture with a D_{50} of 0.150 mm. 97
A20 Shear stress versus horizontal displacement of a 6% mixture with a D_{50} of 0.150 mm. 97
A21 Results direct shear test of a 8% mixture with a D_{50} of 0.150 mm. 98
A22 Shear stress versus horizontal displacement of a 8% mixture with a D_{50} of 0.150 mm. 98

A23 Results direct shear test of a 10% mixture with a D_{50} of 0.150 mm. 99
A24 Shear stress versus horizontal displacement of a 10% mixture with a D_{50} of 0.150 mm. 99
C1 Reduction of permeability coefficient as function of the added bentonite volume percentage for the M32 sand type. 103
C2 Reduction of permeability coefficient as function of the added bentonite volume percentage for the M32 sand type (vertical log scale). 103
C3 Reduction of permeability coefficient as function of the added bentonite volume percentage for the S90 sand type. 104
C4 Reduction of permeability coefficient as function of the added bentonite volume percentage for the S90 sand type(vertical log scale). 104
D1 Water level (upper line) and bed level (lower line) measurements with an average discharge of 10.35 l/s. 106
D2 Water level (upper line) and bed level (lower line) measurements with an average discharge of 10.67 l/s. 107
D3 Water level (upper line) and bed level (lower line) measurements with an average discharge of 12.13 l/s. 108
D4 Water level (upper line) and bed level (lower line) measurements with an average discharge of 12.50 l/s. 109
D5 Water level (upper line) and bed level (lower line) measurements with an average discharge of 13.00 l/s. 110
D6 Water level (upper line) and bed level (lower line) measurements with an average discharge of 13.88 l/s. 111
D7 Water level (upper line) and bed level (lower line) measurements with an average discharge of 17.4 l/s. 112
D8 Water level (upper line) and bed level (lower line) measurements with an average discharge of 18.00 l/s. 113
D9 Water level (upper line) and bed level (lower line) measurements with an average discharge of 19.16 l/s. 114
D10 Water level (upper line) and bed level (lower line) measurements with an average discharge of 17.76 l/s. 115
D11 Water level (upper line) and bed level (lower line) measurements with an average discharge of 15.93 l/s. 116
D12 Water level (upper line) and bed level (lower line) measurements with an average discharge of 17.46 l/s. 117
D13 Water level (upper line) and bed level (lower line) measurements with an average discharge of 19.47 l/s. 118
E1 (a) Smooth glass bottom of the flume (b) Simulation of a rough bottom. 119
E2 Water level measurements with a smooth bottom. 120
E3 Water level measurements with a rough bottom. 120
E4 Velocity measurements with a smooth bottom. 121
E5 Velocity measurements with a rough bottom. 121
F1 v_e/k versus bed shear stress for (a) sand mixtures with a D_{50} of 0.256 mm and (b) sand mixtures with a D_{50} of 0.150 mm. 123
F2 v_e/k versus the Shields parameter for (a) sand mixtures with a D_{50} of 0.256 mm and (b) sand mixtures with a D_{50} of 0.150 mm. 124
F3 Averaged erosion velocity versus depth-average flow velocity squared for (a) sand with a D_{50} of 0.256 mm and (b) sand with a D_{50} of 0.150 mm. 125
F4 Erosion velocity versus bed shear stress versus velocity for (a) sand with a D_{50} of 0.214 mm from Lemmens Lemmens (2014) and (b) sand with a D_{50} of 0.208 mm from Gailani Gailani (2001). 126
F5 Reduction of the erosion velocity as function of the bentonite content from depth-averaged flow velocities squared, from Lemmens. 127
G1 (Water) Levels of Scenario A-9. 128
G2 Discharge of Scenario A-9. 128
G3 Development of the breach with in Scenario A-9. 129
G4 (Water) Levels of Scenario A-10. 129
G5 Discharge of Scenario A-10. 130
G6 Development of the breach width in Scenario A-10. 130

G7 (Water) Levels of Scenario A-11. . . . 131
G8 Discharge of Scenario A-11. . . . 131
G9 Development of the breach with in Scenario A-11. . . . 132
G10 (Water) Levels of Scenario A-12. . . . 132
G11 Discharge of Scenario A-12. . . . 133
G12 Development of the breach width in Scenario A-12. . . . 133
G13 (Water) Levels of Scenario B-9. . . . 134
G14 Discharge of Scenario B-9. . . . 134
G15 Development of the breach with in Scenario B-9. . . . 135
G16 (Water) Levels of Scenario B-10. . . . 135
G17 Discharge of Scenario B-10. . . . 136
G18 Development of the breach width in Scenario B-10. . . . 136
G19 (Water) Levels of Scenario B-11. . . . 137
G20 Discharge of Scenario B-11. . . . 137
G21 Development of the breach with in Scenario B-11. . . . 138
H1 Vertical concentration profiles (a) with a relatively low bed shear stress and (b) with a relatively high bed shear stress. . . . 140
H2 Influence of the near bed concentration on the erosion velocity (a) for the courser sand ($D_{50} = 0.256$ mm) and (b) for the finer sand ($D_{50} = 0.150$ mm). . . . 141

List of Tables

1 Characteristic sand diameters of the Zwin'94 experiment . . . 10
2 Characteristic parameters of the Zwin'94 experiment . . . 11
3 Run plan for the erosion test . . . 18
4 Characteristics permeability tests . . . 26
5 Run plan permeability test . . . 27
6 Characteristics direct shear tests . . . 29
7 Run plan direct shear test . . . 30
8 Properties of the sand used in the tests . . . 32
9 Mixture perparation of the M32 sand . . . 34
10 Mixture perparation of the S90 sand . . . 34
11 Measured erosion velocities for several mixtures, mean flow velocities and sand-types. . . . 38
12 Reduction coefficient f for several mixtures and sand types based on linear regression. . . . 39
13 Predictions of corrected bed shear stresses and Shields parameters using various methods. . . . 41
14 Reduction coefficient f for several mixtures and sand types based on linear regression of corrected bed shear stress data. . . . 43
15 Reduction coefficient f for several mixtures and data sets based on linear regression of corrected bed shear stress data. . . . 46
16 Reduction coefficient f for several mixtures and data sets based on linear regression of mean flow velocity data. . . . 46
17 Summarized results of the permeability tests . . . 50
18 Specifics and results of the direct shear test . . . 53
19 Input parameters erosion function for the course and fine sand. . . . 65
20 Duration of the breaching process, the breach width, the flow through the breach and the rise rate for several retardation mixtures. . . . 67
21 Comparison of the mortality rate for several retardation mixtures. . . . 70
22 Water level and sediment characteristics for the Borssele case study. . . . 72
23 Characteristic parameters of the Borssele case study for the Citterspolder I. . . . 74
24 Characteristic parameters of the Borssele case study for the Citterspolder II. . . . 74
25 Run plan for Scenario A. . . . 75
26 Run plan for Scenario B. . . . 75
27 Duration of the breaching process, the breach width, the flow through the breach and the rise rate for several retardation mixtures in the Van Citterspolder I. . . . 76
28 Duration of the breaching process, the breach width, the flow through the breach and the rise rate for several retardation mixtures in the Van Citterspolder I. . . . 76
D1 Actual run plan for the erosion test . . . 105
D2 Test conditions and results of Run 1. . . . 106
D3 Test conditions and results of Run 2. . . . 107
D4 Test conditions and results of Run 3. . . . 108
D5 Test conditions and results of Run 4. . . . 109
D6 Test conditions and results of Run 5. . . . 110
D7 Test conditions and results of Run 6. . . . 111
D8 Test conditions and results of Run 7. . . . 112
D9 Test conditions and results of Run 8. . . . 113
D10 Test conditions and results of Run 9. . . . 114
D11 Test conditions and results of Run 10. . . . 115
D12 Test conditions and results of Run 11. . . . 116
D13 Test conditions and results of Run 12. . . . 117
D14 Test conditions and results of Run 13. . . . 118
H.1 Characteristic parameters of the..... . . . 140

1 | Introduction

1.1 Background

People all around the world live and work in low-lying areas. Low-lying areas have to be protected against high water levels in rivers and at sea by a water protection system (e.g. by dunes, dikes and barriers). A well-known example of a low-lying country, which has dealt with major flooding events in the past, is the Netherlands. Two well-known flood events in the Netherlands are the St. Elisabeth Flood of 1421 and the North Sea Flood of 1953 (in Dutch: Watersnoodramp). Afterwards a quite extensive and ingenious water protection system was developed, known as the Delta Works.

Dikes are an important component within water protection systems. Generally, dikes are described as elongated naturally occurring or artificially constructed (earthen) structures, which prevent flooding of the hinterland. Dikes are mainly found along seas, estuaries, rivers, canals, lakes and water courses. Many dikes contain sand cores, which are covered by a protection layer (e.g. clay, asphalt etc.) to prevent erosion of the core. Especially during extreme storm events the impact on the protection layer of the dike can be enormous. Unfortunately, there are times that one of the many known failure mechanisms of a dike causes (local) dike failure, exposing the sand core to the water (Rijkswaterstaat, 2006). A so-called initial breach is formed. Once the sand core is no longer fully covered by a protection layer, the sand core start to erode and the core is prone to fast breaching (Visser, 1998).

The water flowing through the breach is eroding the sandy sediment and the breach keeps growing. A clear phased description of the breaching process is given by Visser (1998). As a result of a growing breach more and more water will flow into the hinterland (polder). Inundation of a polder can have significant economical consequences and can also lead to loss of human life and animal life. Loss of life happens mainly due to the relatively fast rising water level and/or high flow velocities caused by the characteristics of the breach (see Rijkswaterstaat, 2006 and Jonkman, 2004). In this thesis an option to retard the breaching process and thus indirectly increasing the safety is investigated.

1.2 Relevance of the research

In Section 1.1 safety and increasing safety have been mentioned. In this study the safety level is determined by the risk of loss of life. An indicator for the risk of a loss of life due to a flood event is the LIR (Localized individual Risk) (see Deltares, 2011 and De Bruijn, 2009) and is defined as:

$$LIR = P_f \cdot (1 - f_{evacuation}) \cdot M_L \tag{1}$$

in which:

- LIR = Localized Individual Risk of loss of life due to a flood event
- P_f = the probability of inundation
- $f_{evacuation}$ = the fraction of the inhabitants that is evacuated
- M_L = the mortality, as in number of casualties as a fraction of the inhabitants left in the zone of flooding (estimated to be 0.01 (Jonkman, 2007))

This definition makes it possible to define a local level of safety and includes all relevant failure mechanisms, evacuation and mitigation effects (Lemmens, 2014).

The Delta Committee recommends an increase in safety level by a factor 10 (see Deltacommissie, 2008 and Smolders, 2010). In order to realize the factor 10 increase in safety, and thus indirectly a reduction of the LIR by a factor 10, the following two options are possible (Deltares, 2011):

- To reduce the number of casualties of the inhabitants that stay behind
- To reduce the number of inhabitants left in the flood zone (evacuation)

Considering the first option, it might be possible to significantly decrease the total water entering the polder and indirectly reduce the rise of the water level in the polder by retarding or even completely stop the breach growth. This potentially leads to significantly lower mortality rates and may even lower the economical consequences. If the vertical growth of the breach, for example, is significantly retarded, the outside water level may already lower below the base of the breach before the breach can grow in horizontal direction (e.g. due to the tide). In this case the total amount of water entering the polder is minimized. The second option also gives opportunities to improve. In order to reduce the number of inhabitants left in the flood zone, the people have to be evacuated. The more time available for an unforeseen evacuation, the more people can theoretically be evacuated. Within the scope of this study the safety criteria is used to asses the increase in safety level as a results of the retardation of the breaching process.

1.3 Problem description

Several retardation options have been investigated by Lemmens (2014). In Chapter 3 these options will be briefly discussed. Based on laboratory experiments, especially a mixture of sand and bentonite (in the core of the dike) seems to significantly slow down the breaching process. Based on these experiments it was hypothesized that 5.4% bentonite in the mixture should be able to increase the safety by a factor of 10 in case of the Zwin'94 experiment (Lemmens, 2014).

Thus far, this theory has only been tested for relatively low flow conditions in the order of 1 m/s. However, during the breaching process high flow conditions in the order of 2-10 m/s can be reached (Visser, 1998). Under high flow velocities dilatant behaviour of the sediment is going to play a role (Van Rhee, 2010). As a result an inward directed hydraulic gradient will hinder the erosion and is expected to have a significant impact on the breaching process (see Robijns, 2012, Foortse, 2013, and Lemmens, 2014). In Section 2.3 a more elaborate explanation of the dilatant behaviour is given. At this moment it is uncertain what the effect of adding a bentonite mixture to the sand core of a dike will be under high flow velocities.

1.4 Research questions

The aim of this Msc Thesis project is to find an answer to the following main question:

"How does bentonite reduce the erosion velocity of sand under high flow velocity conditions?"

In order to find a suitable answer to this question several additional questions are defined:

- "What physical processes affect erosion at high flow velocities?"
- "What percentage of bentonite mixed with sand significantly increases the safety level? "
- "Does the sand-bentonite mixture still show sand-like behaviour or does a certain used percentage bentonite additive influence the soil characteristics?"

1.5 Approach

In this Msc Thesis project a five-step phased approach is pursued. The following phases can be distinguished:

Phase 1 Literature review of the relevant processes of breach growth and retardation of breach growth.
Phase 2 Arrangements for the laboratory experiments and the experimental setup.
Phase 3 Performance of the experiments.
Phase 4 Implementation of the relevant processes found in the previous phases and assessment of the modified BRES model.
Phase 5 Application of the modified BRES model on a case study

1.6 Structure of the thesis

First, a literature review of the most relevant concepts and principles is presented in Chapter 2. This chapter discusses sediment transport, initiation of motion, hindered erosion, the breach growth process, the BRES model and several erosion functions. In Chapter 3 several options to retard the breaching process are briefly described. Chapter 4 presents the hypotheses defined in this thesis. This chapter also contains the proposed research method. In Chapter 5 the experimental setup of three different experiments, along with the experimental run plans are presented. These experiments made it possible to test the proposed hypotheses. In Chapter 6 the results and Chapter 7 the discussion of the experiments will be presented. During and after the experiments a specific erosion and soil behaviour was observed, which enhances the development of an adapted erosion function. In Chapter 8 the development of this adapted erosion function is discussed. In Chapter 9 a case study is presented and discussed. This main purpose of this chapter is to illustrate the effectiveness of the bentonite measure on the safety level of this specific system. Finally, Chapter 10 gives the conclusions of this Msc Thesis. Next to that recommendations containing directions for future research are provided.

2 | Theoretical Background

This chapter covers the most important terminology, processes and concepts, which are dealt with during this study. First, it is explained what sediment transport is and which different sediment transport modes are distinguished. Next the concepts of initiation of motion and of hindered erosion are discussed. After this a phased description of the breaching process is given. Finally, modeling of breach growth with the BRES model (Visser, 1998) is discussed, including a brief discussion of the BRES model, the erosion functions used in the model and the Zwin'94 experiment.

2.1 Sediment transport and sediment transport modes

Sediment transport can be described as the movement of sediment particles through a well-defined plane over a certain period of time (Bosboom and Stive, 2013). Net sediment transport takes place once the sedimentation and entrainment rate are not equal. Entrainment is the pick-up of sediment particles, which happens once the flow velocity is large enough to start moving the particles (see Section 2.2). Sedimentation is the settlement of the particles on the bottom and happens when the flow velocity is not strong enough to keep the particles in the water column. In case there is a net sediment transport there are two possible outcomes based on the sediment continuity balance: accretion and erosion. Accretion happens when the sedimentation rate is bigger than the entrainment rate and causes the bottom to rise. Erosion happens when the entrainment rate is higher than the sedimentation rate and causes a bottom level fall.

As mentioned before, the sediment transport significantly depends on the flow velocity. The bed level response, in turn, depends on a gradient in sediment transport. The relation between the sediment transport and the bed level response is given by the sediment continuity equation, also know as the Exner equation. Gradients in transport rate are for instance occurring when there is a strong change in flow velocity as a result of a narrowing flow profile in a breach. This sediment continuity relation is described mathematically by:

$$B\frac{\partial z_b}{\partial t} = -\frac{1}{1-n}\left(\frac{\partial S_x}{\partial x} + \frac{\partial S_y}{\partial y}\right) \tag{2}$$

where n is the porosity, B the width of the stretch, z_b, the bed level and S the sediment transport in specific direction.

In addition, generally two different modes of sediment transport are distinguished (Bagnold, 1956):

I **Bed-load transport**. In this mode the particles roll, shift or make slight jumps, but stay close to the bed. Once the shear stresses acting on the bed are above a certain threshold, particles are transported in layers. This is called **sheet flow transport** and is a special case of bed-load transport (Bosboom and Stive, 2013).

II **Suspended load transport**. In the suspended load mode the particles are lifted from the seabed and are transported in suspension with the water. Sediment becomes suspended at flow velocities (far) above the critical flow velocity/shear stress (see also Section 2.2).

The different transport modes are also visualized in Fig. 1.

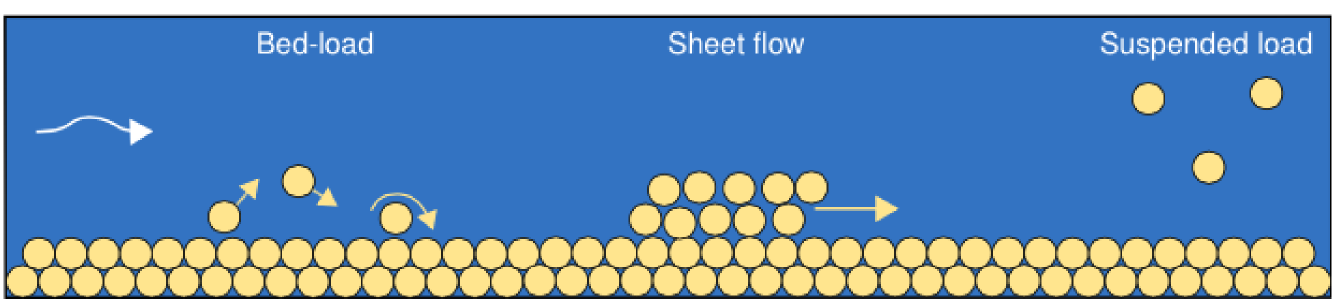

Figure 1: The sediment transport modes, from De Vet (2014).

2.2 Concept of initiation of motion

In order to move individual non-cohesive particles the water movement has to exert a force that is large enough to overcome the resistance of the particle. Shields (1936) introduced the concept of initiation of motion of individual particles. The condition of initiation of motion is defined as the moment at which the particles are just starting to move.

By looking at the forces that act on a particle Shields (1936) assumed that the lift force F_L, the drag force F_D and the gravity force F_g are playing a role. Fig. 2 presents the considered forces on a single grain. The drag- and lift forces are trying to move the particle, whereas the gravity force tries to keep the particle on its place. The drag force is a combination of a pressure difference caused by the flow separation at the downstream end of the particle and a skin friction at the surface of the particle. The gravity force is directly linked to the underwater mass of the particle. Finally, the lift force is caused by a combination of flow separation and flow contraction. These effects combined give a lower local pressure at locations where the flow velocity is high (Bernoulli's Law). This difference in local vertical pressure leads to a lift force.

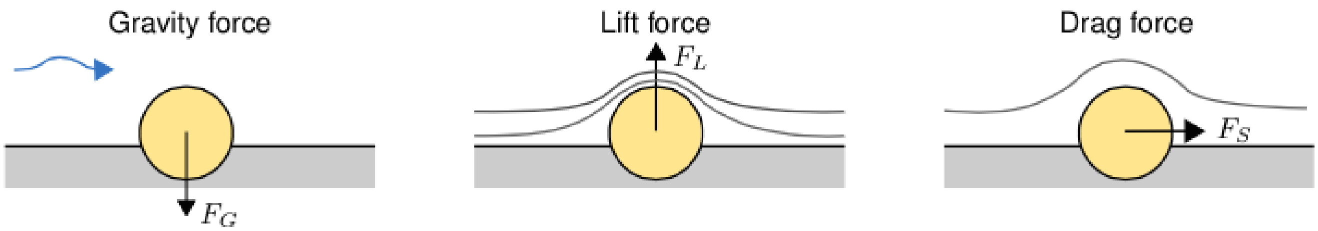

Figure 2: Initiation of motion as proposed by Shields, from De Vet (2014).

When these forces are in equilibrium (horizontal, vertical or rotational) the following expression can be found based on proportionality and spherical geometry principles:

$$(\rho - \rho_s)gD^3 \propto \rho U_{cr}^2 D^2 \propto \tau_{b,cr} D^2 \tag{3}$$

From the proportionality of Eq.(3) the following ratio, known as the critical Shields parameter or the critical mobility parameter θ_{cr}, can be the deduced:

$$\theta_{cr} = \frac{\tau_{b,cr}}{(\rho - \rho_s)gD} \tag{4}$$

in which g is the gravitational acceleration, D the sediment diameter, U_{cr} the critical depth-averaged velocity at which the particles start to move, $\tau_{b,cr}$ the critical bed shear stress, ρ_s the sediment density and ρ represent the density of the water. In addition it has to be remarked that the critical Shields parameter θ_{cr} has to be determined experimentally.

The actual balance of lift-, drag- and gravity forces, which is not necessarily equal or bigger than the critical Shields parameter, is given by the Shields parameter θ and is defined as:

$$\theta = \frac{\tau_b}{(\rho - \rho_s)gD_{50}} = \frac{u_*^2}{\triangle g D_{50}} \tag{5}$$

where $\triangle$ represents the relative density, D_{50} is the median diameter of the sediment and u_* is the shear stress velocity, which is directly linked to the shear stress τ_b.

Empirical sediment transport formulae often use the Shields and critical Shields parameter in order to determine the transport rate (see also Section 2.6).

2.3 Concept of hindered erosion

Most sediment transport formulae are calibrated based on river conditions under relatively small flow velocities ($<$ 1m/s). As mentioned before, in Section 1.3, during the breaching process high flow conditions in the order of 2-10 m/s can be reached (Visser, 1998). At high velocities Van Rhee (2010) states that dilatancy effects will hinder the erosion.

At higher flow velocities sand is picked up in layers. This is also known as sheet flow transport (see also Section 2.1). As a result the top layer of the sand bed will be sheared. This shearing leads to a volume change. Under the assumption that the porosity is lower than the critical porosity (the critical porosity defines the porosity above which the soil becomes loosely packed) the total volume will increase under shear (Fig. 3). This is called dilatancy. The increased volume has to be filled with water, since the particles can be considered incompressible. An inflow of water means that a drop in pore pressure in the top of the sand bed is needed in the control volume. This drop in pressure introduces an inwards directed hydraulic gradient that hinders the entrainment of sediment.

Traditional pick-up functions were developed for relative low velocities and bed shear stresses; hence they overestimate erosion for high flow velocities. In order to solve this problem Van Rhee (2010) proposed the following modified critical Shields parameter, which takes the hydraulic gradient into account:

$$\theta_{cr}{}^{1} = \theta_{cr}\left(1 + \frac{v_e}{k_l}\frac{n_l - n_0}{1 - n_0}\frac{A}{\triangle}\right) \tag{6}$$

in which:

- v_e = the erosion velocity [m/s]
- k_l = the permeability given a loose soil packing [m/s]
- n_0 = the in-situ porosity [-]
- n_l = the porosity in the sheared zone (loose packing) [-]
- A = a tune parameter, which is equal to 3/4 for a single particle and approximately 1.7 for a continuum [-]

The modified critical Shields parameter can be used in conventional erosion functions to deal with high velocity regimes as long as the conventional erosion functions contain a critical Shields parameter (Van Rhee, 2010).

Figure 3: Increase of volume due to shearing from De Vet (2014); original figure from Van Rhee (2010).

2.4 The breaching process

There are several (geotechnical) failure mechanisms known, which might initiate the breaching process (Rijkswaterstaat, 2006). A few of these failure modes are summarized in Fig. 4. After a (local) failure the protective layer (often clay) is damaged, which means that the sand core is no longer protected and erosion is no longer prevented.

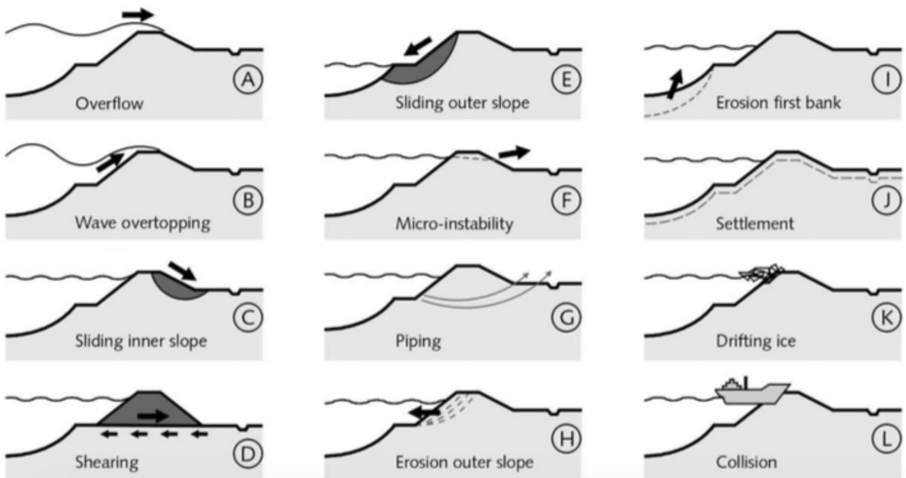

Figure 4: Several failure modes of dikes from Tonneijck and Weijers (2008).

The breaching process can be decomposed in five different phases according to Visser (1998). These five phases are:

1. The steepening of the inner slope of the dike towards a critical value.
2. Retrograde erosion of the inner slope at the critical slope, decreasing the crest width of the dike in the breach to zero, which is the end of this stage.
3. Lowering of the crest height in the breach until the level of the base of the dike is reached. At the same time the width of the breach grows in lateral direction, because the side slopes also remain at a critical slope.
4. Both vertical and lateral directed erosion can take place. The lateral erosion is more important in this phase, since the vertical erosion depends on the erodibility of the base of the dike.
5. The flow has become subcritical and the breach continues to grow in lateral direction at the critical side slope angle. The growth of the breach stops once the flow velocity through the breach is too low to initiate sediment transport. This is due to the fact that the water level difference between the polder and outside the dike is getting too small. Once the water level gradient is zero the breaching process ends completely.

The five phases approach is shown in Fig. 5.

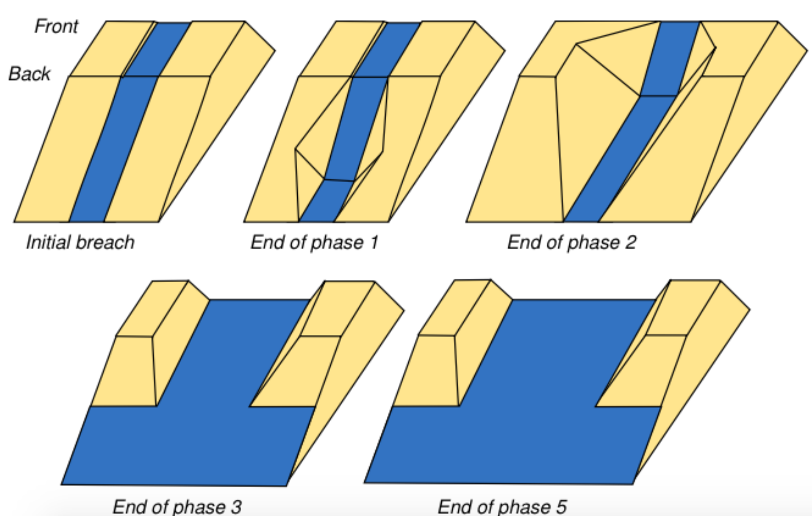

Figure 5: The five stage breaching process from De Vet (2014), original figure from Visser (1998).

2.5 Modeling of the retardation of breach growth

Breach models have to fulfill two major tasks: to predict the breach characteristics and to estimate the flow through the breach (Peeters et al., 2011). Although currently multiple breach growth models exist, the focus in this study will be on the BRES-Visser breach growth model for sand dikes (Visser, 1998). For the simple reason that this model is freely available for the author and since the main goal is to asses the retardation effect of bentonite under high flow velocities. In addition, the BRES-Visser model appears to perform well for homogeneous sand dikes according to an evaluation based on a process approach and a real test cases approach (Peeters et al., 2011).

A SWOT analyses stating the important assumptions, limitations, strengths and opportunities for the BRES model is summarized in Fig. 6; from (Peeters et al., 2011). An important remark has to be made concerning the applicability of the BRES model (see the threats and weaknesses in Fig. 6). Zhu (2006) developed the BRES-Zhu model for cohesive sediment; this model increases the applicability significantly. Especially the erosion mechanisms for cohesive sediment (e.g headcut erosion) are very different from the mechanism of non-cohesive sediment. A more elaborate discussion can be found in the SWOT analysis by Peeters et al. (2011).

STRENGTHS	WEAKNESSES
- Hydrodynamic aspects easily adjustable - Model structure easily to extend - Detailed physically-based description of surface erosion, especially breach initiation processes - Validation for real-world case studies, e.g. ZWIN94-test - Stand-alone model - Short simulation time	- Currently unavailable for use in practical cases - Limited number of breach process incorporated (only for homogeneous, sandy dikes) - Not tested during IMPACT & FLOODSITE Hence, performance in practice is unclear. - Erosion at toe determines erosion rate of entire dike (breach initiation) - Breach shape always trapezoidal - No head-cut erosion - Only sediment transport equation - No piping - Model relatively insensitive to water levels on land-side
OPPORTUNITIES	**THREATS**
- Enormous potentials due to detailed physically-based description - Detailed physically-based - Development of a user-friendly interface - Erosion equations can be built-in rather easily	- Model structure not easily adjustable - Limited applicability for inexperienced users - Only for homogeneous, sandy dikes - Some less known model parameters

Figure 6: SWOT analysis from Peeters et al. (2011).

From sensitivity studies it can be concluded that breach parameters are highly affected by the critical angles of the side slopes (see Robijns, 2012 and Foortse, 2013). In addition, it is recommended to be careful with selecting erosion functions only in the range and conditions for which they are developed (Robijns, 2012).

For an elaborate explanation of the model equations and setup, reference is made to the dissertation of Visser (1998).

2.6 Erosion functions in the BRES model

Within the BRES model several sediment transport formulae and an erosion function have been implemented (see Visser, 1998 and Robijns, 2012). In the current model the following functions can be selected:

1. Bagnold-Visser (see Visser, 1988), abbreviated as BV

$$s_b = \frac{e_b}{(\tan(\phi) - \tan(\beta))\cos(\beta)} \frac{c_f U^3}{\Delta g} \tag{7}$$

$$s_s = \frac{e_s}{(w_s/u)(\cos(\beta))^2}\frac{c_f U^3}{\Delta g} \tag{8}$$

2. Engelund and Hansen (1967), abbreviated as EH

$$s_t = 0.05{c_f}^{-1}\left(\triangle g D_{50}^3\right)^{0.5}\theta^{2.5} \tag{9}$$

3. Van Rijn (1984), abbreviated as VR

$$s_{b(T<3)} = 0.053\left(\triangle g {D_{50}}^3\right)^{0.5}\frac{T^{2.1}}{{D_*}^{0.3}} \tag{10}$$

$$s_{b(T>3)} = 0.1\left(\triangle g {D_{50}}^3\right)^{0.5}\frac{T^{1.5}}{{D_*}^{0.3}} \tag{11}$$

$$s_s = F c_a U d \tag{12}$$

4. Wilson (1987), abbreviated as WL

$$s_b = 12.1\cdot\left(\triangle g D^3\right)^{0.5}(\mu\theta - 0.047)^{1.5} \tag{13}$$

5. Bisschop & Van Rhee (see Bisschop et al., 2010), Abbreviated as RH

$${v_e}^5 = \alpha^2 D_*^{0.6}\left(\frac{\theta-\theta_{cr}}{\theta_{cr}}\right)^3\left(\frac{k}{\delta}\right)^3 \tag{14}$$

$$\alpha = 0.00033\frac{\sqrt{\triangle g D_{50}}}{1-n_0} \tag{15}$$

$$D_* = D_{50}\left(\frac{\triangle g}{\nu^2}\right)^{1/3} \tag{16}$$

$$\delta = \frac{n_1-n_0}{1-n_1}\frac{1}{\triangle(1-n_0)} \tag{17}$$

where c_f represents a friction coefficient, δ is called the dilatancy factor (see Eq.(17)), ν the kinematic viscosity, μ a ripple factor, F is a dimensionless form factor, U the depth-averaged flow velocity, d is the water depth, $T = (\tau_b - \tau_{b,cr})/\tau_{b,cr}$ is a dimensionless transport parameter, c_a is the sediment concentration at 'a' meters above the bottom, w_s is the settling velocity, ϕ is the angle of internal repose, β is the slope angle, e_s is a measure for the efficiency of the suspended load transport, e_b is a measure for the efficiency of the bed load transport and s the sediment transport capacity. For an explanation on how to determine certain parameters reference is made to the work of the authors mentioned above. The subscript b, s and t in the sediment transport equations refer to the bed load transport mode, suspended load transport mode and total load transport respectively (see also Section 2.1).

It has to be remarked that within the BRES model the erosion functions are combined with the simplified Galapatti (1983) mechanism to obtain sediment transport formulae. The erosion functions itself do not take into account that at a certain point the sediment capacity can be reached. Once the sediment capacity is reached no further erosion takes place. Hence, the erosion velocity becomes zero. In this study the underlying assumptions of the erosion functions are not further investigated.

For every phase one of the erosion formulae can be manually selected. Robijns (2012) and Foortse (2013) conclude that a combination of the Bisschop & Van Rhee (2010) formula in phase I, II and III and the Van Rijn (1984) formula in phases IV and V lead to a reasonable results as compared to the Zwin'94 experimental data (see Fig. 7).

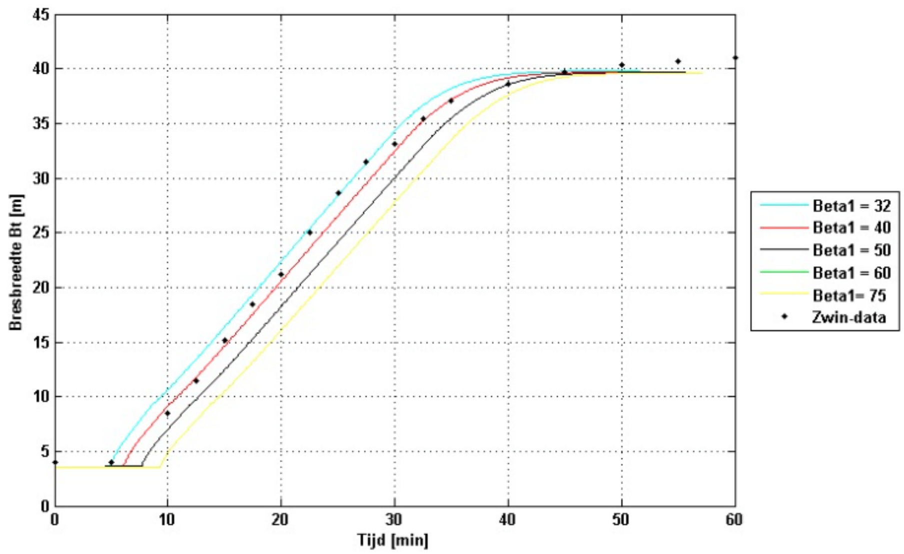

Figure 7: Comparison BRES-model output and Zwin'94 dataset, from Foortse (2013).

Lemmens (2014) implemented several other erosion functions in the BRES-Visser model. These were: the erosion function of Van Rhee (2010), the erosion function of Van Rijn (1984), the erosion function of Nakagawa and Tsujimoto (1980) and the erosion function of Fernandez-Luque (1974). In addition, the adapted critical Shields number was implemented in these erosion functions. A comparison was made with the simplified Bisschop & Van Rhee erosion function (see Bisschop et al., 2010) and it was concluded that the Bisschop & Van Rhee (2010) formula is still a favourable option.

2.7 The Zwin'94 experiment

In this section a brief overview of the full-scale dam breach experiment, known as the Zwin'94 experiment is presented. For a more elaborate description reference is made to Visser et al. (1995) and Visser et al. (1996).

The Zwin'94 experiment was performed on 6 and 7 October 1994 in the Zwin Channel. This is a tidal inlet connecting the nature reserve "Het Zwin" with the North Sea. The main goal of the experiment was to obtain data in order to calibrate and validate breach models. The sand-dam was built with local sand from the Zwin Channel and from suppletion sand. In Table 1 the characteristics of both sand types are outlined. The experimental cross-section is provided in Fig. 8 and the relevant parameters for the experiment are listed in Table 2. NAP is the reference level in the Netherlands, at about mean sea level.

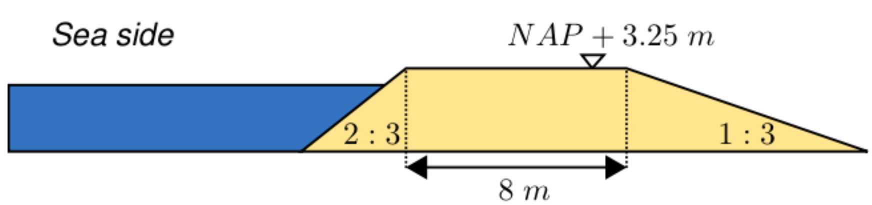

Figure 8: Cross-section Zwin dike from De Vet (2014).

Table 1: Characteristic sand diameters of the Zwin'94 experiment

Origin sand	D_{10} in $[\mu m]$	D_{50} in $[\mu m]$	D_{90} in $[\mu m]$
ZWIN sand	155	185	285
Suppletion sand	215	315	600

Table 2: Characteristic parameters of the Zwin'94 experiment

Parameter	Value
Seaside bottom level Z_w in [m]	NAP + 0.7
Polder bottom level Z_p in [m]	NAP + 0.7
Initial polder water level H_p in [m]	NAP + 1.3
Crest height H_d in [m]	NAP + 3.3
Bottom of the breach Z_{br} in [m]	NAP + 2.5
Initial breach width at the bottom b in [m]	1.0
Crest width W_d in [m]	8.0
Outer slope α in [-]	1:1.6
Inner slope β in [-]	1:3
Side slope angle γ in [deg]	60
Angle of repose ϕ in [deg]	32
Water temperature T in [°C]	17
Initial porosity n_0 in [-]	0.40
Sheared porosity n_i in [-]	0.48
Density of the water ρ_w in [kg/m^3]	1025
Density of the sand ρ_s in [kg/m^3]	2650

The increase in breach width was both videorecorded and photographed from a measuring vessel. In Fig. 9 the development of the width of the breach in time and the end of each phase are shown. It was observed that the breach width had grown to 41 meters within one hour! The flow velocity in the breach was also measured by using floats.

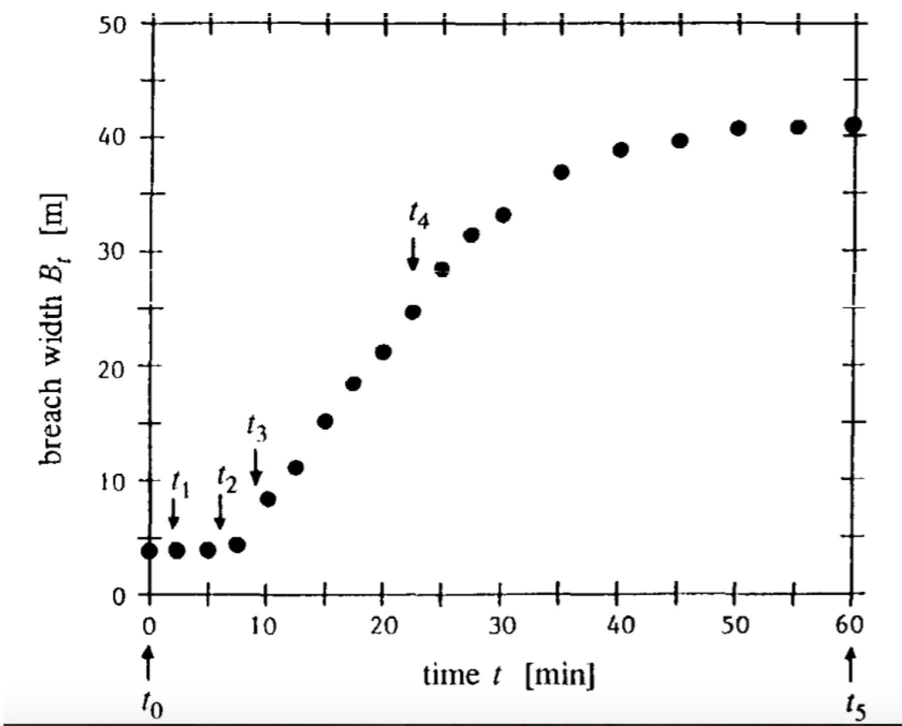

Figure 9: Observed breach with in time and the end on each subsequent phase from Visser (1998).

In this study the obtained data from the Zwin'94 experiment will be used as a reference scenario for a dike with a sand core. The effects of the retardant bentonite additive as obtained during the experiments will be compared to this reference scenario. The comparison takes place based on breach width, flow through the breach and duration of the breaching process.

3 | Retardation of the breaching process

Although the aim of this study is to investigate the possibility to retard the breaching process by adding bentonite to the sand core of a dike, many other possibilities to retard the breaching process have been proposed in the literature. In this chapter a summary of these options is given in order to give a complete overview of the research performed on this topic. The options are categorized in the following four categories: alteration of the shape of the dike, changing the characteristics of the soil, addition of erosion resistant components and alternative approaches.

3.1 Alteration of the shape of the dike

For the alteration of the dike shape two options have been proposed and analyzed in the literature (Smolders, 2010). These two options are:

1. **To reduce the angle of the inner slope**

   After an initial breach is formed the water will start to flow over the inner slope. By reducing the inclination angle of the inner slope the flow velocity on the slope will be decreased. As a consequence also the erosion rate is decreased. In this way the duration of the first stage of the breaching process, as discussed in Section 2.4, is increased and the overall breaching process is retarded. Fig. 10 shows the results of a changed inner slope on the duration of stage I. A change in inner slope from 1:3 to 1:50 increases the duration with a factor of about 15 (Smolders, 2010). Unfortunately, a decrease in inner slope automatically enlarges the dike profile.

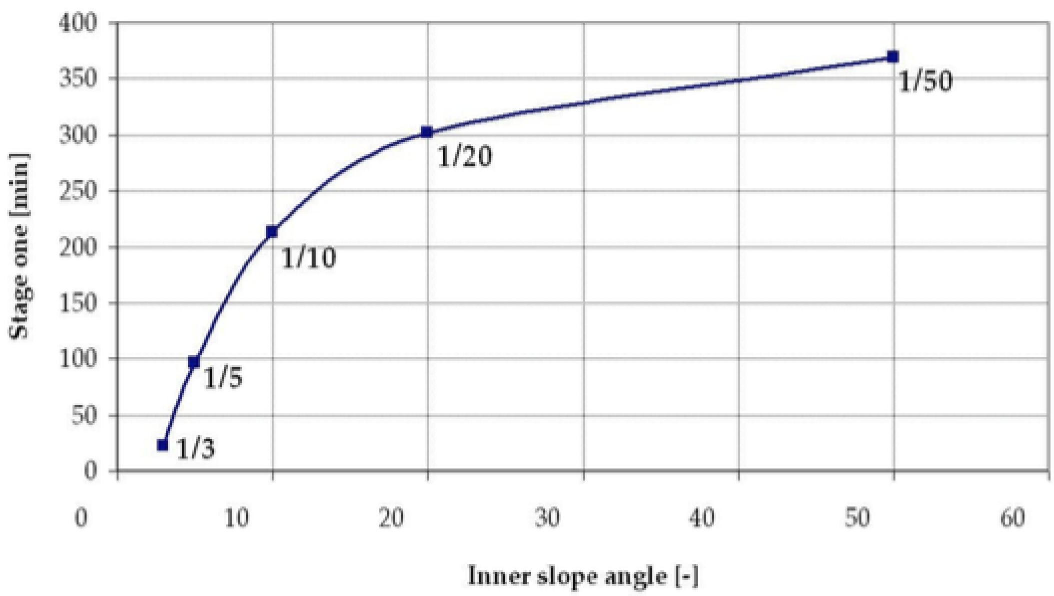

Figure 10: Retardation of the breaching process by decreasing the inner slope angle from Smolders (2010).

2. **To increase the crest width**
   By increasing the width of the crest the retrograde erosion in phase II will be slowed down. An almost perfect linear relation between the increase in crest width and the duration of stage II is observed (Smolders, 2010). This is also shown in Fig. 11. Unfortunately, again the dike profile is enlarged by applying this option, which might not be applicable everywhere.

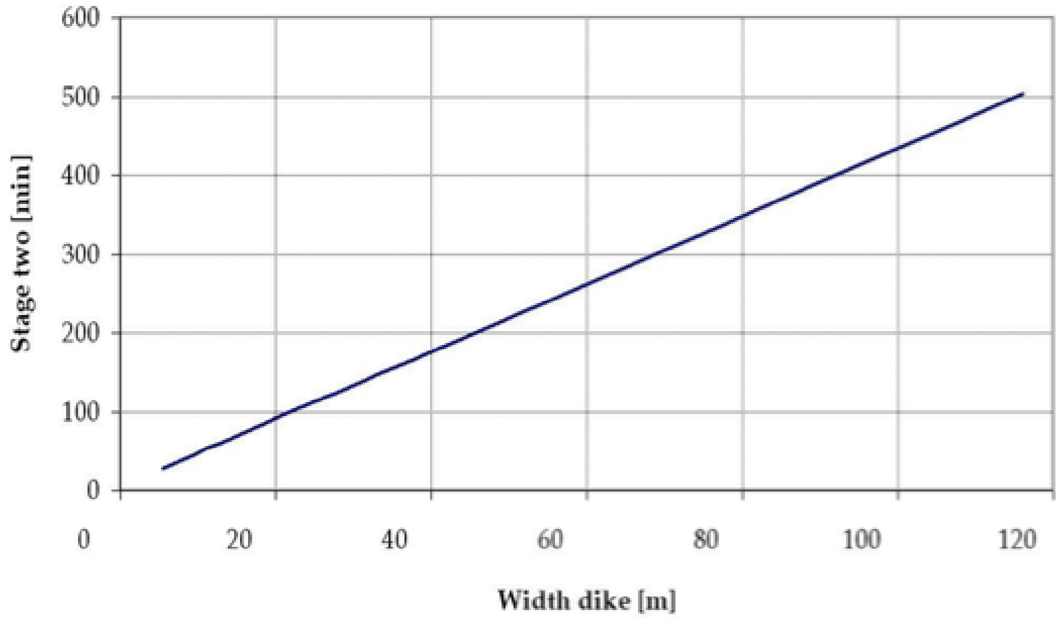

Figure 11: Retardation of the breaching process by increasing the crest width from Smolders (2010).

3.2 Changing the characteristics of the soil

In order to change the characteristics of the soil a distinction is made between changing the cohesion and permeability of the soil and increasing the strength of the sand by reinforcement. Both options are briefly discussed.

1. **Increase the cohesion and decrease the permeability of the dike**
   The duration of the breaching process is positively influenced when the cohesion of the dike is increased (Zhu, 2006). Experiments with a sand dike and a clay dike under similar hydraulic conditions and dimensions clearly show a significant increase in the duration of the breaching process. Fig. 12 and Fig. 13 show that it takes 3 minutes to breach the sand dike and about 3 hours to breach the clay dike. It is important though, to keep the total strength of a dike at a sufficient level. The strength of a dike highly depends on the sand properties.

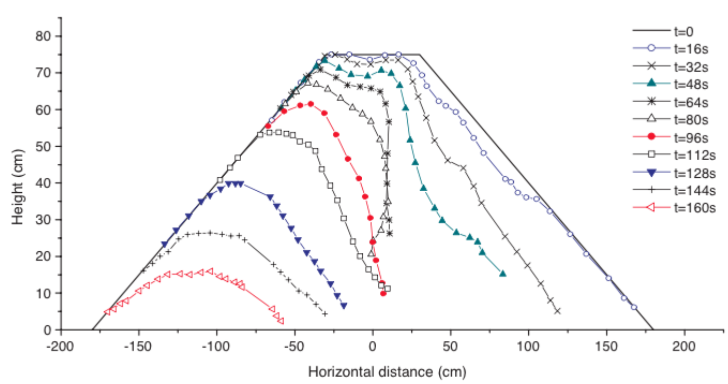

Figure 12: Development of the breaching process in a sand dike experiment from Zhu (2006).

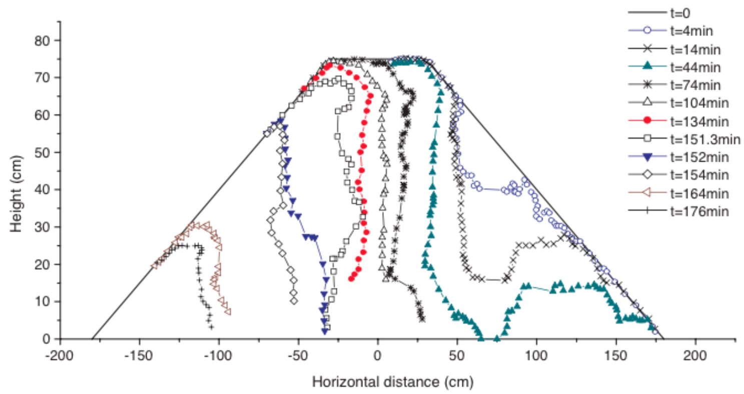

Figure 13: Development of the breaching process in a clay dike experiment from Zhu (2006).

One method is to use bentonite as an additive to retard the breaching process (Gailani, 2001). Bentonite is well-known for its absorbent properties. The volume of bentonite increases when it gets in contact with water and by doing this the permeability of the sand decreases. The lower the permeability, the higher the extra downward forcing due to the extra hydraulic gradient and thus the longer the erosion process takes. This has been discussed in Section 2.3. Even adding a small percentage of bentonite is able to significantly lower the erosion rate, inundation velocity and corresponding breaching process duration (Lemmens, 2014). This is also visualized in Fig. 14. However, the strength properties of the sand should be maintained while decreasing the permeability. The sand particles are not allowed to loose direct contact with neighbouring particles and consequently lose its strength characteristics.

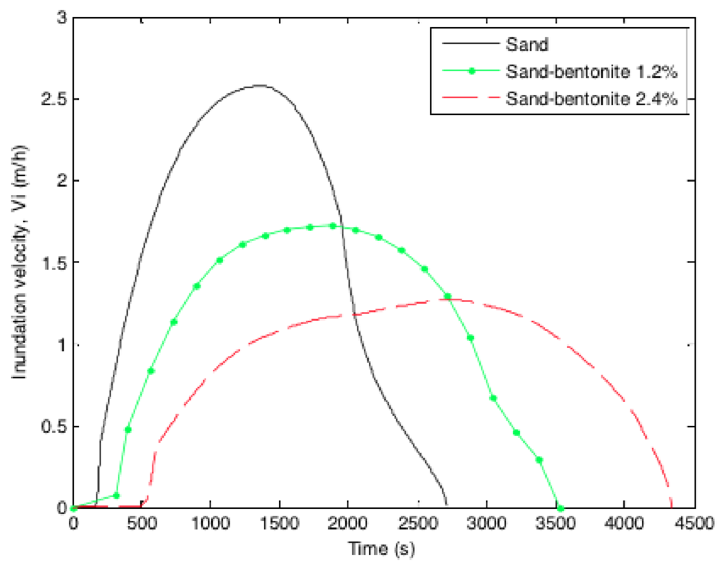

Figure 14: Retardation of the breaching process with bentonite under low flow velocities from Lemmens (2014).

2. **Increase the strength of the sand**
   In the literature four different techniques have been found. These are: reinforcement by grout injection, biological reinforcement of the sand, reinforcement by fibers and reinforcement by vegetation. Each of these options is briefly discussed.

   (a) **Reinforcement by grout injection**
   Grouting is a technique to improve the soil characteristics (e.g. cohesion and strength) by injecting a cement mixture or chemical mixture. In order to be effective a certain minimum permeability has to be present. The reduction of the permeability reduces the erodibility, but also limits the penetration distance within the soil (Anagnostopoulos, 2005). An important remark is that the a dike is often prone to

settlement of the underlying soil. The grouted dike body is not likely to be able to follow this settlement and crack formation can occur, which limits the applicability to retard the breaching process (Lemmens, 2014).

(b) **Biological reinforcement of the sand**
With this option the characteristics of sand to cementate under specific biological conditions is used. This natural phenomena can be enhanced by using a specific enzyme (De Jong et al., 2006). During and after the cementation the soil properties will change. The strength increases and the permeability decreases. Initial studies indicate that especially the reduction of the permeability reduces the erodibility of the soil (Ferris et al., 1997).

(c) **Reinforcement by fibers**
Two important parameters influence the peak shear strength of the sand reinforced with fibers. These are the ratio between the area of the fibers A_R and the area of the sample A, and the length of the fibers (Gray and Ohashi, 1983). Although a slight increase in friction angle of the mixture is observed, no significant reduction of the erosion velocity is taking place (Lemmens, 2014). The effectiveness in reducing the erosion velocity of the fibers in comparison with the bentonite mixture is shown in Fig. 15.

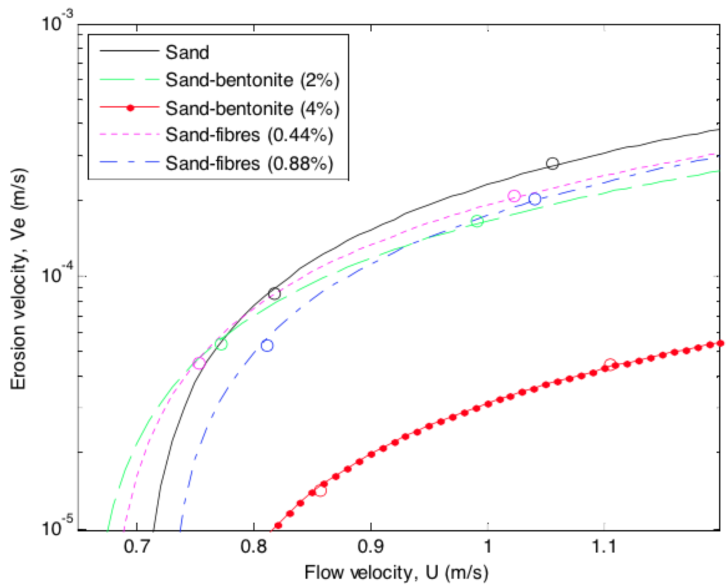

Figure 15: Retardation with bentonite and fibers under low flow conditions, from Lemmens (2014).

(d) **Reinforcement by vegetation**
The idea of reinforcing the sand by vegetation is quite similar to the reinforcement by fibers. Instead of fibers, the roots of the vegetation are used as natural reinforcement. Erosion of non-cohesive sand-like soil is drastically reduced by the presence of certain types of vegetation (Verhagen et al., 2008). Unfortunately, the reduction of erosion is becoming less and less effective the greater the penetration depth becomes (De Baets and Poesen, 2010).

3.3 Addition of erosion resistant components to the dike

Another approach is to add erosion resistant components in the dike body. The aim of these components is to prevent the growth of a breach after it reaches those components. Two possibilities are briefly discussed.

1. **Compartmentation**
A possibility to limit/pre-determine the lateral growth of the breach is to create compartments in the cross section of the dike (Visser, 1998). The compartments can be created using the following materials (see also Lemmens, 2014): sheet piling, vertical clay layers or cores and a geo-textile.

2. **Erosion resistant core**
An erosion resistant core is preventing erosion in vertical direction. In certain dikes and dams these erosion

resistant cores are already present, however, the effects of breaching in those structures is not well-known. Three types of materials are proposed by Lemmens (2014): sheet piling, concrete and clay (Zhu, 2006).

3.4 Alternative approaches

Two alternative approaches are also discussed in the literature (see Lemmens, 2014). These are:

1. **Increase erosion resistance by applying a pressure difference**
   By applying a pressure difference it is theoretically possible to create an inward directed hydraulic gradient (see also Section 2.3). If this is applied well, the entrainment of sediment is hindered.
2. **Reduction of the flow through the breach**
   Instead of altering the soil properties it is also possible to reduce the flow through the breach. The flow reduction can be realized by decreasing the area of inflow. An erosion resistant sill/toe-structure reduces the depth over which the water flows and thus reduces the area of inflow (see Visser, 1998). In this way the breach width, the water entering the hinterland and thus inundation velocity can be reduced (see also Van Gerven, 2004). This is shown in Fig. 16 and Fig. 17. Unfortunately, the dike body behind the sill can still be eroded away.

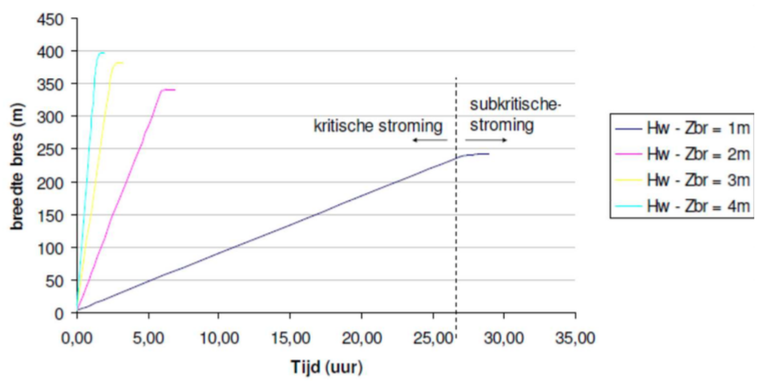

Figure 16: Reduction in lateral breach width for different sill heights from Van Gerven (2004).

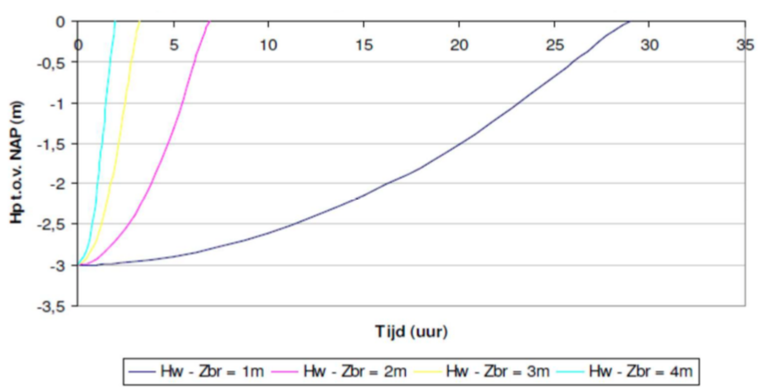

Figure 17: Rise in water level of the polder for different sill heights from Van Gerven (2004).

4 | Hypotheses

In order to focus the research in the direction of answering the research questions several hypotheses are formulated. These hypotheses will especially be useful in setting up the laboratory experiments. The main research questions was:

“How does bentonite reduce the erosion velocity of sand under high flow velocity conditions?"

and the additional questions were:

- “What physical processes affect erosion at high flow velocities?”
- “What percentage of bentonite mixed with sand significantly increases the safety level? ”
- “Does the sand-bentonite mixture still show sand-like behaviour or does a certain used percentage bentonite additive influence the soil characteristics?”

From the literature review it can be concluded that hindered erosion might be an important process affecting the erodibility of the dike material under high flow velocities. In addition, the permeability will decrease significantly if bentonite is added. Several presumptions from the literature review are translated into hypotheses. The hypotheses proposed in Section 4.1 and Section 4.2 will be tested in the further part of this thesis. In Section 4.3 the research method is outlined.

4.1 Hypotheses regarding the physical behaviour of erosion

The following hypotheses are proposed regarding the physical behaviour:

1. The effect of dilatancy significantly reduces the erosion velocity at high flow velocities (>2 m/s) as compared to low flow velocities (<1 m/s).
2. A bentonite-sand mixture still shows sand-like behaviour when the bentonite content is up to 10% of the total mixture content.
3. The turbulence affects the erosion velocity at high flow velocities.
4. Reducing the permeability by adding bentonite is responsible for the decrease in erosion velocity.

4.2 Hypotheses regarding the modeling of breach growth

The following hypotheses are proposed regarding the modeling of the observed behaviour:

5. The adapted erosion function implemented in the BRES model is able to predict the breach growth process for the ZWIN’94 experiment relatively accurately.
6. Adding bentonite to the sand core of a dike is a highly effective measure to retard the breaching process.
7. The implementation of bentonite in the mixture is practically feasible for new dikes.

4.3 Research method

In order to check these hypotheses and to answer the research questions several experiments were executed. These experiments are similar to the bentonite-sand mixture experiments executed by Lemmens (2014) under relatively low flow velocity conditions. These experiments are:

1. Erosion tests;
2. Permeability tests;

3. Direct shear tests;

Erosion tests: The erosion tests were executed in a flume of the Laboratory for Fluid Mechanics at the Delft University of Technology. The aim of the erosion tests is to determine the erosion velocity of the bentonite-sand mixture for several added bentonite percentages (see the run plan in Table 3). First, the bed had to be prepared. After compaction and saturation of the bed, erosion test were executed at two different flow velocities. These were 1 and 2 m/s, respectively. The water levels and bed levels were recorded in time with a video camera. From this record the exact flow and erosion velocity have been determined. In addition, two different types of sand were tested, i.e. one with a D_{50} of 0.256 mm and the other with a D_{50} of 0.150 mm. A more elaborate discussion of the setup follows in Chapter 5. The plan for the different erosion runs is summarized in Table 3.

Permeability tests: With the permeability tests the effect of the added bentonite percentages on the mixtures' permeability was assessed. In this study the falling head test has been used to determine the permeability of the mixtures. With the falling head test the subsidence rate of the water on top of the sample is a measure for the permeability. With the results of these experiments it is possible to investigate whether the change in permeability due to addition of bentonite is indeed decreasing the erosion velocities significantly, as stated in the literature (Van Rhee, 2010). The falling head tests were executed in the Laboratory of Geoscience and Engineering at the Delft University of Technology.

Direct shear tests: The direct shear tests were executed to determine the friction angle and (apparent) cohesion of the material. Experiments were carried out for different percentages of bentonite, since it has been expected that addition of bentonite will change the soil behaviour at a certain percentage. Hence, these experiments will investigate if the mixture will behave sand-like or clay-like. The direct shear tests were executed in the Laboratory of Geoscience and Engineering at the Delft University of Technology.

During and after the experiments a specific erosion behaviour and soil behaviour have been observed, enhancing the development of an adapted erosion function. However, first the observed erosion behaviour is compared with the existing erosion function of Van Rhee (2010). Next, the adapted erosion function is implemented in the BRES model. Afterwards the model will be calibrated with the dataset of the Zwin'94 experiment. Finally, the effectiveness of the bentonite measure is tested in a case study.

Table 3: Run plan for the erosion test

Run #	Percentage bentonite [%]	D_{50} in [mm]	Flow velocity in [m/s]
1	0	0.256	1
2	2	0.256	1
3	4	0.256	1
4	6	0.256	1
5	0	0.256	2
6	2	0.256	2
7	4	0.256	2
8	6	0.256	2
9	0	0.150	1
10	6	0.150	1
11	0	0.150	2
12	3	0.150	2

5 | The experimental setup

The experimental tests were executed in the Laboratory for Fluid Mechanics and the Laboratory of Geoscience and Engineering at the Delft University of Technology, as mentioned in Section 4.3. This chapter explains the setup of the erosion tests, the direct shear tests and the permeability tests in more detail. In addition, an elaboration of the used measurement equipment, the used sediment and the preparation of the sand bed and samples is given.

5.1 Experimental setup of the erosion tests

The erosion experiments were carried out in a tilting flume with a length of about 14 m, an effective height of 0.40 m, a width of 0.40 m and a maximum discharge of about 0.025 m^3/s. The maximum inclination of the flume is 1%. For all the experiments one wall was of transparent glass and the other wall consisted of smooth plywood. The flow in the flume was generated with a pump. Water was pumped from a tank beneath the flume into the flume, was flowing through the flume and exited the flume into the lower tank again. The eroded sand-bentonite mixture had to be captured in the lower tank to comply with environmental regulations. The flow was regulated with the pump, since the experiments were performed under supercritical conditions. A tailgate was used to completely fill the flume before the start of a test in order to let the sand bed get saturated. An overview of the flume is given in Fig. 18.

Figure 18: Side and top view of the flume.

The flume was divided into four segments: a wide inflow section (with a length of about 1.5 m) including a honeycomb structure to reduce the turbulence and straighten the flow, a narrow inflow section partly with a fixed concrete bottom (about 5 m long), a test section with a sand bed (about 6 m long) and a narrow outflow section (about 1.5 m long). The width of the flume was artificially reduced to 0.145 m with a constriction over almost the entire length of the flume. As a result the flow velocities increased significantly in the constricted section. To minimize the generation of a scour hole at the upstream end of the bed, a fixed concrete bottom with a height of 0.10 m was implemented. All erosion experiments were performed under supercritical conditions. As a consequence of this flow regime, the preferred equilibrium flow velocities (1 and 2 m/s) were hard to regulate. The equilibrium velocity only depended on the roughness of the bed and the slope of the bed. The only parameter that could be optimized was the slope of the bed. This resulted in two different setups. One with a slope of 1% and one with an intended equilibrium slope of 3%. The experimental setups are shown in Fig. 19 and in Fig. 20. The first setup, with a slope of 1%, had a bed with a height of 0.15 m over the total length of the bed, since the flume was tilted to its maximum inclination of 1%. The second setup, with a slope of 3%, had the same 1% inclination from the flume as the previous setup. However, the bed level had to gradually decrease (2 cm/m) in downstream direction to guarantee a total inclination of 3%.

The height of the bed was chosen to be 0.15 m. Estimations with the Bisschop & Van Rhee model indicated that the erosion velocity v_e at a depth-averaged flow velocity U of 2 m/s could be in the order of cm/s (Bisschop et al., 2010). With a height of the bed of 0.15 m an experimental run without bentonite additive was thus estimated to take about 20 seconds.

The fixed concrete bottom was mainly applied to minimize the effects of turbulence in the measurement area, caused by the sudden transition in bed level between the flume bottom and the height of the sand bed of 0.15 m. Although there would still be a transition in bed roughness from the fixed concrete bottom to the sand bed, the turbulence effects were expected to be less significant than in case of a sudden transition in height. The length of the bed was chosen to be about 6 m to give the flow enough length to reach equilibrium conditions so that the slope of the water level would be equal to the slope of the bottom. General empirical formulations state that the flow needs a length of about 20 times the water depth to reach equilibrium conditions.

Finally, it has to be mentioned that each test consisted of an adjustment period, during which the equilibrium flow conditions were established, and a measuring period. The measuring period was kept as short as possible to prevent turbulence effects, as a result of possible bed form formations. These turbulence effects would influence the results too much. After the tests were stopped, the bed was photographed and samples of the bed were taken (see also Section 5.4.4).

5.1.1 Preparation of the erosion test

In order to execute the experiments, the first step was to mix the bentonite and sand mixtures as dry soils using a concrete mixer (see also Section 5.4.3). Afterwards the desired mixture was transported towards the flume, where the bed was built. Next, the sand bed was compacted by means of vibration with a strip of wood and a rubber hammer, which leaves some ingenuity for improvement. After compaction the sand bed would ideally have a dry bulk density of 1588 kg/m^3. and a porosity of 0.40. The final step of the preparation phase was to allow the bed to become saturated with water for a period of about 24 hours. This was specifically needed to activate the bentonite and to let it reach its full swelling capacity.

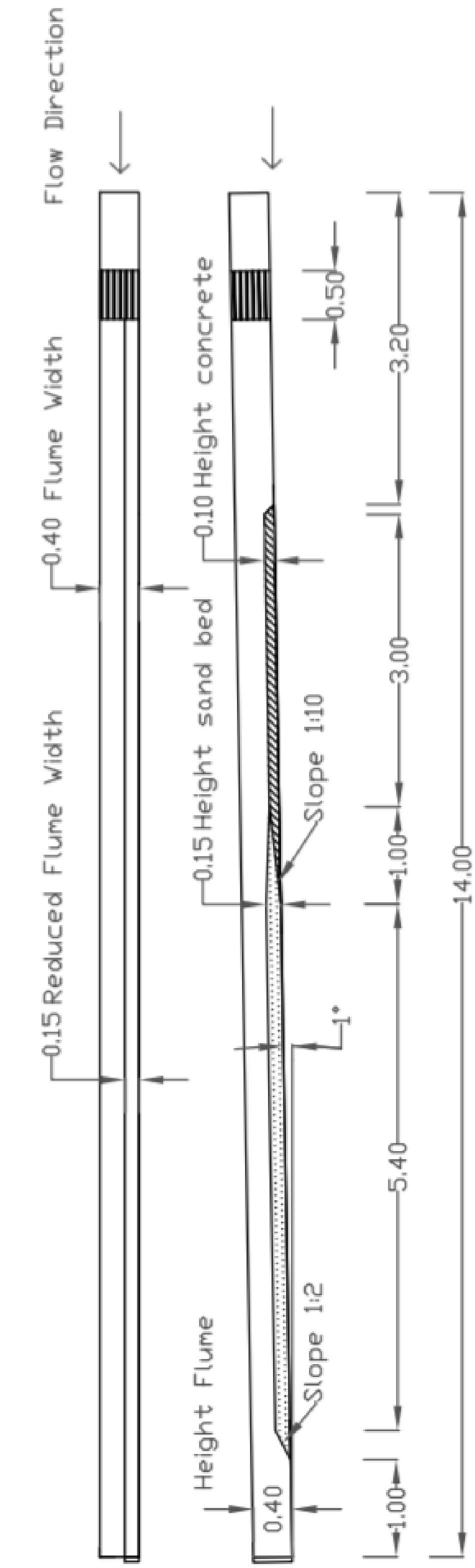

Figure 19: Experimental setup 1 of the erosion test: top view (above) and side view (bottom) with measures in meters.

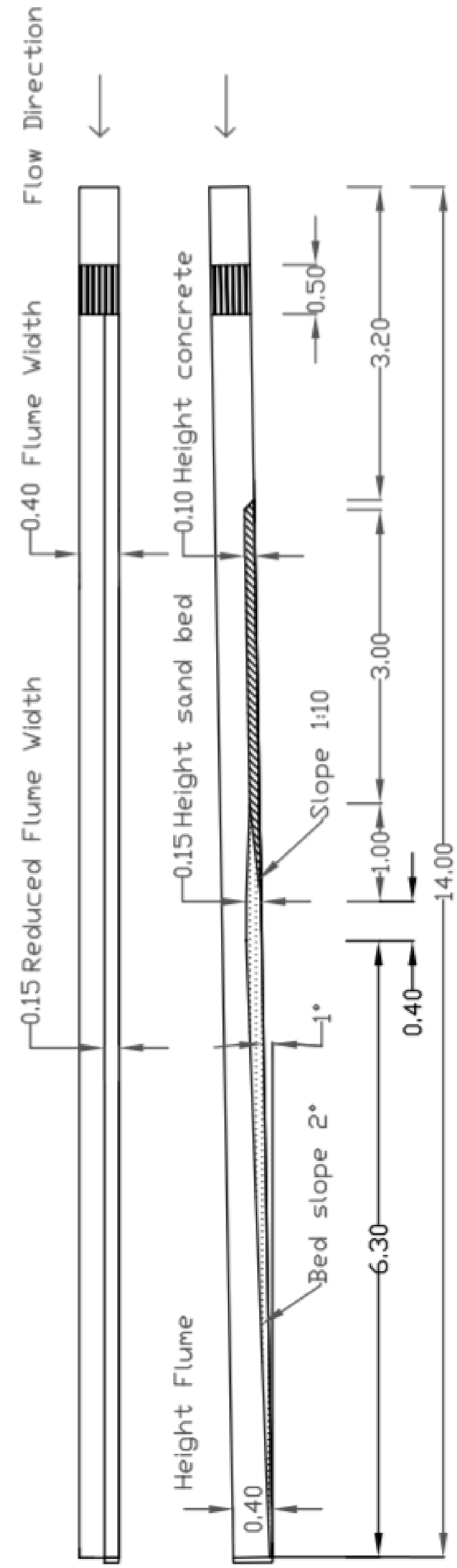

Figure 20: Experimental setup 2 of the erosion test: top view (above) and side view (bottom) with measures in meters.

5.1.2 Measuring equipment

Important variables in a typical sediment experiment are the water discharge, the width of the flume, the average water depth, the mean flow velocity (averaged over the depth, the width and in time), the energy gradient, bed roughness and the sediment characteristics. In these laboratory experiments with a movable sand bed the only known variables were the sediment characteristics, the width of the flume and the energy gradient (in case of reasonable uniform conditions). The other variables were unknown and had to be measured during the experiments. During the erosion tests the flow rate was measured and video recordings were made. In addition, during some experiments, flow velocity profile measurements were performed with a flow velocity meter and water-surface level measurements with an adjustable staff gauge. This section elaborates on the instrumentation used in the erosion experiments.

A flow rate meter (EMS)
The flow rate as discharged by the pump was continuously measured with a so-called Electromagnetic Flow Meter (EMS) and continuously stored in a computer. The proper installation of the flow velocity sensors on the inflow pipe is shown in Fig. 21. Together with a known pipe diameter the device automatically gave its output as a flow rate.

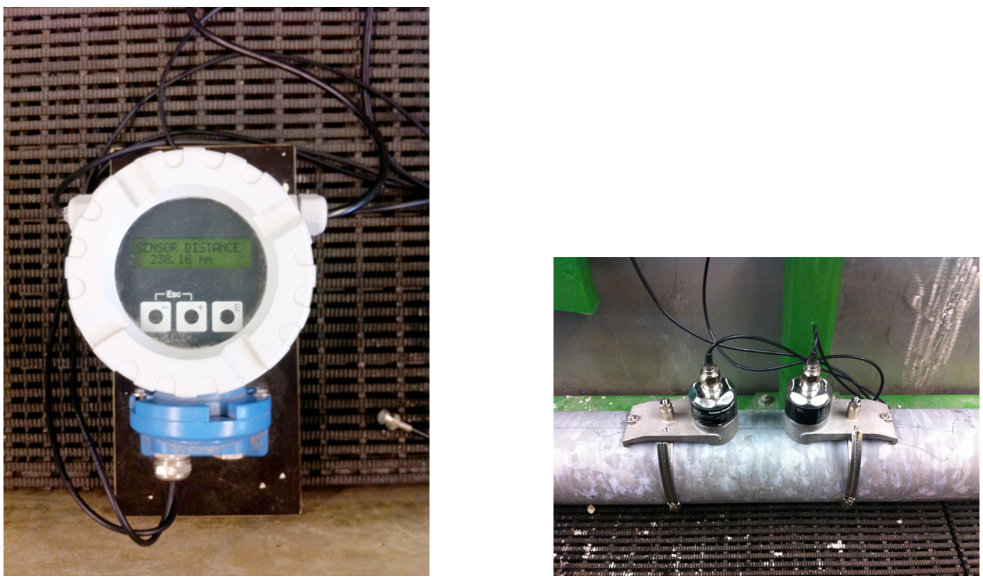

Figure 21: (a) Flowmeter display and (b) Acoustic flow meter attached to the inflow pipe.

A flow velocity meter (EMS)
The flow velocity measurements were also performed with an Electromagnetic Flow Meter (EMS) and only in the area of interest. This device, however, measured the fluid velocity in x- and y-direction at a specific position in the water column. The EMS had to be positioned under water in still water for a few hours prior to the measurements in order to reduce the reading inaccuracy as much as possible. After this time a small but fairly constant offset of $\pm$ 0.01 m/s was noted. The flow velocity measurements were mainly performed to determine the velocity profile in the flume and to verify the position of the mean velocity in the water column. The mean flow velocity equals the discharge divided by the product of the mean depth times the constricted width of the flume and could be determined with the discharge meter and the video recordings.

A staff gauge
The adjustable staff gauge was used to determine the water surface level and the bed level surface in the area of interest during some experiments. The inaccuracy of the staff gauge was in the order of 1 to 2 mm. The vertical positioning of the instrument relative to the bottom was manually controlled.

The camera setup

During the tests video recordings were made. The video camera was positioned in such a way that the water levels and bed levels in the area of interest could later be extracted (see also Fig. 22). To simplify the data analysis a grid was drawn on the glass side window of the flume (see Fig. 22). In vertical direction a total height of 0.40 m was divided in parts of 0.01 m and in horizontal direction an area of 0.90 m was divided into parts of 0.10 m. A second camera was positioned on the next window (more upstream) and functioned as a back-up recording.

Figure 22: (a) Setup of the camera and (b) Grid on the glass wall in the area of interest.

5.2 The permeability tests

In this section the permeability test is explained in more detail. A falling head test is used for measuring the permeability of soils of intermediate and low permeability (Mulder and Verwaal, 2006). In this study falling head tests were executed, because the permeability of the sand was expected to decrease significantly due to the addition of bentonite.

5.2.1 Experimental setup of the permeability tests

The tests were performed with the device as provided in Fig. 23. Fig. 24 gives a conceptual sketch of the test. The device consists out of a sample area, a vertical water column (also called a standpipe) with a standard diameter (see also Table 4) and a connection between the sample area and the water column. This connection can be closed with a valve. The concept is simple: the drop in water level in the standpipe, in time, ($h_0 - h_t$ see Fig. 24) is a measure for the permeability of the sample. The vertical water column provides both a means of measuring the water quantity and the water head to drive the flow. It has to be mentioned that the test procedure follows generally accepted practice, but is not covered by (British) Standards (see also Mulder and Verwaal, 2006).

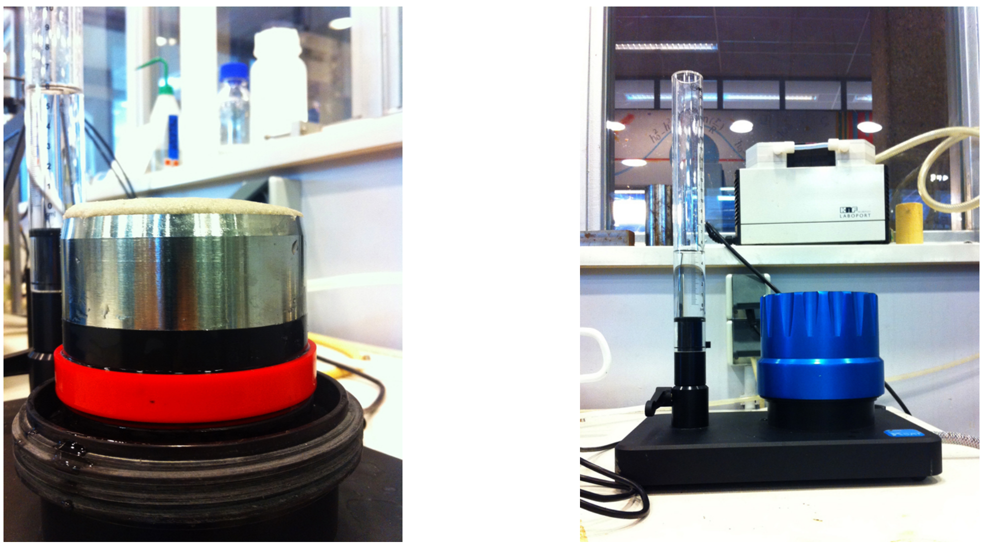

Figure 23: (a) Device falling head test and (b) Sample positioning.

Once the water column is completely filled and the sample area starts to overflow (which is a constant reference level due to the overflow) a flow will be driven in the direction of the sample. The flow is driven by the difference in water level between the water column and the reference level. The water has to flow through the sample over a distance of L (see Fig. 24), which takes time. In the water column the water level is changing in time and since the diameter of the water column is known, also the change in water volume is known. The change in water volume in time is also known as the water flow Q, which can be directly implemented in Darcy's law. Darcy's law also contains the permeability k. Hence the falling head test can be used to determine the permeability k and, after some mathematical manipulation, is calculated with Eq.(18) (see also Fig. 24):

$$k = -\frac{La}{At} \ln \left[\frac{h_t}{h_0} \right] \tag{18}$$

For a complete derivation reference is made to Barends and Uffink (2011).

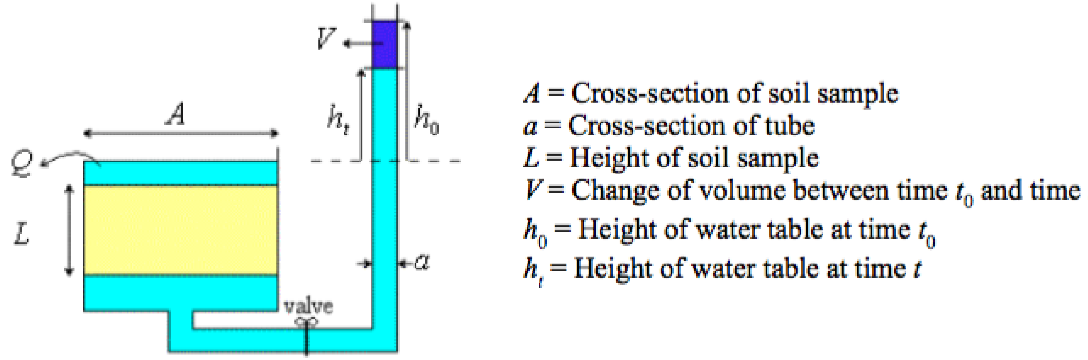

Figure 24: Conceptual sketch of the falling head test, from Barends and Uffink (2011).

Table 4: Characteristics permeability tests

Parameter and dimension	Value
Cross-sectional area of the samples A in [cm^2]	50
Height of the samples L in [cm]	5.0
Volume of the samples in [ml]	250
Weight of the samples in [g]	400 - 420
Porosity in [-]	0.40 - 0.41
Dry bulk density in [kg/m^3]	1446 - 1481
Height of the column in [cm]	20
Cross-sectional area of the water column a in [cm^2]	4.536
Initial head difference/water level h_0 in [cm]	6 - 9

5.2.2 Preparation of the permeability test samples

First, a sample is prepared with a desired density and with pre-defined dimensions (see Table 4). Afterwards the sample needs time to get saturated. This takes about a day. Once the sample is saturated the actual test can be executed. During the entire procedure (the preparation and execution phase) the temperature of the area has to be monitored to incorporate the effect of the temperature on the results at a later time. The permeability coefficients are later normalized to represent the permeability at a temperature of 25 °C . For a full description of the procedures reference is made to Mulder and Verwaal (2006).

5.2.3 Run plan permeability tests

The permeability tests were executed according the run plan as given in Table 5.

Table 5: Run plan permeability test

Run #	**Percentage bentonite [%]**	**D_{50} in [mm]**
1	0	0.256
2	2	0.256
3	4	0.256
4	6	0.256
5	8	0.256
6	10	0.256
7	0	0.150
8	2	0.150
9	4	0.150
10	6	0.150
11	8	0.150
12	10	0.150

5.3 The direct shear tests

In this section the direct shear test is explained in more detail. The test is executed in order to determine the shear strength, the friction angle and the (apparent) cohesion. The tests can be executed under drained, undrained and consolidated-undrained conditions.

5.3.1 Experimental setup of the direct shear tests

The tests were performed with the setup as provided in Fig. 25 and Fig. 26. The soil samples are confined inside an upper- and a lower rigid ring (see Fig. 27). In this case the top and bottom of the sample are provided with drainage plates. These allow the sample to become saturated and to drain the water during the test to prevent water pressures. The confined sample is submerged underwater and is subjected to a normal load during the test. The normal loads are pre-defined by the user. Each mixture is subjected to three different pre-defined normal stresses during the shearing process (see also Table 6). The normal forces are often converted into normal stresses. This is simply the normal load divided by the surface at which the force works (Surface CD in Fig. 27).

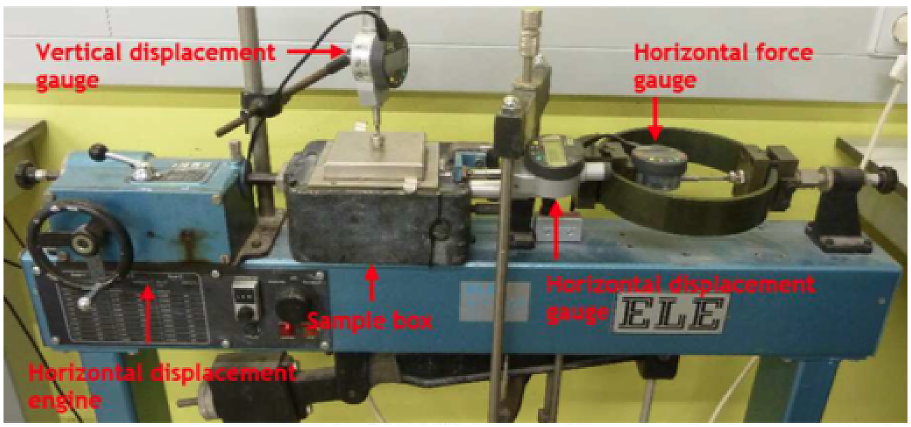

Figure 25: Device direct shear test, from Lemmens (2014).

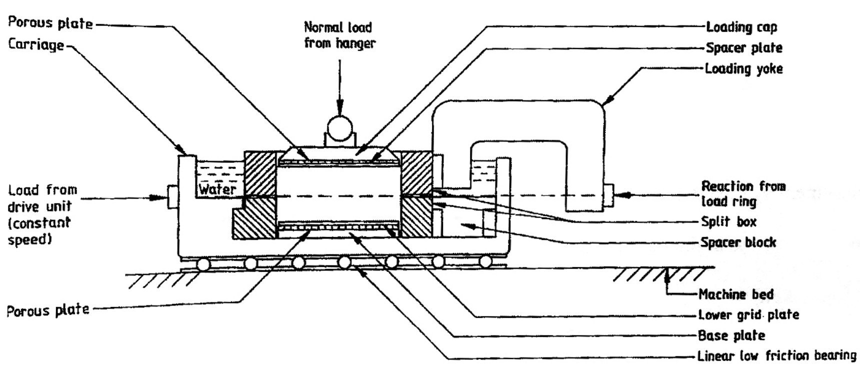

Figure 26: Setup direct shear test, from Mulder and Verwaal (2006).

The shear force is applied by a motorized drive, which adds a horizontal displacement at a pre-defined speed. Only the bottom ring is displaced by the motorized drive, while the top ring is kept at its place. The horizontal and vertical displacements, together with the horizontal shear force are measured and registered.

The soil shear strength is defined by the Mohr-Coulomb theory as:

$$\tau = C + \sigma \tan(\phi) \tag{19}$$

where τ is the shear stress (the shear force/area of surface CD in Fig. 27), σ the normal stress (normal load/area of surface CD) and C the (apparent) cohesion.

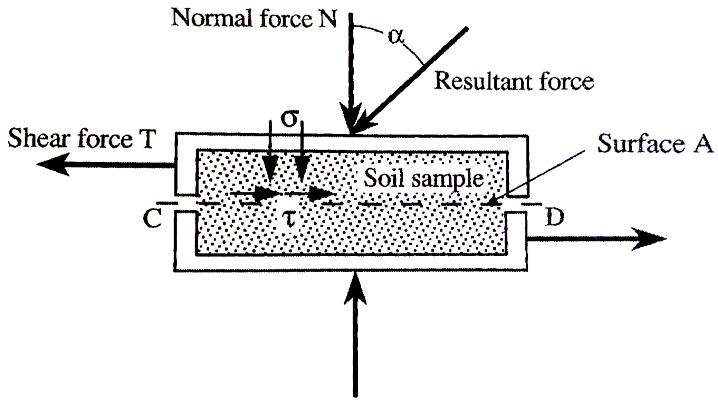

Figure 27: Upper and lower rigid ring containing the sample, from Mulder and Verwaal (2006).

Preparation of the direct shear test samples
The samples are prepared according the CEN ISO/TS 17892-10:2004 Standard (CEN, 2004). In addition, the guidelines of Mulder and Verwaal (2006) are extensively used. First the sample is prepared with the desired density (compacted by vibration) and dimensions as stated in Table 6. Afterwards the sample needs time to get saturated. The sand mixture will be saturated very quickly, but the sand-bentonite mixtures will need about a day to become saturated. Next, the samples need time to consolidate under the pre-defined normal stress. Once the primary consolidation is complete, the minimum time to failure and the rate of shear displacement can be determined. The rate of shear is determined according to the CEN ISO/TS 17892-10:2004 Standard (CEN, 2004). The rate of shear for a cohesive soil has to be very slow in order to allow the excess pore pressure to dissipate. In this way it is guaranteed that the effective stress is equal to the total stress.

For a full description of the procedures reference is made to Mulder and Verwaal (2006).

Table 6: Characteristics direct shear tests

Parameter and dimension	Value
Width of the samples in [mm]	100
Height of the samples in [mm]	31
Area of the samples in [mm^2]	10000
Weight of the samples in [kg]	0.49 - 0.54
Shear rate in [mm/min]	0.035 - 0.1
Porosity in [-]	0.40 -0.42
Dry bulk density in [kg/m^3]	1536 - 1582
Normal weight 1 in [kg]	5.9813
Normal weight 2 in [kg]	15.9813
Normal weight 3 in [kg]	25.9813

5.3.2 Run plan direct shear tests

The direct shear tests were executed according the run plan as given in Table 6.

Table 7: Run plan direct shear test

Run #	Percentage bentonite [%]	D_{50} in [mm]
1	0	0.256
2	2	0.256
3	4	0.256
4	6	0.256
5	8	0.256
6	10	0.256
7	0	0.150
8	2	0.150
9	4	0.150
10	6	0.150
11	8	0.150
12	10	0.150

5.4 Sediment properties

Two different types of sand were used in the tests. In addition, each test was performed with a different amount of bentonite additive. In this section the characteristics of the sand, the bentonite and the applied mixture ratios of the sand-bentonite mixtures are presented. In addition the most important characteristics of the bentonite are briefly discussed and are further summarized in appendix B.

5.4.1 The sand

Two different types of pure quartz sand were used in the tests (see the run plan in Table 3). An overview of the fraction sizes of both sand is given in Table 8 and the gradation curves are given in Fig. 28 and Fig. 29.

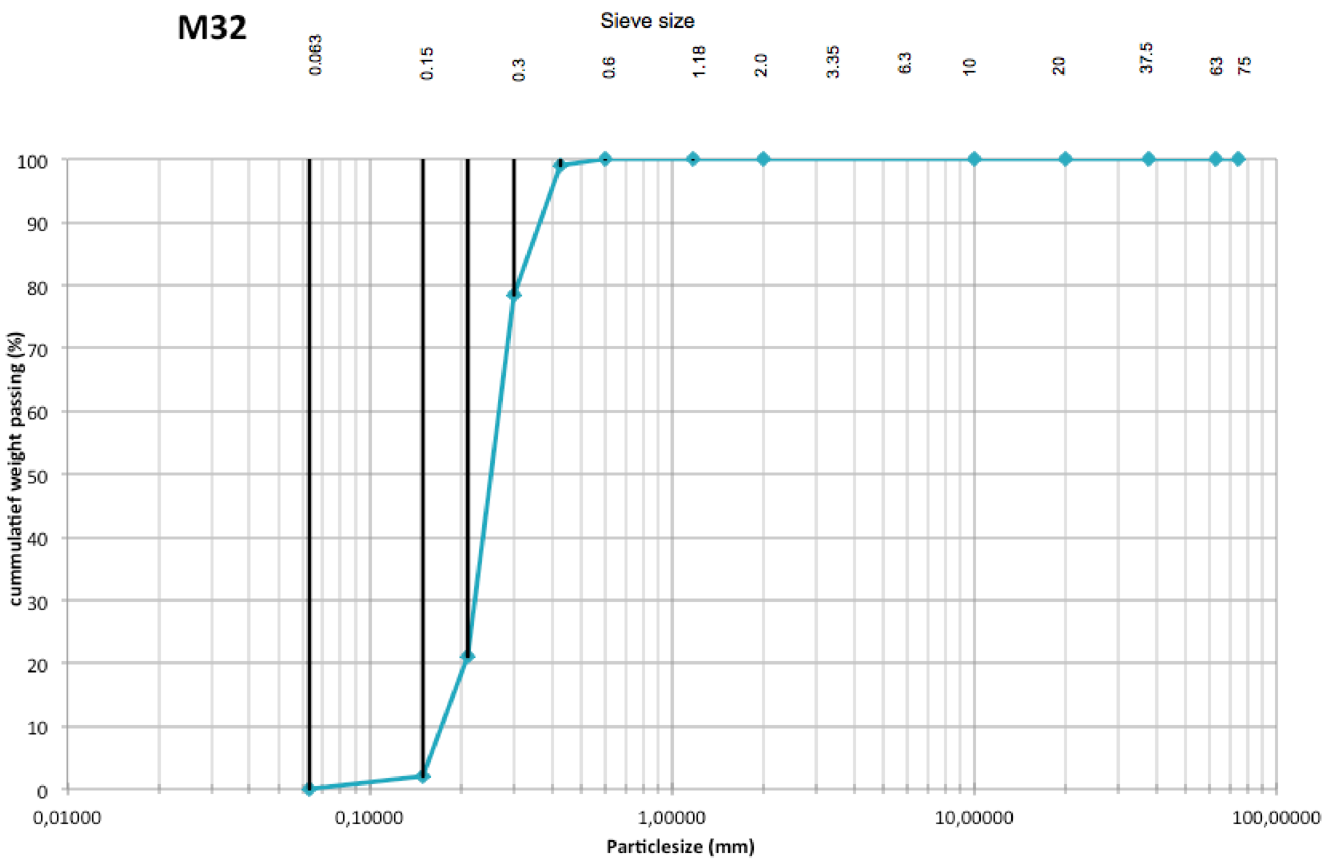

Figure 28: Gradation curve sand with a D_{50} of 0.256 mm

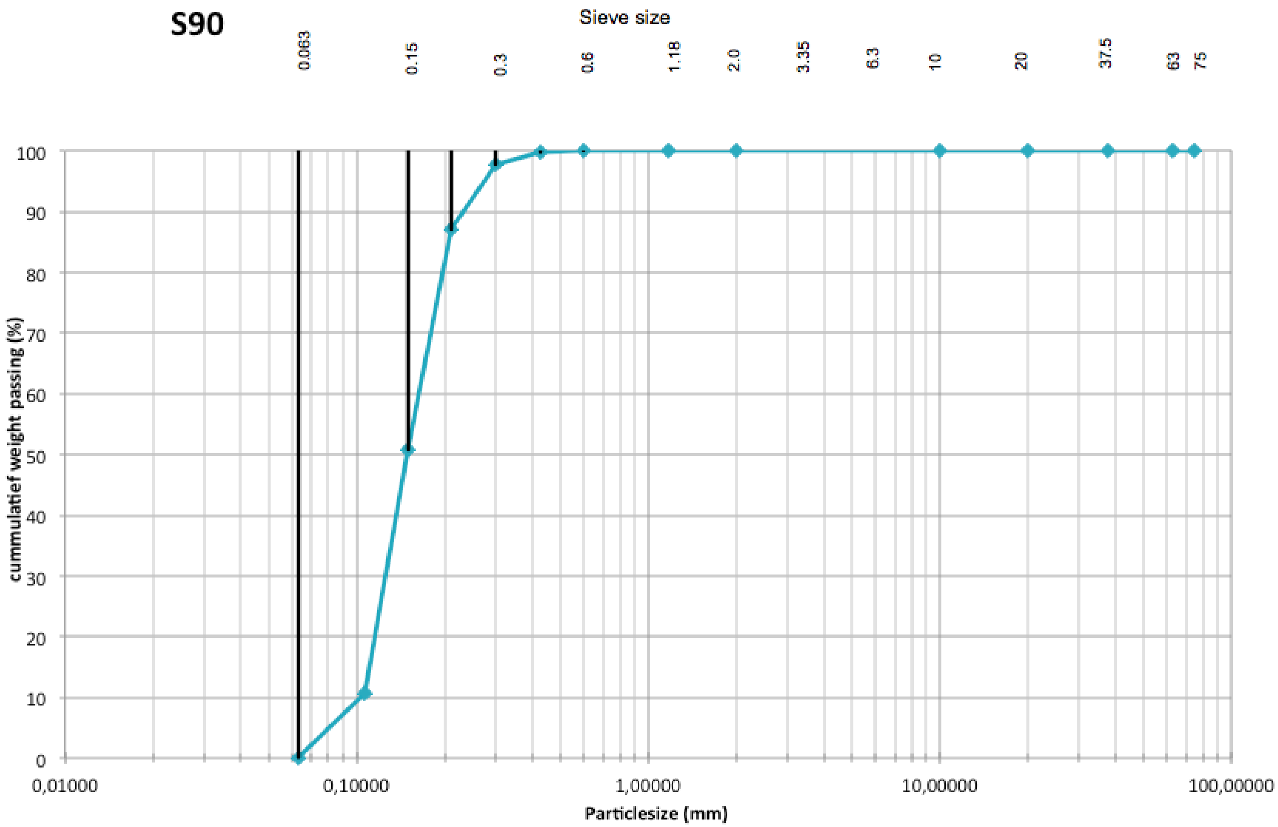

Figure 29: Gradation curve sand with a D_{50} of 0.150 mm

Table 8: Properties of the sand used in the tests

Sandtype	D_{10} [mm]	D_{15} [mm]	D_{30} [mm]	D_{50} [mm]	D_{60} [mm]	D_{85} [mm]	D_{90} [mm]
Courser M32	0.176	0.192	0.226	0.256	0.272	0.340	0.370
Finer S50	0.103	0.111	0.127	0.149	0.166	0.208	0.236

With the data from Table 8 the coefficient of uniformity C_u and the coefficient of curvature C_c are calculated. These coefficients are crude shape parameters and are used to characterize the sand. The coefficients are defined as:

$$C_u = \frac{D_{60}}{D_{10}} \tag{20}$$

$$C_c = \frac{{D_{30}}^2}{D_{10}D_{60}} \tag{21}$$

The coefficient of uniformity C_u and the coefficient of curvature C_c for the M32 sand-type are 1.55 and 1.07, respectively. For the S90 sand-type the values are 1.61 and 0.94, respectively. Sand is classified as well graded if the following criteria is met: $C_u \geq 6$ & $1 < C_c < 3$ (Holtz and Kovacs, 1981). Since both criteria are not met, both sands are classified as poorly graded.

Determination of the relative density

Most granular soils have a widely varying density state in which the soil may occur in situ. In Fig. 30 the soil is modelled as perfectly spherical grains with an equal diameter. The soil state with the largest possible spaces in between the particles is defined as the minimum bulk density ρ_{min}. The opposite of the minimum bulk density is the maximum bulk density ρ_{max}. In this state the particles will be as close together as possible without pulverizing the soil material or fracturing the particles in smaller pieces. This state is reached by compacting the soil by vibration and/or weight of material above.

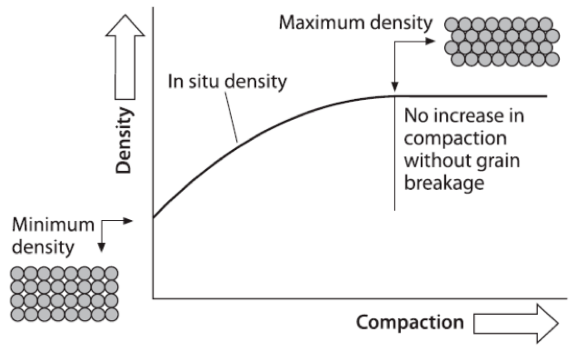

Figure 30: In situ density related to the minimum and maximum densities, from Price (2009).

Generally, the in situ density ρ_{insitu} is somewhere in between those minimum and maximum limits (see Fig. 30). The relative position of the in situ density in between those limits is defined as the relative density. The relative density (abbreviated as RD) thus characterizes the state of compaction which the soil has reached and is defined as:

$$RD = \frac{\rho_{max}}{\rho_{insitu}} \left[\frac{\rho_{insitu} - \rho_{min}}{\rho_{max} - \rho_{min}} \right] 100\% \tag{22}$$

The minimum and maximum limits of both the S90 (D_{50}=0.150 mm) and M32 (D_{50}=0.256 mm) sand-types were determined according Japanese standards of the Japanese Geotechnical Society (JGS, 1996). The Japanese Geotechnical Society-method or JGS-method determines the limit densities by using a mold with an inner diameter of 6 cm and a height of 4 cm. This results in a volume of 113.1 cm^3. A detailed English procedure of the Japanese procedure is given by Anakari (2008). In short the procedure to determine the minimum density is to gently pour sand in the mold (without color) through a funnel. Once the mold is full and the top is smoothed off straight, the mold with sand is weighed. The maximum density procedure is slightly more complicated. The mold is filled to $1/5^{th}$ of the height using a funnel. Next, the soil is compacted by tapping the mold 100 times. This procedure is repeated for each layer ($1/5^{th}$ of the total height of the mold) until the mold is completely filled. After the mold is completely filled, the color is removed and the top is smoothed off. The mold with sand is again weighed. Since the weight, the volume of the mold and the mass of the soil in the mold are now known, the density of the soil in both states can be calculated.

The following values of the minimum and maximum limits were determined: a ρ_{min} of 1471 kg/m^3 and a ρ_{max} of 1694 kg/m^3 for the M32 sand-type. Together with a ρ_{min} of 1328 kg/m^3 and a ρ_{max} of 1608 kg/m^3 for the S90 sand type.

5.4.2 The bentonite

The Sealfix Benonite has a green-greyish color (see Fig. 31), it mainly consists of montmorillonite and it is known for its high plastic behaviour. In addition, bentonite is famous for its high swell capacity. The swelling leads to an increase in bentonite volume and, when mixed with sand, fills the pores between the sand grains. In order to obtain the maximum swelling potential, the bentonite needs at least 24 hours to saturate and has a dry bulk density of about 900 kg/m^3.

Figure 31: The green-greyish fine bentonite particles.

5.4.3 Preparation of the mixtures

To get a fairly homogenous sand-bentonite mixture a mixer and a concrete mixer were used to dryly mix the sand and bentonite. The Cebogel Sealfix Bentonite (see Appendix B) was added, given a pre-determined mixture ratio, to 50 kg of sand. Since each erosion test run roughly needed 200 kg, several batches had to prepared for each run. Mixtures were prepared with a volume bentonite content of 0, 2, 4, 6, 8 and 10%. For the permeability tests and direct shear tests the same procedure was applied. The only difference is the amount of materials used. Table 9 and Table 10 summarize the volume percentage, dry weight percentage and mixture ratio of the different runs. These tables are based on a dry bulk density of about 900 kg/m^3 for bentonite and dry bulk densities of 1400 kg/m^3 and 1500 kg/m^3 for the M32 (D_{50}=0.256 mm) and S90 (D_{50}=0.150 mm) sand types respectively. The difference in mixture ratio is caused by the slight difference in dry bulk densities of the sands.

Table 9: Mixture perparation of the M32 sand

Dry volume percentage bentonite %	Dry weight percentage bentonite %	Mixture ratio [g/kg]
2	1.2	12
4	2.4	24
6	3.6	36
8	4.8	48
10	6.0	60

Table 10: Mixture perparation of the S90 sand

Dry volume percentage bentonite %	Dry weight percentage bentonite %	Mixture ratio [g/kg]
2	1.286	12.86
4	2.571	25.71
6	3.857	38.57
8	5.143	51.43
10	6.429	64.29

5.4.4 Classification of the mixtures

Classification of fine grained soils is often based on its consistency limits (often called Atterberg limits).The consistency of a soil is its physical state at a given moisture content. Four different consistency states can be distinguished: solid, plastic, semi-plastic solid and liquid (Mulder and Verwaal, 2006). The most important are the liquid and the plastic limits. They represent the upper and lower bounds of the plastic state. The PI-index summarizes the range of the plastic state by subtracting the plastic limit from the liquid limit and is often a very important parameter used to classify fine grained soils.

Four samples were taken of the bed in the erosion tests. One sample contained the M32 sandtype with 4% bentonite additive, the second the S90 sandtype with a 4% bentonite additive. The third and fourth samples contained M32 sand with 6% additive and S90 with a 6% additive respectively. The plastic limit experiments were performed according the British Standards (BS 1377: Part 2 1990). A description of the experimental procedures is given by Mulder and Verwaal (2006). However, the plastic limit could not be determined for any of the samples. Rolling of the soil was hardly possible and crumbling occurred before the necessary 3 mm soil thread was reached. The best attempt is shown in Fig. 32. Since the plastic limit could not be determined, the samples are reported as non plastic.

Figure 32: Best attempt to determine the plastic limit of a 6% mixure.

6 | The experimental results

In this chapter the results of the physical model tests are presented. First, an overview of the erosion test results is given. This includes the effectiveness of the sand-bentonite mixtures in reducing the erosion velocity. The effectiveness is determined with two different methods. Next, the results of the permeability and direct shear tests are briefly presented. Generally it is described how the results were obtained and what the results represent. Appendices A, C and D are referenced regularly.

6.1 Results erosion test

In this section the results of the erosion tests are discussed. Thirteen different tests runs were executed. During these tests, the volume percentage of bentonite additive, the diameter of the sand and the mean flow velocity were varied (see also Table 3). First, the visual observations from the video recordings are presented and explained. The effectiveness of the sand-bentonite mixtures in reducing the erosion velocity is also presented. Next, the corrected bed shear stresses are calculated with several methods and one method is chosen as the most representative method. The effectiveness of the sand-bentonite mixtures in reducing the erosion velocity is also tested for this method. The data set is also compared with data sets from Gailani (2001) and Lemmens (2014). This chapter concludes with a comparison of the effectiveness of bentonite mixtures on the permeability and the erosion velocity.

Visual results from the video recordings
During the test runs the discharge was constantly measured and the bed levels and water levels in the area of interest were videotaped. From the recorded videos the water levels and bed levels were extracted with a Matlab script. The Matlab script was using the Videoreader function to extract frames from the videos at a preset interval. The time between each of the consecutive frames was between 10 and 60 s. For each frame the Matlab script required the user to input coordinates for the water levels and bed levels in order to give a time series of the water level and bed level as output. Next, the script automatically converted the amount of pixels to a height using a pixel : distance ratio by specifying a known distance. The results of these surface water level and bed level positions in time are given in Appendix D. In the final step the mean flow velocity U and erosion velocity v_e between each of the consecutive frames in time were calculated with Eq.(23) and Eq.(24).

$$U = \frac{Q \cdot 10^{-3}}{b \cdot (h - h_b)} \tag{23}$$

$$v_e = \frac{h_{b(n)} - h_{b(n+1)}}{t_{n+1} - t_n} = \frac{\Delta h_b}{\Delta t} \tag{24}$$

in which b the constricted width of the flume, h_w the water surface level, $h_{b(n)}$ the bed level at a specific time, t_n the specific time of the measurement, Δh_b the difference in bed level and Δt the time interval between two measurements.

For each test run data from 5 measurement locations were analyzed. The measurement locations were all in the area of interest and evenly spaced at a 10 cm interval from each other. The most upstream measurement location was at the 0 line of the grid (see Fig. 22). The results of all the test runs are graphically presented in Fig. 33 and more details are given in Table 11. Fig. 33 relates the erosion velocity v_e to the mean flow velocity squared U^2 and displays the results for different mixture ratios and sand-types. Linear regression lines through the measurements have also been included. It is important to note that the regression lines go through the origin, which is a simplification. In reality the erosion velocity v_e is zero if the critical velocity that initiates motion of the sand particles U_{cr} is not yet exceeded. However, since the critical velocity that initiates motion is very low (about 0.10 m/s) and erosion behaviour at flow velocities > 1 m/s is of main concern in this study, this critical velocity is simplified to be zero. This simplification leads to generic quadratic equations for the erosion velocity in the form of $v_e = aU^2$ and are not verified at flow velocities below 1 m/s.

The main objective of the experiments was to determine the erosion behaviour of sand or sand-bentonite mixtures given a mean flow velocity of 1 and 2 m/s. With the bed level inclination of 1% and 3% these conditions were reasonably established. However, slight differences in mean flow velocity occurred. Mainly as a result of a small varying discharge delivered by the pump, which was very difficult to control better. At first notice, the only peculiar results are those of a 6% mixture at a intended mean flow velocity of about 2 m/s. For some unexplainable reason the mean flow velocity was only about 1.7 m/s ($U^2 \approx 3.0$ m/s). Nevertheless, the results for the 6% mixtures are very interesting. It appears that the erosion velocity at a mean flow velocity of about 1.7 m/s is of the same order as, or even lower than, the erosion velocity at a mean flow velocity of about 1 m/s. Although, this is most likely the result of a more homogeneous mixture, it was still unexpected (see also Chapter 7). It is definitely worthwhile pursuing further research with 6% mixtures at 2 m/s or higher in order to verify if the erosion velocity is indeed no longer increasing with an increase in mean flow velocity.

The reproducibility of the tests is confirmed to be reasonably well. Test runs 7 and 13 both contained sand with a D_{50} of 0.256 mm and were executed at a mean flow velocity U of about 2 m/s. The erosion velocity, obtained from the video recordings, was almost identical. The reproducibility will be discussed in more detail below.

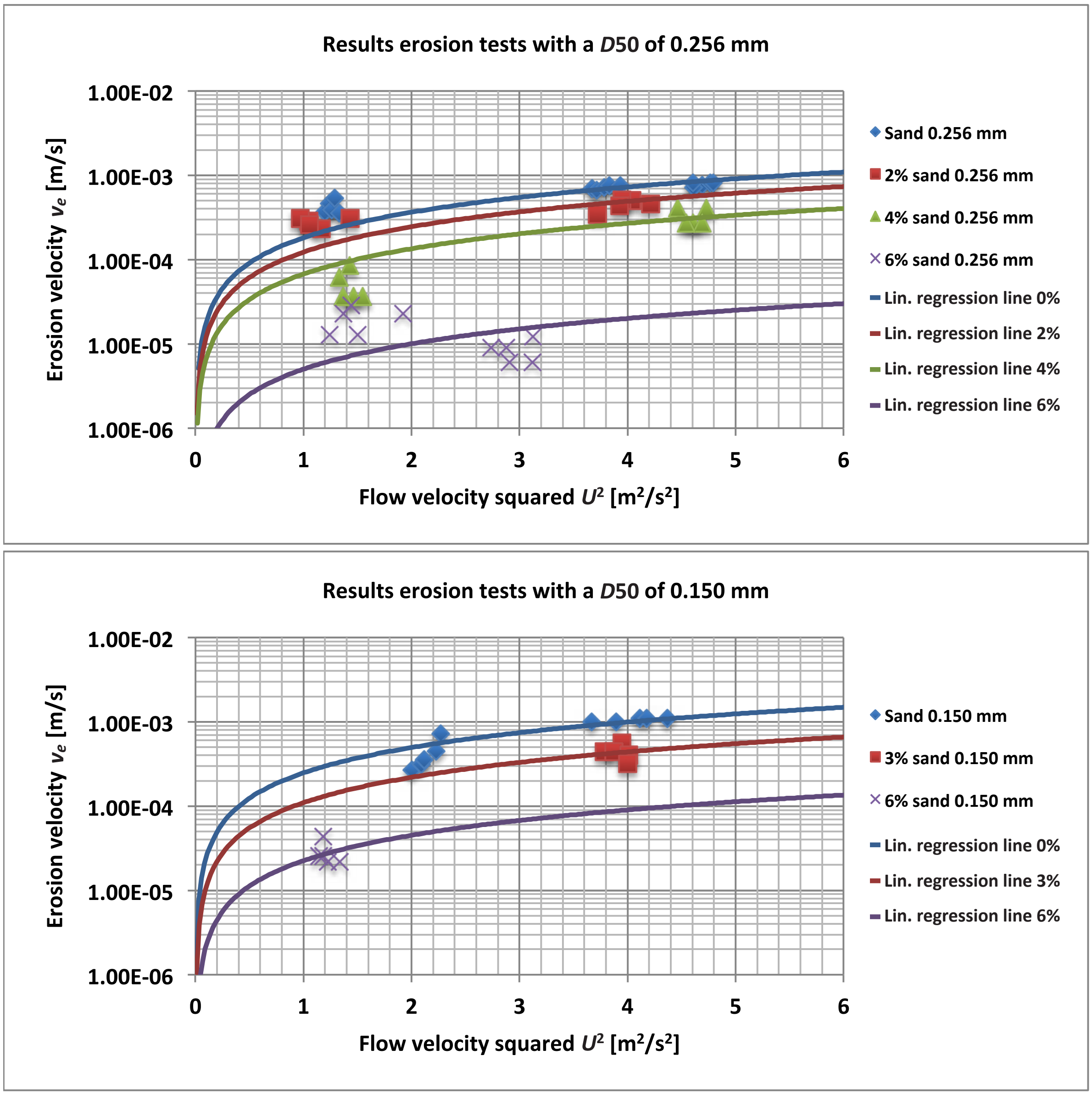

Figure 33: Erosion velocity versus mean flow velocity squared for (a) sand with a D_{50} of 0.256 mm and (b) sand with a D_{50} of 0.150 mm.

In order to objectively calculate the effectiveness of a bentonite additive, the erosion velocity of the bed of a mixture is compared with the erosion velocity of the sand mixture at the same mean flow velocity. The effectiveness of the different bentonite mixtures is given by the ratio of the mixture's erosion velocity and the erosion velocity of the sand (see Eq.(25)) and is based on the average erosion velocity for each test:

$$f = \frac{v_{e,mixture}}{v_{e,sand}} \tag{25}$$

The averages of the results presented in Fig. 33 are given in Fig. F3 in Appendix F. The ratio f for each mixture is calculated from the coefficients of the linear regression lines in relation to the coefficient of the linear regression line of sand. Or in mathematical terms $v_e = faU^2$, with a the coefficient of the sand regression line. The effectiveness of the different bentonite contents are given in Table 12. In this table mixtures with the same D_{50} are clustered together and compared, and the clusters are separated with a horizontal line between the results. The effectiveness of the different bentonite contents are also graphically displayed in Fig. 34. An exponential relationship between the reduction f and the amount of bentonite additive $B_{\%}$ is also presented in Fig. 34. Significant reductions in erosion velocity are obtained by adding bentonite to a sand mixture. A 2% mixture already reduces the erosion velocity by about 50%, a 3% or 4% mixture by 50 to 65 % and a 6% mixture by at least 90%. Furthermore, it appears that the effectiveness of adding bentonite to the finer and courser sand, both with a porosity of about 0.40 - 0.41, is about the same.

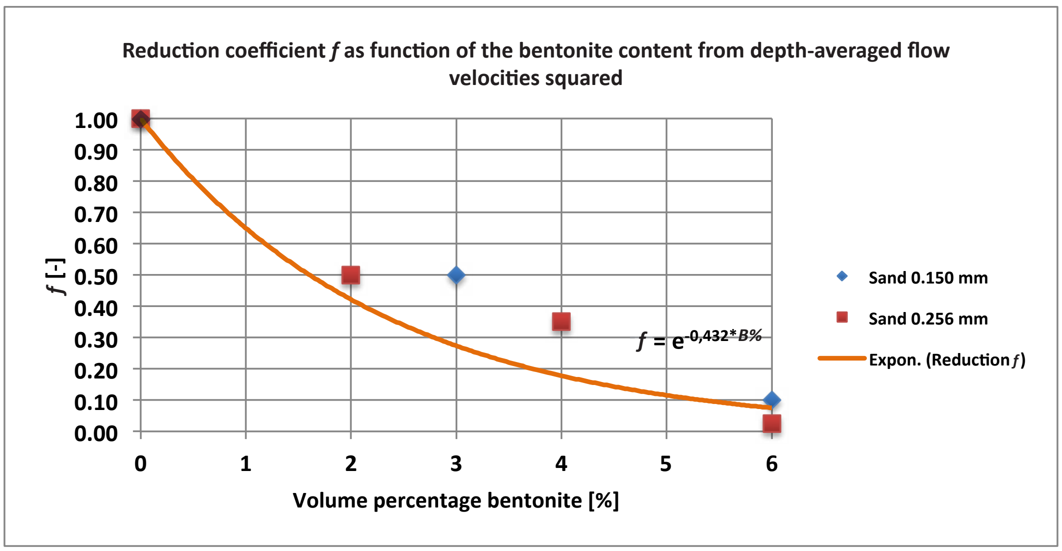

Figure 34: Reduction coefficient f as function of the bentonite content from mean flow velocities squared.

Table 11: Measured erosion velocities for several mixtures, mean flow velocities and sand-types.

Run #	Bentonite [%]	D_{50} [mm]	U [m/s]	v_e [m/s]	n_0 [-]	$\rho_{dry,mixture}$ [kg/m^3]
1	0	0.256	1.12	4.21E-04	0.40	1581
2	2	0.256	1.06	2.79E-04	0.41	1575
3	4	0.256	1.19	5.15E-05	0.41	1575
4	6	0.256	1.22	1.99E-05	0.41	1564
7	0	0.256	2.17	7.82E-04	0.40	1582
9	2	0.256	2.00	4.48E-04	0.41	1572
10	4	0.256	2.15	3.25E-04	0.41	1568
11	6	0.256	1.72	8.50E-06	0.41	1575
6	0	0.150	1.46	4.20E-04	0.41	1570
5	6	0.150	1.10	2.76E-05	0.41	1560
8	0	0.150	2.01	1.06E-03	0.40	1579
12	3	0.150	1.98	4.32E-04	0.41	1572
13	0	0.256	1.95	7.16E-04	0.41	1571

Table 12: Reduction coefficient f for several mixtures and sand types based on linear regression.

Bentonite [%]	D_{50} [mm]	coefficient a [-]	f [-]
0	0.256	2.00E-04	1.00
2	0.256	1.00E-04	0.50
4	0.256	7.00E-05	0.35
6	0.256	5.00E-06	0.03
0	0.150	2.00E-04	1.00
3	0.150	1.00E-04	0.50
6	0.150	2.00E-05	0.10

Determination of the bed shear stress

Sediment transport directly depends on the bed shear stress (see also Section 2.1 and Section 2.2). In this study the bed shear stresses are used to compare the erosion theories with the test results, registered by the video camera. In order to predict the transport rate in laboratory open-channel flows with good precision, it is often necessary to remove side-wall and non-uniformity effects for computing effective bed shear stresses (see Cheng and Chua, 2005 and Guo, 2014). This is needed, because the evaluation of the bed shear stress often uses bulk flow parameters, such as: flow depth, depth-averaged flow velocity and energy slope (Cheng and Chua, 2005). Hence, correcting shear stresses for these sidewall effects is considered an essential procedure. In this study four methods are used for this purpose: the Flow-depth method, the Hydraulic radius method, the Vanoni & Brooks method (Vanoni and Brooks, 1957) and the Einstein method (Einstein, 1941). The non-uniformity correction was neglected for these tests, since reasonable uniform conditions had developed in the area of interest (see also Appendix E).

1. **The flow-depth method**
   The flow-depth method states that the bed shear stress τ_b causes the following energy loss in the water column per unit area above the bed (see also Guo, 2014):

   $$\tau_b = \rho g h S \tag{26}$$

   in which h is the measured water depth with the bottom of the flume as reference level and S the energy slope gradient. For narrow flumes with a water depth h and the width of the flume b, the total energy loss above the bed affected by the bottom and side walls becomes:

   $$b\tau_b + 2h\tau_w = \rho g b h S \tag{27}$$

   in which τ_w is the wall shear stress. This results in the following upper bound expression for the corrected bottom shear stress:

   $$\tau_b = \rho g h S - \frac{2h}{b}\tau_w \leq \rho g h S \tag{28}$$

   In this study τ_w was estimated using the following expresion:

   $$\tau_w = c_f \rho U^2 \tag{29}$$

   The c_f value was estimated at roughly 0.0024 (depending on the hydraulic radius R of the test run), which corresponds with a wall-related Manning roughness coefficient n_w of 0.009 for glass walls (Daugherty et al., 1989).

2. **The hydraulic radius method**
   The hydraulic radius method states that the bed shear stress τ_b causes the following energy loss in the water column per unit area above the bed (see also Guo, 2014):

   $$\tau_b = \rho g R S \tag{30}$$

in which the hydraulic radius R is calculated according to:

$$R = \frac{hb}{2h + b} \tag{31}$$

For narrow flumes with a water depth h and the width of the flume b, the total energy loss above the bed as a result of the bottom and side walls becomes:

$$b\tau_b + 2h\tau_w = (b + 2h)\tau_0 \tag{32}$$

If a rough bed and relatively smooth sidewalls are assumed a lower bound of τ_b is found by replacing τ_w by τ_b in Eq.(32):

$$\tau_b > \rho g R S \tag{33}$$

3. **The Vanoni and Brooks approach**
The approach as described by Vanoni and Brooks (1957) is typically used in research, even though the bed shear stress is generally overestimated by this approach (Cheng and Chua, 2005). This approach uses the Darcy-Weisbach friction factor f_D, which has a sound theoretical basis. With this friction factor the bed shear stress can be expressed as:

$$\tau_b = \frac{b}{b + 2h}\frac{f_b}{f_D}\rho g h S \tag{34}$$

where the friction factors are defined as:

$$f_D = \frac{8gRS}{U^2} \tag{35}$$

$$f_b = f_D + \frac{2h(f_D - f_w)}{b} \tag{36}$$

$$f_w = \left[20\left(\frac{4UR}{f_D\nu}\right)^{0.1} - 39\right]^{-1} \tag{37}$$

in which f_b the bed friction factor and f_w the wall friction factor. The wall friction factor relation, given by Eq.(37), is obtained by curve fitting and depends on ratio Re/f_D the Reynolds number over the Darcy Weisbach friction factor (see also Cheng and Chua, 2005).

4. **The Einstein approach**
The approach as described by Einstein (1941) is also often used. This approach generally underestimates the bed shear stress (Cheng and Chua, 2005). In this method, Einstein originally accounts for the wall resistance component by correcting the Manning roughness coefficient. Einstein defined the average bed shear stress as:

$$\tau_b = \rho g R S \left(\frac{n_b}{n}\right)^{1.5} \tag{38}$$

where n_b and n are the bed-related and total Manning roughness coefficients, respectively.

An alternative form is using the Darcy-Weisbach friction factor to account for the effects of the wall friction. It is assumed that the wall-related friction can be estimated using the following Blasius experession (see Cheng and Chua, 2005):

$$f_w = \frac{0.316}{\left(\frac{4UR_w}{\nu}\right)^{0.25}} \tag{39}$$

in which R_w is the wall-related hydraulic radius. After an extensive substitution and manipulation procedure as explained by Cheng and Chua (2005) this finally yields the following corrected bed shear stress:

$$\tau_b = \rho g h S \left(1 - \frac{0.114}{b} \left(\frac{U^7 \nu}{S^4 g^4} \right)^{0.2} \right) \tag{40}$$

With this method, the sidewall correction of the bed shear stress is determined by measuring the water depth, energy slope and the depth-averaged flow velocity.

The corrected bed shear stresses τ_b are given in Table 13. The four methods (Flow-depth, Hydraulic radius, Vanoni & Brooks and Einstein) are abbreviated as τ_{bR}, τ_{bh}, τ_{bv} and τ_{be}, respectively. The corresponding Shields parameters are also calculated with Eq.(41).

$$\theta = \frac{\tau_b}{\rho g \Delta D_{50}} \tag{41}$$

From Table 13 it can be concluded that the values of the corrected bed shear stresses τ_b obtained with four different methods show close resemblance. This is also graphically represented in Fig. 35. Especially the bed shear stresses at mean flow velocities close to 1 m/s for the courser sand are clustered. For mean flow velocities of about 2 m/s and the courser sand this resemblance is less strong. For the finer sand, this is exactly the opposite. Linear regression lines are determined as a sample estimate of the true, unknown relationships for each method. The regression lines through the data points of Vanoni & Brooks and of the hydraulic radius method best explain the variance in data and are thus preferred. In this case the Vanoni & Brooks is chosen, because the Vanoni & Brooks method is the most widely used method according to literature (Cheng and Chua, 2005). Therefore, the corrected bed shear stresses using the Vanoni & Brooks method will be used in the forthcoming chapters.

The values of the corrected bed shear stress are of the same order of magnitude as in the experiments executed by Auel et al. (2014) and analysed by Guo (2014). The experimental setup used by Auel et al. (2014) is reasonably comparable with the setup used in this study and gives some extra confidence to these values.

Table 13: Predictions of corrected bed shear stresses and Shields parameters using various methods.

Test	τ_{bR} [Pa]	τ_{bh} [Pa]	τ_{bv} [Pa]	τ_{be} [Pa]	θ_{bR} [-]	θ_{bh} [-]	θ_{bv} [-]	θ_{be} [-]
1	3.37	3.63	3.96	4.01	0.81	0.88	0.96	0.97
2	3.50	4.27	4.48	4.52	0.85	1.03	1.08	1.09
3	3.50	3.56	4.00	4.08	0.84	0.86	0.97	0.99
4	3.54	3.52	4.01	4.10	0.85	0.85	0.97	0.99
5	3.77	4.79	5.04	5.09	1.55	1.97	2.07	2.10
6	3.42	1.76	2.83	3.02	1.41	0.73	1.17	1.24
7	9.31	7.38	9.72	10.08	2.25	1.78	2.35	2.43
8	10.43	11.06	12.92	13.25	4.30	4.56	5.32	5.46
9	10.21	10.70	12.49	12.80	2.46	2.58	3.01	3.09
10	9.44	7.79	10.07	10.42	2.28	1.88	2.43	2.52
11	10.05	12.56	13.08	13.65	2.42	3.03	3.16	3.29
12	9.79	9.88	11.60	11.88	4.03	4.07	4.78	4.89
13	10.41	11.60	13.23	13.51	2.51	2.80	3.19	3.26

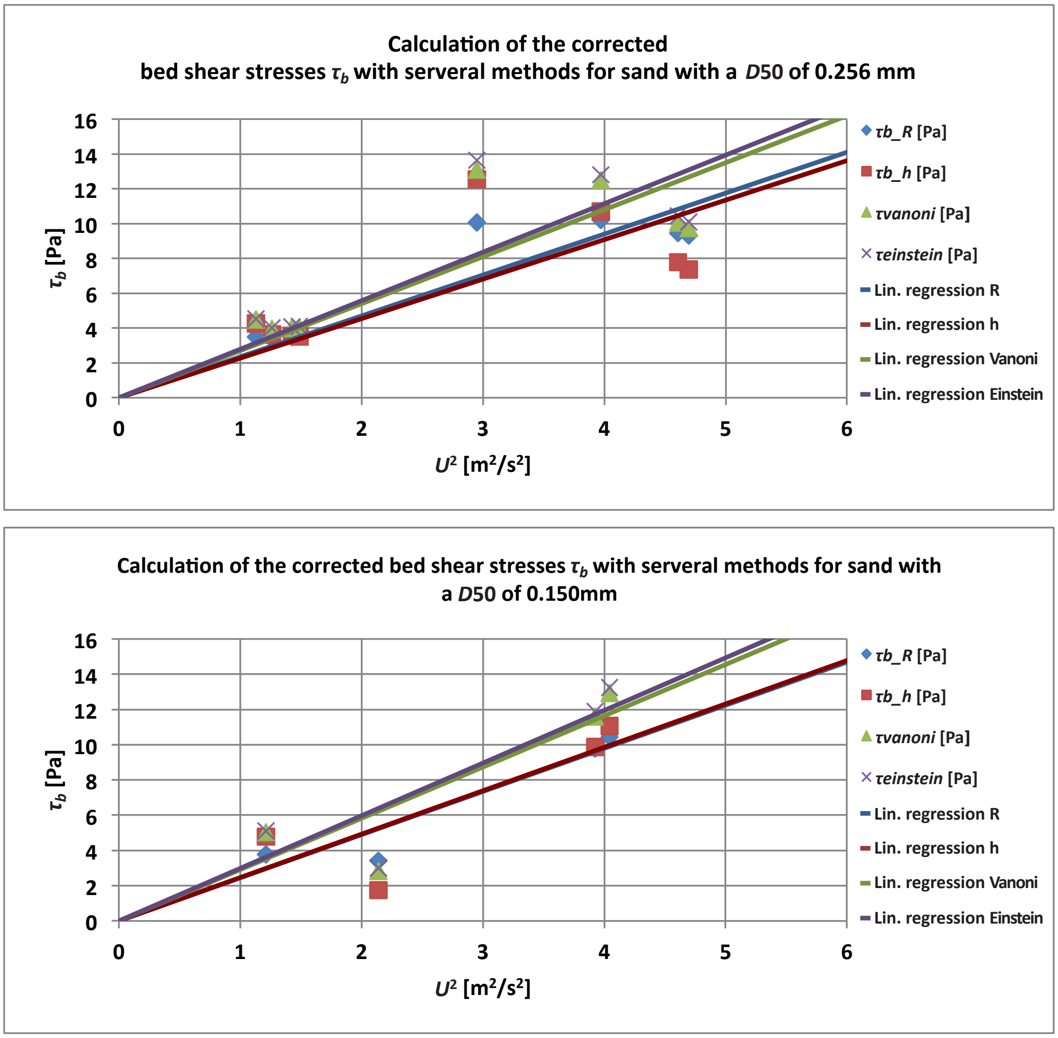

Figure 35: Prediction of bed shear stresses using different theories versus velocity squared for (a) sand with a D_{50} of 0.256 mm and (b) sand with a D_{50} of 0.150 mm.

Results calculated from the corrected bed shear stresses

In order to objectively calculate the effectiveness of a bentonite additive from the corrected bed shear stresses, the erosion velocity of the bed of a mixture is again compared with the erosion velocity of the sand mixture at the same flow velocity. The effectiveness of the different bentonite mixtures is given by the ratio of the mixture's erosion velocity and the erosion velocity of the sand (see Eq.(25)) and is based on the average erosion velocity for each test. The average erosion velocities versus corrected bed shear stresses are presented in Fig. 36. Linear regression lines through the measurements are also included. It is important to note that the regression lines go through the origin as explained before in Section 6.1. This simplification leads to generic quadratic equations for the erosion velocity in the form of $v_e = aU^2$ and are not verified at mean flow velocities below 1 m/s.

The ratio f for each mixture is calculated from the coefficients of the linear regression lines in relation to the coefficient of the linear regression line of sand. Or in mathematical terms $v_e = faU^2$, with a the coefficient of the sand regression line. The effectiveness of the different bentonite contents are given in Table 14. The effectiveness of the different bentonite contents are also graphically displayed in Fig. 37. An exponential relationship between the reduction f and the amount of bentonite additive $B_{\%}$ is also presented in Fig. 37 and differs slightly from the exponential relations displayed in Fig. 34. Significant reductions in erosion velocity are again obtained by adding bentonite to a sand mixture. A 2% mixture already reduces the erosion velocity by about 50%, a 3% or 4% mixture by 56 to 62 % and a 6% mixture by at least 94%. Furthermore, it appears that the effectiveness of adding bentonite to the finer and courser sand, both with a porosity of about 0.40 - 0.41, is about the same.

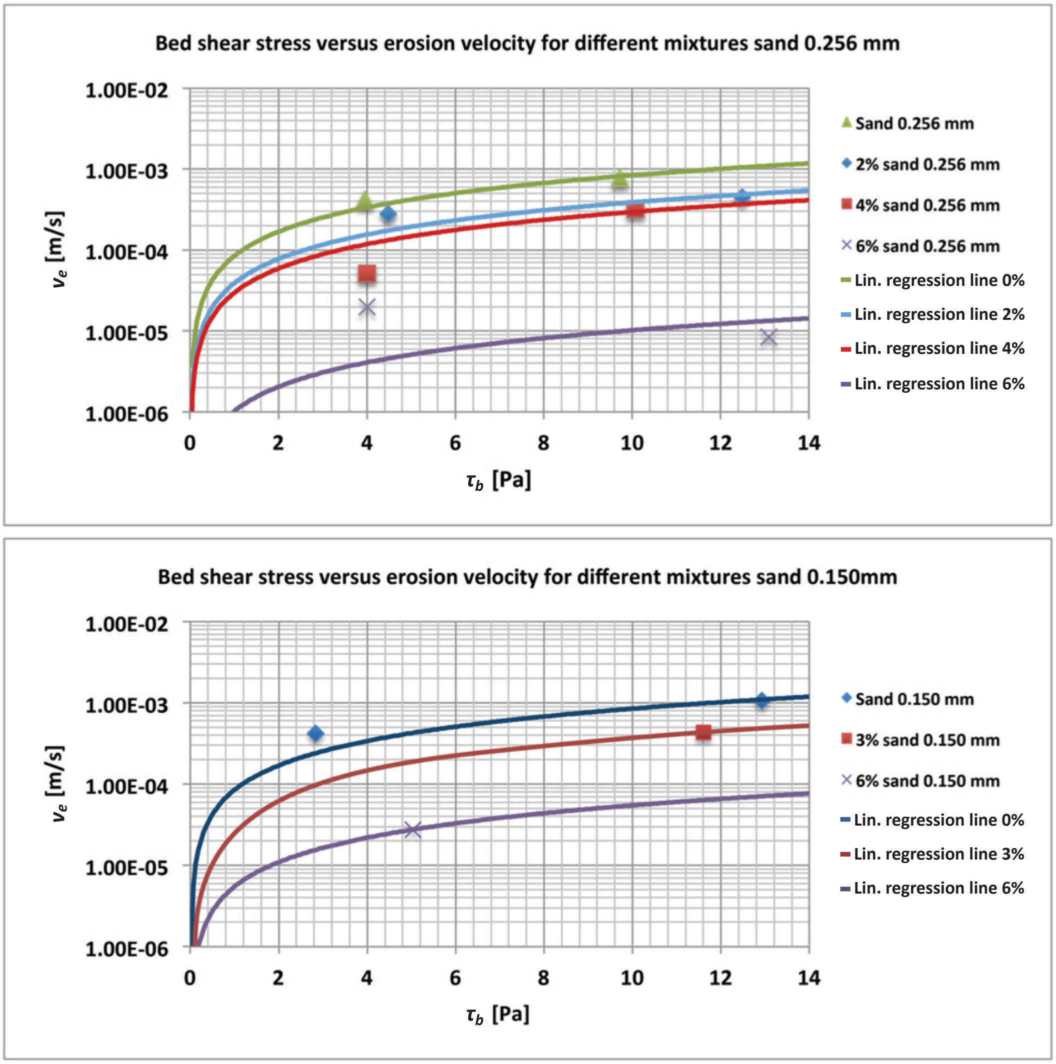

Figure 36: Erosion velocity versus bed shear stress for (a) sand with a D_{50} of 0.256 mm and (b) sand with a D_{50} of 0.150 mm.

Table 14: Reduction coefficient f for several mixtures and sand types based on linear regression of corrected bed shear stress data.

Bentonite [%]	D_{50} [mm]	coefficient a [-]	f [-]
0	0.256	8.00E-05	1.00
2	0.256	4.00E-05	0.50
4	0.256	3.00E-05	0.38
6	0.256	1.00E-06	0.01
0	0.150	9.00E-05	1.00
3	0.150	4.00E-05	0.44
6	0.150	5.00E-06	0.06

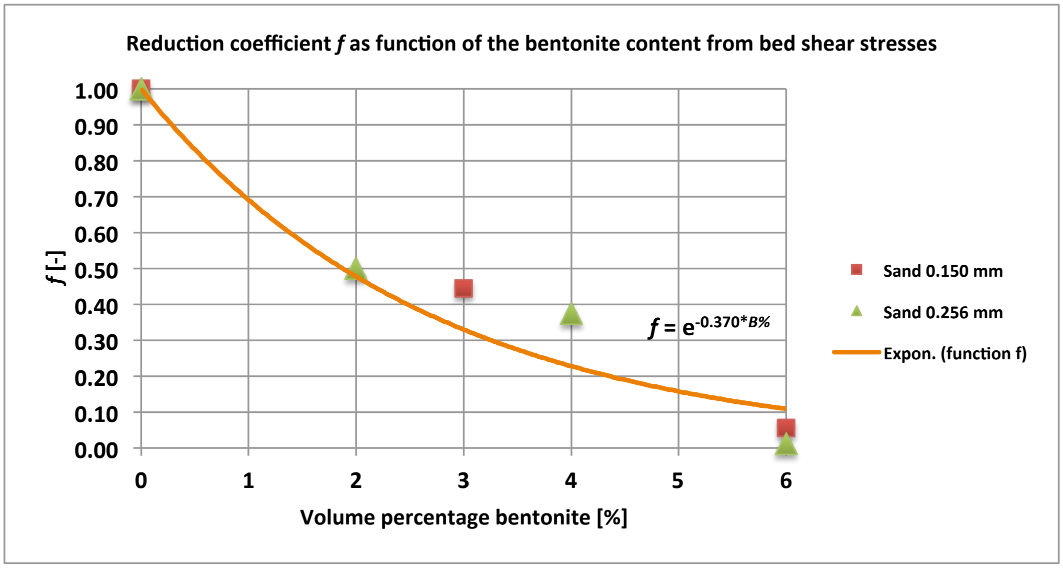

Figure 37: Reduction coefficient f as function of the bentonite content from corrected bed shear stresses.

Comparison of data from different erosion experiments with sand-bentonite mixtures

A literature study concerning the erosion behaviour of sand-bentonite mixtures, has resulted in the conclusion that very few data are available. At higher flow velocities these are even non-existent. For this reason it has been decided to collect all the data currently present. Data for the sand tests, without any bentonite, is visualized in Fig. 38 and shows the dependance of the erosion velocity on the (predicted) bed shear stresses. Note that the vertical axis is on logarithmic scale. The data set consist of data from Gailani (2001) with a D_{50} of 0.214 mm, Lemmens (2014) with a D_{50} of 0.208 mm and data collected in this study (called Foortse) with a D_{50} of 0.256 mm and 0.150 mm. It also has to be noted that average erosion velocities and depth-averaged flow velocities are used. Furthermore, the Vanoni & Brooks method is used to predict the bed shear stresses in the Foortse and Lemmens data sets.

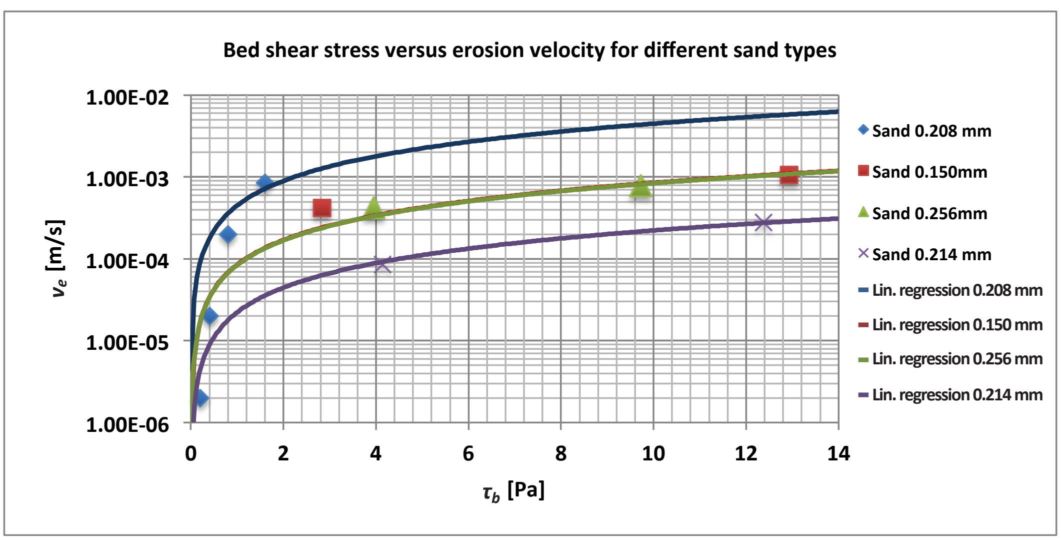

Figure 38: Erosion velocity versus bed shear stress for sands with a different D_{50}.

From Fig. 38 it can be concluded that the measurements executed by Gailani generally gave higher erosion velocities at the same bed shear stresses as both data from Lemmens and Foortse. This might be the result of the method used to calculate the bed shear stress τ_b. In Gailani's case the bed shear stress might be determined with a theoretical roughness prediction based on k_s, where the roughness of the particles protruding the water flow are governing. However, in sheet flow conditions, particles are partly in suspension and move as a sheet. Large shear stresses cause entrainment of large amounts of sediment resulting in high sediment concentrations, especially near the bed. These high sediment concentrations, in turn, cause an increase of the viscosity of the flowing sand-water mixture. This results in higher values for the roughness height k_s and thus higher values of the friction coefficient c_f. This means that the particle protrusion is no longer governing and that the roughness is increasing significantly. If this would be the case, the data of Gailani would have to be corrected. At the same erosion velocities, the measurement will have a higher bed shear stress and thus, as a result, the regression line will shift to the right.

The measurements from Lemmens show exactly the opposite trend. The erosion velocity, given a bed shear stress, is generally lower than those of Gailani and Foortse. Since both Foortse and Lemmens used the Vanoni & Brooks method to calculate the bed shear stresses, a comparison of shear stresses versus depth-averaged flow velocities squared was performed. This comparison is shown in Fig. 39. Fig. 39 also shows theoretical bed shear stresses calculated with Eq.(42), Eq.(43) and Eq.(44).

$$\tau_b = \rho c_f U^2 \tag{42}$$

$$c_f = \frac{\kappa^2}{\left[\ln(\dfrac{12R}{k_s})\right]^2} \tag{43}$$

$$k_s = \begin{cases} 3D_{90} \\ 2D_{50} \\ 3\theta D_{90} \end{cases} \tag{44}$$

in which κ is the Von Karman coefficient (=0.40). These theoretical bed shear stresses are not corrected for any side-wall effects. The comparison clearly shows that the corrected bed shear stresses calculated by Lemmens are much higher than those calculated by Foortse or the theoretical bed shear stresses. And since the theoretical bed shear stresses are not corrected for any side wall effect, this suggests that the measurements performed by Lemmens might overestimate the real bed shear stresses. In this case the regression line from Lemmens would shift to the left. Furthermore, the relatively low values for shear stresses from Foortse might be explained by the fact that the theoretical predictions are not corrected for side-wall effects.

Finally, it appears that the measurements from Foortse for sand with a D_{50} of 0.256 mm and a D_{50} of 0.150 mm show only slight differences. It was expected that the courser sand would be eroded earlier than the finer sand. However, these data suggest it does not matter. The only explanation is that some inaccuracy is present in the data. It is expected that this inaccuracy is mainly caused in the preparation phase of the bed. Especially the compaction of the bed to the desired density and porosity was difficult to control. In addition, there might also be differences in all the data sets, because all the measurement setups were different.

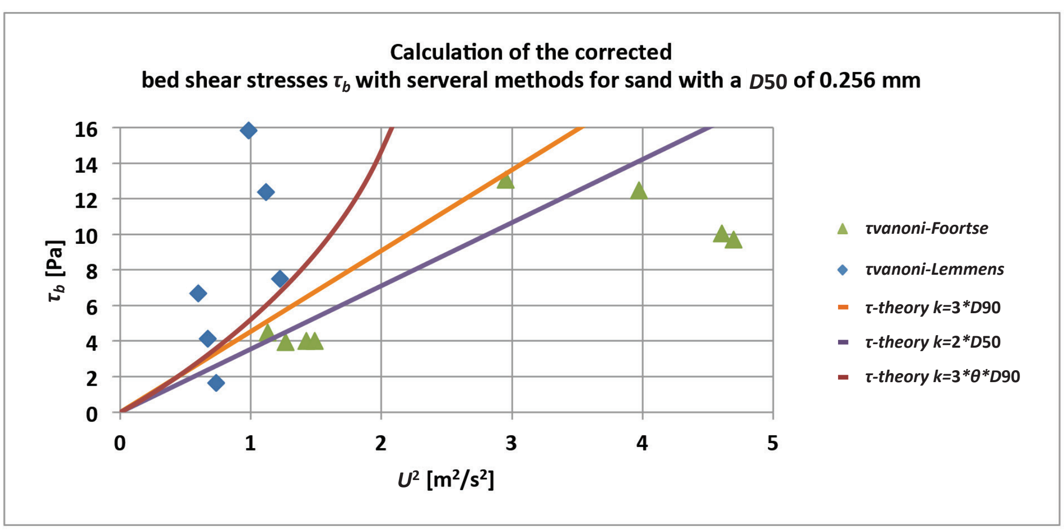

Figure 39: Bed shear stress versus velocity squared with data from Lemmens (2014), Foortse and theoretical predictions.

From Fig. 39 it can be concluded that a comparison based on absolute values of τ_b is not reliable enough. Significant variance between the different datasets is present. However, it might be instructive to compare the relative effectiveness of the bentonite-mixtures. The relative effectiveness f for each mixture is calculated from the coefficients of the linear regression lines in relation to the coefficient of the linear regression line of sand. Or in mathematical terms $v_e = faU^2$, with a the coefficient of the sand regression line. It is important to note that the regression lines go through the origin as explained before in Section 6.1. The linear regression lines for the data of Lemmens and Gailani are presented in Fig. F4 attached in Appendix F. From Table 15 it can be concluded that the relative reduction of adding bentonite for data of Lemmens and Foortse show close resemblance. On the contrary, the relative reduction based on data from Gailani differs much from the data of Foortse and Lemmens. However, it has to be remarked that the regression lines through the data of Gailani are of poor quality.

Table 15: Reduction coefficient f for several mixtures and data sets based on linear regression of corrected bed shear stress data.

Bentonite [%]	$f_{Foortse0.256}$ [-]	$f_{Lemmens}$ [-]	$f_{Gailani}$ [-]
0	1.00	1.00	1.00
2	0.50	0.50	0.15
4	0.38	0.30	0.02

When the same comparison is made with data from Lemmens (2014) and Foortse based on the erosion velocity versus the mean flow velocity squared, the result is slightly different (see Table 16). The reduction effect of a 4% mixture is stronger according to the measurements executed by Lemmens than measured by Foortse. The relative effectiveness f is again determined with the coefficients of the regression lines. The regression lines go through the origin as explained before in Section 6.1. This simplification leads to generic quadratic equations for the erosion velocity in the form of $v_e = faU^2$ and are not verified at mean flow velocities below 1 m/s. Fig. F5 attached in Appendix F presents the regression lines through the data of Lemmens. Finally, it has to be remarked that data from Gailani (2001) is excluded, because the exact flow velocities during these tests were not available.

Table 16: Reduction coefficient f for several mixtures and data sets based on linear regression of mean flow velocity data.

Bentonite [%]	$f_{Foortse0.256}$ [-]	$f_{Lemmens}$ [-]
0	1.00	1.00
2	0.50	0.50
4	0.38	0.15

Characterization of the flow conditions during the erosion tests

The Shields parameters (Table 13) are roughly in the range of 1 to 5, depending on the mean flow velocity. Based on these values of the Shields parameter and video recordings it can be concluded that the dominant erosion process was sheet flow erosion (see Section 2.1). In Tables D2 to D14 in Appendix F the values of v_e/k (erosion velocity over the in-situ permeability) and the Froude number Fr for each test are given. The Froude numbers are all above 1, indicating that all tests were executed under supercritical conditions. The v_e/k values for the tests were generally above 3 for the mixtures, indicating that a high erosion regime was often present. However, very large differences, from 1.5 up to about 30 were calculated. It also seems that a higher bentonite content leads to a steeper positive relationship between the bentonite content and v_e/k (see also Fig. F1 and Fig. F2 in Appendix F. This basically means that the high erosion regime is generally reached faster with sand-bentonite mixtures than with pure sand only.

The bottom line

The data analysis of the erosion tests in Section 6.1 clearly indicates that it is very difficult to predict and verify the absolute reduction in erosion velocity for different bentonite mixtures. Large variances in bed shear stresses and corresponding erosion velocities exist in the existing data sets and a comparison based on absolute values of (corrected) shear stresses is deemed not to be reliable enough. The significant differences in bed shear stresses are most likely caused by the difficulty in accurately measuring the energy loss of the system. Many methods are available to determine the friction coefficient, which accounts for this energy loss. Some even account for the extra viscosity of the flowing sand-water mixture, because of the high sediment concentrations near the bed. These high sediment concentrations near the bed (and thus higher viscosity) lead to higher energy loss, which is accounted for in the friction coefficient. The side-wall correction also influences the corrected bed shear stresses. This correction is related to the depth-averaged flow velocity and has a high impact on the bed shear stress at high velocities. It is hypothesized that the used side-wall correction methods might be over-correcting the bed shear stresses at higher flow velocities and might not be perfectly valid at flow velocities of about 2 m/s and higher. Relative reductions in erosion velocities for different bentonite mixtures proved to be more fruitful and even made it possible to compare data from different data sets.

This chapter concludes with a comparison of the effectiveness of bentonite mixtures on the permeability and the erosion velocity. For this comparison the exponential trend lines of Fig. 34, Fig. 37 and Fig. 42 are used. The comparison is visualized in Fig. 40. The effectiveness in reducing the permeability with sand-bentonite mixtures - derived in Section 6.2 - is denoted as f_{k1} for the courser sand with a D_{50} of 0.256 mm and f_{k2} for the finer sand with a D_{50} of 0.150 mm (see Eq.(45) and Eq.(46)). The subscript B indicates the permeability of the sand-bentonite mixture and the subscript *sand* the permeability of the sand mixture.

$$f_{k1} = k_B/k_{sand} = e^{-0.691*B_{\%}} \tag{45}$$

$$f_{k2} = k_B/k_{sand} = e^{-0.674*B_{\%}} \tag{46}$$

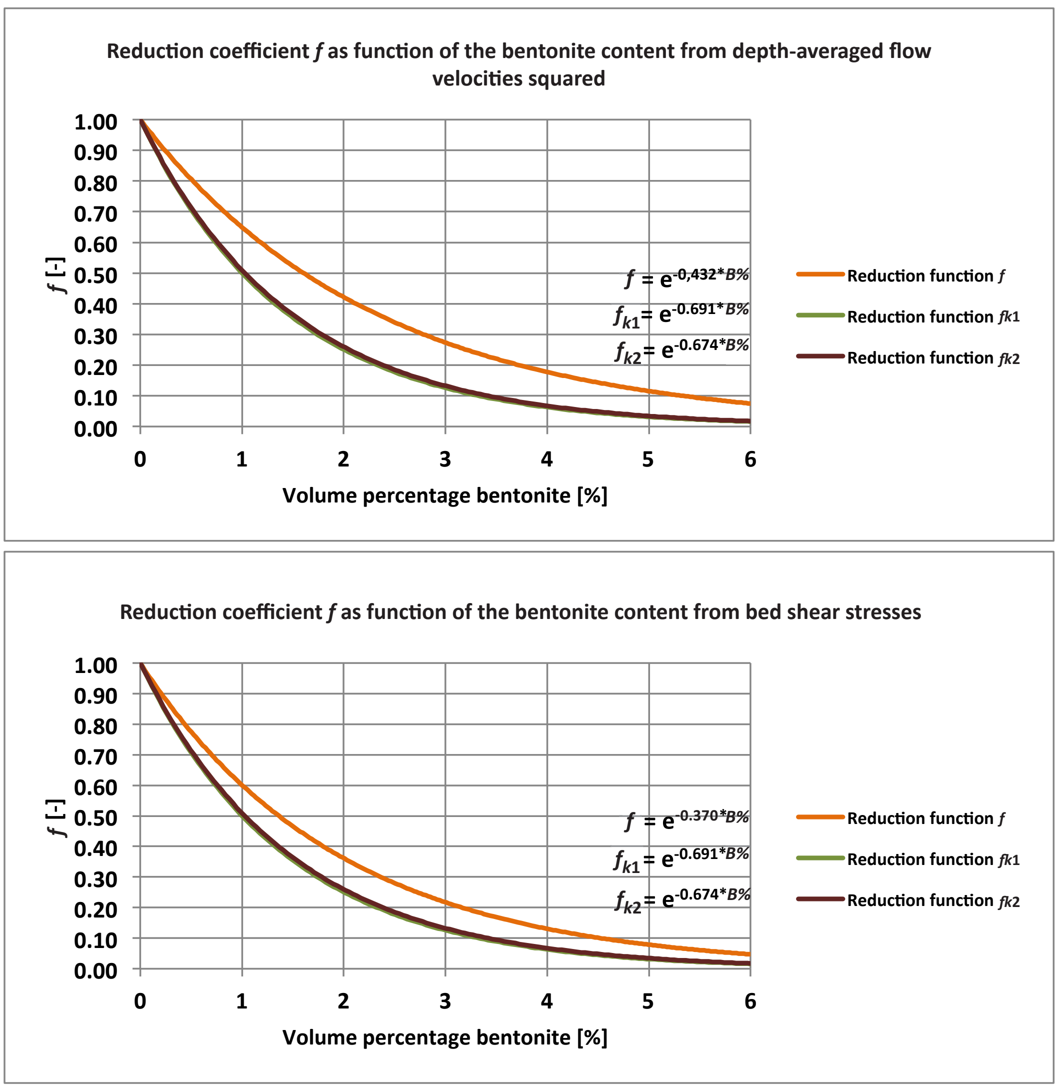

Figure 40: Reduction of the erosion velocity and permeability as function of the bentonite content (a) from depth-averaged flow velocities squared (b) from bed shear stresses.

$$f_{U^2} = f_B/f_s = e^{-0.432*B_{\%}} \tag{47}$$

$$f_\tau = f_B/f_s = e^{-0.370*B_{\%}} \tag{48}$$

The effectiveness in reducing the erosion velocity with sand-bentonite mixtures is denoted as f_{U^2} (Eq.(47) for the exponential relationship based on the mean flow velocity squared and f_τ (Eq.(48) for the exponential relationship based on the bed shear stresses. The ratio f_B/f_s gives the reduction in erosion velocity of the mixture as compared to the erosion velocity of the sand.

Finally, an empirical relationship between the reduction of the erosion velocity and the reduction of the permeability is derived (see Eq.(49) and Eq.(50)). There is some difference between the method based on the mean flow velocity squared and the one based on the bed shear stresses. However, both relationships indicate that there is a relatively strong dependence of the erosion velocity on the permeability. The reduction of the erosion velocity seems also to be related to the reduction in permeability (${f_k}^{0.54-0.63}$), which approaches the relationship between the erosion velocity and the permeability ($k^{0.6}$) as obtained by the model of Bisschop et al. (2010).

$$f_{U^2} \propto {f_k}^{0.63} \tag{49}$$

$$f_\tau \propto {f_k}^{0.54} \tag{50}$$

6.2 Results permeability tests

In this section the results of the permeability tests are presented. The objective of the falling head test was to determine the in-situ permeability of sand and sand-bentonite mixtures (see also Table 5). With the setup and input conditions as explained in Section 5.2.1 the permeability was calculated with Eq.(18). Additional information can be found in Appendix C. The average permeability for each mixture, the reduction of the mixture permeability relative to the permeability of the sand and soil conditions are summarized in Table 17. The relative densities were determined with the minimum and maximum density as discussed in Section 5.4.1. The absolute values of the in-situ permeability of each mixture, including the data from Lemmens (2014), are also graphically presented in Fig. 41.

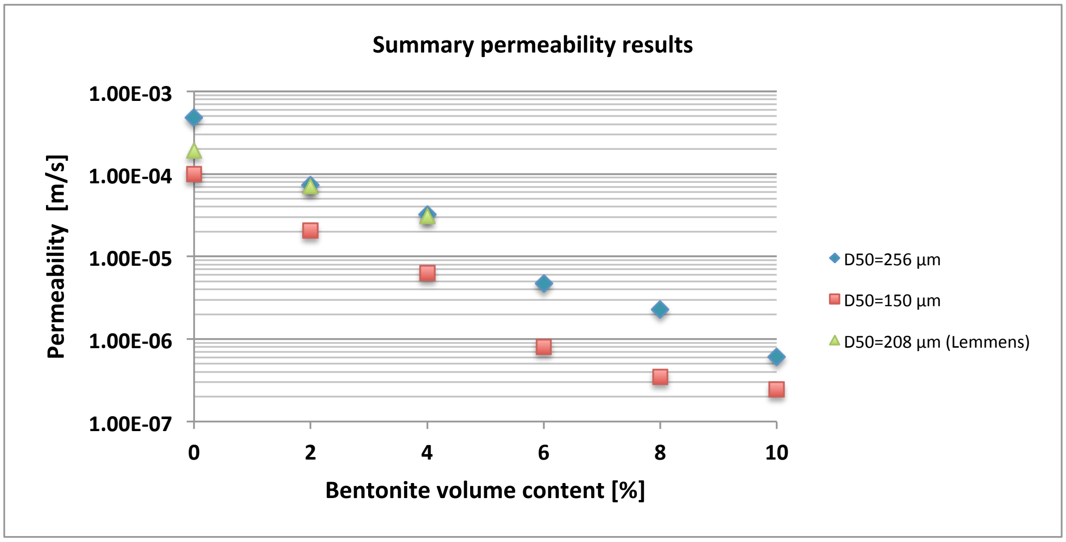

Figure 41: Results of the permeability coefficients for different sand diameters.

Adding bentonite clearly reduces the permeability significantly. A 2% volume bentonite content already reduces the original permeability to 20% or below for both sand types. A 4% volume bentonite content even reduces the original permeability to 7%. Increasing the bentonite content to 6% or higher this is 1%. Empirical functions have been derived based on this data set. The reduction ratio k/k_{sand} is a function of the volume percentage of added bentonite. This is graphically displayed in Fig. 42. It appears that the relationship is almost identical for the sand types with a D_{50} of 0.256 mm and a D_{50} of 150 mm and suggest that the reduction ratio is almost irrespective of the sand diameter. These equations have been used in this study to model the erosion behaviour of the dike core.

The permeabilities of the sand with the largest particles (D_{50} of 0.256 mm) are higher than the smaller particles sizes. The same is valid for the sand with a D_{50} of 0.208 mm as compared to sand with a D_{50} of 0.150 mm. The permeability measurements executed by Lemmens (2014), with a D_{50} of 0.208 mm, were obtained with porosities in the order of 0.43 - 0.44. These higher porosities might explain the relatively high permeabilities measured for the 2% and 4% mixtures. These permeabilities are almost identical to the results of the courses sand diameter (a D_{50} of 0.256 mm) executed at porosities in the order of 0.40 - 0.41. Unfortunately, no information regarding the relative density of the measurements executed by Lemmens (2014) was available.

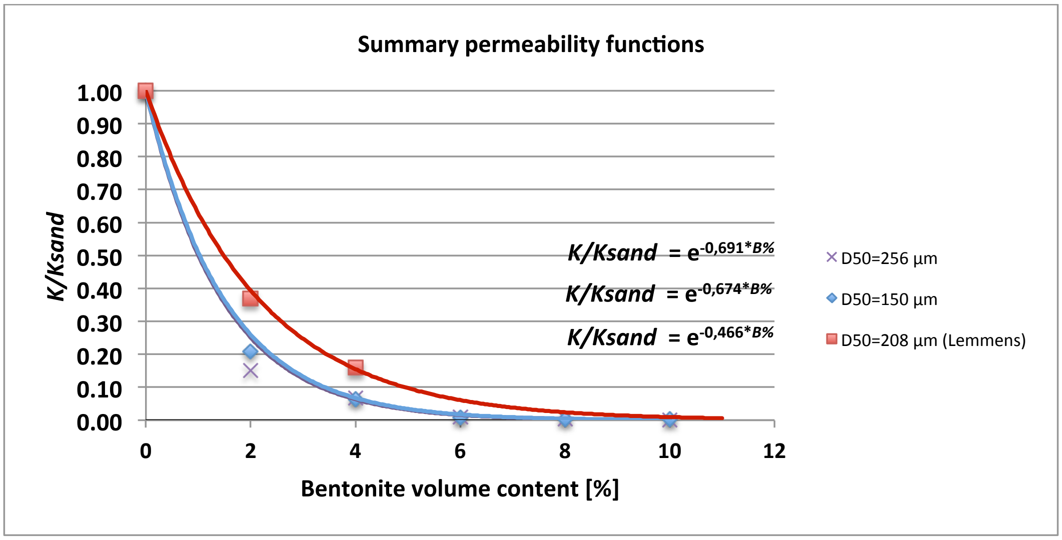

Figure 42: Reduction of the permeability coefficients as functions of the volume percentage of bentonite.

Table 17: Summarized results of the permeability tests

Bentonite [%]	D_{50} [mm]	k [m/s]	k/k_{sand} [-]	n_0 [%]	$\rho_{dry,mixture}$ $[kg/m^3]$	RD [%]
0	0.256	4.83E-4	1.000	40.3	1582	53.3
2	0.256	7.29E-5	0.151	40.3	1581	52.9
4	0.256	3.23E-5	0.067	40.9	1567	46.5
6	0.256	4.65E-6	0.010	40.3	1581	52.9
8	0.256	2.29E-6	0.005	40.6	1575	50.2
10	0.256	6.11E-7	0.001	40.8	1570	47.9
0	0.150	9.88E-5	1.000	41.4	1552	82.9
2	0.150	2.06E-5	0.208	40.8	1568	87.9
4	0.150	6.31E-6	0.064	40.4	1580	91.6
6	0.150	8.09E-7	0.008	41.3	1556	84.1
8	0.150	3.46E-7	0.004	40.8	1568	87.9
10	0.150	2.45E-7	0.002	41.7	1546	81.0

6.3 Results direct shear tests

In this section the results of the direct shear tests are presented. Additional information is provided in Appendix A. The tests were executed with the continuing loading method. The continuing loading method can be explained as follows. A test starts with shearing the sample with the lowest normal load until the peak shear is reached. After this peak is reached, extra normal load is added and the shearing is continued. This procedure is repeated until three different peak shear stresses, given their normal load pair, are obtained. In Appendix A the shear stress versus displacement graphs of all the individual tests are given. In these graphs three obvious peak shear stresses can be detected. The benefit of this method is that the same sample can be used continuously. This method was the only viable option given the time span, since every sample had to be saturated for at least 24 hours before the test could commence.

Sample area correction
The shear and normal stresses are calculated from the lateral force, the normal forces and the horizontal contact area. During the tests the contact area between the two specimen halves is reducing in time (see Fig. 43). This reduction varies with relative displacement δ between the upper and lower halves and in case of a square box (with length a) the corrected sample area is defined as:

$$A_c = a(a - \delta) \tag{51}$$

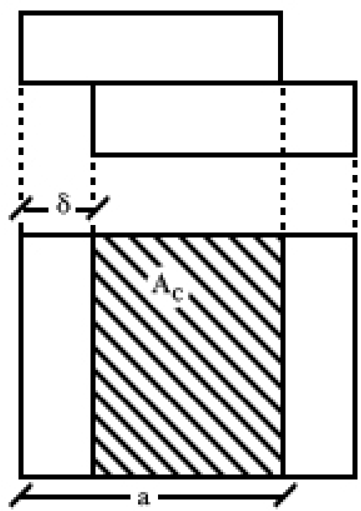

Figure 43: Visualization of the sample area correction, adapted from Bardet (1997).

The corrected normal and shear stress pairs are plotted for the M32 and S90 sand type in Fig. 44 and Fig. 45. Linear regression lines have been plotted through the data points and represent the Mohr-Coulomb failure enveloppes as discussed in Section 5.3.1. With Eq.(19) the apparent cohesion and friction angle are determined. These results, including soil characteristics, are summarized in Table 18. Graphs of each individual test can be found in Appendix A.

The results in Fig. 44 and Fig. 45 show insignificant differences. The apparent cohesion is not changing drastically by adding more bentonite ($<$ 3 kPa). The friction angle is also not significantly decreasing as a result of adding bentonite. It remains in the range of 34 to 43 degrees. The internal friction angles of the S90 sand type are higher than those of the M32 sand type. This is a result of a higher degree of compaction (expressed by the higher relative density). Based on these results it can be concluded that sand-bentonite mixtures with volume percentage bentonite up to 10 do not show any sign of cohesion-like behaviour and are thus still behaving as a non-cohesive sand.

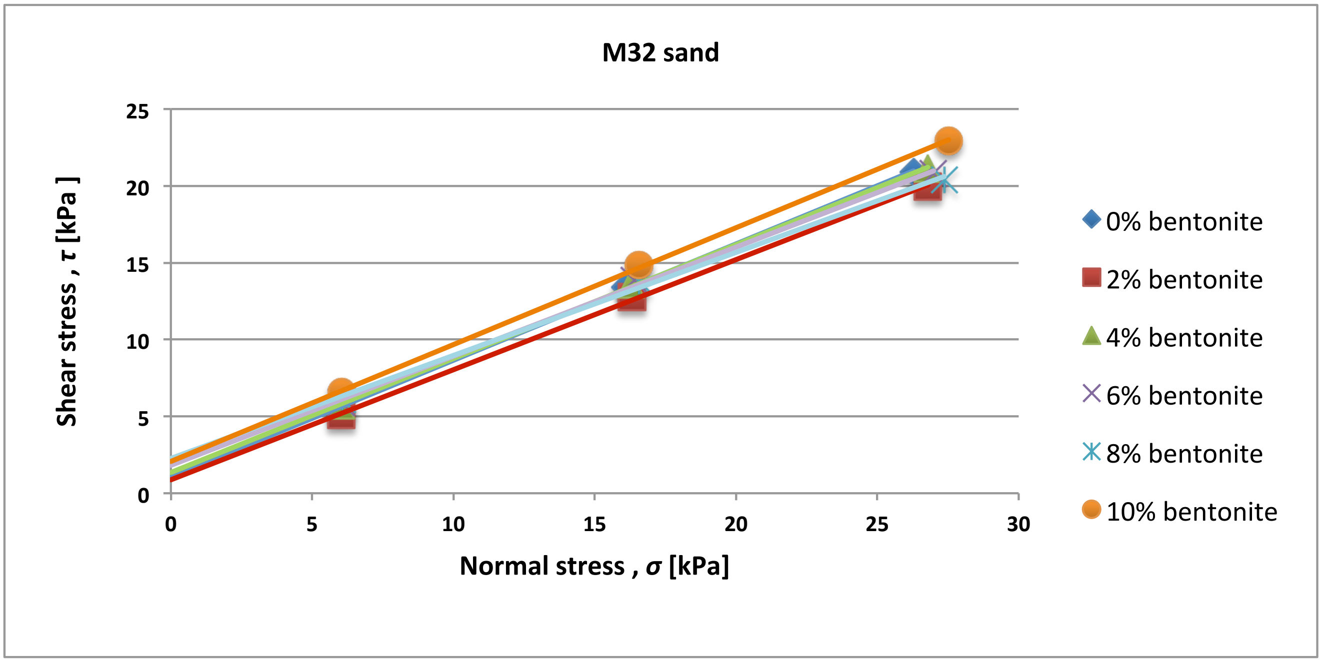

Figure 44: Results direct shear tests of sand with a D_{50} of 0.256 mm.

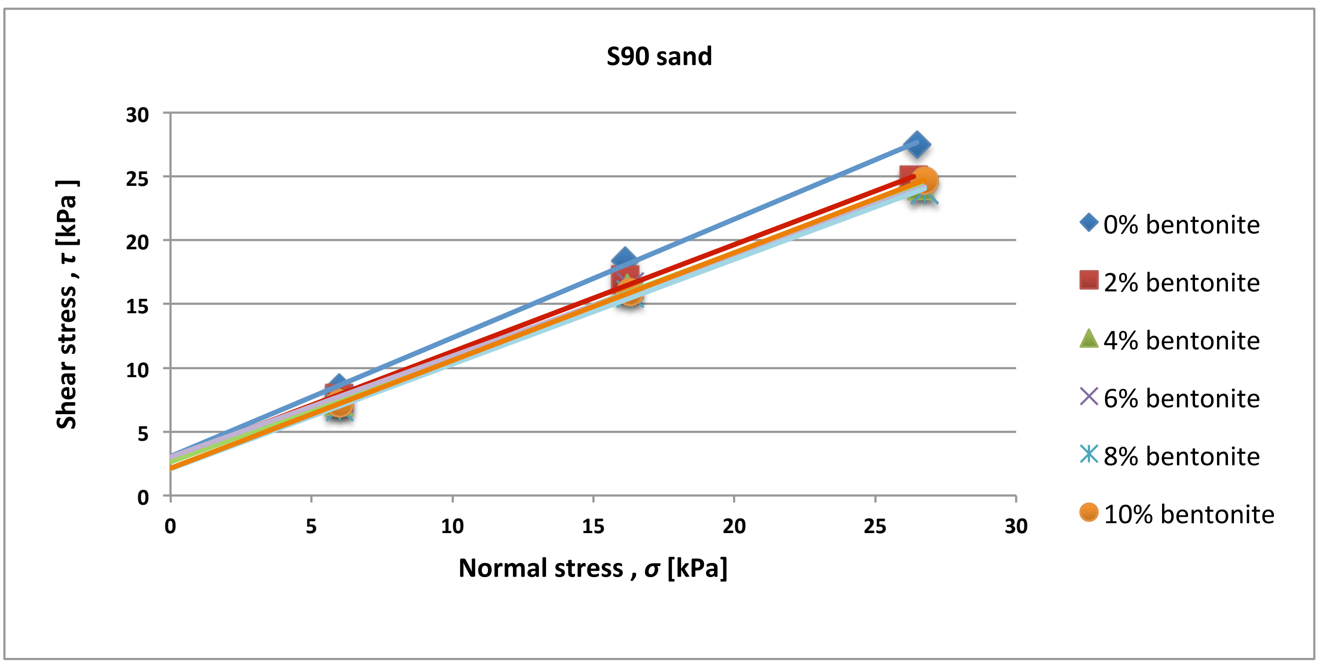

Figure 45: Results direct shear tests of sand with a D_{50} of 0.150 mm.

Table 18: Specifics and results of the direct shear test

Bentonite [%]	D_{50} **[mm]**	C **[kPa]**	ϕ **[°]**	$\rho_{dry,mixture}$ $[kg/m^3]$	n_0 **[%]**	RD **[%]**
0	0.256	1.07	37.1	1581	40.3	52.9
2	0.256	0.88	35.6	1581	40.3	52.9
4	0.256	1.35	36.5	1569	40.8	47.4
6	0.256	1.81	35.3	1581	40.3	52.9
8	0.256	2.27	33.8	1575	40.6	50.2
10	0.256	2.07	37.2	1575	40.6	50.2
0	0.150	3.06	42.9	1554	41.4	83.5
2	0.150	2.88	40.0	1568	40.8	87.9
4	0.150	2.63	39.3	1580	40.4	91.6
6	0.150	3.01	38.4	1554	41.4	83.5
8	0.150	2.09	39.4	1565	40.9	87.0
10	0.150	2.14	40.2	1536	42.0	77.8

7 | Discussion of the experimental tests

This chapter briefly focusses on the unexpected experimental results of the direct shear tests. In addition, the (un)expected occurrences and important observations during the erosion tests are discussed extensively. The permeability results are also briefly discussed. The chapter concludes with a few general remarks about the assumptions used and choices made in the experimental phase of this study.

7.1 The directs shear tests

As expected low cohesion values (< 3kPa) and friction angles in the order of 33 - 43 degrees were observed for the mixtures with a bentonite volume content lower than 6%. In contrast, a sharp increase in cohesion and significant drops in friction angles were expected for higher bentonite volume percentages ($>$6 %). Fully saturated specimens swell and loosen the packing of the sand particles. At a certain point the sand particles were expected to loose direct contact with neighbouring particles and consequently lose its strength characteristics. Although it is noted in literature (see Chalermyanont and Arrykul, 2005) that fully saturated and inundated mixtures lost their cohesion as a direct result of the swelling bentonite, this still does not explain the high friction angles. The only possible explanation is that the sand grains still have direct contact with neighbouring particles and thus show typical sand-like behaviour at these mixture ratios.

As expected, smaller horizontal strain (displacement) was also observed for stiffer material (as in mixtures with a low bentonite content) than for softer material (mixtures with higher bentonite contents) (see appendix A).

7.2 The erosion tests

During the experiments many expected and unexpected occurrences were observed. These findings may add incremental value to the dataset of Chapter 6. These findings may be used as guidelines in similar future experiments, and may prove useful in designing other erosion experiments as well. The following occurrences will be discussed: scour holes, bed forms, inhomogeneity of the bed, softening of the clay, mass erosion and erosion with even steeper bottom slopes.

Scour holes, bedforms and inhomogeneity of the bed
As indicated in Section 5.1, a fixed concrete bottom was applied in part of the flume. The fixed concrete bottom was mainly applied to minimize the effects of turbulence in the measurement area, caused by the sudden transition in bed level between the flume bottom and the height of the sand bed of 0.15 m. Although there would still be a transition in bed roughness from the fixed concrete bottom to the sand bed, the turbulence effects were expected to be less significant than in case of a sudden transition in height. During the erosion experiments the designs given in Fig 19 and Fig. 20 proved to be almost flawless. This was unexpected, but most certainly beneficial. Although some erosion took place at the transition from the fixed concrete plate to the bed and after some time even bedforms appeared (see Fig. 46) no indication of a starting scour hole was present in any of the thirteen test runs.

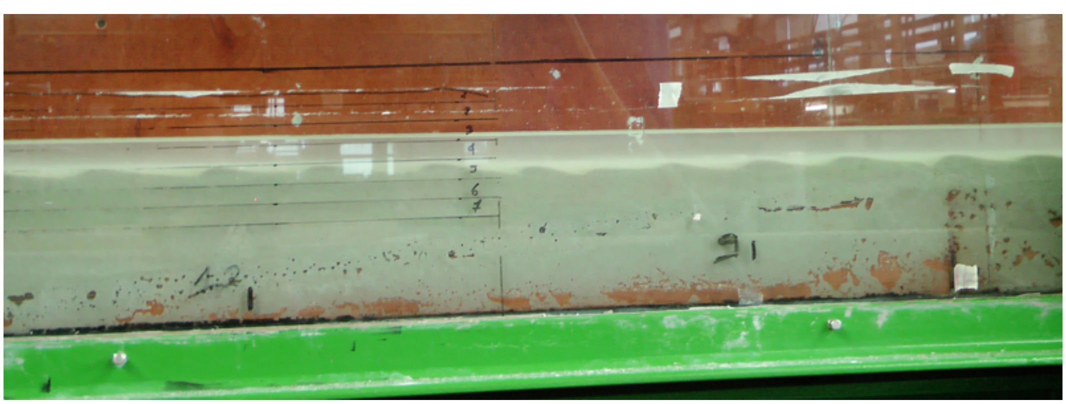

Figure 46: No formation of a scour hole and appearance of bedforms.

Local weak spots appeared during the erosion experiments as a result of a not perfectly homogeneous mixture. Preparation of the sand or sand-bentonite mixtures was extremely time-consuming and laborious. First, the sand and bentonite were mixed using a concrete mixture (see also Section 5.1.1). Next the mixture was transported towards the flume using a wheelbarrow. Finally, the flume was filled using a bucket. In addition, the bed had to be compacted towards its ideal density of about 1580 kg/m^3 and porosity of about 0.40. The compaction method was vibration by means of a wooden strip of wood and a hammer. The quality control was based on the bed height and the total volume needed for the bed. All these steps combined could easily influence the homogeneity of the bed and certainly leaves some ingenuity for improvement. If during the tests a local weak spot became apparent, this soon became an undulation. The undulation, in turn, disturbed the flow, causing local acceleration and deceleration of the flow. These accelerations and decelerations disturbed the flow pattern even more, resulting in rapid erosion (see Fig. 47). In contract, also some local stronger parts in the bed were visible. At locations where the bentonite content was higher than average, soil lumps were formed. Fig. 48 shows an example of a soil lump that was completely eroded away and is a clear example of more cohesive erosion behaviour than non-cohesive behaviour.

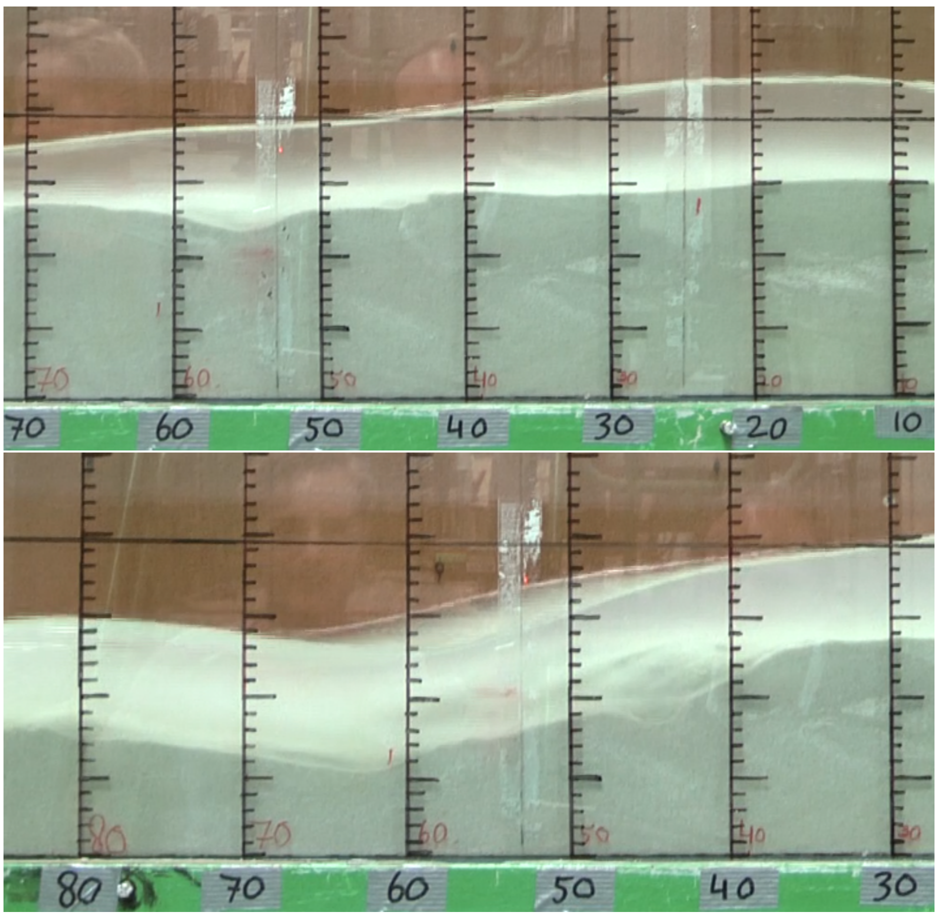

Figure 47: (a) Local weak spot in a 1 m/s test (b) Local weak sport in a 1 m/s test, 10 seconds later.

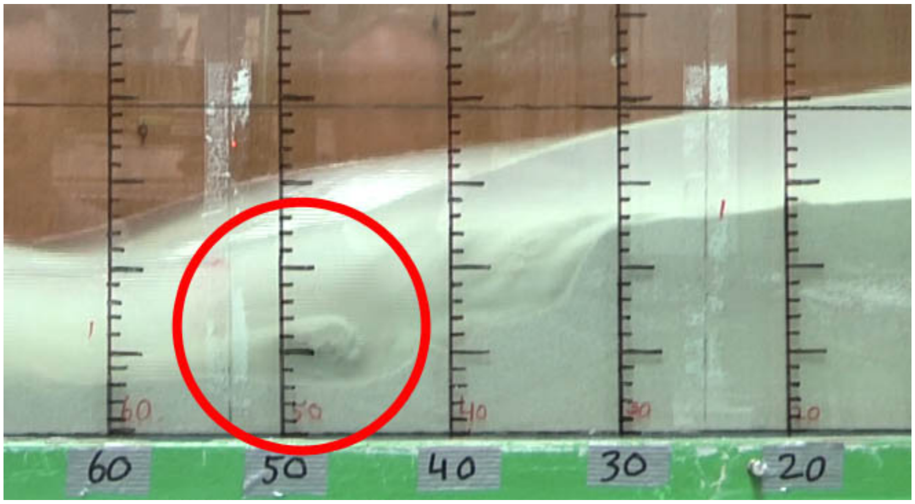

Figure 48: Local inhomogeneous erosion of a soil lump.

It was only a matter of time before a hydraulic jump appeared as a result of bedform formations or after a local inhomogeneous weak spot started to erode. In a hydraulic jump the flow regime is in transition from supercritical flow to subcritical flow. Since the flow has to dissipate much of its energy a very turbulent flow is formed (Fig. 49). Erosion caused by this turbulence disturbed further measurements, but may certainly happen in case of a real breach.

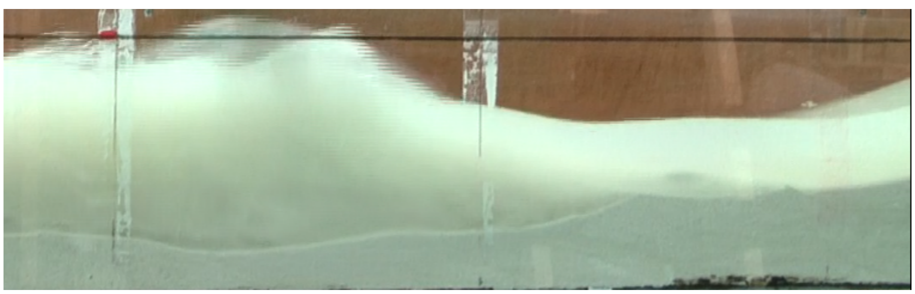

Figure 49: Formation of a hydraulic jump.

Due to the local weak spots and the formation of bedforms the duration of the tests was usually short in order to prevent the influence of these instabilities on the test results. Another observation was that certain parts of the bed were still not saturated after 24 to 48 hours. This is also supporting the earlier observation that it is almost impossible to get an ideal homogeneous bed (or core in a dike), which might be a limitation for the practical implementation.

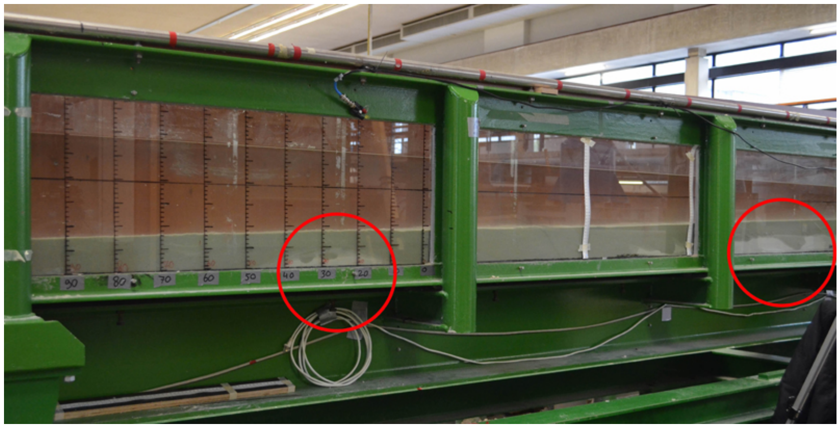

Figure 50: Part of the bed has still not been in contact with water after 24 hours.

Cohesive behaviour of the bed

During and after the erosion tests with a sand-bentonite mixture two additional phenomena were observed. These were: mass erosion and softening of the soil bed after the tests. Although direct shear tests and the attempt to find a plasticity limit clearly indicate that the mixtures still behave as a sand, visual observations and camera recordings indicated a mass erosion of the bed (Fig. 52 and Fig. 51). Mass erosion is generally characterized as cohesive behaviour. The geotechnical results and visual observations clearly contradict each other.

Figure 51: Topview of the bed after an erosion test.

Figure 52: Inhomogeneous mass erosion of a 6% mixture.

The softening of the soil layer was also very peculiar. During the tests (especially the 6% mixture runs) there was hardly any erosion visible. However, the bed started to soften after the tests were stopped and hardly any water was flowing over the bed. This is clearly depicted in Fig. 53. It appears that a bed, containing bentonite, prevents erosion only temporarily during extreme shear stresses. After the extreme endeavor, it looked as if the bentonite was exhausted and simply let itself erode without significant resistance. This might suggest that a dike core will be protected during extreme water conditions and will soften, as butter getting heated, afterwards.

Figure 53: (a) Softening of the soil bed with a 6% mixture (b) Softening of the soil bed with a 6% mixture, 10 seconds later.

Influence of the bed slope on the erosion velocity

The tests executed with setup 1 (Fig. 19) had a bed height of 15 cm. However, about 1 m after the area of interest, the bed had to go down towards the bottom level of the flume again. The transition was quite sudden and corresponded with a steep slope of 1:3. The steep slope resulted in an acceleration of the flow in downstream direction. Acceleration of the flow, means higher flow velocity, and thus higher erosion velocities. This is clearly visualized in Fig. 54. In a time frame of a few seconds the bed was eroded 20 cm in horizontal direction at a flow velocity of about 1 m/s. This observation is a clear demonstration of inner slope erosion in a real breach scenario and clearly shows how fast a dike with a sand core might get eroded away.

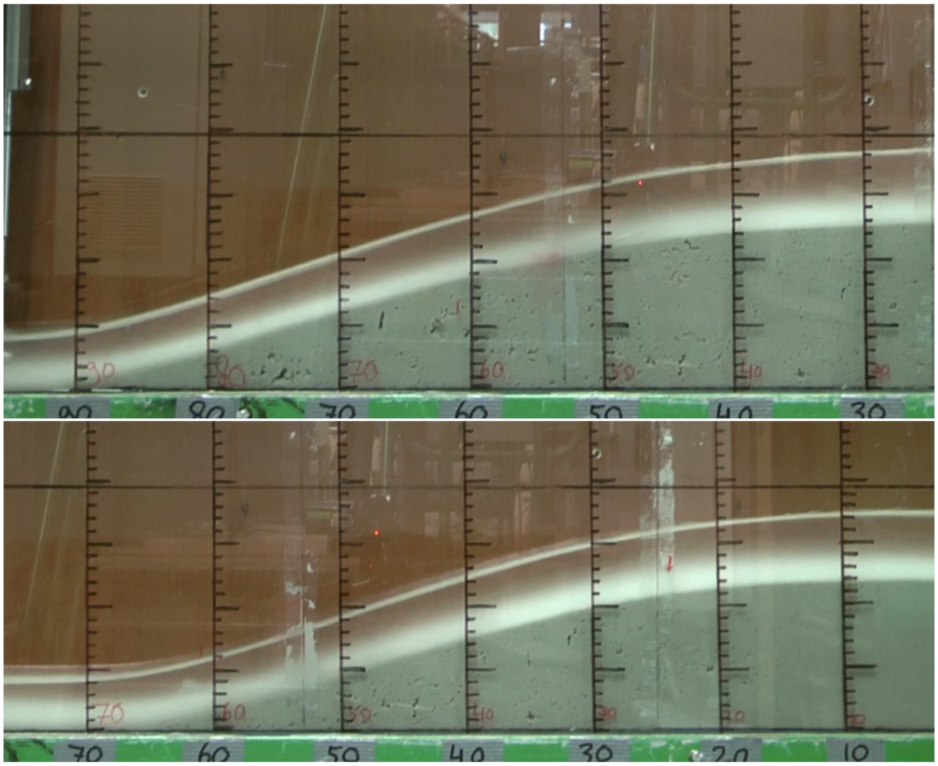

Figure 54: (a) Horizontal erosion as a result of downstream effects. (b) Horizontal erosion as a result of downstream effects, a few seconds later.

7.3 The permeability tests

In general, sand is a quite permeable natural material. Adding a certain amount of bentonite to sand certainly yields a high decrease in permeability. This is the result of the swelling potential of the bentonite. It appears that the most significant decrease in permeability happens with bentonite contents up to 6% volume percentage. Adding more bentonite still reduces the permeability, but the overall effect is starting to flatten out for bentonite contents higher than 8%. Overall, the approximate decrease in permeability is almost three orders of magnitude (from 10^{-4} to 10^{-7}) with bentonite volume percentages up to 10%.

Furthermore, it was observed that the swelling of the samples kept increasing and that the specimen expanded with bentonite contents higher that 8%. This increase of swell even lead to the appearance of cracks in the specimen (Fig. 55). This crack formation is expected to be responsible for the decrease in effectiveness of a bentonite mixture with bentonite contents $> 8\%$.

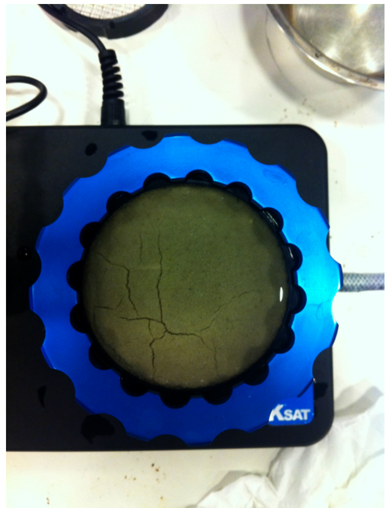

Figure 55: The appearance of cracks for a mixture with 8% bentonite.

7.4 General remarks

During this study many assumptions and choices were directly or indirectly made. In this section these assumptions and choices are explicitly stated and discussed.

- The continuous loading method for the direct shear tests was chosen simply in view of time. Although the normal and shear stress couples give a reasonable good estimate of the peak shear stress under a specific normal load, the samples were not sheared until failure. Although these shear stresses might be higher in reality than indicated in the results of this study, a fairly good indication is obtained with the continuous loading method.
- During the preparation and design phase it was assumed that the bed would be perfectly homogenous. However, the preparation of the bed and the preparation of the sample specimen is not a perfectly robust method and is prone to imperfections. This might be a serious limitation for the practical implementation and future research into mixing techniques and compaction methods for this application is recommended.
- Although the video recordings are perfectly accurate, data analysis always introduces inaccuracies. By programming an algorithm to extract data series for the bed levels and water levels the inaccuracies were minimized as much as possible. The algorithm automatically converted pixels to lengths using a preset pixel/length ratio. However, the exact location of the bed level and water level still had to be indicated in the videos and still were a source of subjectivity and inaccuracy.
- The porosity $n_{mixture}$ and dry bulk density $\rho_{mixture}$ are calculated for just the sand with Eq.(52) and Eq.(53). This means that it is indirectly assumed that all the bentonite particales will position itself between the sand grains in the voids. This is a reasonable assumption for lower bentonite volume percentages, but the assumption is probably violated at higher percentages (see also Fig. 55).

$$\rho_{mixture} = \frac{M_{mixture} - M_{additive}}{V_{bed}} \tag{52}$$

$$n_{mixture} = 1 - \frac{\rho_{mixture}}{\rho_s} \tag{53}$$

  in which $M_{mixture}$ is the total mass of the mixture (sand + bentonite), $M_{additive}$ the mass of the bentonite additive only, V_{bed} the total volume of the bed or sample and ρ_s the density of the sand grains (generally accepted as 2650 kg/m^3).
- A final remark is made about the flume setup. During the tests it appeared that quite some height in the flume is needed in order to reach the required high flow velocities. Steep bed slopes are needed in order to reach high equilibrium flow velocities (when supercritical flow conditions prevail). Flow velocities $>$ 2 m/s will be extremely difficult to reach in the current setup and it is strongly recommended to look for open channel flumes with a height clearly exceeding 40 cm or to design experiments with a conduit flow setup. Furthermore, it is recommended not to forget to check the environmental regulations of the laboratory and not to underestimate

the troubles related to discharging the bentonite out of the experimental system. Bentonite is characterized by its very small particle size and cannot easily be filtered out of the water.

8 | Modelling the performance of the bentonite additive

This chapter focusses on modelling of the bentonite additive behaviour. The BRES-Visser model (see Sections 2.4 and 2.5), along with the Zwin'94 data (see Section 2.7), is used to model the performance of the bentonite additives. The data from the Zwin'94 experiment will be used as a reference scenario for a dike with a sand core. The effects of the retardant bentonite additive will be compared to this reference scenario. The comparison takes place based on breach width, flow through the breach and duration of the breaching process.

8.1 The critical Shields parameter

The concept of initiation of motion, as discussed in Section 2.2, indicates the initiation of the sediment transport and is an important parameter in modelling the erosion behaviour. The initiation of motion is often defined with de critical Shields parameter θ_{cr} and can be determined using the Shields curve. The Shields curve gives the critical Shields parameter θ_{cr} for specific conditions and is based on experimental results. Van Rijn (1993) determined that the Shields curve can also be represented with:

$$\theta_{cr} = 0.24{D_*}^{-1} \quad \text{for} \quad 1 < D_* \leq 4 \tag{54}$$

$$\theta_{cr} = 0.14{D_*}^{-0.64} \quad \text{for} \quad 4 < D_* \leq 10 \tag{55}$$

$$\theta_{cr} = 0.04{D_*}^{-0.1} \quad \text{for} \quad 10 < D_* \leq 20 \tag{56}$$

$$\theta_{cr} = 0.013{D_*}^{0.29} \quad \text{for} \quad 20 < D_* \leq 150 \tag{57}$$

$$\theta_{cr} = 0.055 \quad \text{for} \quad D_* > 150 \tag{58}$$

where D_* can be calculated with Eq. (16).

8.2 The erosion function

The next step in modelling the performance of the bentonite additive is to derive an erosion function. In this study the Van Rhee erosion function (Van Rhee, 2010) is adapted to the experimental data of the erosion tests (see Section 6.1). This erosion function is chosen, because this function includes the hindered erosion process, as discussed in Section 2.3. The inclusion of the hindered erosion concept is very important at high flow velocities. The erosion function of Van Rhee (2010) is defined as:

$$v_e = \frac{1}{1 - n_0 - c_b}\left(\Phi_p\sqrt{g\Delta D_{50}} - c_b w_s\right) \tag{59}$$

where c_b is the near bed concentration. The dilatancy factor δ_p is calculated with Eq.(17) and the dimensionless pick-up flux Φ_p is defined as:

$$\Phi_p = 0.00033{D_*}^{0.3}\left[\frac{\theta - {\theta_c}^1}{\theta_c^1}\right]^{1.5} \tag{60}$$

where θ_c^1 is defined as:

$${\theta_c}^1 = \theta_c\left[\frac{sin(\phi - \beta)}{sin(\phi)} + \delta_p\frac{v_e}{k_l}\right] \tag{61}$$

From Fig. 56 and Fig. 57 it can be concluded that the erosion function of Van Rhee (2010) does not perfectly agree with the experimental data. Generally, the erosion rates are overestimated. Especially, the erosion rate of the 6% mixture with a D_{50} of 0.256 mm is not corresponding with the erosion function of Van Rhee. However, the credibility of one of the measurements of the 6% mixture with a D_{50} of 0.256 mm has already been questioned in Chapter 6.1. In case of a sand mixture, a 2% mixture and a 4% mixture with a D_{50} of 0.256 mm and all mixtures with a D_{50} of 0.150 mm, the overestimation is less than a factor 10. The agreement between the erosion function and all mixtures with a D_{50} of 0.150 mm is reasonably well. These results include the effect of the permeability of sand-bentonite mixtures on the erosion velocity (see also Section 6.2). However, in the calculations the in-situ porosity k_0 is used instead of the loose state permeability k_l, since the permeability at the loose state and corresponding value of the loose state porosity n_l are not easy to determine.

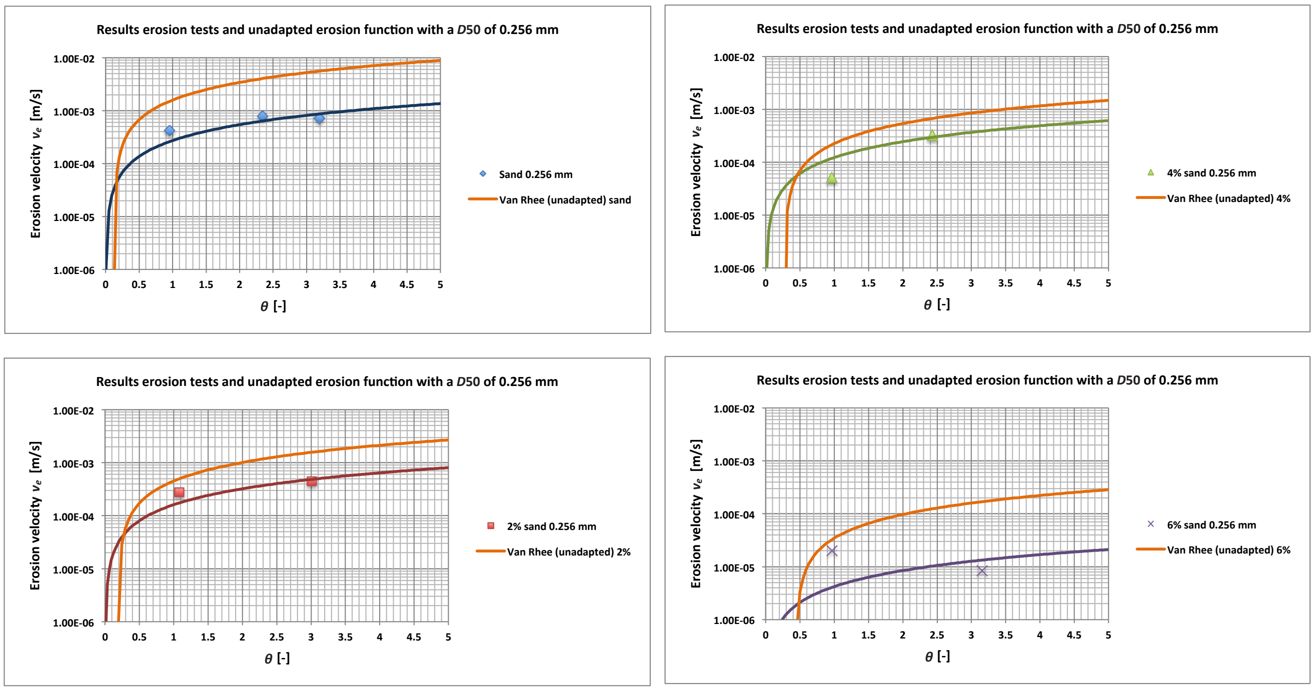

Figure 56: Comparison between the results of the erosion tests and the unadapted erosion function of Van Rhee for (a) sand only (b) a 2% mixture (c) a 4% mixture and (d) a 6% mixture sand with a D_{50} of 0.256 mm.

In order to get a more meaningful estimate Van Rhee (2015), recently, proposed that the in-situ permeability k_0 and the loose state permeability k_l are related as follows:

$$(1 - n_0)\,\frac{k_l}{\Delta n} = F k_0 \tag{62}$$

where F is assumed to be constant and generally reads:

$$F = \frac{(1 - n_0)}{\Delta n}\frac{k_l}{k_0} = \frac{{n_l}^3}{{n_0}^3}\frac{(1 - n_0)^3}{(n_l - n_0)(1 - n_l)} \tag{63}$$

and the relative porosity change Δn is defined as:

$$\Delta n = \frac{n_l - n_0}{1 - n_l} \tag{64}$$

The porosity at the loose state n_l is often assumed to be the maximum porosity (=0.48). Typical values for the in-situ porosity n_0 are between 0.40 and 0.42 (see also Chapter 6). In this case the value of F thus varies between 9 and 9.4. When the relation between the in-situ porosity k_0 and the loose state porosity k_l (Eq. (62)) is used, the value of k_l appears to be 1.87 to 2.3 times bigger than the value of k_0. This results in even higher erosion rates (1.5 times higher for the courser sand and 2.0 times higher for the finer sand) and a poorer fit with the experimental data.

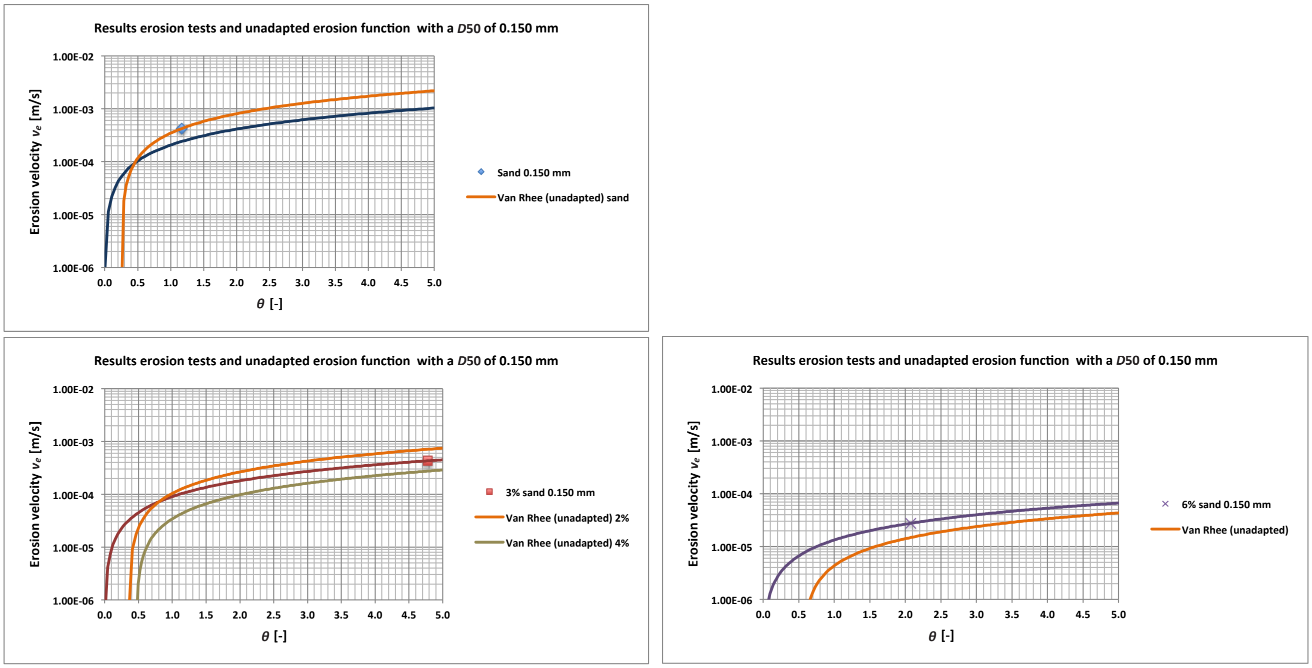

Figure 57: Comparison between the results of the erosion tests and the unadapted erosion function of Van Rhee for (a) sand only (b) a 3% mixture (c) a 6% mixture sand with a D_{50} of 0.150 mm.

Part of the inaccuracy can also be attributed to the estimated near-bed concentration (see Appendix H). Unfortunately, the near-bed concentrations could not be measured during the experiments. For this reason a near bed concentration of 0.03 has been used in the calculations of Fig. 56 and Fig. 57. However, a sensitivity analysis shows that when a near bed concentration of 0.10 or 0.20 is used, erosion rates are lower (see also Appendix H). For higher flow velocities (θ>2) the difference in erosion velocity has a maximum of a factor 2 (see also Fig. H2). For low flow velocities the difference becomes more significant. The effect of a higher near-bed concentration, which is likely at higher flow velocities, results in a better fit with the experimental data.

It is not uncommon to find discrepancies between experimental data and results predicted by erosion functions. This may be due to the introduction of inaccuracies in the experimental setup and procedures as mentioned before. However, it may also be that the erosion function of Van Rhee (2010) does not fully capture all the physical processes. Three possible causes for the overestimation of the erosion function of Van Rhee (2010) are proposed:

1. **As a consequence of the experimental setup the depth-averaged flow velocity is used in the erosion function.**
   The erosion function of Van Rhee (2010) indirectly uses the depth-averaged flow velocity to determine the erosion rate. However, the near-bed flow velocity is the governing parameter in sediment transport. It is often assumed that the near-bed flow velocity and depth-averaged flow velocity are related by a log-law flow velocity profile. However, it is expected that the velocity profile is significantly influenced by sediment transport, especially, sediment transport (sheet flow transport) under high flow velocities. The validity of using the depth-averaged flow velocity as an input parameter for the erosion rate can be tested by measuring the entire velocity profile during erosion tests. The velocity profile can, for instance, be continuously measured with an ADV (Acoustic Doppler Velocity) meter. Unfortunately, this was not a viable option in this study.

2. **The sediment transport capacity of the flow is reached, which limits the erosion function.**
   The erosion rate is also, theoretically at least, allowed to continue indefinitely with increasing flow velocities (and thus Shields parameters). However, the sediment capacity of the flow is limited. It is impossible to pick-up more sediment than the water flow can carry and transport away. For this reason, it might be useful to couple the erosion function of Van Rhee (2010) to a sediment transport equation, which incorporates the carrying capacity of the flow and thus limits the erosion rate.

3. **There is a difference in erosion behaviour between conduit flow and open channel flow setup caused by an unknown physical process.**

The final aspect, that might explain the discrepancies between the experimental data and the results predicted by the erosion function, is that some physical process is not accounted for. In particular, there might be an unknown difference between the physical processes of conduit flow and open channel flow. The erosion function of Van Rhee (2010) is, most of the time, applied in conduit flow environments and the erosion experiments of this study were a clear example of an open-channel flow environment.

8.3 The adapted erosion function

The original erosion function of Van Rhee (2010) does not perfectly agree with the experimental data. Especially the mixtures with a D_{50} of 0.256 mm. In Section 8.2 it has been concluded that the erosion rates are generally overestimated. A sensitivity analysis is executed, where the Van Rhee function (Van Rhee, 2010) is fitted to the experimental data. An additional coefficient c is added in front of the permeability to fit the erosion function to the experimental data. It appears that the best fits are possible with a value of c ranging from 1/3 to 1. The coefficient of 1 indicates that there is no adaptation of the function needed (resulting in Fig. 56 and Fig. 57).

The input conditions as used in the erosion function of Van Rhee (2010) are given in Table 19. In addition, it has to be noted that it is assumed that the critical Shields parameter θ_{cr} for a sand-bentonite mixture is equal to the critical Shields parameter of sand with an equal diameter. Furthermore, the near bed concentration c_b is chosen to be 0.03 to account for a near bed concentration present in the erosion tests. This near bed concentration was clearly visible during erosion tests. Finally, Table 19 shows some slight differences in input parameters between the different sand types.

Table 19: Input parameters erosion function for the course and fine sand.

Parameter and dimension	Value course sand	Value fine sand
D_{10} in [mm]	0.176	0.103
D_{50} in [mm]	0.256	0.150
D_{90} in [mm]	0.370	0.235
g in [m/s^2]	9.81	9.81
ρ in [kg/m^3]	1000	1000
ρ_s in [kg/m^3]	2650	2650
Δ in [-]	1.65	1.65
n_0 in [-]	0.40	0.40
n_1 in [-]	0.48	0.48
Flume width b in [m]	0.145	0.145
c_b in [-]	0.03	0.03
ϕ in [°]	36	40
β in [°]	0	0
ν in [m^2/s]	1.0E-6	1.0E-6
Permeability k in [m/s]	4.83E-4	9.88E-5
θ_{cr} in [-]	0.042	0.063

The effect of the coefficient c of 1/3 on the erosion function is visualized in Fig. 58 and Fig. 59. It seems that the agreement between the erosion function and all mixtures with a D_{50} of 0.150 mm is negatively affected by the coefficient c. Although the agreement of a sand mixture is better, the erosion velocities of the bentonite mixtures are now underestimated by the erosion function. The agreement of a sand mixture, a 2% mixture and a 4% mixture, with a D_{50} of 0.256 mm, is reasonably good. The difference between the measurements and the erosion function has a maximum of a factor 3. Although the agreement of a 6% mixture, with a D_{50} of 0.256 mm is by far not perfect, the difference between the measurements and the erosion function is minimized. However, since the credibility of one of the measurements of the 6% mixture with a D_{50} of 0.256 mm has already been questioned in Chapter 6.1, the agreement of the erosion function with the other measurements is deemed more important.

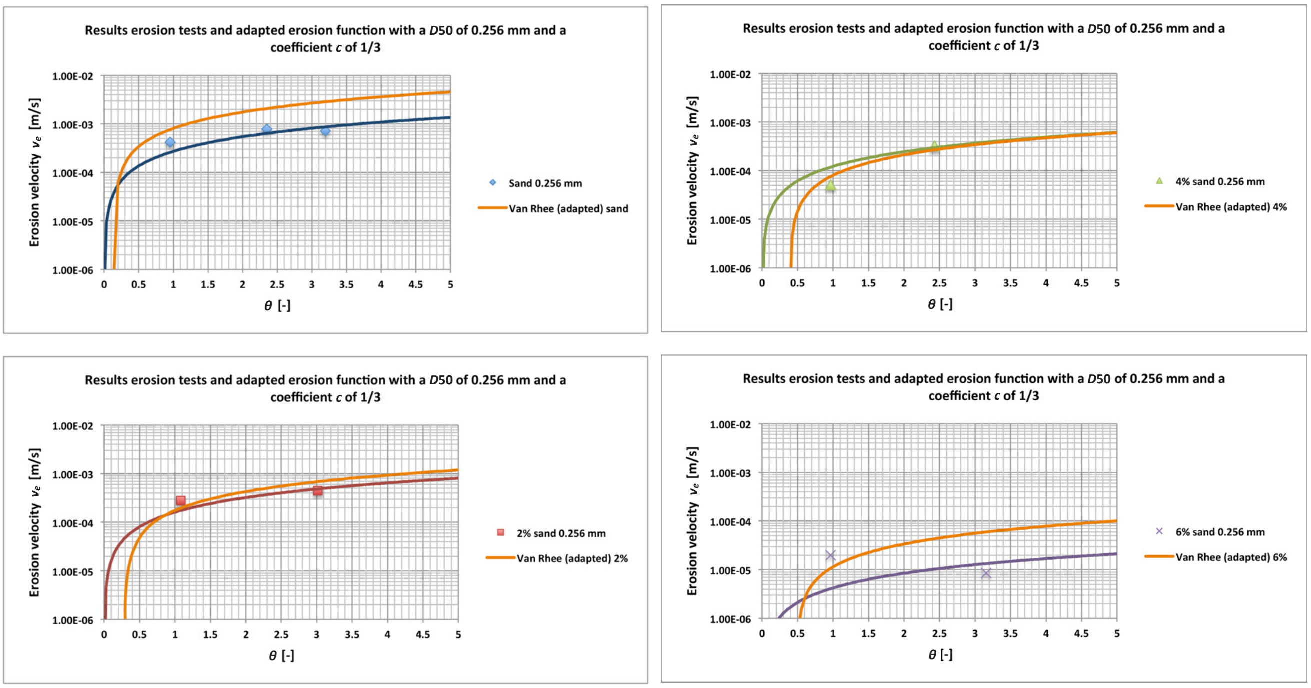

Figure 58: Comparison between the results of the erosion tests and the adapted erosion function of Van Rhee for (a) sand only (b) a 2% mixture (c) a 4% mixture and (d) a 6% mixture of sand with a D_{50} of 0.256 mm.

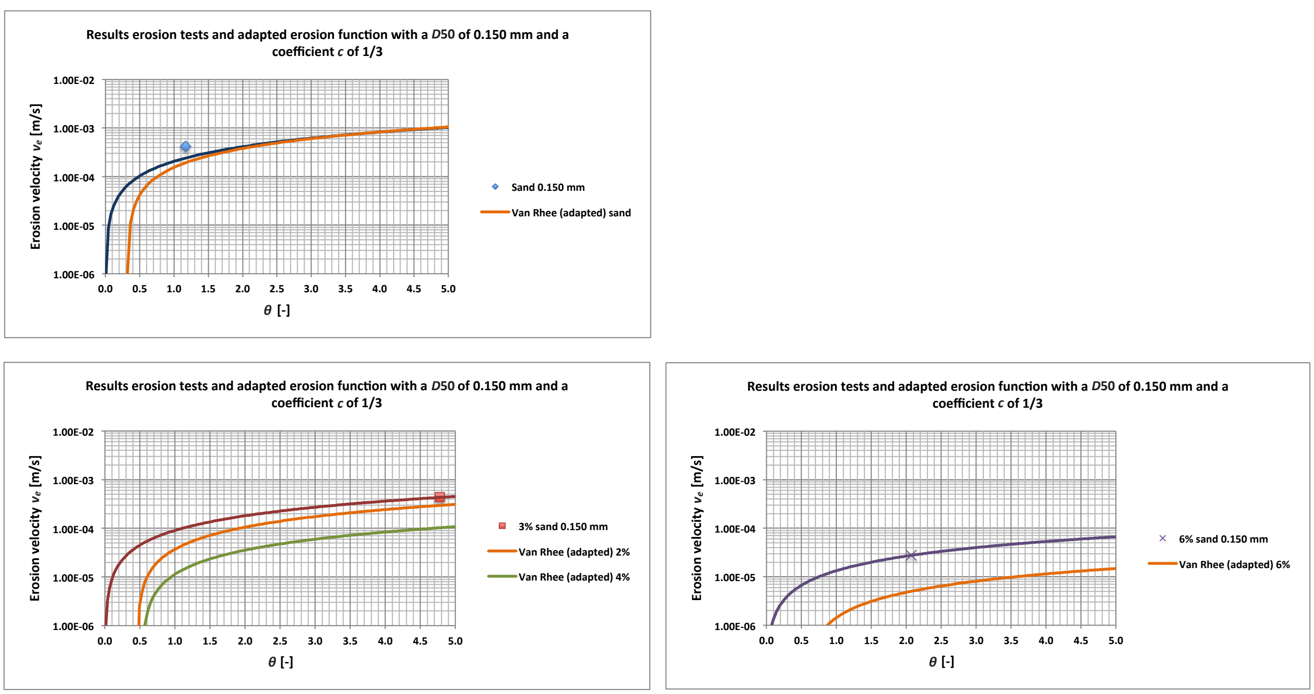

Figure 59: Comparison between the results of the erosion tests and the adapted erosion function of Van Rhee for (a) sand only (b) a 3% mixture (c) a 6% mixture of sand with a D_{50} of 0.150 mm.

8.4 Inclusion of the effect of the bentonite content on the erosion velocity

The final step in the derivation of the adapted erosion function, is to include the effect of the bentonite content on the erosion velocity (as a continuous function). This effect is indirectly taken into account by adapting the permeability in the original erosion function. The relationship between the bentonite content of the mixture and the permeability of the mixture with respect to the permeability of unaltered sand has been derived in Section 6.2. The empirical relations for the courser sand ($k_{0.256mm}$) and the finer sand ($k_{0.150mm}$) are given by:

$$k_{0.256mm} = k_{sand} * e^{-0.691*B\%} \tag{65}$$

$$k_{0.150mm} = k_{sand} * e^{-0.674*B\%} \tag{66}$$

in which $B\%$ is the volume percentage of added bentonite and k_{sand} is the permeability of the original sand without bentonite.

Since the empirical relationships of Eq.(65) and Eq.(66) are almost identical it is concluded that the permeability of the mixture is (most likely) independent of the particle size. For this reason the relationship between the bentonite content of the mixture and the permeability of the mixture will be modelled with the following empirical equation:

$$k = k_{sand} * e^{-0.68*B\%} \tag{67}$$

where the exponent is chosen to be the rounded off average of 0.691 and 0.674, which is 0.68.

By implementing the adapted erosion function in the BRES model, the model can simulate the breaching process for different volume percentages of added bentonite. This is the topic of Section 8.5.

8.5 Calibration of the erosion function and the performance of the bentonite additive in the core of a dike

The adapted erosion function with a coefficient c of 1, including the relationship between the bentonite content and the permeability of the mixture, Eq.(67), has been implemented in the BRES model. Next, the BRES model has been calibrated using data from the Zwin'94 experiment (see also Table 2).

The performance of different volume percentages of added bentonite on the breaching process has also been modelled with the BRES model. A comparison of the effectiveness of different bentonite mixtures in reducing the breach width B, flow through the breach Q, the inundation velocity V_i and duration t of the breaching process is visualized in Fig. 60 and the maximum values are given in Table 20. From Fig. 60 and Table 20 it can be concluded that adding bentonite to a sand core of a dike has a phenomenal effect on the breaching process. By adding 6% of bentonite to the total volume to the sand core, the duration of the process is increased by roughly four times and the inundation rate is almost 0.5 m/h. An inundation velocity V_i below 0.5 m/h is preferred, since at an inundation of 0.5 m/h or higher (fast rising water) the mortality will start to increase (Jonkman, 2004).

Table 20: Duration of the breaching process, the breach width, the flow through the breach and the rise rate for several retardation mixtures.

Bentonite [%]	Duration [s]	B_{max} [m]	Q_{max} $[m^3/s]$	$V_{i,max}$ [m/h]
0	2527	38.7	194	2.70
2	3868	24.5	103	1.59
4	5293	15.1	60	0.95
6	9747	9.7	28	0.53

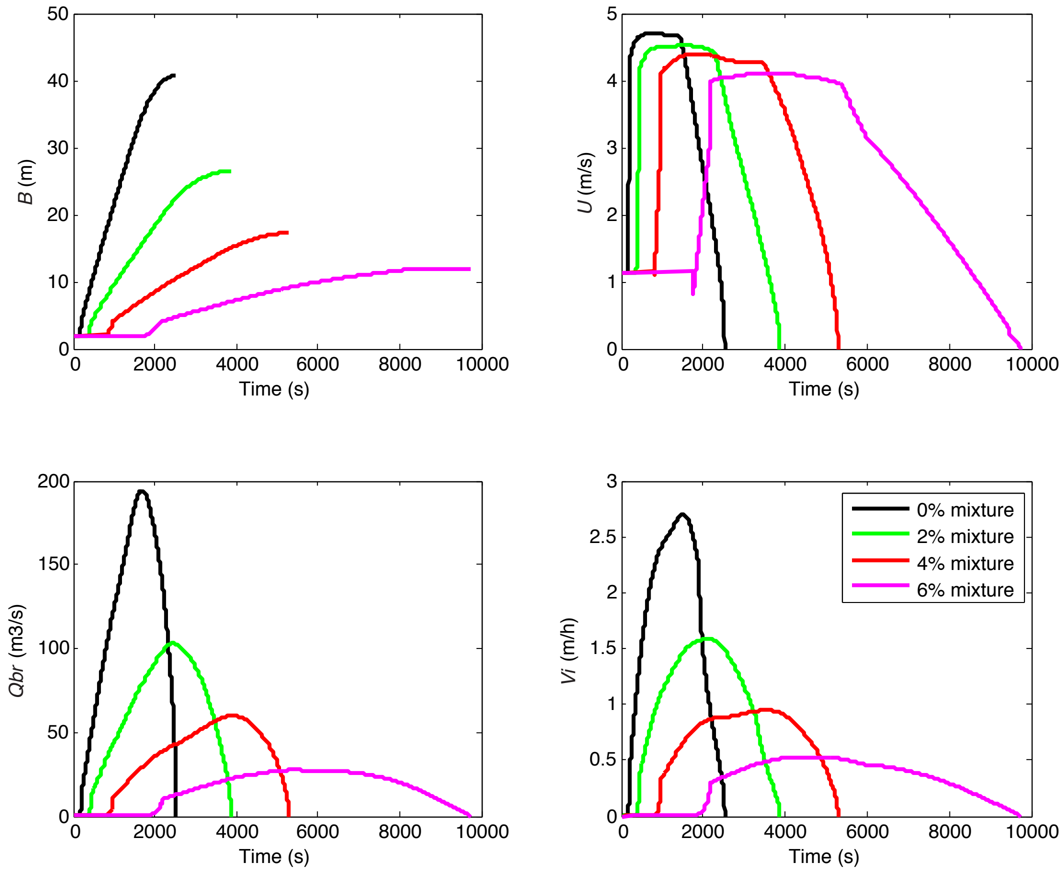

Figure 60: Comparison of the effectiveness of different bentonite mixtures in reducing the breach width, flow through the breach, the inundation velocity and duration of the breaching process.

In order to decrease the inundation rate slightly more, below a value of 0.5 m/h, the bentonite content should be above 6%. An exponential relationship between the reduction of the inundation velocity and the volume bentonite percentage is derived with data from Table 20. With this relationship, the needed volume bentonite percentage is guesstimated by means of extrapolation.

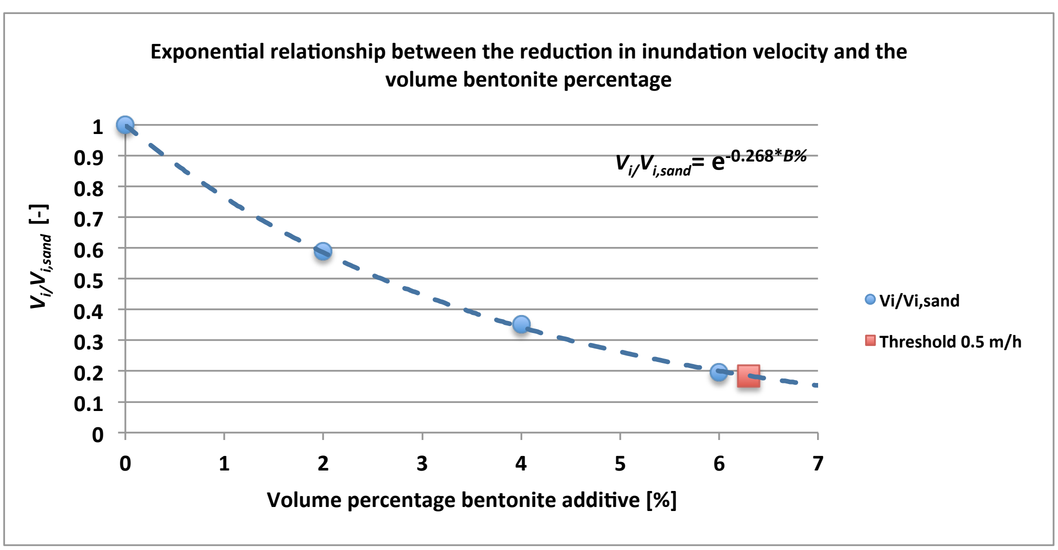

Figure 61: Exponential relationship between the reduction in inundation velocity and the volume bentonite percentage.

From this extrapolation, it seems that in order to achieve an inundation velocity equal to the threshold value, a reduction of the original inundation velocity of more than 80% is necessary. This gives a reduction ratio $V_i/V_{i,sand}$ of 0.185, which corresponds with a bentonite percentage of 6.3%. Thus, a sand-bentonite mixture with a bentonite volume percentage of 6.3% theoretically reduces the inundation velocity V_i below the threshold value of 0.5 m/h (see also Fig. 62). It should be noted that this result is true for the dike, polder and conditions of the Zwin'94 experiment. However, the general conclusion that bentonite mixtures significantly reduce the erosion of a breach is still valid.

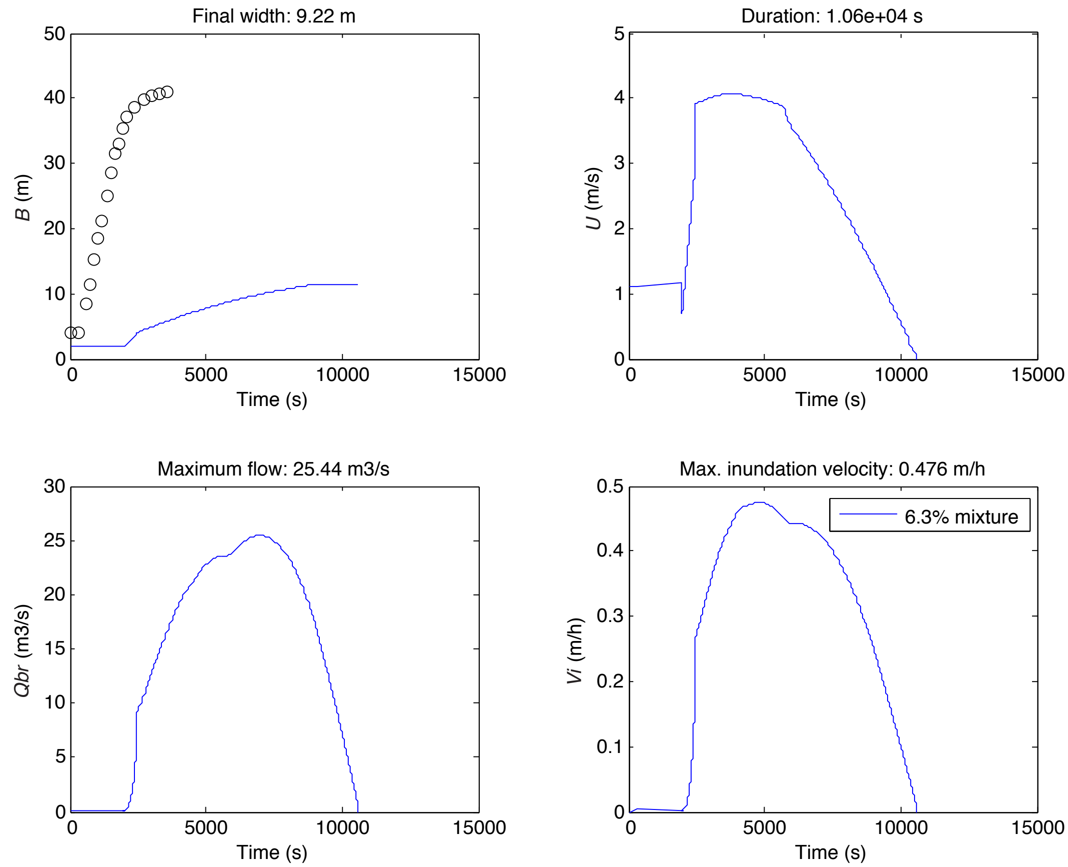

Figure 62: Breach width, flow through the breach, the inundation velocity and duration of the breaching process for a 6.3% mixture.

8.6 Effect of bentonite mixtures on the mortality

This section further clarifies the effectiveness of the bentonite mixtures. This time the effectiveness of the mixtures is measured by the reduction in mortality (with a sand core as reference), where the mortality is defined as the number of casualties divided by the number of people present in a flooding polder (Jonkman, 2004). A quick method for the estimation of loss of life caused by the flooding of low-lying areas protected by flood defences is used in this study. This method is proposed by Jonkman (2004) and uses mortality functions to relate the mortality amongst the exposed populations to the characteristics of the flood. The characteristics of the flood are water depth h, the depth-averaged flow velocity U and rise rate (or inundation velocity) V_i. The characteristics of the flood can be obtained from flood simulations. In this case the BRES model is used. In addition, the method also takes the possibilities for warning, evacuation and shelter, and the loss of shelter due to the collapse of buildings, into account. The output of the mortality functions was compared with historical flood events and it was shown that the functions give an accurate approximation of the number of observed fatalities during these events. For a more elaborate description and the assumptions reference is made to Jonkman (2004).

The mortality functions, based on empirical historical data, are defined as follows:

Given $V_i \geq 0.5$ m/h & $h < 1.5$ m or $V_i < 0.5$ m/h & $h > 0$ m, the mortality is calculated with:

$$M = 1.34 \cdot 10^{-3} * e^{0.59h} \tag{68}$$

If $V_i \geq 0.5$ m/h & $1.5 \leq h \leq 4.7$ m, the mortality is calculated with:

$$M = 1.45 \cdot 10^{-3} * e^{1.39h} \tag{69}$$

And if $V_i \geq 0.5$ m/h & $h > 4.7$ m, the mortality is:

$$M = 1 \tag{70}$$

From Eq.(68), Eq.(69) and Eq.(70) it can be concluded that the mortality rates are the highest in areas with a large water depth and a high rise rate (also called the inundation velocity). The combination of fast rising water and high water depths is disastrous. When the rising rate exceeds the threshold of 0.5 m/h it is called fast rising water and the number of fatalities will steadily increase. It is also important to note that people in the vicinity of the breach, where very high flow velocities are reached, often all become fatalities. This effect, however, is not taken into account in this study.

The effectiveness of the bentonite mixtures in reducing the mortality is demonstrated in a fictitious case for the Zwin'94 polder. Fictitious in the sense that the Zwin polder is (part of) an estuary and thus uninhabited. The results of the absolute mortality and the reduction in mortality as compared to the scenario with a pure sand core, are given in Table 21. From these results some conclusions can be drawn. A theoretical 6.3% bentonite mixture or higher will reduce the inundation velocity to values lower than 0.5 m/h (see also Fig. 62). For this reason Eq.(68) is used and a relatively low mortality is obtained (see also Table 21. In all other cases (with mixtures $\leq 6\%$ bentonite) the inundation velocity exceeds the threshold value. If the threshold of 0.5 m/h is exceeded Eq.(69) is used. This results in a significantly increase in mortality (see Table 21). By reducing the inundation velocity below the threshold value the maximum mortality is almost reduced by a factor 10. Indirectly this also means that the LIR (Localized individual risk) is reduced by a factor 10.

Table 21: Comparison of the mortality rate for several retardation mixtures.

Bentonite [%]	h_{max} [m]	Mortality rate [-]
0	2.4724	0.041
2	2.3725	0.039
4	2.2056	0.031
6	2.1072	0.027
6.3	2.1065	0.0046

9 | Case study Borssele

In this section a case study of a hypothetical breach in the sea dike near Borssele is presented. Borssele is located in the south of the Netherlands in the province of Zeeland (see also Fig. 63). In 2013, Horvat & Partners, studied the threats of an extreme high water event for EPZ, client and proprietor of the nuclear power plant in Borssele. The power plant is located along the Westerschelde and is protected by a sea dike. The Department of Hydraulic Engineering of Delft University of Technology contributed breach growth calculations of the larger Van Citterspolder I and the smaller Van Citterspolder II (see Fig. 63) to this study. In this chapter data from the breach growth study of Visser and Robijns (2013) is used as input in the BRES model. The BRES model uses a five-phased description of the breach growth process as proposed by Visser (1998) (see also Section. 2.4). Simulations with different core compositions (sand or sand-bentonite mixtures) of the sea dike and several initial breach heights are made and discussed. The main purpose of this study is to get more insight in the breach growth processes and the retardation of breach growth with sand-bentonite mixtures

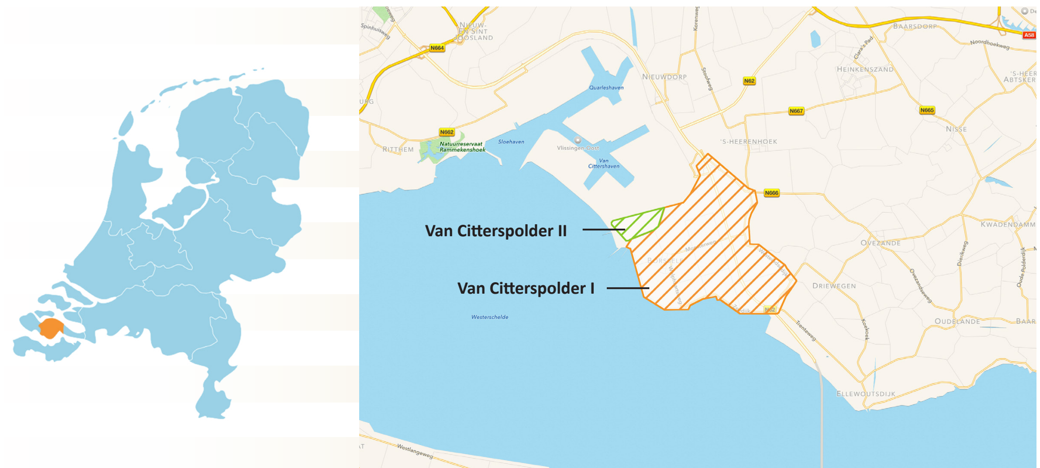

Figure 63: The Van Citterspolder I and II are located in the province of Zeeland in the Netherlands, partly adapted from Rijkswaterstaat (2014) .

9.1 Assumptions

In order to start the simulations and to study the breaching process in the sea dike of Borssele as a function of time, all the input parameters required by the BRES model had to be implemented. Some of these input parameters required assumptions. These assumptions are briefly discussed below. These assumptions concern the polder area, the initial breach, the secondary water protection system, the foreland of the dikes, the geometries of the dikes and the sediment characteristics of the dikes.

- **Polder area**
  The polder areas have been estimated from topographical maps and charts. The area of the larger Van Citterspolder I is about $9.8 \cdot 10^6$ m^2 and is positioned at a height of roughly NAP +1.0 m (NAP is the reference level in the Netherlands, at about mean sea level). The smaller Van Citterspolder II has a varying topography. The maximum area at a height of NAP +4.0 m is 670.000 m^2, reducing to 603.000 m^2 at a height of NAP +3.0 m and 425.000 m^2 at a height of NAP +1.6 m.

- **Initial breach**
  It is assumed that an initial breach in the crest of the dike is formed at the maximum water level of NAP + 7.0 m (with a maximum tidal and storm surge amplitude). The sand core of the dike is thus already exposed from the start of the simulations. The dimensions of the initial breach are: an initial breach width of 1.0 m at the bottom of the breach, the initial bottom of the breach is 0.5 m below the maximum water level (this level is varied in this study) and the side slope angles are 60°. In addition, it is assumed that the cover layers are not retarding the breaching process.

- **Secondary water protection system**
  In this study it is assumed that no secondary water protection system is present.

- **Foreland of the dikes**
  Based on the local geometry of the foreland of the Van Citterspolder II, it is assumed that the foreland is easily erodible by the flow caused by the breach. It is assumed that upstream of the breach a circular spillway is formed, which controls the breach inflow. In this case the spillway has a discharge coefficient of $\pi/2$. In addition, it is assumed that the foreland is located at NAP + 3.0 m. The Van Citterspolder I has no foreland. It is, however, conservatively assumed that there is a foreland present at NAP + 0.8 m. In this particular case, it is assumed that upstream of the breach a spillway is formed with a discharge coefficient of 1.

- **Geometries of the dikes**
  The BRES model uses a simplified trapezoidal dike geometry. For this reason the geometries of the dike segments are schematized. The width of the crest, the height of the crest, the horizontal and vertical positions of the toe and heel of the dikes are assumed to be equal over the total length of the dike segments. In addition, the angles of the inner slopes and outer slopes are determined by connecting the the location of the inner crest with the heel of the dike and the crest with the toe of the dike.

- **Sediment characteristics of the dike**
  Some soil samples were taken in the dike segment of the Van Citterspolder II. These soil samples indicated that fine sediment with a particles size between 0.150 mm and 0.210 mm are present in this dike segment. However, the client preferred conservative estimations. For this reason, courser sand diameters were chosen, because courser sediment diameters lead to more erosion and larger breach widths. In this particular case, the sediment diameters of the sand as found in the Zwin'94 experiment were used (as suggested by Visser and Robijns (2013)).

9.2 Model setup

In this section the settings of the model are discussed. An overview of the imposed boundary conditions is given in Fig. 64. The boundary condition is composed of a tidal effect and surge effect. The combined effect represents a rare 1/10.000 storm event. The total variation in water level in time h_t is given by Eq.(71).

$$h_t = h_0 + h_a \cdot cos(\frac{2 * \pi * t}{T_a}) + h_s \cdot cos^2(\frac{\pi * t}{T_s}) \tag{71}$$

in which h_0 denotes the average water level, h_a the first order tidal amplitude, T_a the standard duration of the astronomical tide, h_s the maximum surge height, T_s the typical storm duration and t the time. The values of these parameters are given in Table 22. In this case the maximum water level equals 7 m ($h_0 + h_a + h_s$). In addition, it is assumed that an initial breach is formed at the maximum water level. After 17.5 hours the surge effect is reduced to zero again and the water level signal returns to its astronomical character (see Fig. 64).

Table 22: Water level and sediment characteristics for the Borssele case study.

Parameter	Value
Average waterlevel h_0 in [m]	NAP - 0.08
Amplitude of the semi-diurnal tide h_a in [m]	1.93
Storm surge amplitude h_s in [m]	5.15
Duration of the surge conditions T_s in [hr]	35
D_{10} in [mm]	0.155
D_{50} in [mm]	0.185
D_{90} in [mm]	0.285

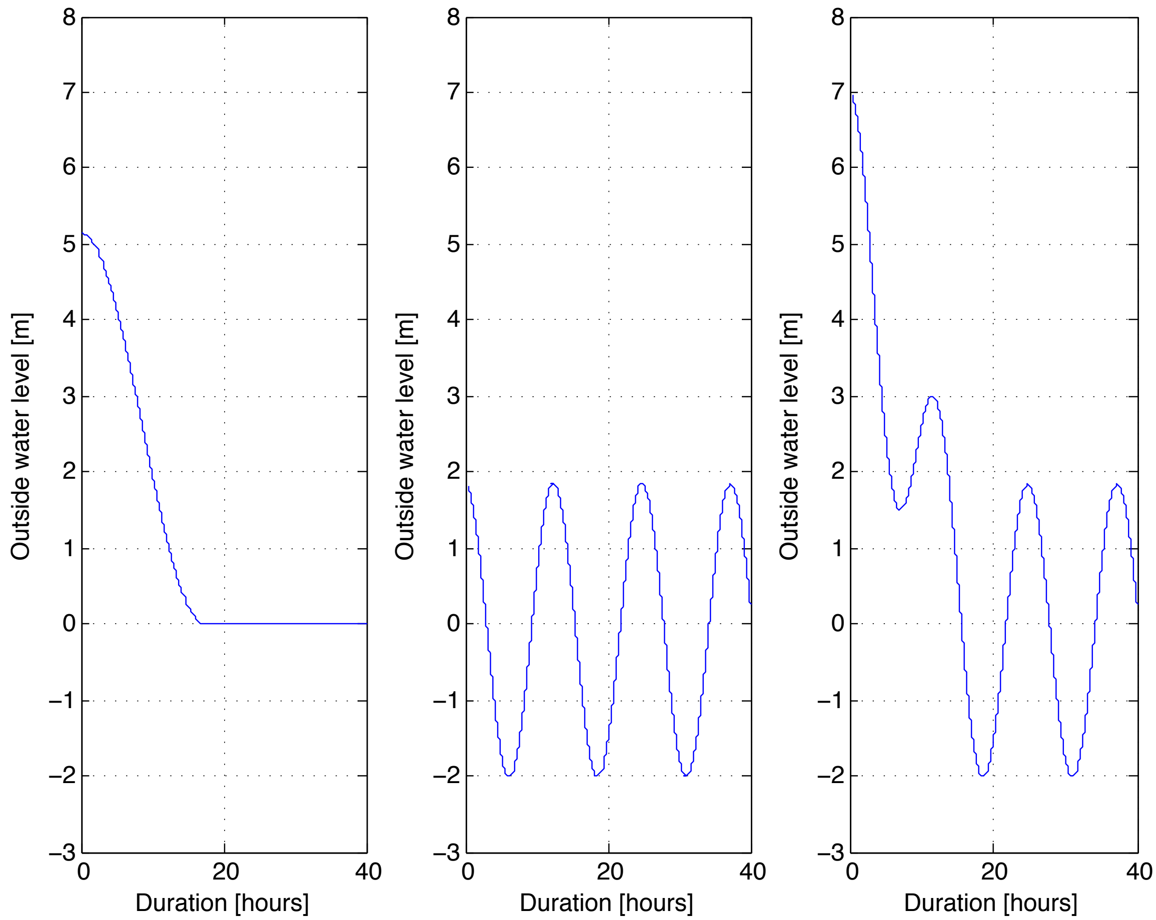

Figure 64: The water level signal (right) is composed of a tidal effect (middle) and a surge effect (left).

Regarding the geometry of the dikes of both polders, data from Visser and Robijns (2013) are used. These are given in Table 23 and Table 24. The definitions - as used in Table 23 and Table 24 - are proposed by Visser (1998) and are visualized in Fig. 65. Finally, the sediment diameters are given in Table 22.

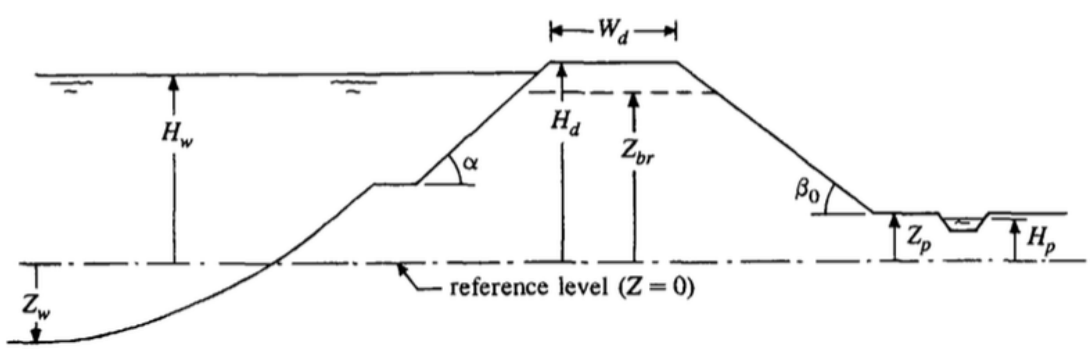

Figure 65: Schematization of the system including a cross-section of the dike as proposed by Visser (1998).

Dike segment Van Citterspolder I

Table 23: Characteristic parameters of the Borssele case study for the Citterspolder I.

Parameter	Value
Seaside bottom level Z_w in [m]	NAP + 0.8
Polder bottom level Z_p in [m]	NAP + 1.0
Initial polder water level H_p in [m]	NAP + 1.0
Crest height H_d in [m]	NAP + 11.4
Bottom of the breach Z_{br} in [m]	NAP + 6.5
Initial breach width at the bottom b in [m]	1.0
Crest width W_d in [m]	5.0
Outer slope α in [°]	12.53
Inner slope β in [°]	19.65
Side slope angle γ in [deg]	60
Angle of repose ϕ in [deg]	32
Water temperature T in [°C]	17
Initial porosity n_0 in [-]	0.40
Sheared porosity n_i in [-]	0.48
Density of the water ρ_w in $[kg/m^3]$	1025
Density of the sand ρ_s in $[kg/m^3]$	2650

Dike segment Van Citterspolder II

Table 24: Characteristic parameters of the Borssele case study for the Citterspolder II.

Parameter	Value
Seaside bottom level Z_w in [m]	NAP + 3.0
Polder bottom level Z_p in [m]	NAP + 3.3
Initial polder water level H_p in [m]	NAP + 1.6
Crest height H_d in [m]	NAP + 10.6
Bottom of the breach Z_{br} in [m]	NAP + 6.5
Initial breach width at the bottom b in [m]	1.0
Crest width W_d in [m]	3.8
Outer slope α in [°]	9.95
Inner slope β in [°]	20.32
Side slope angle γ in [deg]	60
Angle of repose ϕ in [deg]	32
Water temperature T in [°C]	17
Initial porosity n_0 in [-]	0.40
Sheared porosity n_i in [-]	0.48
Density of the water ρ_w in $[kg/m^3]$	1025
Density of the sand ρ_s in $[kg/m^3]$	2650

9.3 Run plan

This section contains the run plan for the simulations of the Borssele case study. In these simulations the core composition (sand or sand-bentonite mixtures) of the sea dike and the initial breach height are varied. The maximum water level and storm duration are kept constant. The run plan is divided in two scenarios: Scenario A for the dike segment of the Van Citterspolder I and Scenario B for the dike segment of the Van Citterspolder II (see also Table 25 and Table 26). The initial breach bottom level $Z_{br,0}$ is calculated by subtracting the initial breach height from the maximum high water level.

Scenario A - Van Citterspolder I

Table 25: Run plan for Scenario A.

Run	Bent. [%]	Initial breach height [m]	Initial breach bottom level $Z_{br,0}$ above NAP [m]
A-1	0	0.5	6.5
A-2	2	0.5	6.5
A-3	4	0.5	6.5
A-4	6	0.5	6.5
A-5	0	1.0	6.0
A-6	2	1.0	6.0
A-7	4	1.0	6.0
A-8	6	1.0	6.0
A-9	0	2.0	5.0
A-10	2	2.0	5.0
A-11	4	2.0	5.0
A-12	6	2.0	5.0

Scenario B - Van Citterspolder II

Table 26: Run plan for Scenario B.

Run	Bent. [%]	Initial breach height [m]	Initial breach bottom level $Z_{br,0}$ above NAP [m]
B-1	0	0.5	6.5
B-2	2	0.5	6.5
B-3	4	0.5	6.5
B-4	6	0.5	6.5
B-5	0	1.0	6.0
B-6	2	1.0	6.0
B-7	4	1.0	6.0
B-8	6	1.0	6.0
B-9	0	2.0	5.0
B-10	2	2.0	5.0
B-11	4	2.0	5.0
B-12	6	2.0	5.0

9.4 Results

In this section the results of the different simulations are presented. Table 27 and 28 contain values for the maximum breach width B_{max}, the maximum water level in de polder H_p, the maximum inundation velocity V_i and mortality for each scenario. Appendix G provides detailed information - for the simulations with an initial breach height of 2.0 m - of the outside water level in time, the water level in the polder in time, the height of the breach in time, the discharge in time and the width of the breach in time.

Table 27: Duration of the breaching process, the breach width, the flow through the breach and the rise rate for several retardation mixtures in the Van Citterspolder I.

Run	Bent. [%]	B_{max} [m]	$V_{i,max}$ [m/h]	$H_{p,max}$ [m] *	Mortality [-]
A-1	0	179.3	0.67	1.97	0.022
A-2	2	50.6	0.20	1.02	0.002
A-3	4	- **	-	-	0.000
A-4	6	-	-	-	0.000
A-5	0	187.1	0.74	2.17	0.030
A-6	2	69.0	0.27	2.33	0.005
A-7	4	73.2	0.06	0.40	0.002
A-8	6	-	-	-	0.000
A-9	0	156.8	0.77	2.26	0.034
A-10	2	76.9	0.31	1.42	0.005
A-11	4	86.4	0.10	0.57	0.002
A-12	6	28.3	0.02	0.12	0.001

* The polder water level is corrected by subtracting the the initial polder water level, since the bottom polder level is already located at NAP +1.0 m.
** When no value is present in the column, this simply means that the outside water level is already lower than the bottom of the breach Z_{br} in phase 3. The breach is no longer growing vertically and no water is entering the polder.

Table 28: Duration of the breaching process, the breach width, the flow through the breach and the rise rate for several retardation mixtures in the Van Citterspolder I.

Run	Bent. [%]	B_{max} [m]	$V_{i,max}$ [m/h]	$H_{p,max}$ [m] *	Mortality [-]
B-1	0	69.0	4.88	4.63	0.904
B-2	2	75.9	2.49	3.36	0.155
B-3	4	-**	-	-	0.000
B-4	6	-	-	-	0.000
B-5	0	114	5.29	4.76	1.000
B-6	2	40.7	2.78	3.71	0.252
B-7	4	58.8	0.77	1.43	0.003
B-8	6	-	-	-	0.000
B-9	0	70.8	5.30	4.82	1.000
B-10	2	70.9	3.05	4.05	0.404
B-11	4	20.3	1.34	2.40	0.041
B-12	6	-	-	-	0.000

* The polder water level is corrected by subtracting the initial polder water level, since the bottom polder level is already located at NAP +1.6 m.
**When no value is present in the column, this simply means that the outside water level is already lower than the bottom of the breach Z_{br} in phase 3. The breach is no longer growing vertically and no water is entering the polder.

From Table 27 and 28 it can be concluded that the inundation velocity V_i, the water level in the polder H_p and the mortality are positively influenced by the bentonite additive in the core of the dike. In both polders the safety increases with a factor 2.5 to 10 when a 2% sand-bentonite mixture is added to the core. Higher percentages of bentonite in the core of the dike increase the safety even more and in some cases even completely stop the breach growth (this also depends on the initial breach bottom level). The main difference between the larger Van Citterspolder I and the smaller Van Citterspolder II is that the smaller polder fills much faster and reaches significantly higher water levels in the polder.

Fig. 66 and Fig. 67 show the development of the breach and the development of the breach bottom in time. Although the final breach width is not always reduced with increasing percentages of bentonite additive in the core, the growth of the breach in time is slower with increasing bentonite percentages. This automatically implies that less water is flowing into the polder over time, which affects the inundation velocity V_i. The less water is flowing into the polder, the longer it takes to fill the polder. In the end this might also lead to a lower polder water level. This conclusion is also supported by the development of the breach bottom in time. Sand-bentonite mixtures with increasing percentages significantly increase the duration of the first three phases (from minutes to few hours). In Fig. 66 and Fig. 67 the end of phase 3 can be observed when the vertical erosion of the bottom of the breach stops and thus becomes a flat line.

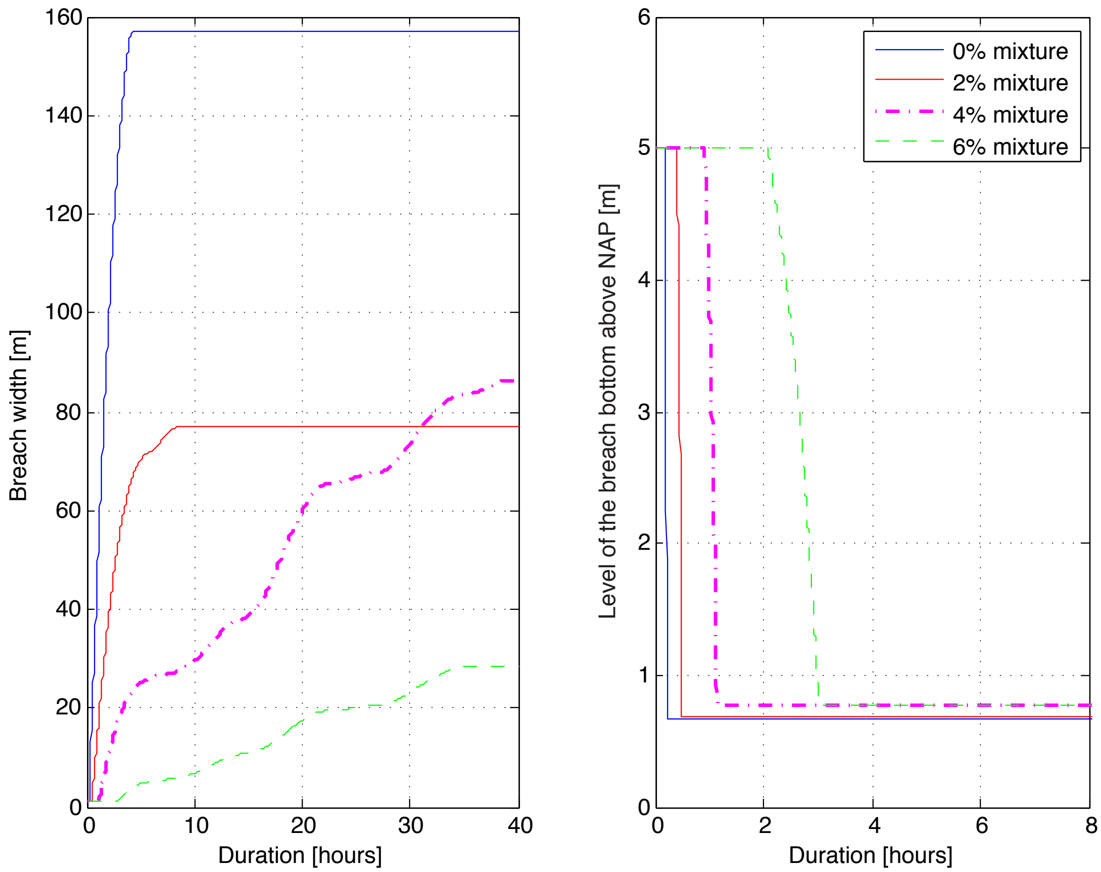

Figure 66: (a) The development of the breach width in time and (b) the development of the breach bottom in time for several sand-bentonite mixtures in the Van Citterspolder I.

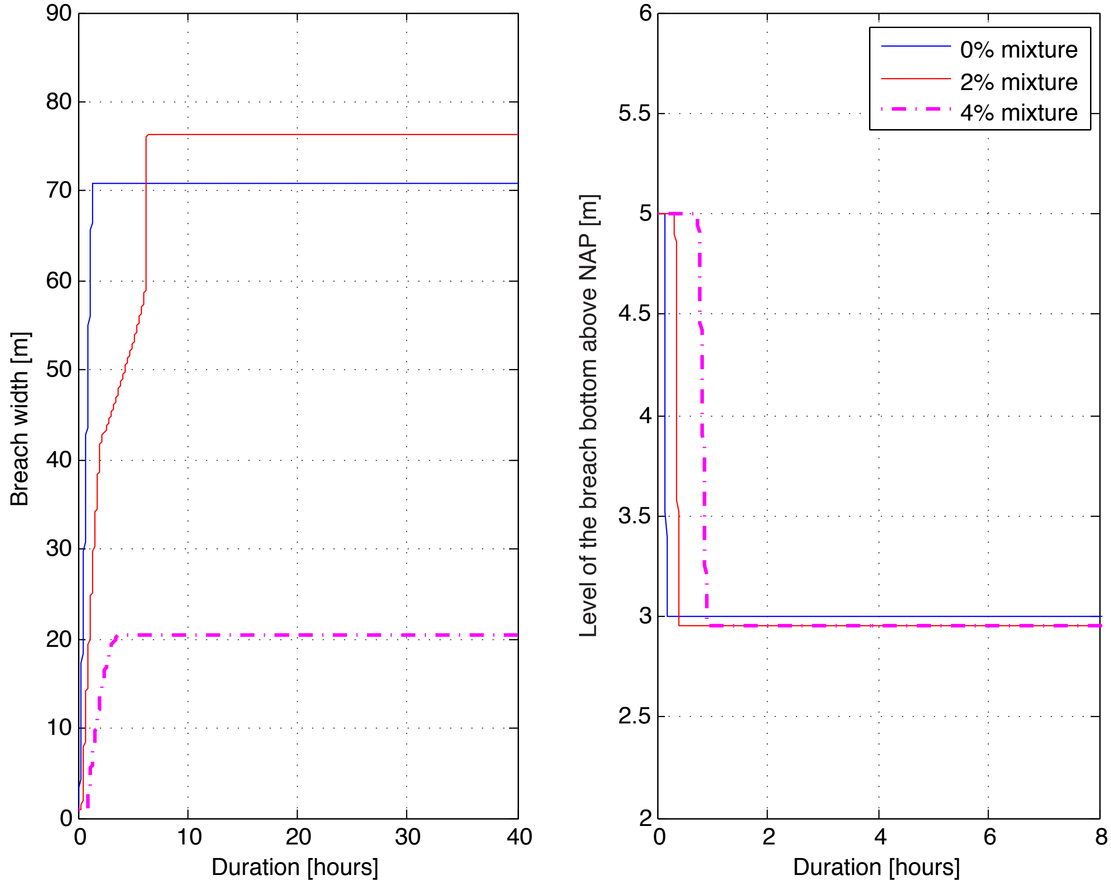

Figure 67: (a) The development of the breach width in time and (b) the development of the breach bottom in time for several sand-bentonite mixtures in the Van Citterspolder II.

Two important remarks about this case study are that the results - especially the development of the breach width in time - are very sensitive to the side slope angle of the breach and that a secondary water protection system in the Van Citterspolder I is present in reality. This means that the polderlevel in the Van Citterspolder I will not easily reach water levels above NAP +4.0 m, because the water will overflow the secondary dike into the Van Citterspolder II.

To conclude, the polder area has a big influence on the inundation velocity and the polder water levels. A small polder fills much faster and reaches significantly higher polder levels. In both the Van Citterspolder I and the Van Citterspolder II the safety increases with a factor 2.5 to 10 when a 2% sand-bentonite mixture is added to the core. Higher percentages of bentonite additive increase the safety even more and in some cases even completely stop the breach growth.

10 | Conclusions & Recommendations

10.1 Conclusions

The objective of this research has been to determine if and how bentonite would be able to reduce the erosion velocity of sand under high flow velocity conditions. In this chapter, the conclusions are presented in which reference is made to the hypotheses of Chapter 4.

At high flow velocities (>2 m/s) the erosion velocity depends on the properties of the soil mass, not only on the properties of a particle. Important parameters of the soil mass are the permeability and dilatancy. From the erosion experiments it can be concluded that the effect of dilatancy, which plays a role at higher flow velocities, indeed hinders erosion and thus reduces the erosion velocity at higher flow velocities (supporting hypothesis 1). This is caused by volume change, as a result of shearing of the bed. The volume change generally leads to a drop in pore pressure in the top of the sand bed. This pressure drop introduces a hydraulic gradient and thus an inflow of water that hinders the entrainment of sediment.

The permeability also significantly influences the erosion behaviour. Falling head tests were executed to determine the effectiveness of adding bentonite to a dike with a sand core. Adding a certain amount of bentonite to sand certainly yields a high decrease in permeability (supporting hypothesis 4). This is the result of the swelling potential of the bentonite, which is assumed to fill the empty space between the sand particles. It appears that the most significant decrease in permeability happens with bentonite contents up to 6% volume percentage (see also Fig. 42). Adding more bentonite still reduces the permeability, but the overall effect is starting to flatten out for bentonite contents higher than 8%. Overall, the approximate decrease in permeability is almost three orders of magnitude (from 10^{-4} to 10^{-7}) with bentonite volume percentages up to 10%

Direct shear tests were executed to determine the friction angle and (apparent) cohesion of the sand and several sand-bentonite mixtures. The bentonite percentages varied from 0 to 10%. As expected low cohesion values (< 3 kPa) and friction angles in the order of 33 - 43 degrees were observed for mixtures with a bentonite volume content lower than 6%. In contrast, a sharp increase in cohesion and significant drops in friction angles were expected for higher bentonite volume percentages (>6%). At a certain point the sand particles were expected to loose direct contact with neighbouring particles and consequently lose its strength characteristics. However, this appeared not to be the case (see also Fig. 44 and Fig. 45). The only possible explanation is that the sand grains still had direct contact with neighbouring particles. Hence, sand-bentonite mixtures with a bentonite volume content up to 10% still show sand-like behaviour (hypothesis 2). This indirectly indicates that the strength characteristics of a dike core will not be altered.

Thirteen different erosion tests runs were executed. During these tests, the volume percentage of bentonite additive, the diameter of the sand (D_{50} of 0.256 mm and a D_{50} of 0.150 mm) and the intended flow velocity (1 and 2 m/s, respectively) were varied. In order to objectively calculate the effectiveness of a bentonite additive, the erosion velocity of the bed of a sand-bentonite mixture was compared with the erosion velocity of a sand mixture at the same mean flow velocity. This procedure was applied to two different methods. The first one related the erosion velocities to the mean flow velocities squared U^2 and the second related the erosion velocities to the corrected bed shear stresses. Both methods show a similar trend. Significant reductions in erosion velocity are obtained by adding bentonite to a sand mixture (see Fig. 34 and Fig. 37). A 2% sand-bentonite mixture already reduces the original erosion velocity by about 50%, a 3% or 4% mixture by 50 to 65 % and a 6% mixture at least by 90%. Finally, it has to be added that the reproducibility of the tests has been confirmed to be reasonably well (supporting hypothesis 4 and hypothesis 6).

An additional remark is that it seems that, in general, a higher bentonite content leads to a steeper positive relationship between the bentonite content and v_e/k (see Fig. F1 and Fig. F2). This basically means that the high erosion regime is generally reached faster with sand-bentonite mixtures than with pure sand only. Finally, an empirical relationship between the reduction of the erosion velocity and the reduction of the permeability was derived. This relation indicates a relatively strong dependence of the erosion velocity on the permeability ($k^{0.54-0.63}$) depending on the method used for determination of the reduction in erosion velocity (supporting hypothesis 4).

A literature study concerning the erosion behaviour of sand-bentonite mixtures, has resulted in the conclusion that very few data are available. At higher flow velocities these are even non-existent. For this reason it has been decided to collect all the data currently present. An analysis of the data collection clearly indicates that it is very difficult to predict and verify the absolute reduction in erosion velocities for different bentonite mixtures. Large variances in bed shear stresses and corresponding erosion velocities exist in the data sets and a comparison based on absolute values of (corrected) shear stresses is deemed not to be reliable enough. The significant differences in bed shear stresses are most likely caused by the difficulty in accurately measuring the energy loss of the system.

The Van Rhee erosion function (see Van Rhee, 2010) has been adapted to the experimental data of the erosion tests. This erosion function is chosen, because this function includes the hindered erosion process. Both the dilatancy and permeability effects are included. A sensitivity analysis has been executed and indicated that an additional coefficient c in front of the permeability could be used to fit the data. It appears that the best fits are generally possible with a value of c ranging from 1/3 to 1 (see Fig. 57 and Fig. 58). The adapted erosion function also includes an empirically derived (continuous) relation between the permeability of the mixture and the volume percentage of added bentonite. This study also discusses some possible causes of the discrepancies between the experimental data and the results predicted by the erosion function of Van Rhee (2010).

The BRES-Visser model, calibrated with data from the Zwin'94 experiment has been used to model the performance of the bentonite additives. The adapted erosion function (with a coefficient c of 1), including the relationship between the bentonite content and the permeability of the mixture, has been implemented in the BRES model. The BRES model, using the adapted erosion function, is able to accurately predict the breaching process of the Zwin'94 experiment (hypothesis 5). The data from the Zwin'94 experiment has also been used as a reference scenario for a dike with a sand core. The effects of the retardant sand-bentonite mixtures have been compared to this reference scenario. The comparison is based on breach width, flow through the breach, the inundation velocity and duration of the breaching process. Significant reductions of these parameters are realized with increasing bentonite percentages (see Fig. 60). By reducing the inundation velocity below a threshold value of 0.5 m/h, the mortality and the LIR (Localized Individual Risk), can theoretically be decreased by a factor 10 (hypothesis 6). A sand-bentonite mixture with a bentonite content of 6.3% would be necessary to reduce the inundation velocity to a value below 0.5 m/h for the fictitious case of the Zwin'94 experiment. It should be noted that this result is true for the Zwin'94 experiment. However, the general conclusion that bentonite mixtures significantly reduces the erosion of a breach is still valid.

During the experiments many expected and unexpected occurrences were observed. These findings may add incremental value to the dataset and could be used as guidelines in designing other erosion experiments. The following occurrences, seen during and after the erosion experiments, have been discussed in this study: scour holes, bed forms, inhomogeneity of the bed, softening of the clay, mass erosion and erosion with even steeper bottom slopes. The most important conclusion being that it is very hard to get a perfectly homogeneous sand-bentonite mixture with sand-bentonite mixtures below 6% of added bentonite (hypothesis 7). Inhomogeneity in the bed in turn leads to local weak spots and turbulent flows. The turbulent flows disturbed further measurements due to significant and severe erosion, but may certainly happen in case of a real breach (hypothesis 3). In addition, visual observations and camera recordings indicated a mass erosion of the bed. Mass erosion is generally characterized as cohesive behaviour. The geotechnical results and visual observations clearly contradict each other (contradicting hypothesis 2).

To conclude, sand bentonite mixtures are able to significantly reduce the erosion velocity. The effects of dilatancy and a decrease in permeability have a large impact on the erosion velocity. This is already noticeable at very low percentages of added bentonite. A sand-bentonite mixture with a bentonite volume content of 6% substantially reduces the erosion velocity (also at high flow velocities) and the mixture generally has a reasonably good homogeneity. With lower percentages of added bentonite the homogeneity is less reliable, which might be a considerable practical limitation. Sand-bentonite mixtures with a bentonite content up to 6% also still show sand-like behaviour, indicating that the strength characteristics of a dike will not alter. Finally, case studies with the BRES model indicate that an increase in safety level by a factor of 10 can be achieved using sand-bentonite mixtures in the core of a dike and that the polder area has a big influence on the inundation velocity and the polder water levels. In both the Van Citterspolder I and the Van Citterspolder II the safety increases with a factor 2.5 to 10 when a 2% sand-bentonite mixture is added to the core. Higher percentages of bentonite additive increase the safety even more and in some cases even completely stop the breach growth, because the outside water level drops faster than the breach grows vertically. In the Zwin'94 case study a 6.3% sand-bentonite mixture increases the safety by a factor 10.

10.2 Recommendations

During and after different experiments with sand-bentonite mixtures, understanding has been obtained which can be useful for future research. These recommendations are written with the objective to contribute to future research and especially the applicability of sand-bentonite mixtures in sand dikes to retard the breaching process.

Verification of the soil characteristics of higher percentage sand-bentonite mixtures with triaxial tests

The continuous loading method for the direct shear tests was simply chosen in view of time. Although the normal and shear stress couples give a reasonable good estimate of the peak shear stress under a specific normal load, the samples were not sheared until failure. An increase in cohesion and significant drops in friction angles were expected for higher bentonite volume percentages (>6 %), because at a certain point the sand particles were expected to loose direct contact with neighbouring particles and consequently lose its strength characteristics. Furthermore, visual observations and camera recordings of the erosion tests indicated mass erosion of the bed at mixtures with higher bentonite contents. Mass erosion is generally characterized as cohesive behaviour. The geotechnical results and visual observations clearly contradict each other. For these reasons it is advised to execute some triaxial tests for sand-bentonite mixtures with bentonite volume contents of 6% and higher.

Estimation of the economical consequences and reduction of consequences by using sand-bentonite mixtures in the core of a dike

Although this study gives a clear indication of the effectiveness of bentonite in retarding the breach growth and corresponding mortality, the economical consequences have not been taken into account. However, it is expected that the economical consequences will only be reduced in case the water level in the inundated polder stays really low or the polder is never inundated. Theoretically this is possible by reducing the breaching process in such a way that the outside water level already returns to its normal level before the dike is severely breached. By retarding the breaching process, it is also possible to repair the dike segment or start up mitigation procedures in time. This most certainly has a positive effect on the economical consequences.

Investigate if the erosion function of Van Rhee (2010) generally overestimates the erosion velocity and might possibly not fully capture all the physical processes

Discrepancies were found between the experimental data and the results predicted by the erosion function of Van Rhee (2010). This may be due to the introduction of inaccuracies in the experimental setup and procedures. However, it may also be that the erosion function of Van Rhee (2010) does not fully capture all the physical processes. Three possible causes for the overestimation of the erosion function of Van Rhee (2010) have been proposed in this study. 1) As a consequence of the experimental setup the depth-averaged flow velocity is used in the erosion function of Van Rhee (2010). However, the near-bed flow velocity is the governing parameter in sediment transport. It is often assumed that the near-bed flow velocity and depth-averaged flow velocity are related by a log-law flow velocity profile. However, it is expected that the velocity profile is significantly influenced by sediment transport, especially, sediment transport (sheet flow transport) under high flow velocities. The validity of using the depth-average velocity as an input parameter for the erosion rate can be tested by measuring the entire velocity profile during erosion tests. The velocity profile can, for instance, be continuously measured with an ADV (Acoustic Doppler Velocity) meter. Unfortunately, this was not a viable option in this study. 2) The sediment transport capacity of the flow is reached, which limits the erosion function. For this reason, it might be useful to couple the erosion function of Van Rhee (2010) to a sediment transport equation, which incorporates the carrying capacity of the flow and thus limits the erosion rate. 3) There is a difference in erosion behaviour between conduit flow and open channel flow setup caused by a unknown physical process.

Finding an approach to accurately measure the friction coefficient (energy loss) in order to determine the bed shear stress

The data analysis of the erosion tests have clearly indicated that it is very difficult to predict and verify the absolute reduction in erosion velocity for different bentonite mixtures. Large variances in bed shear stresses and corresponding erosion velocities exist in the existing data sets and a comparison based on absolute values of (corrected) shear stresses is deemed not to be reliable enough. The significant differences in bed shear stresses are most likely caused by the difficulty in predicting the friction coefficient. The friction coefficient is often linked to a bed roughness and is an important unknown during the experiments. However, the friction coefficient has to be linked to the energy loss in the system and not only the bed roughness. Although many methods are available to determine the friction coefficient, many are simply based on the bed roughness and thus not account for all physical processes. High sediment concentrations near the bed (and thus a higher viscosity) lead to higher energy losses, which have to be accounted for in the friction coefficient as well. In order to get more reliable values for the bed shear stresses, the energy loss of the system has to be measured more accurately.

Execute flume experiments to verify the applicability of side-wall correction methods in supercritical flow conditions

The side-wall correction significantly influences the corrected bed shear stresses. Since the corrected bed shear stresses (derived from the erosion experiments) are relatively low in comparison with theoretical bed shear predictions, it is hypothesized that the used side-wall correction methods might be over-correcting the bed shear stresses at higher flow velocities and might not be perfectly valid at flow velocities of about 2 m/s and higher. Hence, flume experiments are recommended to further investigate the extend of the side-wall correction in supercritical flow conditions.

Execute flume experiments to accurately calculate the wall friction factor of the flume

In this study, bed shear stresses have been corrected for side-wall effects using general empirical wall friction coefficients (for a glass wall and a plywood wall) or general empirical formulations. It might be more accurate to measure the wall friction factor for each specific experimental setup.

Finding an approach to create a homogeneous and compacted sand-bentonite mixture to increase the practical feasibility

During the preparation and design phase it was assumed that the bed would be perfectly homogenous. However, the preparation of the bed and sample specimens was not a perfectly robust method and was prone to imperfections (especially for sand-bentonite mixtures with a bentonite content $< 6\%$). As a result of an inhomogeneous bed, local weak spots became apparent and rapid mass erosion would soon follow. In contradiction, also some local stronger parts in the bed were visible. This might be a serious limitation for the practical implementation and future research into mixing and compaction methods for this application (on large scale) is recommended.

Verification of the breaching process on a prototype dike segment with a sand-bentonite core

Up to this moment, the breaching process is predicted with the BRES model combined with the erosion behaviour obtained during the erosion tests. Although this seems a perfectly logical procedure, breaching tests should be executed as a verification step. These breaching tests might also increase the predictability of the (absolute) reduction in erosion rate of the sand-bentonite core. So far, it has also been assumed that the sand-bentonite mixtures were fully saturated. The reality, however, might be different. Most of the time the dike segment is only party saturated and the bentonite will not be activated above the phreatic line. In this case the retardation of the breach growth will be less.

Future erosion experiments at high flow velocities (>2 m/s)

A final remark has to be made about the flume setup. During the tests it appeared that quite some height was needed in the flume in order to reach the required high flow velocities. To reach high equilibrium flow velocities steep bed slopes are needed (in case of supercritical flow). In order to reach flow velocities $>$ 2 m/s it it is strongly advised to look for open channel flumes with a height clearly exceeding 40 cm or design experiments with a conduit flow setup. Although it is easier to reach high flow velocities in a conduit setup, it will be hard to prepare a reasonably homogeneous sand-bentonite bed and thus practically infeasible. Furthermore, it is recommended to check the environmental regulations of the laboratory and take the discharging of the bentonite out of the experimental system in consideration. Bentonite is characterized by its very small particle size and cannot be easily filtered out of the water.

References

Anagnostopoulos, A. (2005). Laboratory study of an injected granular soil with polymer grouts. *Tunelling and Underground Space Technology, Issue 20, pp. 525-533.*

Anakari, K. (2008). Investigating hypoplasticity. parameter determination and numerical simulation. Master's thesis, Delft University of Technology.

Auel, C., Albayrak, I., and Boes, R. (2014). Turbulence characteristics in supercritical open channel flows: Effects of froude number and aspect ratio. *Journal of Hydraulic Engineering, 140, 381-396.*

Bagnold, R. A. (1956). The flow of cohesionless grains in fluids. *Philosophical Transactions of the Royal Society of London. Series A, Mathematical and Physical Sciences, 249(964):pp. 235–297.*

Bardet, J. (1997). *Experimental Soil Mechanics*, volume 1 edition. Prentice Hall.

Barends, F. and Uffink, G. (2011). *Mechanics and Transport of Flow through Porous Media: Online syllabus.* Delft University of Technology.

Bisschop, F., Visser, P., van Rhee, C., and Verhagen, H. (2010). Erosion due to high flow velocities: A description of relevant processes. *Proc. 32nd Int. Conf. Coastal Eng, 1:32, 1:32, Shanghai; China.*

Bosboom, J. and Stive, M. (2013). *Coastal Dynamics I, Lecture Notes CIE 4305.* VSSD. ISBN: 978-90-6562-286-0.

CEN (2004). Geotechnical investigation and testing - laboratory testing of soil - part 10: Direct shear tests (iso/ts 17892-10:2004). Technical report, CEN, European Committee for Standardization.

Chalermyanont, T. and Arrykul, S. (2005). Compacted sand-bentonite mixtures for hydraulic containment liners. *Songklanakarin J. Sci. Technol., 2005, 27(2) : 313-323.*

Cheng, N. and Chua, L. H. C. (2005). Comparison of sidewall correction of bed shear stress in open-channel flow. *Journal of Hydraulic Engineering, ASCE, 131(7), 605-609.*

Daugherty, R. L., Franzini, J. B., and Finnemore, E. J. (1989). *"Fluid mechanics with engineering applications.* McGraw-Hill Book Company, Singapore.

De Baets, S. and Poesen, j. (2010). Emperical models for predicting the erosion reducing effects of plant roots during concentrated flow erosion. *Geomorphology, Issue 188, pp. 425-432.*

De Bruijn, K. (2009). Slachtofferrisico's door overstromingen, voorstel voor indicatoren voor gebruik in de discussie over nieuwe normen voor de waterkeringen. Technical report, Deltares.

De Jong, J., Fritzges, M., and Nüsslein, K. (2006). Microbially induced cementation to control sand response. *Journal of Geotechnical and Geoenvironmental Engineering, 132(11).*

De Vet, P. (2014). Modelling sediment transport and morphology during overwash and breaching events. Master's thesis, Delft University of Technology, The Netherlands.

Deltacommissie (2008). Working together with water: A living land builds for its future. Technical report, Deltacommissie.

Deltares (2011). Analyse van slachtofferrisico's waterveiligheid 21e eeuw (in Dutch). Technical report, Deltares.

Einstein, H. A. (1941). "formulas for the transportation of bed load.". *Transactions, ASCE, 133-149.*

Engelund, F. and Hansen, E. (1967). A monograph on sediment transport. Technical report, Technical University of Denmark.

Fernandez-Luque, R. (1974). Erosion and transport of bed-load sediment. Technical report, KRIPS Repro BV, Meppel ,The Netherlands.

Ferris, F., Stehmeier, L., Kantzas, A., and Mourits, F. (1997). Bacteriogenic mineral plugging. *The Journal of Canadian Petroleum Technology, 35(8).*

Foortse, B. (2013). Bres-model: Onderzoek naar de mogelijkheden om het bres-model te verbeteren (in Dutch). Bachelor Thesis, Delft University of Technology, The Netherlands.

Gailani, J. (2001). Effects of bentonite clay on sediment erosion rates. Technical report, DOER.

Galapatti, R. (1983). A depth-integrated model for suspended transport. In *Communications on Hydraulics, Rep. 83-7, Dept. Civil Eng., Delft University of Technology, The Netherlands.*

Gray, D. and Ohashi, H. (1983). Mechanics of fiber reinforcement in sand. *Journal of Geotechnical Engineering, vo. 109, no. 3.*

Guo, J. (2014). Sidewall and non-uniformity corrections for flume experimens. *Journal of Hydraulic Research, 53:2, p. 218-229.*

Holtz, R. and Kovacs, W. (1981). *An Introduction to Geotechnical Engineering.* Prentice-Hall, inc.

JGS (1996). Soil testing standards, chapter test methods for the minimum and maximum densities of sands, pages 136-138 (in japanese). Technical report, Japanese Geotechnical Society.

Jonkman, B. (2004). Methode voor de bepaling van het aantal slachtoffers ten gevolge van een grootschallige overstroming (in Dutch). Technical report, Rijkswaterstaat.

Jonkman, B. (2007). *Loss of life estimation in flood risk assesment.* PhD thesis, Delft University of Technology, The Netherlands.

Lemmens, D. (2014). Design of a breach retardant dike. Master's thesis, Delft University of Technology, The Netherlands.

Mulder, A. and Verwaal, W. (2006). *Lecture Notes CT5320 Practical Soil Mechanics: Test Procedures.* Delft University of Technology.

Nakagawa, H. and Tsujimoto, T. (1980). Sand bed instability due to bed load motion. *Journal of the Hydraulics Division, 106(12), pp. 2029-2051.*

Peeters, P., Van Hoestenberghe, T., Vincke, L., and Visser, P. (2011). Swot analysis of breach models for common dike failure mechanisms. In *Proceeding of the 34th IAHR World Congress - Balance and Uncertainty, 33rd Hydrology and Water Resources Symposium; 10th Hydraulics Conference.*

Price, D. (2009). *Engineering Geology: Principles and Practice.* Springer.

Rijkswaterstaat (2006). Veiligheid nederland in kaart - inschatting van het aantal slachtoffers ten gevolge van overstroming (in Dutch). Technical report, Rijkswaterstaat.

Rijkswaterstaat (2014). The national flood risk analysis for The Netherlands. Technical report, Rijkswaterstaat, VNK Project Office, The Netherlands.

Robijns, T. (2012). Gevoeligheisstudie van het bres-model (in Dutch). Bachelor Thesis, Delft University of Technology, The Netherlands.

Shields, A. (1936). Anwendung der ähnlichkeits-mechanik und der turbulenz-forschung auf die geschiebebewegung. *Preussische Versuchsanstalt für Wasserbau und Schiffbau, 26:524–526.*

Smith, J. and McLean, S. (1977). Spatially averaged flow over a wavy surface. *Journal of Geophysical Research 82(12):1735-1746.*

Smolders, L. (2010). Feasibility study of a climate dike. Master's thesis, Delft University of Technology, The Netherlands.

Tonneijck, M. and Weijers, J. (2008). *Lecture Notes CIE5314 Flood Defences.* Delft University of Technology.

Van Gerven, K. (2004). Dijkdoorbraken in Nederland. Ontstaan, voorkomen en bestrijden (in Dutch). Master's thesis, Delft University of Technology, The Netherlands.

Van Rhee, C. (2010). Sediment entrainment at high flow velocity. *Journal of Hydraulic Engineering, 136:572–582.*

Van Rhee, C. (2015). Slope failure by unstable breaching. *Proceedings of the Institution of Civil Engineers - Maritime Engineering 168:2 , 84-92.*

Van Rijn, L. C. (1984). Sediment pick-up functions. *Journal of Hydraulic Engineering, 110(10):1494– 1502.*

Van Rijn, L. C. (1993). *Principles of sediment transport in rivers, estuaries and coastal seas.* Aqua Publications, Amsterdam, The Netherlands.

Vanoni, V. A. and Brooks, N. H. (1957). Laboratory studies of the roughness and suspended load of alluvial streams. Technical report, Sedimentation Laboratory, California Institute of Technology, Pasadena, California, U. S. A.

Verhagen, H., Focks, D., Algera, A., and Vu, M. (2008). The use of vetivers in coastal engineering. *COPEDEC VII, Dubai, UAE, Paper No 119.*

Visser, P. J. (1988). A model for breach growth in a dike-burst. In *Proc. 21st Int. Conf. Coastal Eng, Malaga, Spain, pp. 1897-1910.*

Visser, P. J. (1998). *Breach growth in sand-dikes.* PhD thesis, Delft University of Technology, The Netherlands.

Visser, P. J., Kraak, A. W., Bakker, W. T., Smit, M. J., Snip, D. W., Steetzel, H. J., and van de Graaff, J. (1995). A large-scale experiment on breaching in sand-dikes. In *Proc. Coastal Dyncamics'95, Gdansk, Poland, pp 583-594.*

Visser, P. J. and Robijns, T. (2013). Bresontwikkeling dijk bij kerncentrale borssele (in Dutch). Technical report, Delft University of Technology, The Netherlands.

Visser, P. J., Smit, M. J., and Snip, D. W. (1996). Zwin'94 experiment; meetopstelling en overzicht van alle meetresultaten. Technical report, 4-96, Vakgroep Waterbouwkunde, Fac. Civiele Techn., Techn. Univ. Delft, Delft, The Netherlands.

Wilson, K. (1987). Analysis of bed-load motion at high shear stress. In *Journal of Hydraulic Engineering, ASCE , vol. 113, no. 1, pp. 97-103.*

Zhu, Y. (2006). *Breach growth in clay-dikes.* PhD thesis, Delft University of Technology, The Netherlands.

Appendices

A | Data Direct Shear Tests

This appendix contains the individual results of the direct shear tests. For each test two graphs are provided. The first one contains a graph of the shear stress versus the normal stress and the second one the shear stress versus the horizontal displacement.

Test 1: Sand M32

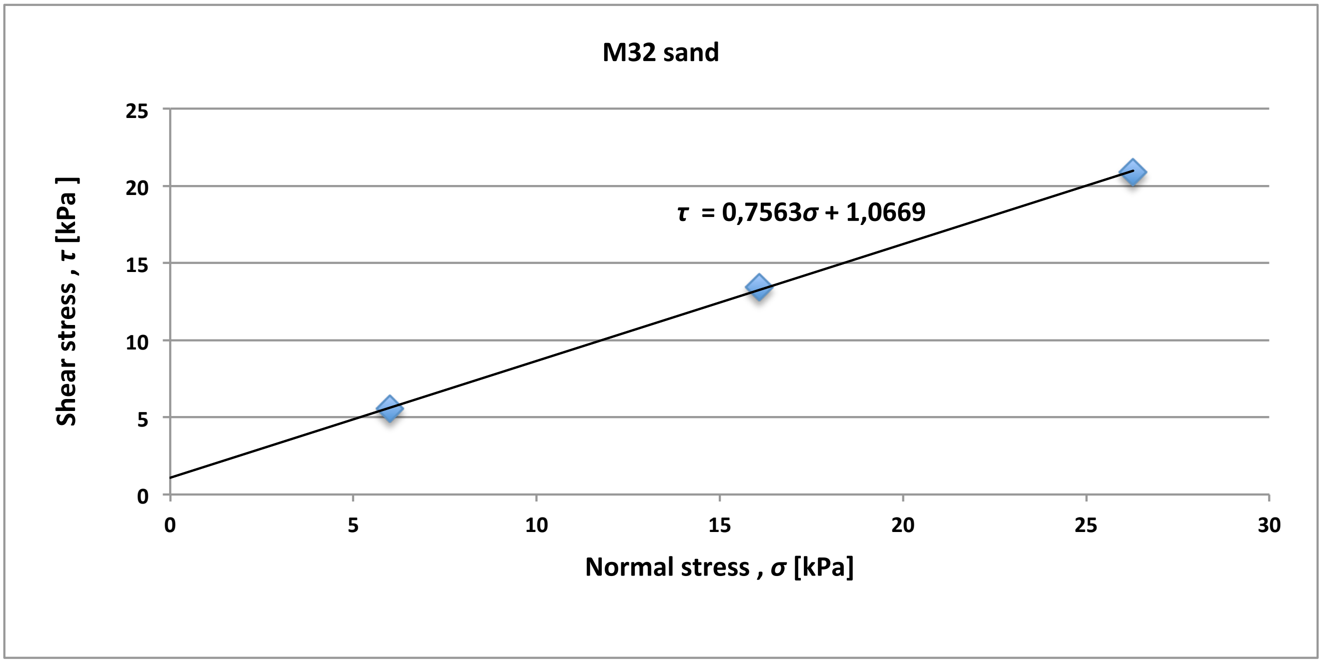

Figure A1: Results direct shear test of sand with a D_{50} of 0.256 mm.

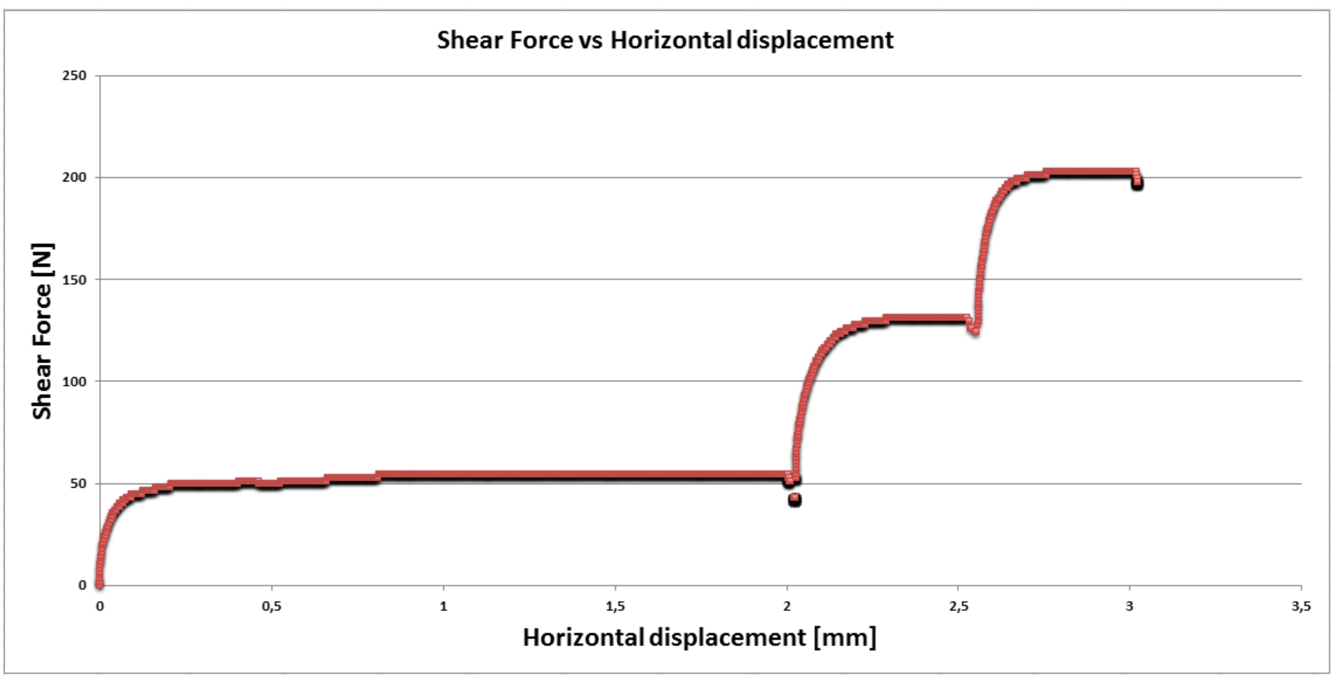

Figure A2: Shear stress versus horizontal displacement of sand with a D_{50} of 0.256 mm.

Test 2: Mixture 2% bentonite M32

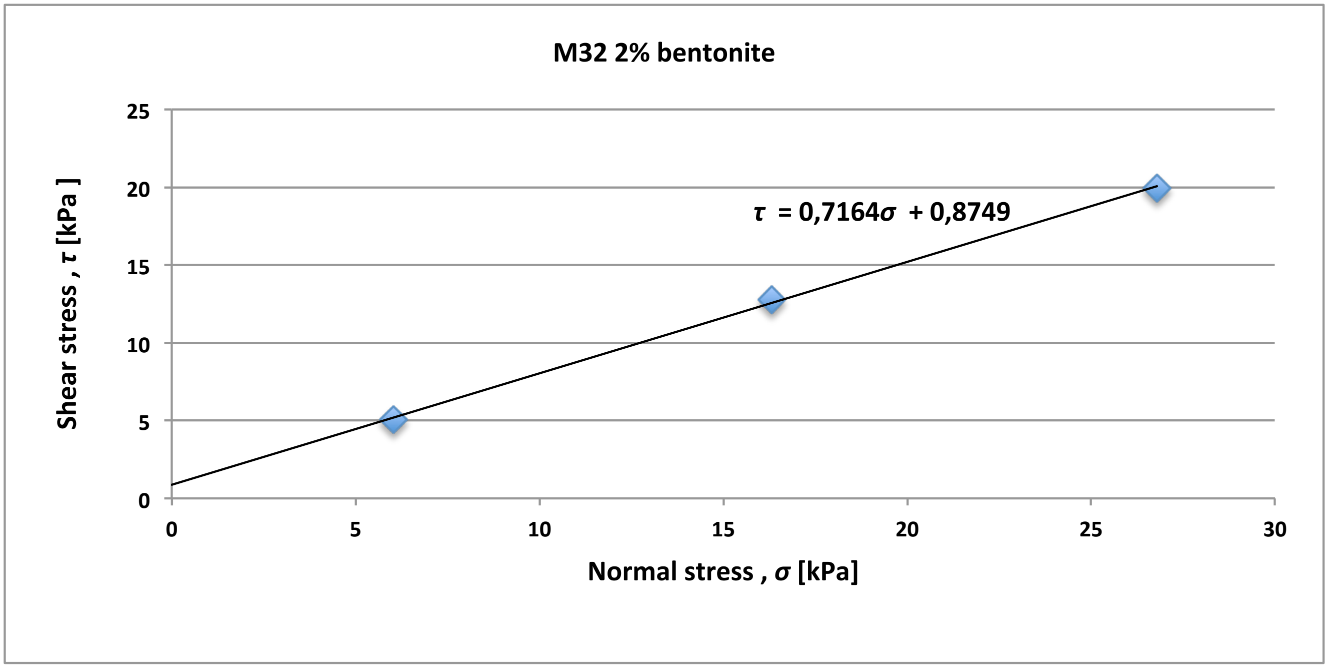

Figure A3: Results direct shear test of a 2% mixture with a D_{50} of 0.256 mm.

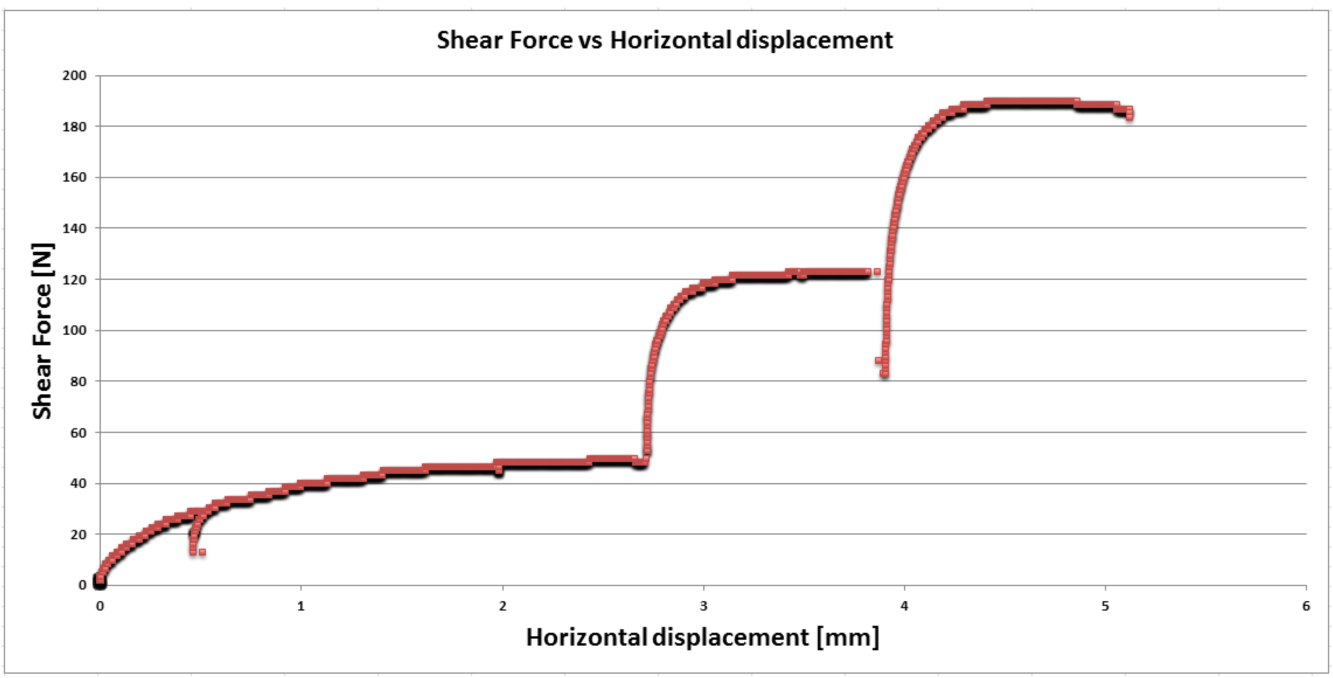

Figure A4: Shear stress versus horizontal displacement of a 2% mixture with a D_{50} of 0.256 mm.

Test 3: Mixture 4% bentonite M32

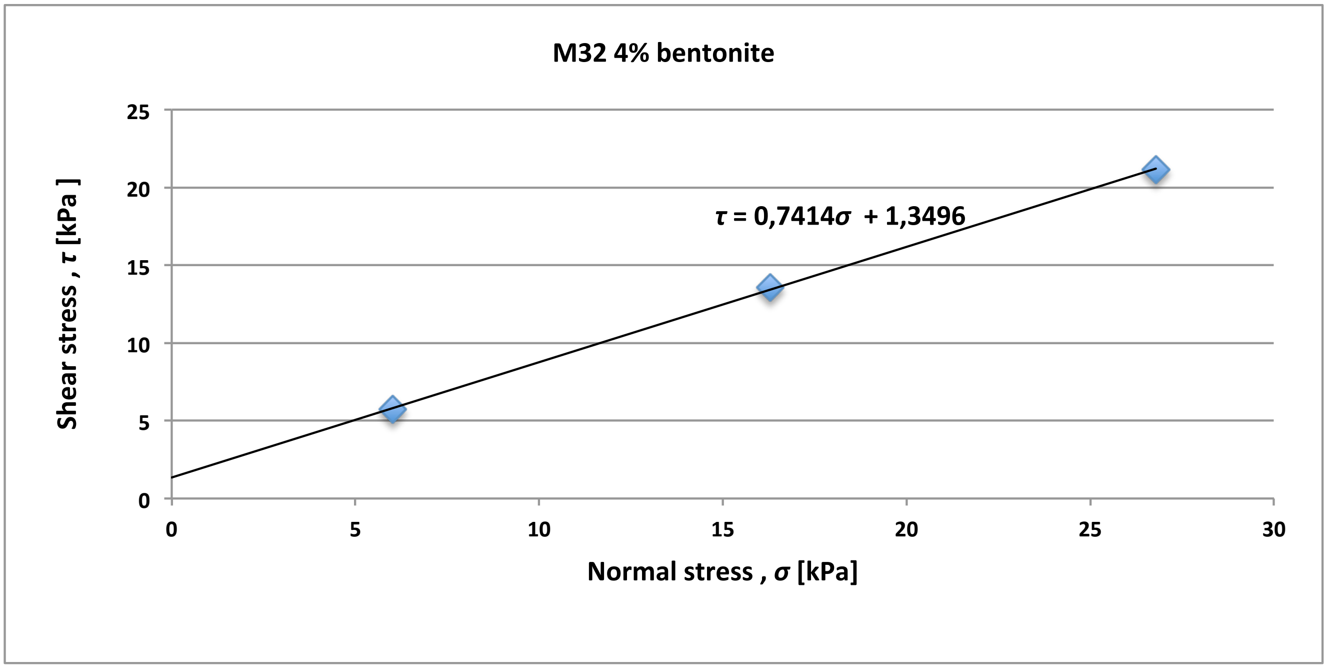

Figure A5: Results direct shear test of a 4% mixture with a D_{50} of 0.256 mm.

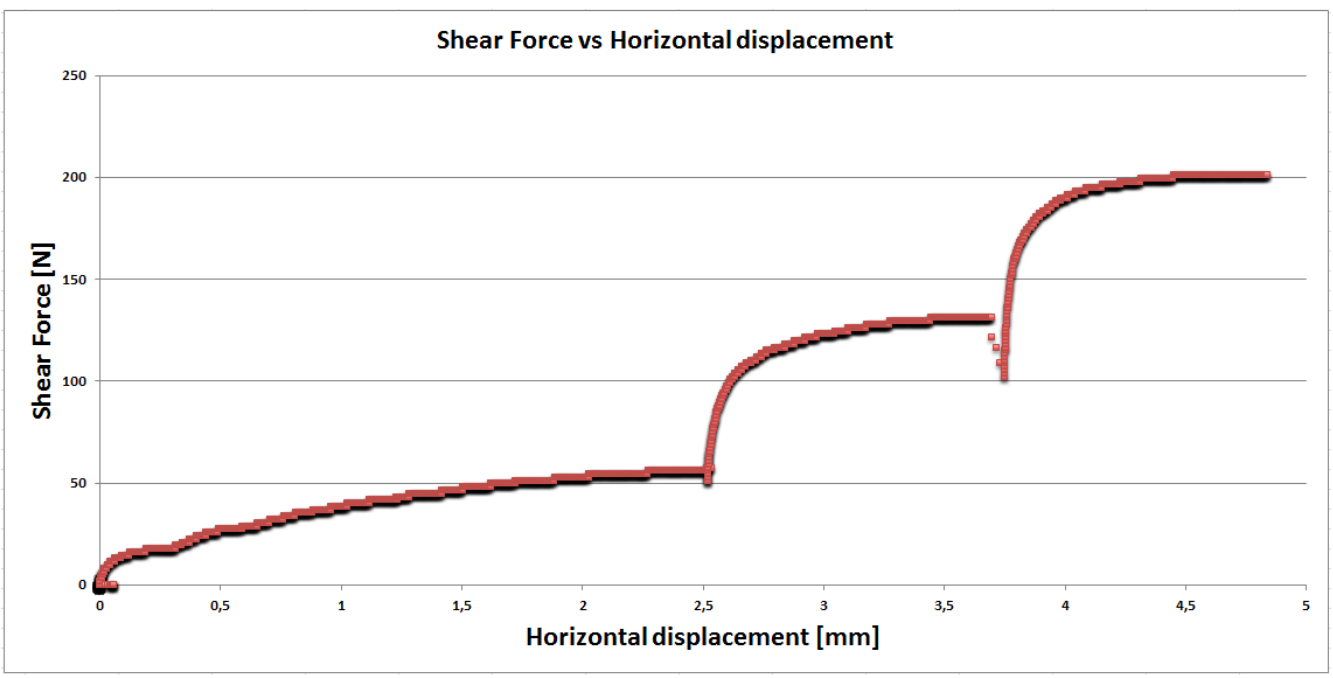

Figure A6: Shear stress versus horizontal displacement of a 4% mixture with a D_{50} of 0.256 mm.

Test 4: Mixture 6% bentonite M32

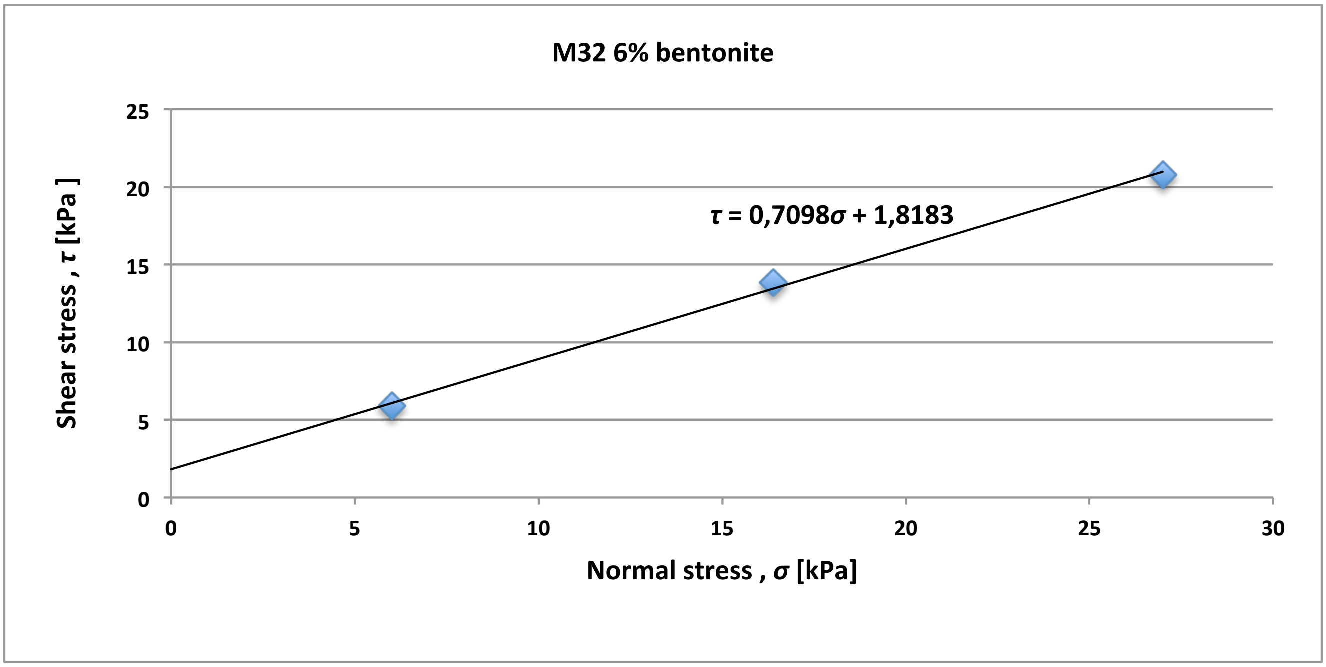

Figure A7: Results direct shear test of a 6% mixture with a D_{50} of 0.256 mm.

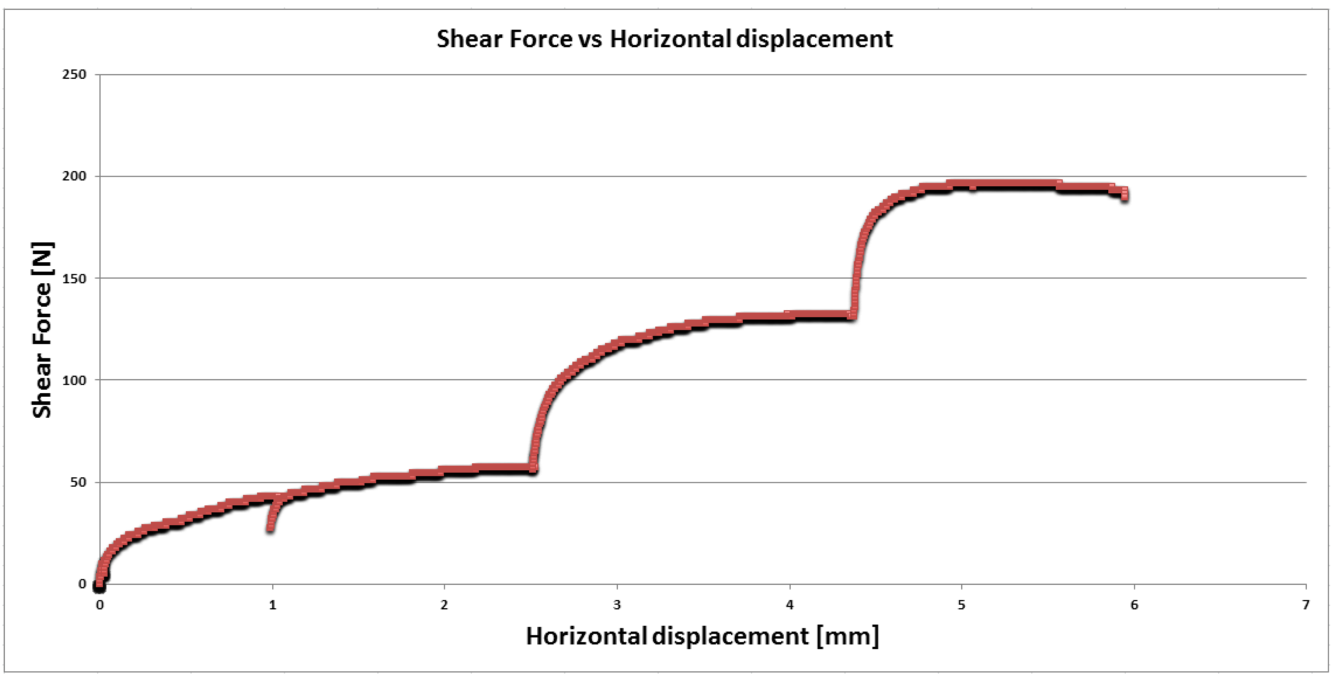

Figure A8: Shear stress versus horizontal displacement of a 6% mixture with a D_{50} of 0.256 mm.

Test 5: Mixture 8% bentonite M32

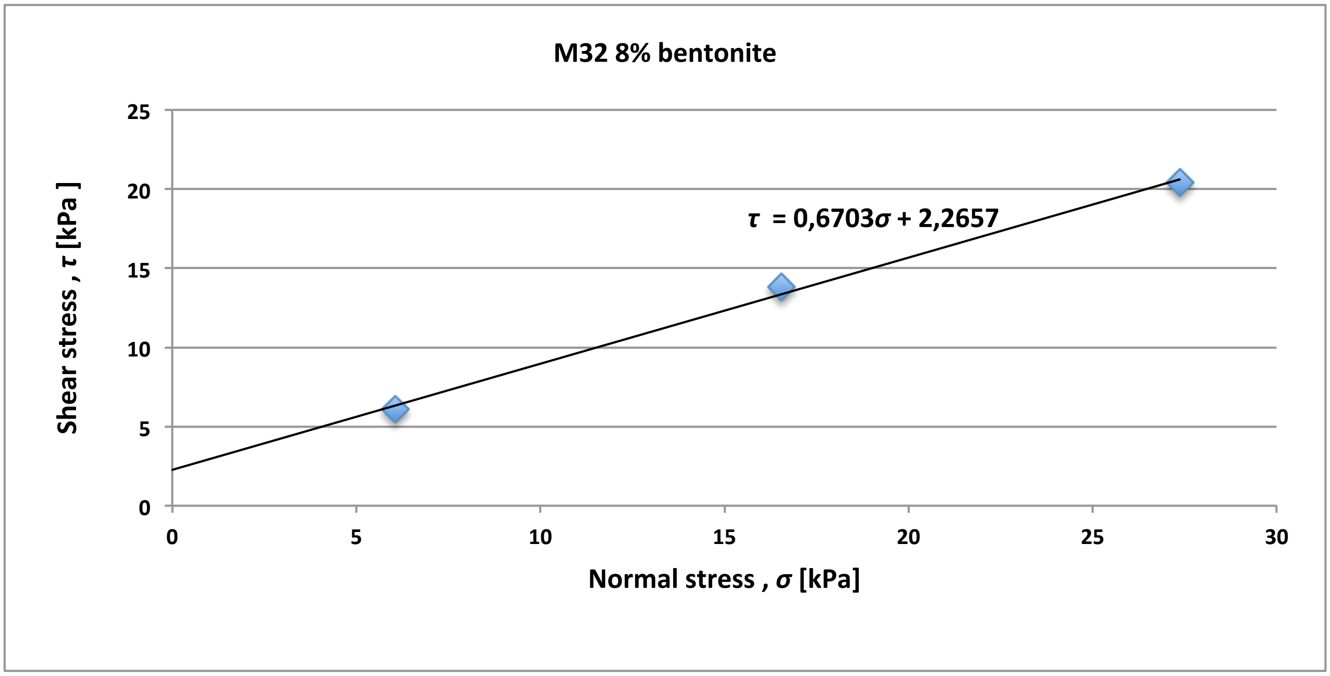

Figure A9: Results direct shear test of a 8% mixture with a D_{50} of 0.256 mm.

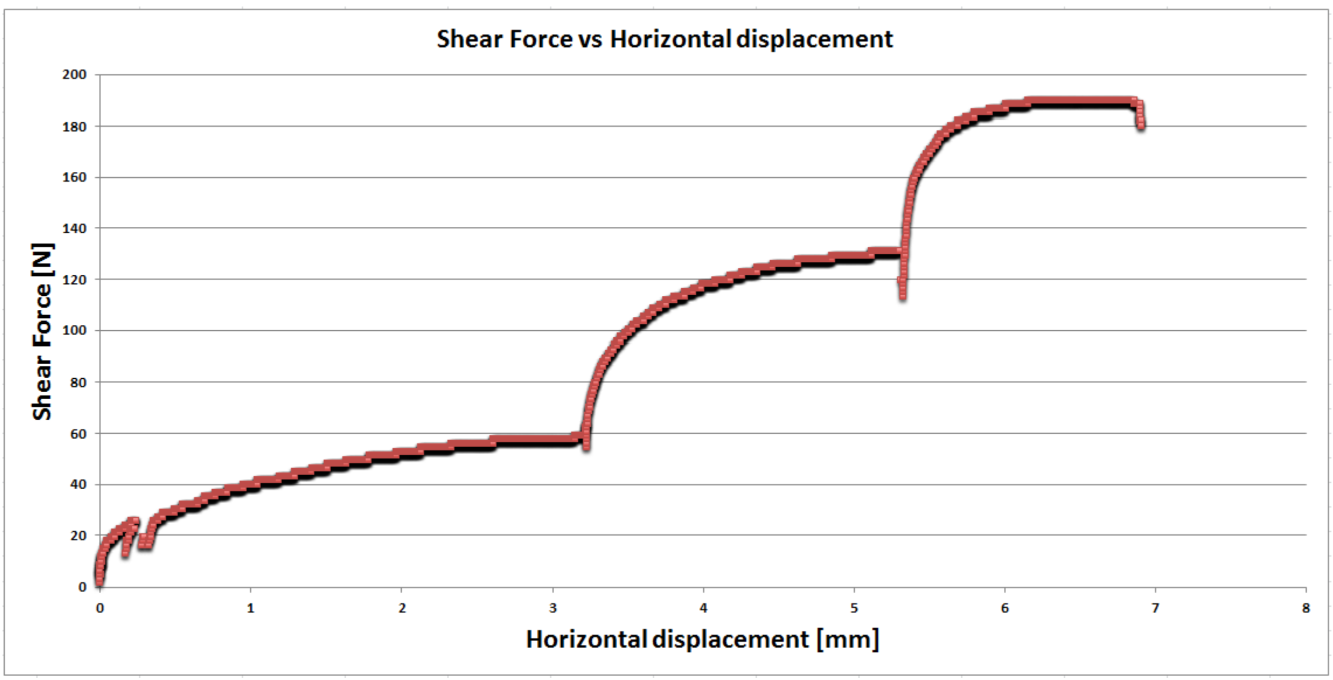

Figure A10: Shear stress versus horizontal displacement of a 8% mixture with a D_{50} of 0.256 mm.

Test 6: Mixture 10% bentonite M32

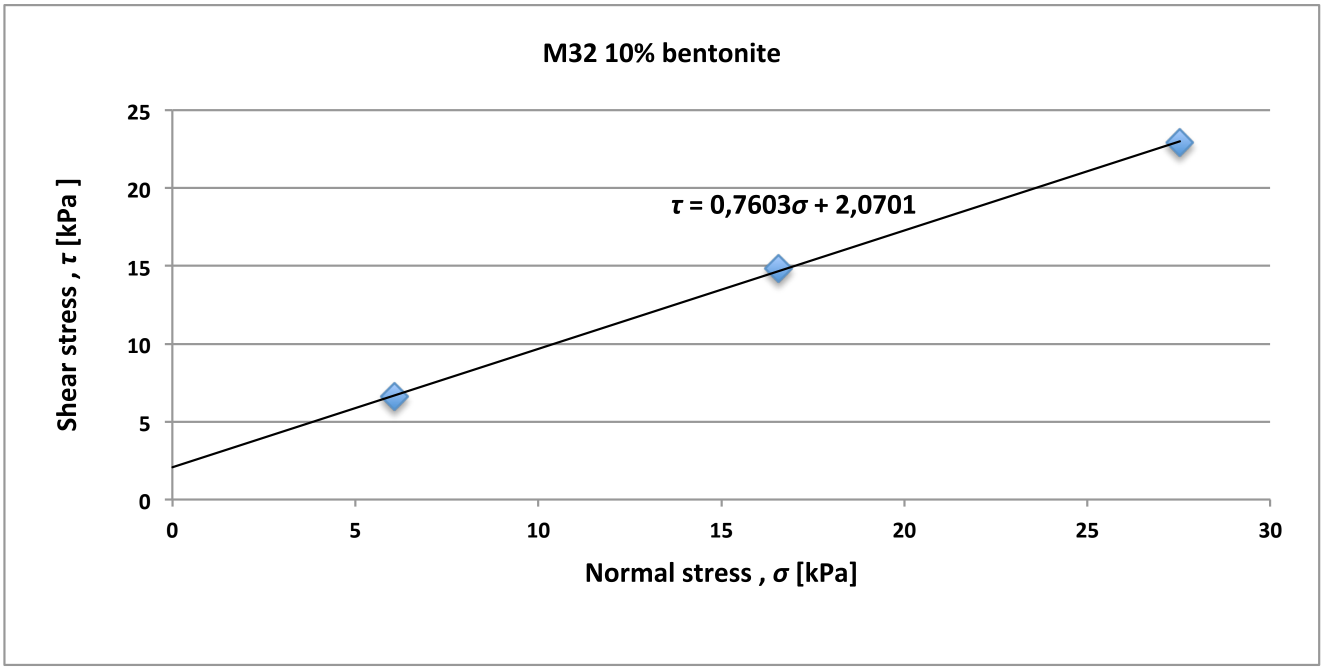

Figure A11: Results direct shear test of a 10% mixture with a D_{50} of 0.256 mm.

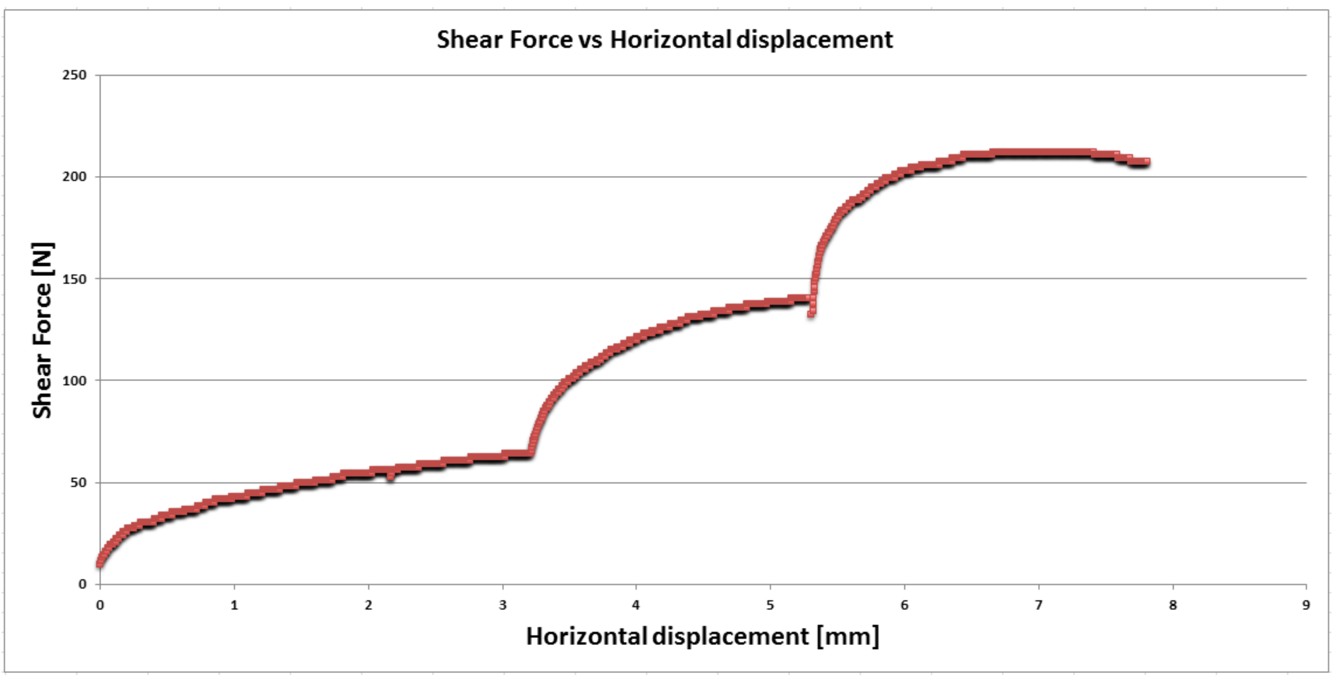

Figure A12: Shear stress versus horizontal displacement of a 8% mixture with a D_{50} of 0.256 mm.

Test 7: Sand S90

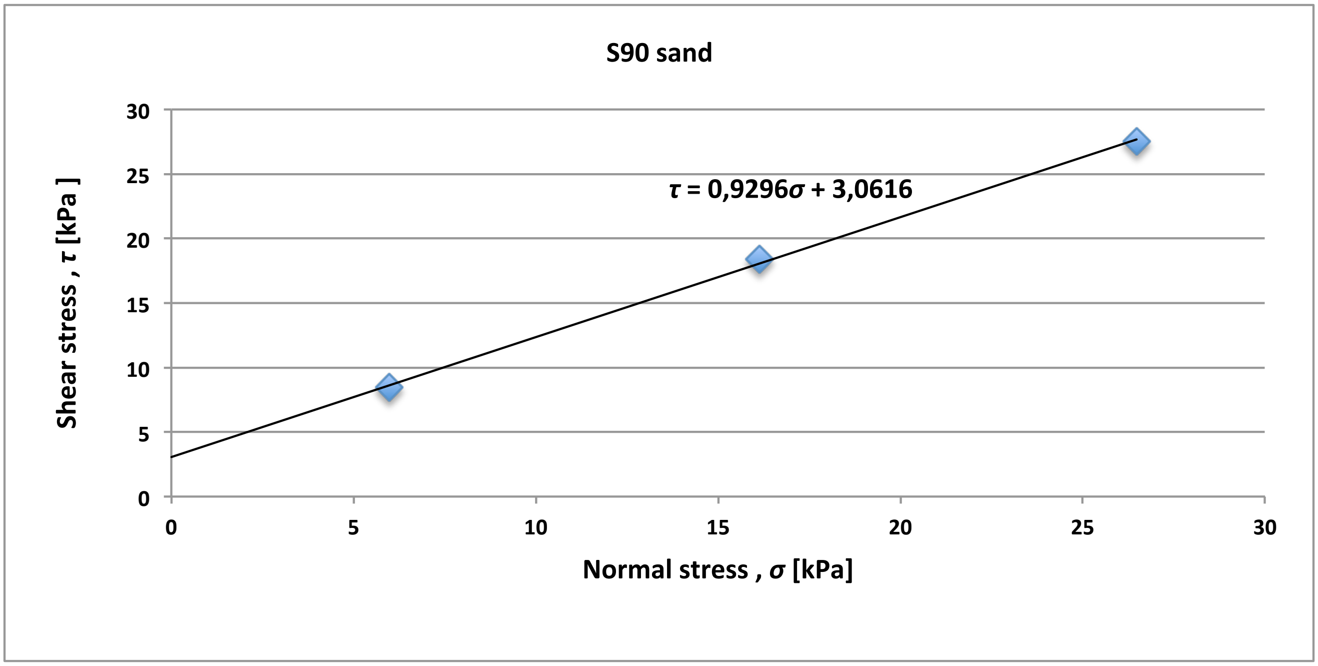

Figure A13: Results direct shear test of sand with a D_{50} of 0.150 mm.

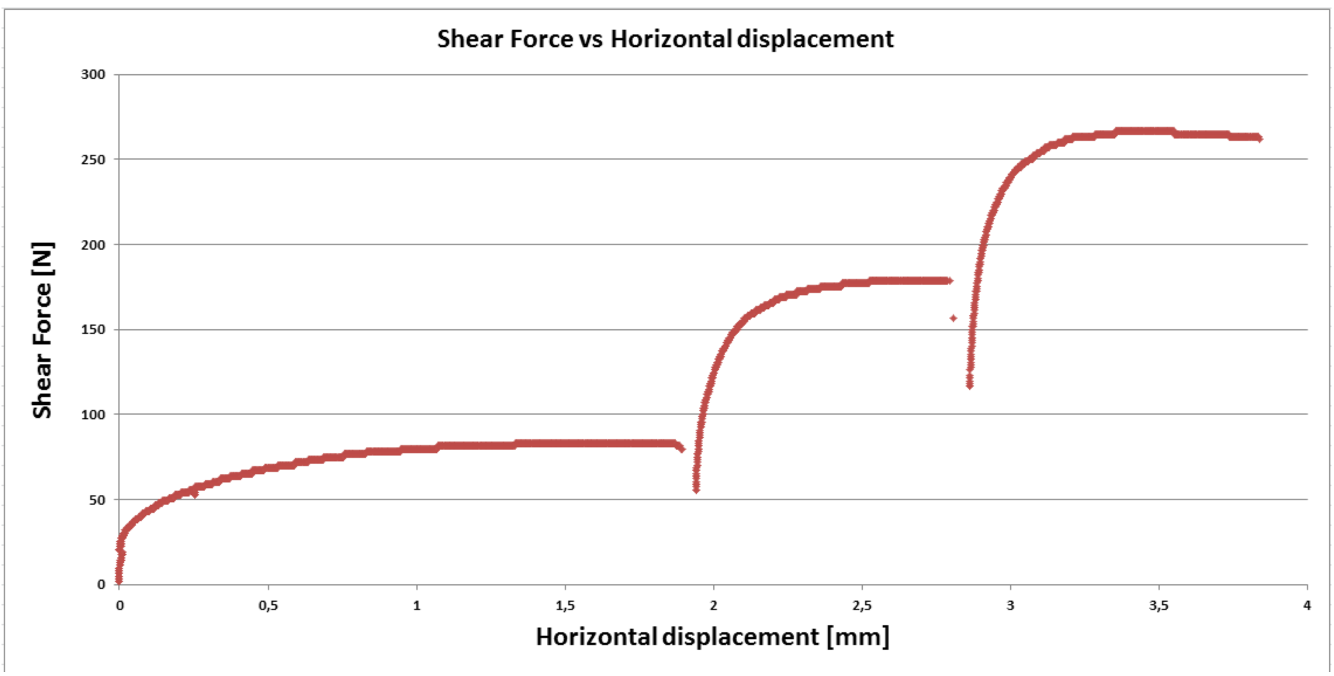

Figure A14: Shear stress versus horizontal displacement of sand with a D_{50} of 0.150 mm.

Test 8: Mixture 2% bentonite S90

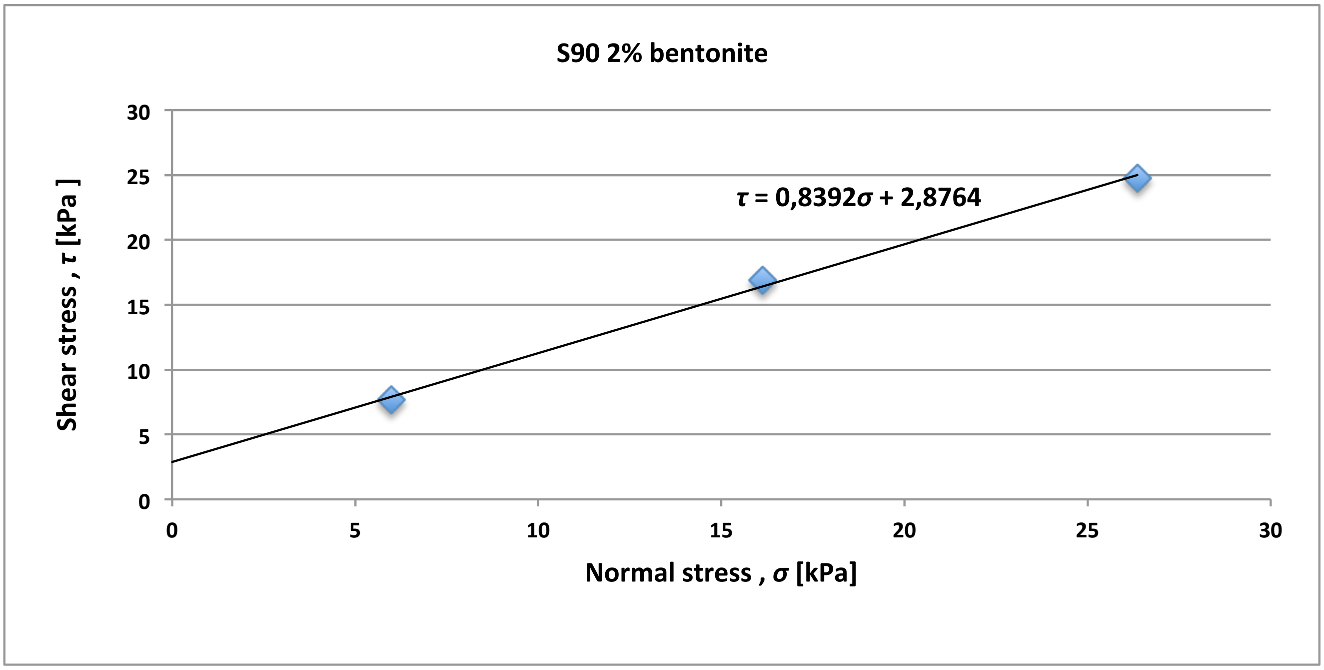

Figure A15: Results direct shear test of a 2% mixture with a D_{50} of 0.150 mm.

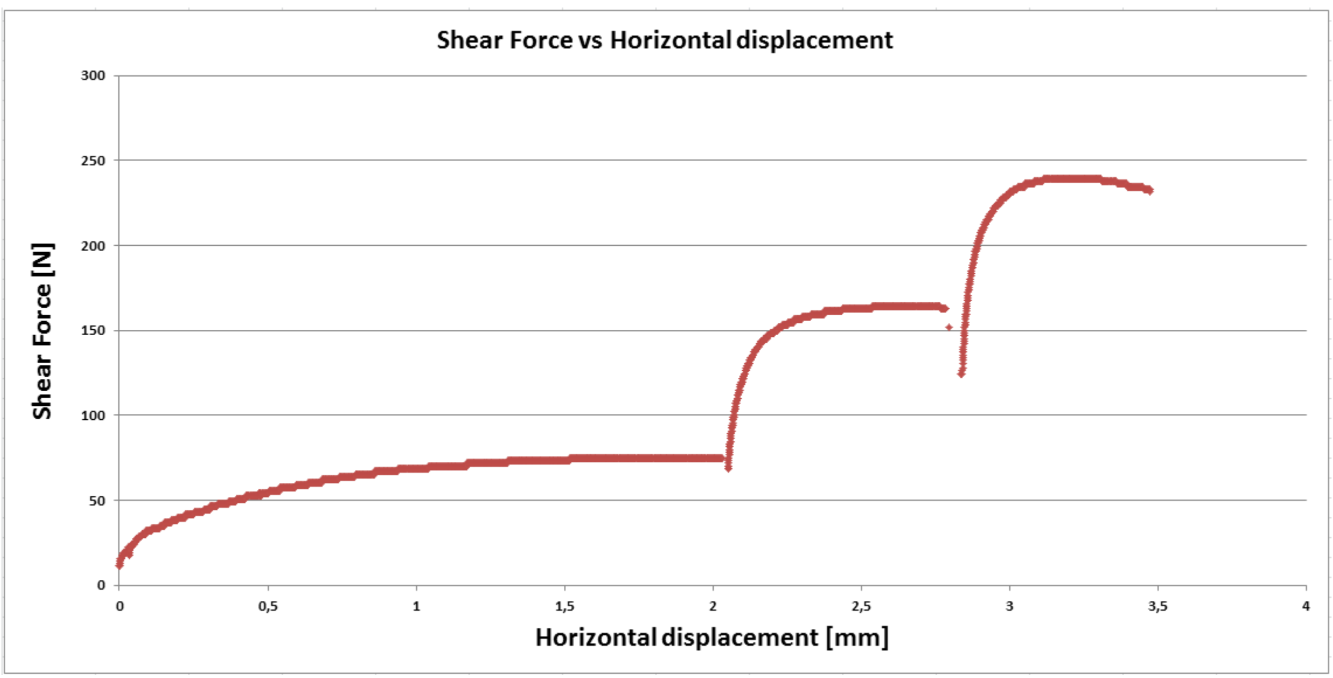

Figure A16: Shear stress versus horizontal displacement of a 2% mixture with a D_{50} of 0.150 mm.

Test 9: Mixture 4% bentonite S90

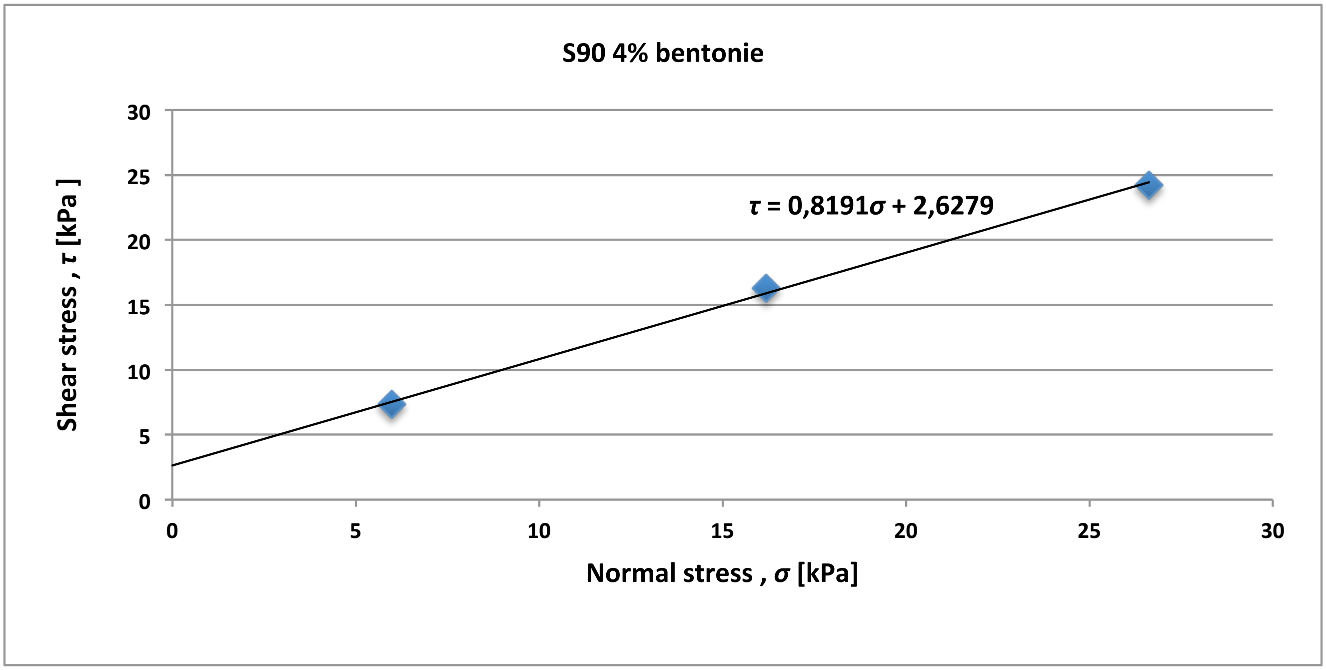

Figure A17: Results direct shear test of a 4% mixture with a D_{50} of 0.150 mm.

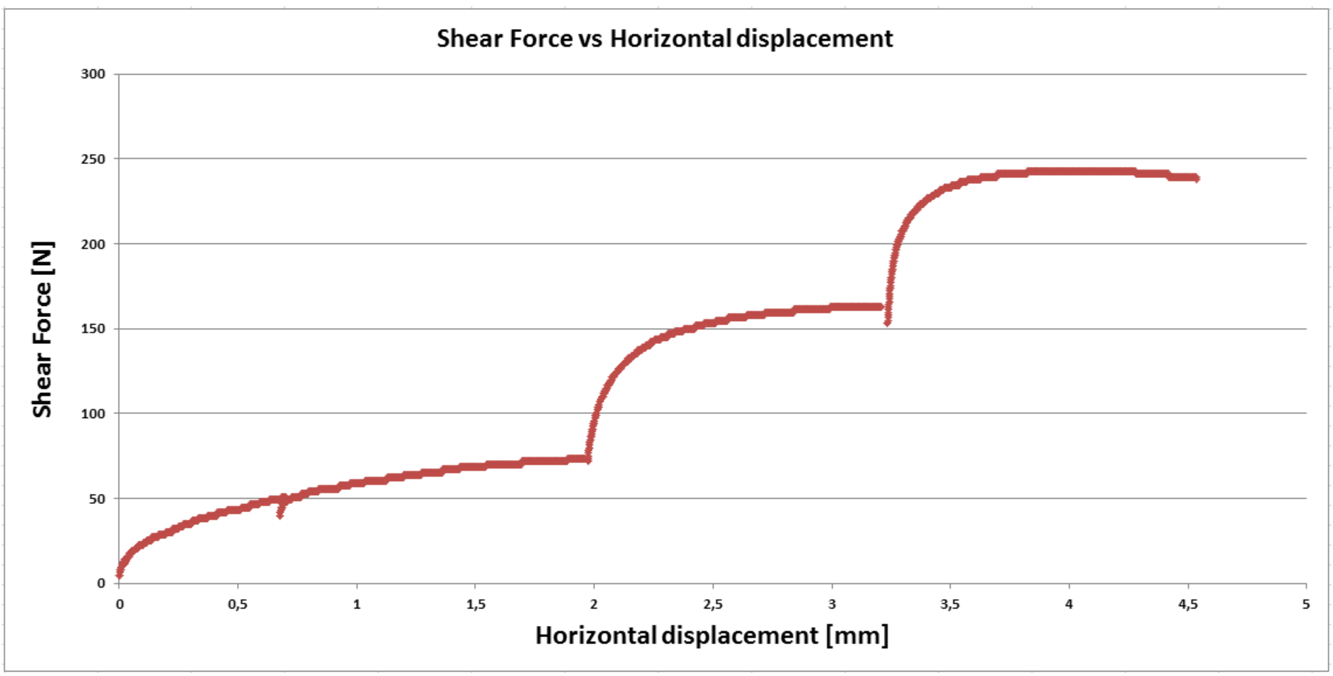

Figure A18: Shear stress versus horizontal displacement of a 4% mixture with a D_{50} of 0.150 mm.

Test 10: Mixture 6% bentonite S90

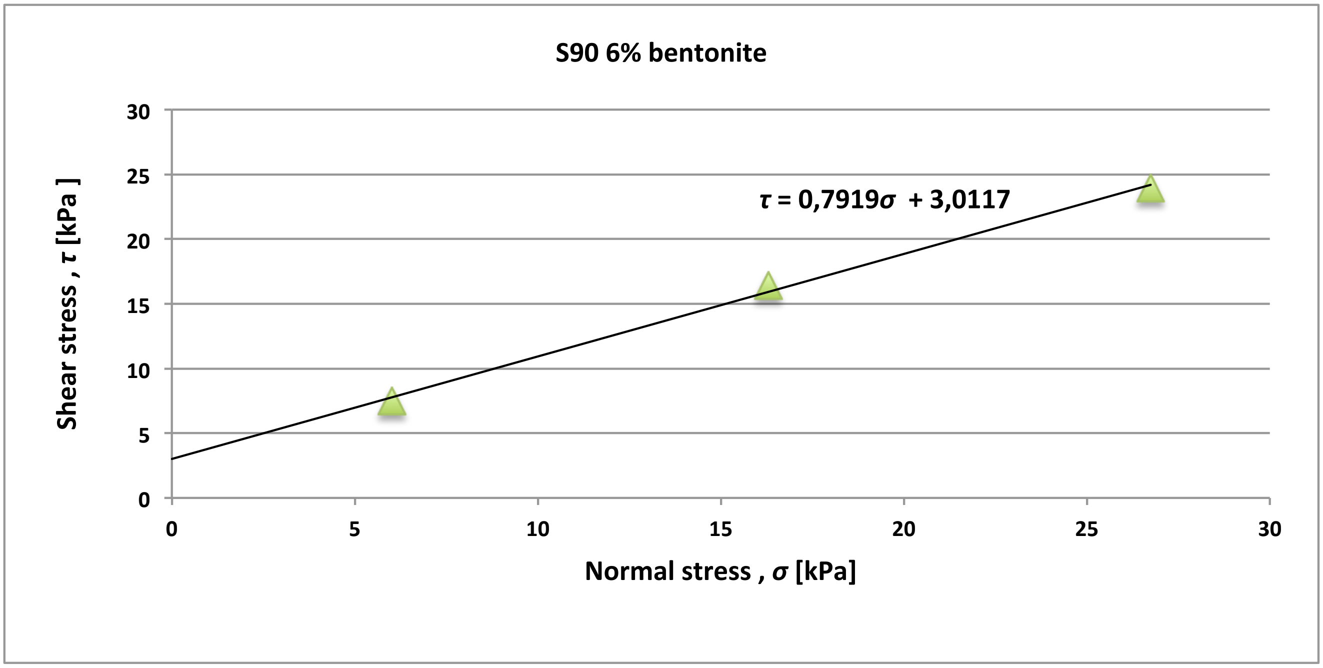

Figure A19: Results direct shear test of a 6% mixture with a D_{50} of 0.150 mm.

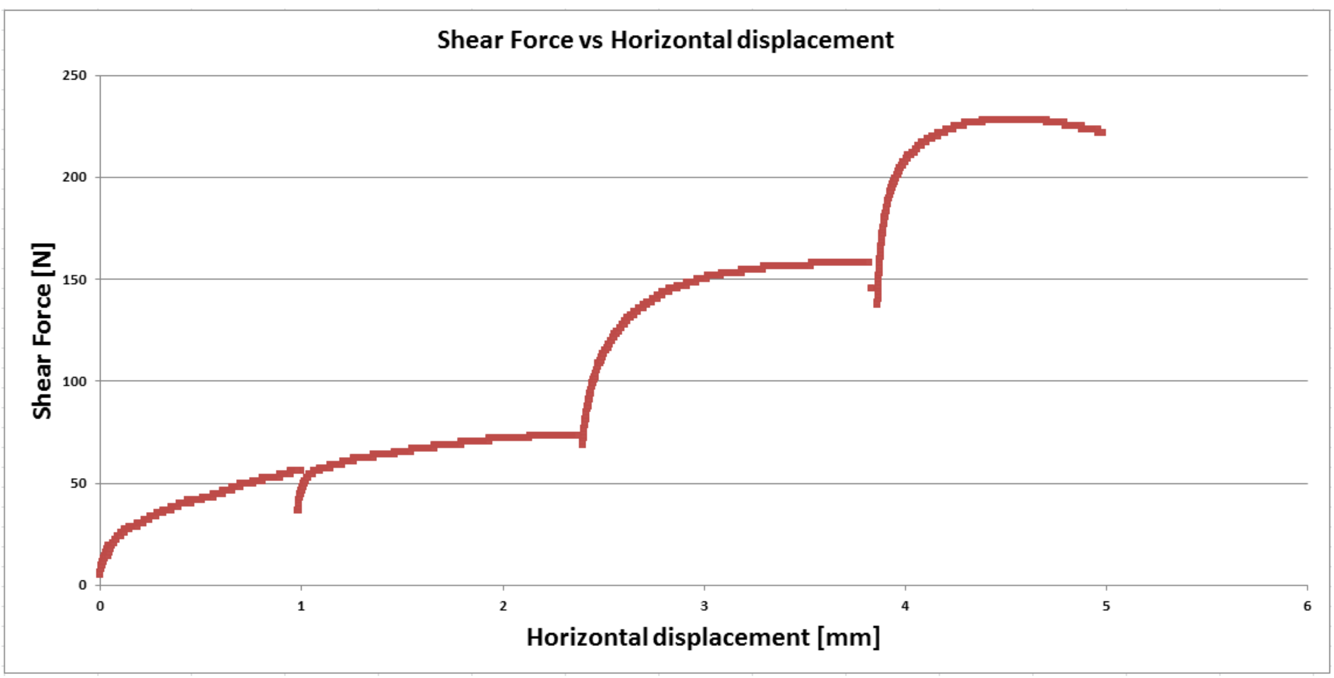

Figure A20: Shear stress versus horizontal displacement of a 6% mixture with a D_{50} of 0.150 mm.

Test 11: Mixture 8% bentonite S90

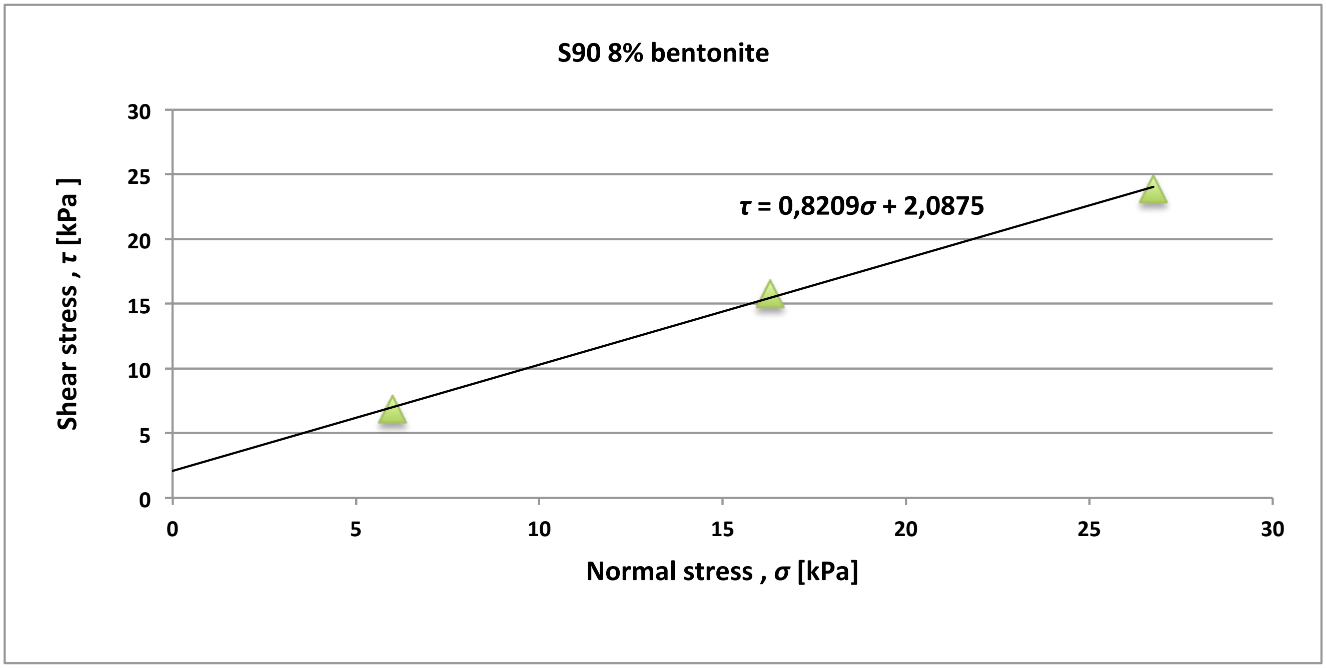

Figure A21: Results direct shear test of a 8% mixture with a D_{50} of 0.150 mm.

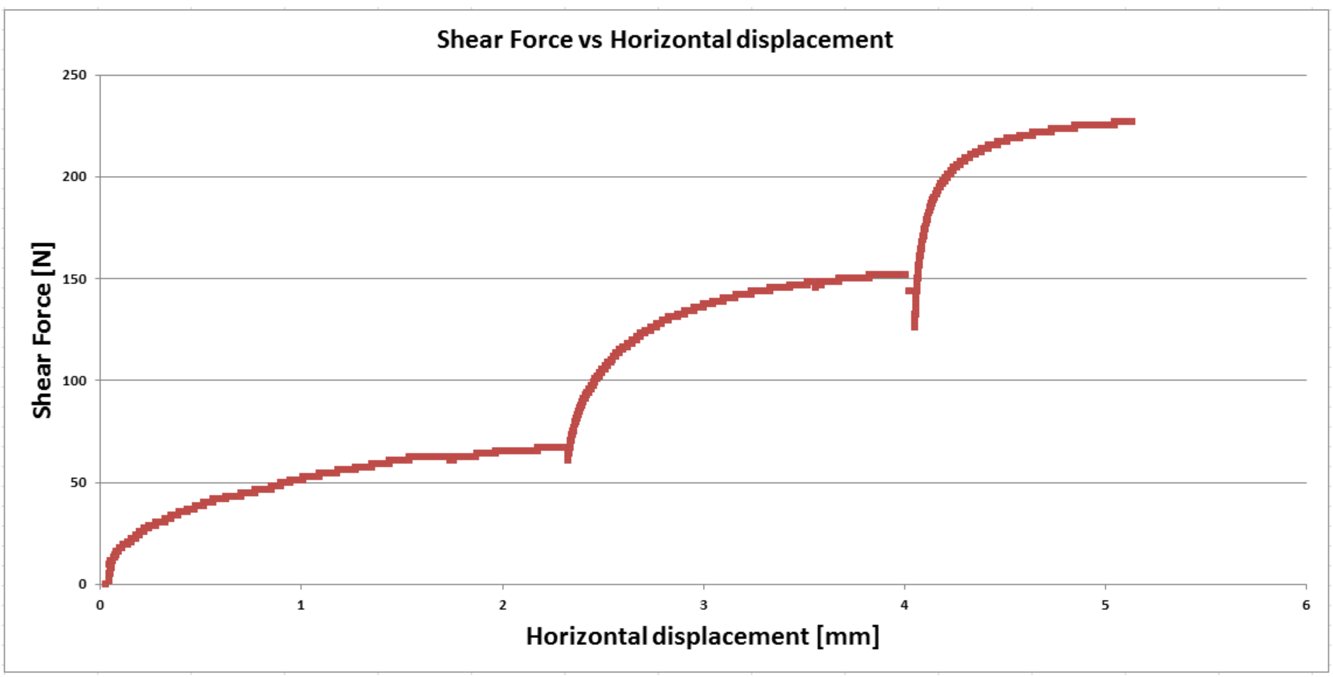

Figure A22: Shear stress versus horizontal displacement of a 8% mixture with a D_{50} of 0.150 mm.

Test 12: Mixture 10% bentonite S90

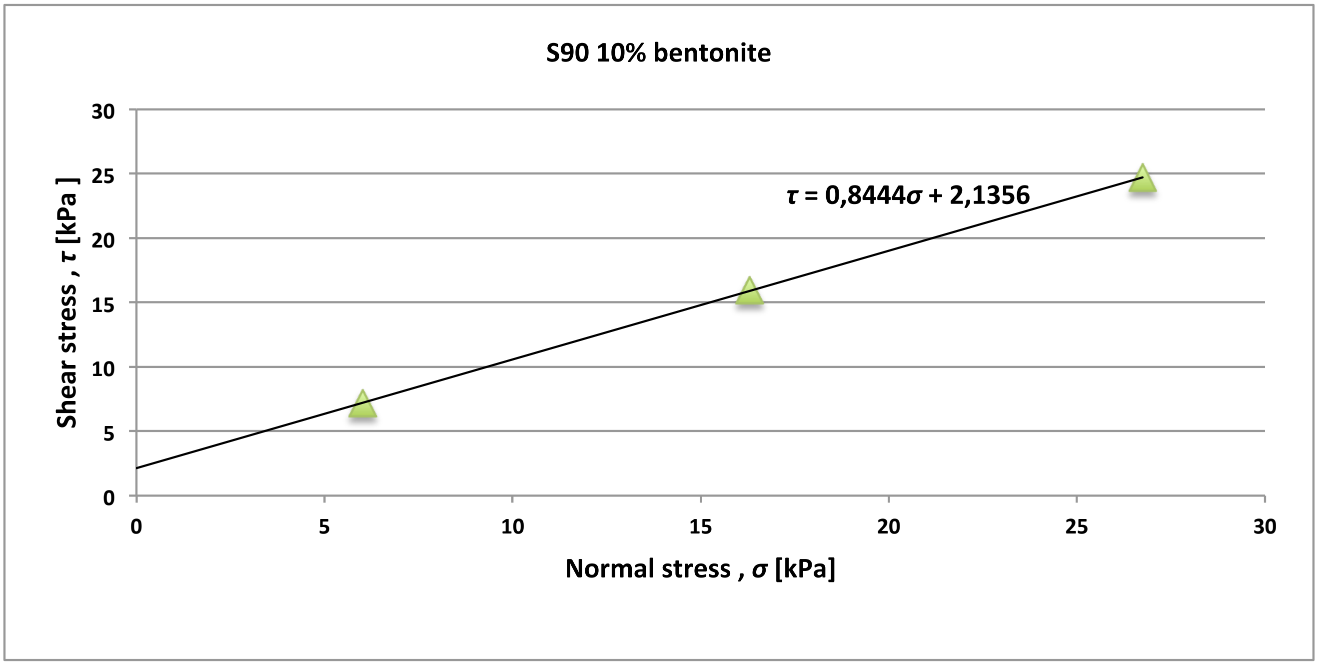

Figure A23: Results direct shear test of a 10% mixture with a D_{50} of 0.150 mm.

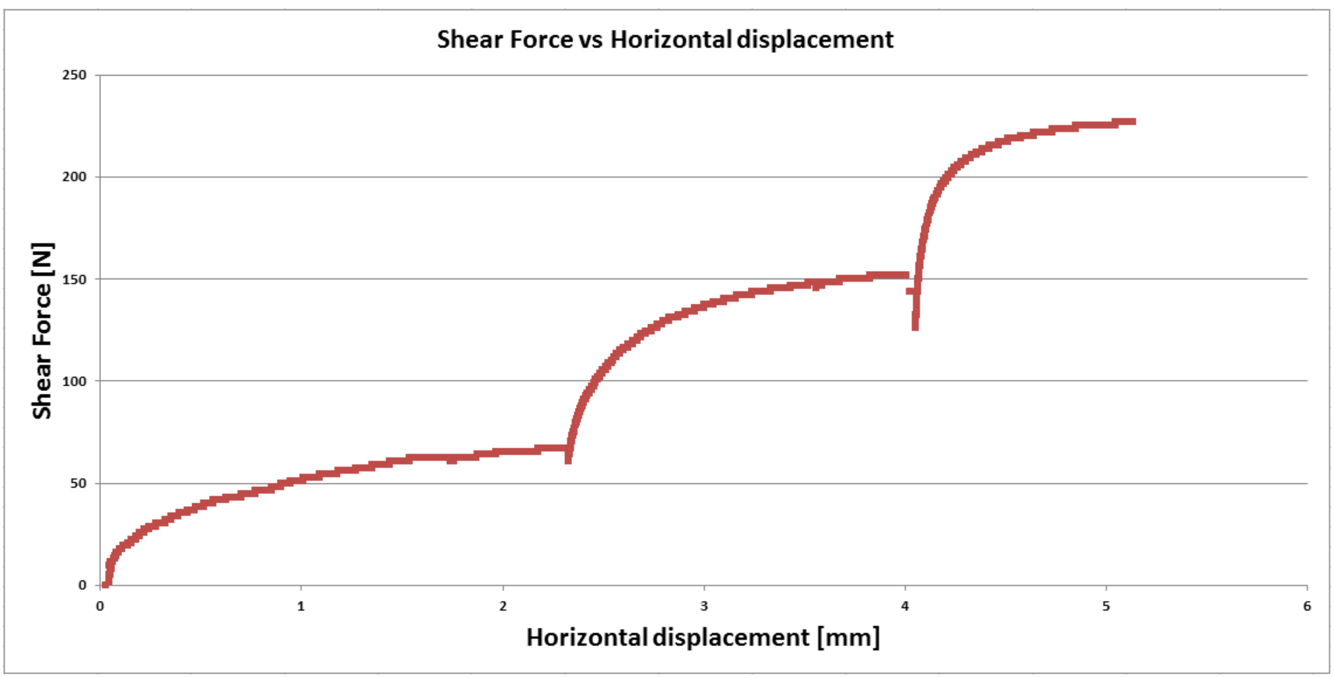

Figure A24: Shear stress versus horizontal displacement of a 10% mixture with a D_{50} of 0.150 mm.

B | Specifics of the Cebogel Sealfix bentonite (Dutch)

PRODUCT DATA

Cebo Holland

CEBOGEL SEALFIX

Toepassing
- In een mengsel met zand voor bodemafdichtingen.
- In boorvloeistof voor grondboringen.

Omschrijving
De basis voor CEBOGEL SEALFIX is een geactiveerde natrium bentoniet. CEBOGEL SEALFIX voldoet aan de CUR aanbeveling 33, die eisen stelt aan bentoniet voor granulaire afdichtingslagen.

Voordelen
- Het grote zwelvermogen maakt een kwalitatief zeer hoogwaardige zandbentoniet afdichting mogelijk.
- Beproefd materiaal voor zandbentoniet afdichtingen: met CEBOGEL SEALFIX is al meer dan 4 miljoen m^2 afgedicht.
- Een spoeling op basis van CEBOGEL SEALFIX is makkelijk te verpompen en zorgt voor een stabiel boorgat.

Specificatie
Voldoet aan de eisen voor bentoniet zoals gesteld in de CUR aanbeveling 33.

Parameter	Methode	CUR 33 Aanbeveling	Typische Waarde
Wateropnemend vermogen na 24 uur	Proef A CUR 33	≥ 700 %	840 %
Methyleenblauw absorptie	Proef B CUR 33	≥ 250 mg MB/gram	330 mg MB/gram
Droge zeefanalyse door 125 μm	Ontw. NEN 33976	≥ 95 %	98 %
Montmorillonietgehalte	Röntgendiffractie	≥ 70 %	80 %
Vochtgehalte (op droog)	NEN 5934	≤ 13,0 % m/m	11,5 % m/m

Cebo Holland BV
Westerduinweg 1
NL-1976 BV IJMUIDEN
P.O. Box 70
NL-1970 AB IJMUIDEN

Tel.: +31 255546262
Fax: +31 255546202
e-mail : sales@ceboholland.com
www.ceboholland.com

PRODUCT DATA

Cebo Holland

Chemische en fysische eigenschappen

Samenstelling	Hoogwaardige geactiveerde natrium bentoniet
Kleur	Beige
Vorm	Zacht poeder

Eigenschappen van de suspensie
Bij verschillende concentraties CEBOGEL SEALFIX aangemaakt in gedestilleerd water.

Parameter	Methode	30 kg/m^3	40 kg/m^3	50 kg/m^3	60 kg/m^3
Vloeigrens kogelnummer	Kugelharfengerät DIN 4126	1	1	2	3
Dichtheid	Mudbalans	1,02 g/ml	1,03 g/ml	1,03 g/ml	1,04 g/ml
Filtraatwaterverlies	DIN 4127	12 ml	10 ml	9 ml	8,5 ml
Marshfunnel API	API RP 13B section 2 (1 liter uit)	30 s	32 s	35 s	38 s

Verpakking
- 25 kg zakken per 1000 kg verpakt op een pallet met krimpfolie
- big bags van 1000 kg
- bulk

Cebo Holland BV
Westerduinweg 1
NL-1976 BV IJMUIDEN
P.O. Box 70
NL-1970 AB IJMUIDEN

Tel.: +31 255546262
Fax: +31 255546202
e-mail : sales@ceboholland.com
www.ceboholland.com

Revisiedatum : 18.03.2009
Document nr. : SF01IP

C | Results Permeability Tests

This appendix contains more elaborate information of the permeability tests. Fig. C1 and Fig. C2 contain the individual emperical functions for the reduction factor k/k_{sand}, which is a function of the volume percentage of added bentonite for the M32 sand type. The second graph has a logarithmic vertical axis. Fig. C3 and Fig. C4 contain the same individual emperical functions for the S90 sand type.

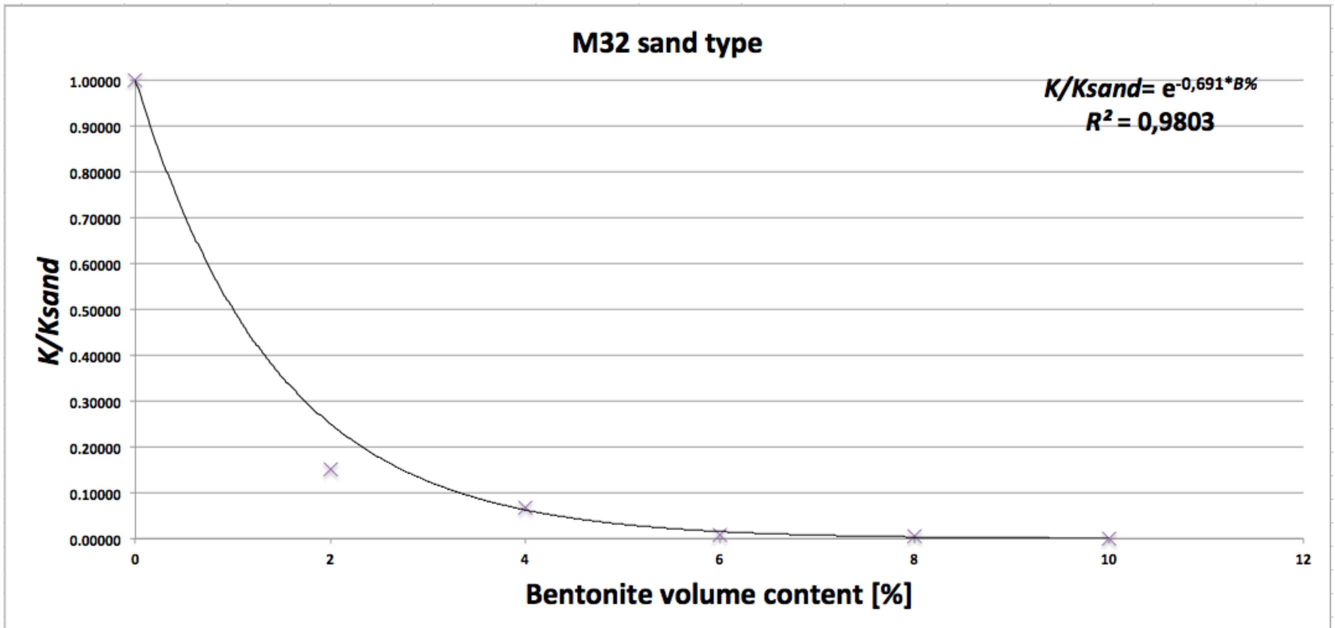

Figure C1: Reduction of permeability coefficient as function of the added bentonite volume percentage for the M32 sand type.

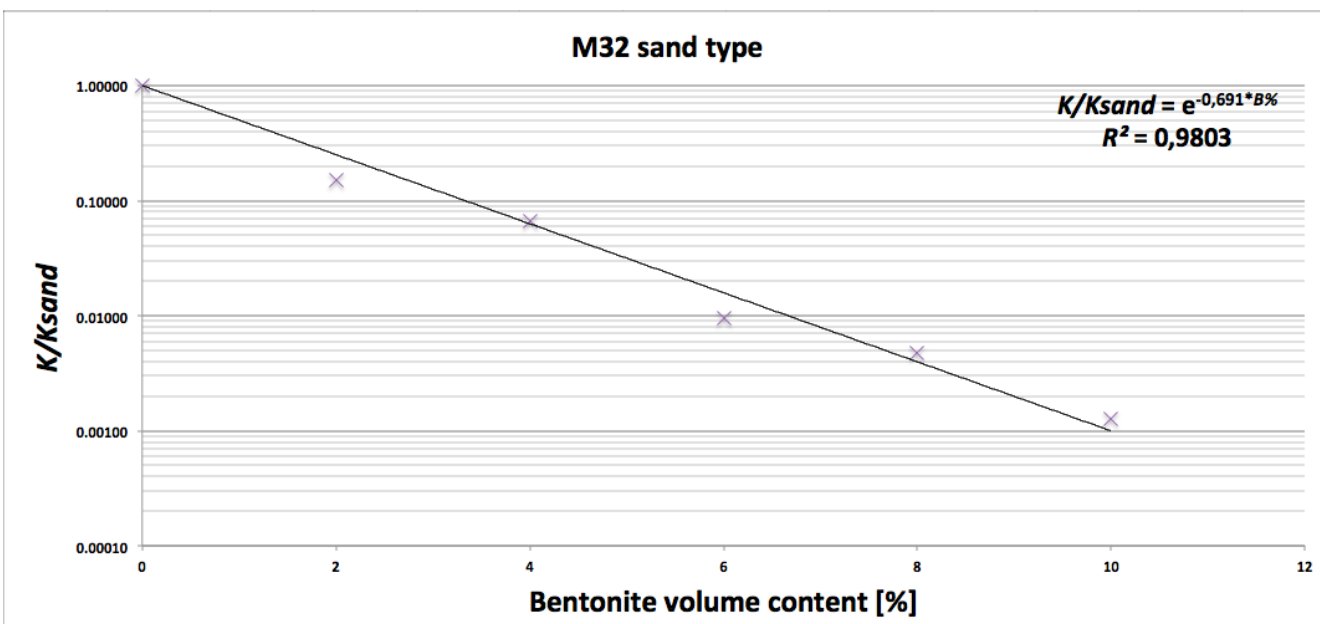

Figure C2: Reduction of permeability coefficient as function of the added bentonite volume percentage for the M32 sand type (vertical log scale).

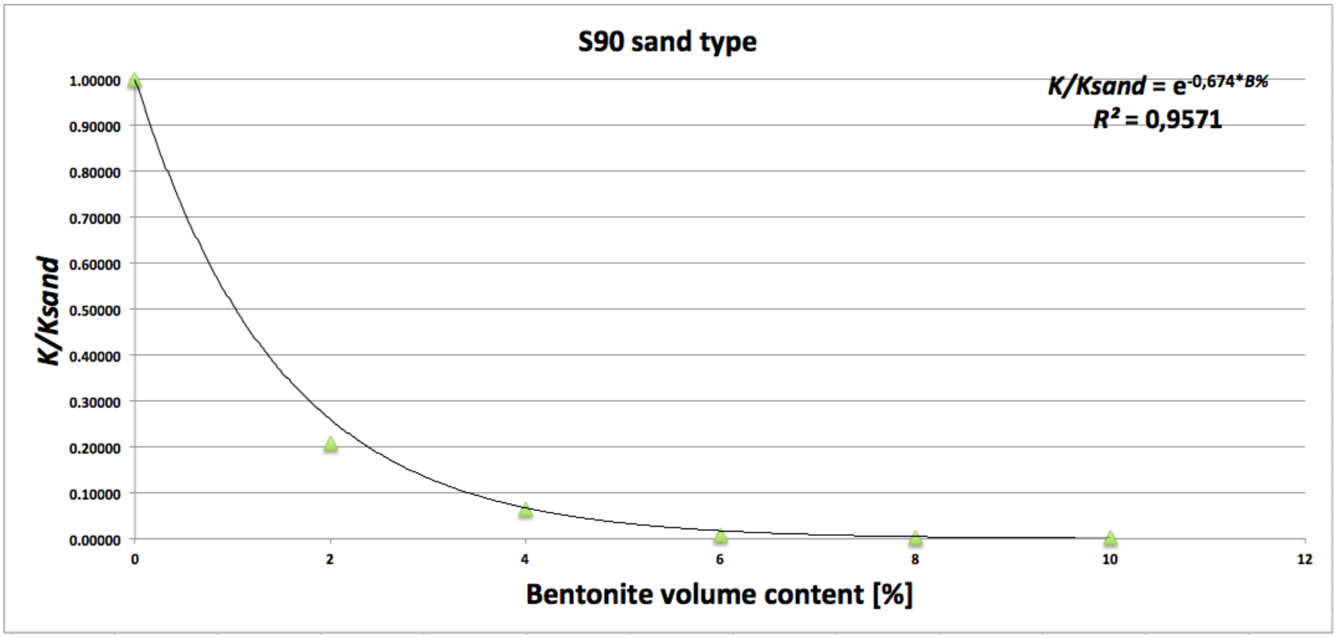

Figure C3: Reduction of permeability coefficient as function of the added bentonite volume percentage for the S90 sand type.

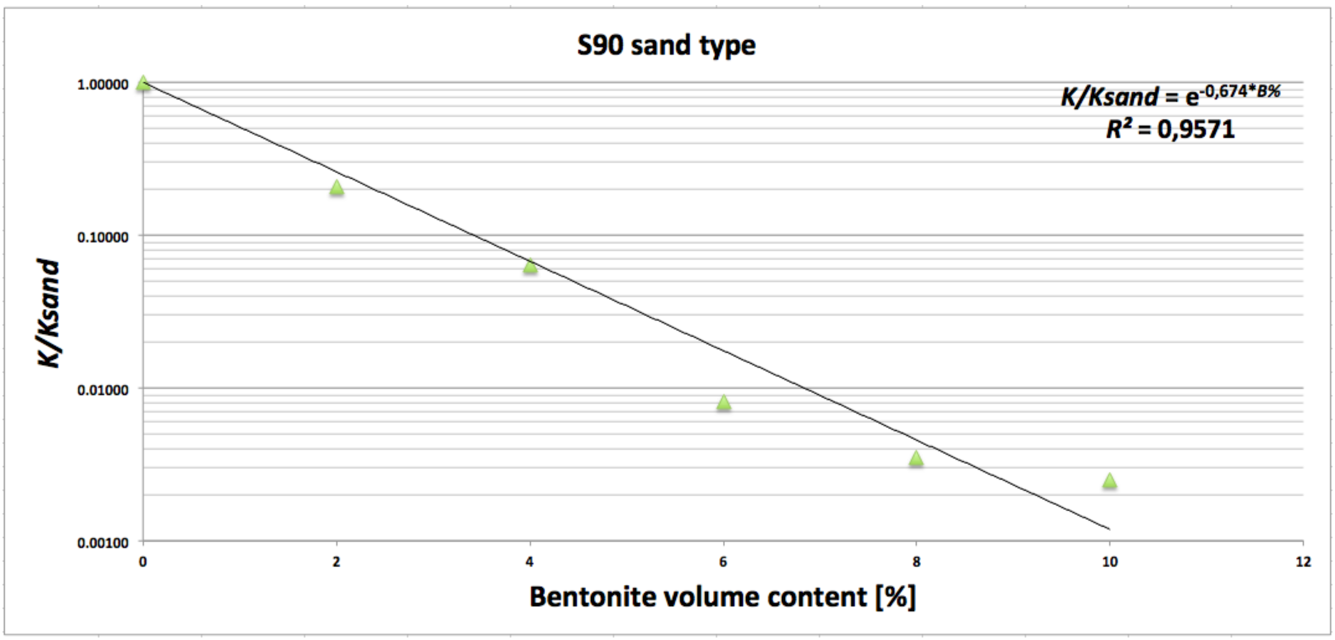

Figure C4: Reduction of permeability coefficient as function of the added bentonite volume percentage for the S90 sand type(vertical log scale).

D | Results Erosion Tests

Test overview
In the test overview the actual test plan as executed is presented (see Table D1). In this overview all the parameters of importance are given. These are: the volume percentage of bentonite additive, the diameter of the sand and the intended mean flow velocity during the tests. During the test runs the discharge was constantly measured and the bed levels and water levels in the area of interest were recorded on video. For each test run data from 5 measurement locations were analyzed. The measurement locations were all in the area of interest and evenly spaced at a 10 cm interval from each other (called Point 0, 10, 20, 30 and 40 in Table D2 to Table D14). The most upstream measurement location was at the 0 line of the grid (see Fig. 22). From these recordings the water levels and bed levels were extracted with a Matlab script. The Matlab script was using the Videoreader function to extract frames from the videos at a preset interval. The time between each of the consecutive frames was between 10 and 60 s (this is also mentioned above Fig. D1 to Fig. D13). For each frame the Matlab script required the user to input coordinates for the water levels and bed levels in order to give a time series of the water level and bed level as output. Next, the script automatically converted the amount of pixels to a height using a pixel : distance ratio which was calculated by specifying a known distance. The results of these surface water level and bed level positions in time are given in Fig. D1 to Fig. D13. In the final step the mean flow velocity U and erosion velocity v_e between each of the consecutive frames in time were calculated with Eq.(23) and Eq.(24). The test conditions and results are given in Table D2 to Table D14. In Table D2 to Table D14 k is the in-situ permeability as measured in the falling head tests.

Table D1: Actual run plan for the erosion test

Run #	Percentage bentonite [%]	D_{50} in [mm]	Flow velocity in [m/s]
1	0	0.256	1
2	2	0.256	1
3	4	0.256	1
4	6	0.256	1
5	6	0.150	1
6	0	0.150	1
7	0	0.256	2
8	0	0.150	2
9	2	0.256	2
10	4	0.256	2
11	6	0.256	2
12	3	0.150	2
13	0	0.256	2

Test 1

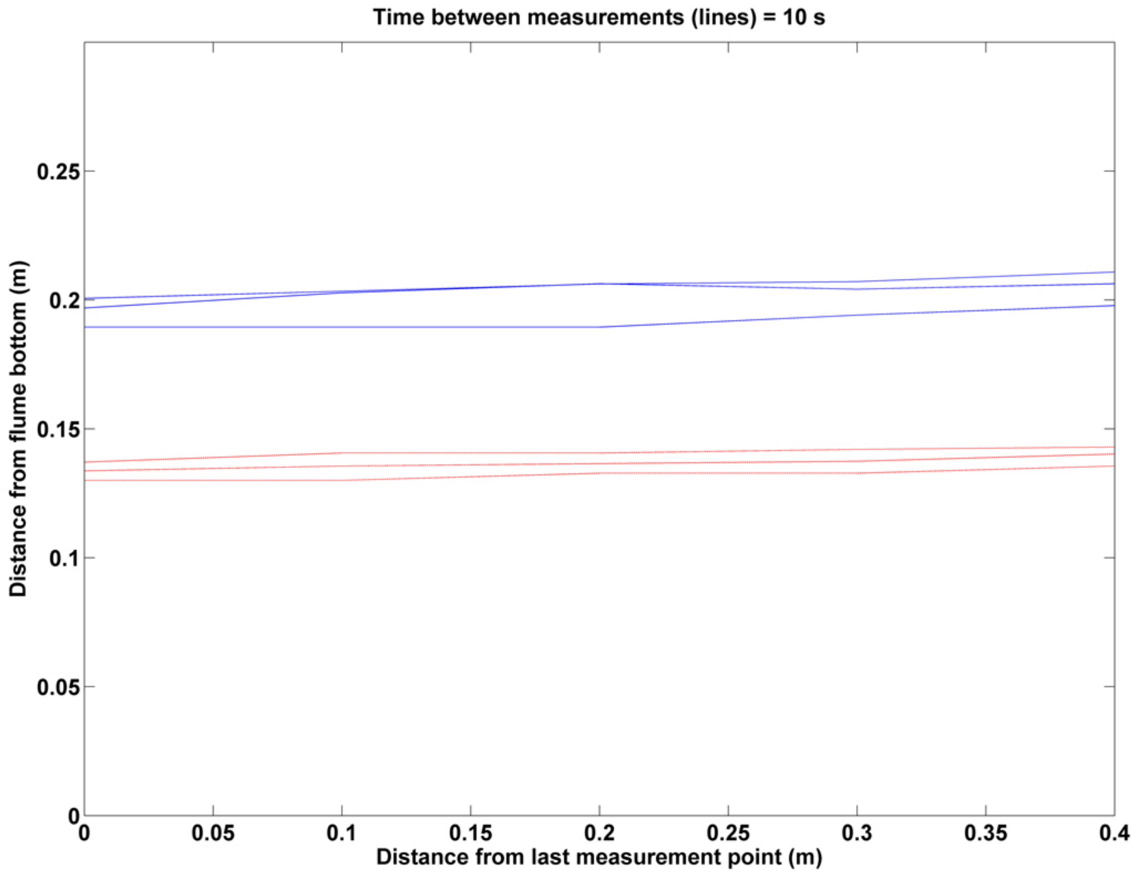

Figure D1: Water level (upper line) and bed level (lower line) measurements with an average discharge of 10.35 l/s.

Table D2: Test conditions and results of Run 1.

Point x	x [m]	h [m]	U [m/s]	v_e [m/s]	R [m]	Fr [-]	k [m/s]	v_e/k [-]	T [°C]
0	0	0.065	1.095	3.69E-04	0.034	1.4	4.83E-04	0.76	21
10	0.1	0.066	1.113	4.62E-04	0.035	1.4	4.83E-04	0.96	21
20	0.2	0.064	1.124	3.91E-04	0.034	1.4	4.83E-04	0.81	21
30	0.3	0.066	1.134	5.30E-04	0.035	1.4	4.83E-04	1.10	21
40	0.4	0.065	1.154	3.55E-04	0.034	1.4	4.83E-04	0.73	21
Average	-	0.065	1.124	4.21E-04	0.034	1.4	4.83E-04	0.87	21

Test 2

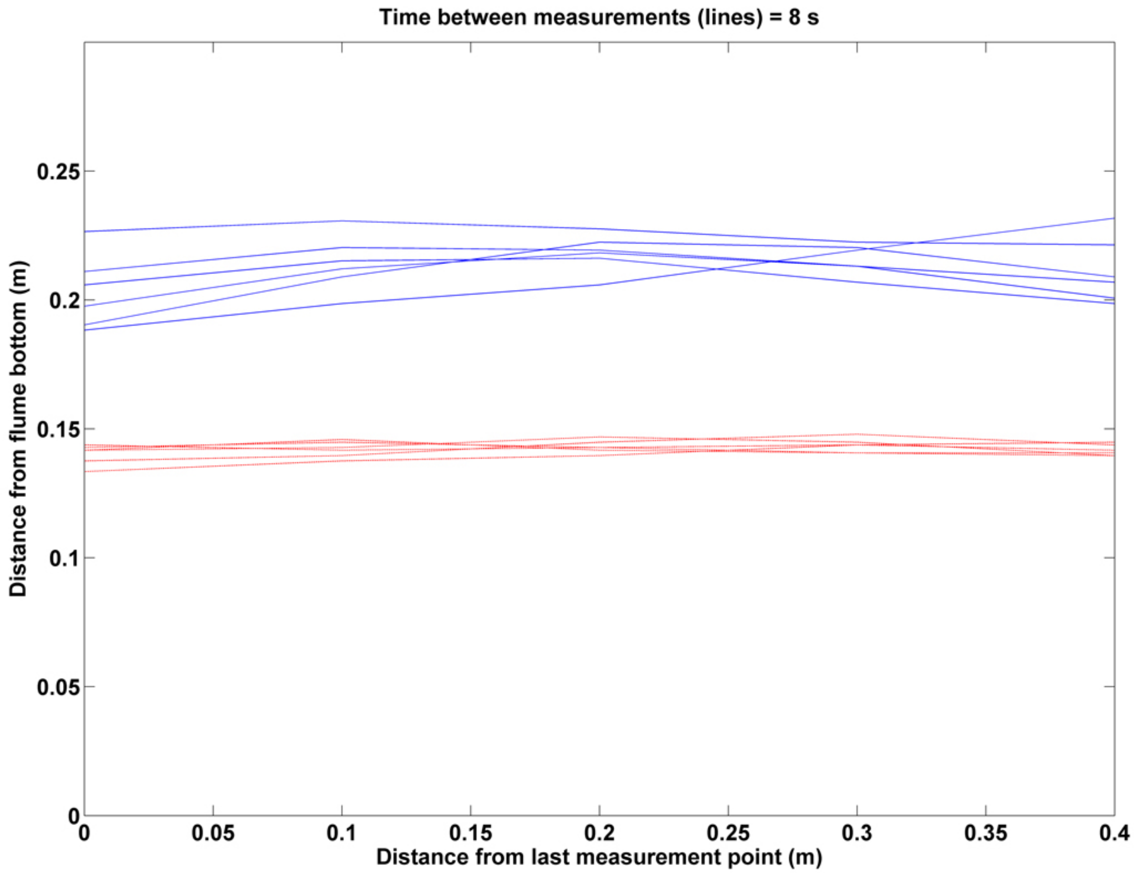

Figure D2: Water level (upper line) and bed level (lower line) measurements with an average discharge of 10.67 l/s.

Table D3: Test conditions and results of Run 2.

Point x	x [m]	h [m]	U [m/s]	v_e [m/s]	R [m]	Fr [-]	k [m/s]	v_e/k [-]	T [°C]
0	0	0.070	1.080	2.33E-04	0.036	1.3	7.29E-05	3.19	21
10	0.1	0.072	1.024	2.85E-04	0.036	1.2	7.29E-05	3.90	21
20	0.2	0.075	0.984	3.10E-04	0.037	1.1	7.29E-05	4.25	21
30	0.3	0.072	1.028	2.59E-04	0.036	1.2	7.29E-05	3.55	21
40	0.4	0.063	1.196	3.10E-04	0.034	1.5	7.29E-05	4.25	21
Average	-	0.070	1.063	2.79E-04	0.036	1.3	7.29E-05	3.83	21

Test 3

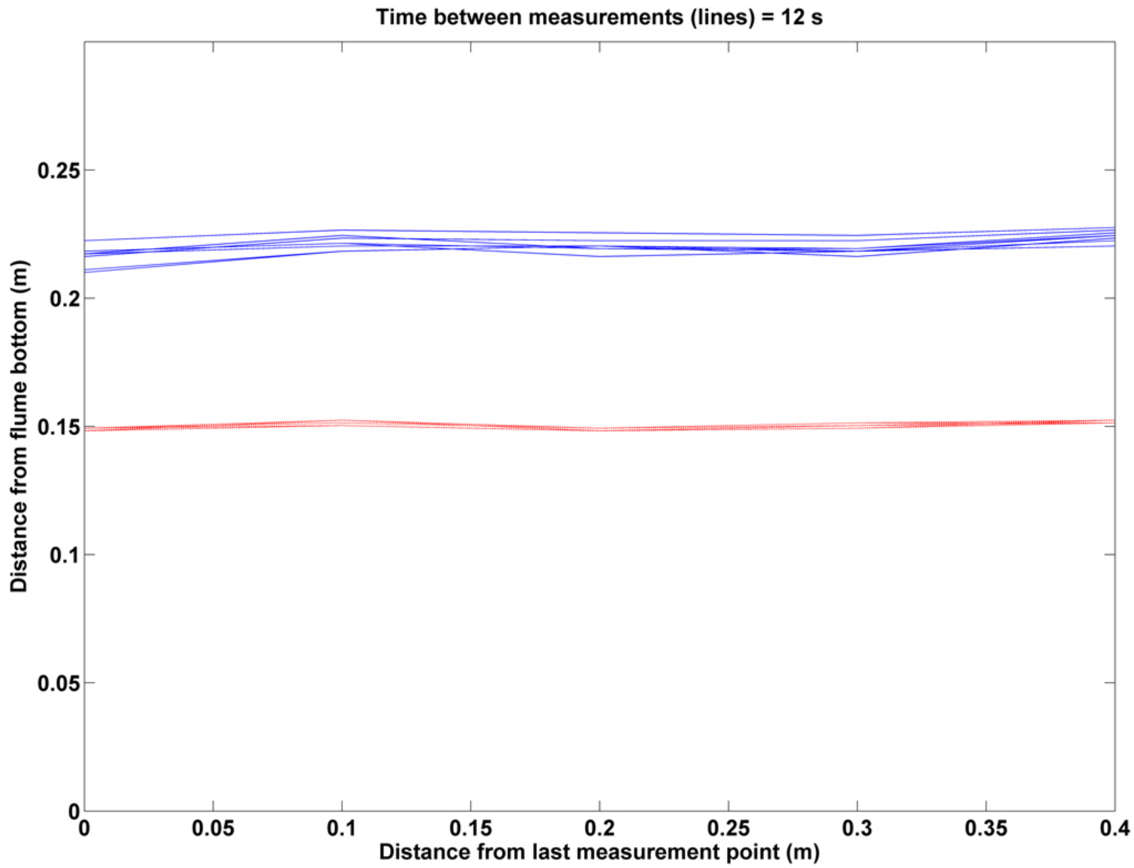

Figure D3: Water level (upper line) and bed level (lower line) measurements with an average discharge of 12.13 l/s.

Table D4: Test conditions and results of Run 3.

Point x	x [m]	h [m]	U [m/s]	v_e [m/s]	R [m]	Fr [-]	k [m/s]	v_e/k [-]	T [$^\circ C$]
0	0	0.073	1.153	6.13E-05	0.036	1.4	3.23E-05	1.90	21
10	0.1	0.069	1.210	3.68E-05	0.035	1.5	3.23E-05	1.14	21
20	0.2	0.072	1.168	3.68E-05	0.036	1.4	3.23E-05	1.14	21
30	0.3	0.070	1.195	8.58E-05	0.036	1.4	3.23E-05	2.66	21
40	0.4	0.067	1.244	3.68E-05	0.035	1.5	3.23E-05	1.14	21
Average	-	0.070	1.194	5.15E-05	0.036	1.4	3.23E-05	1.59	21

Test 4

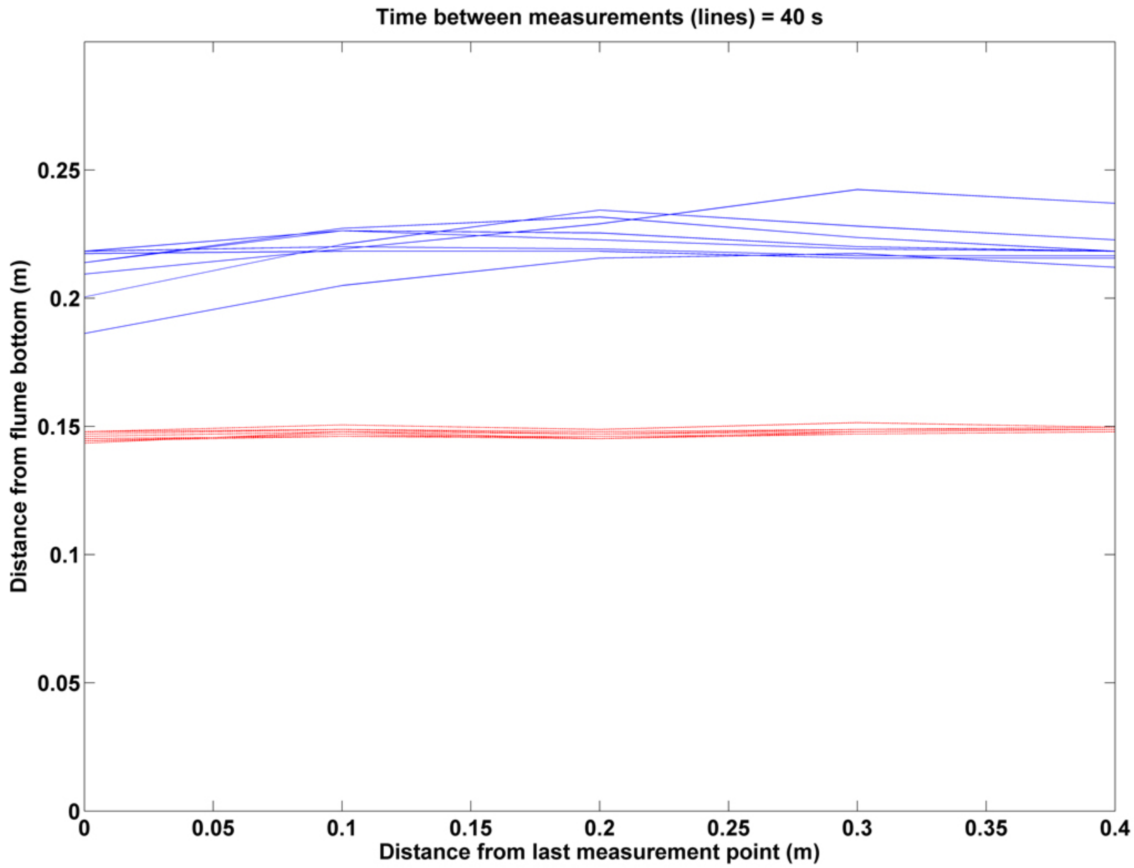

Figure D4: Water level (upper line) and bed level (lower line) measurements with an average discharge of 12.50 l/s.

Table D5: Test conditions and results of Run 4.

Point x	x [m]	h [m]	U [m/s]	v_e [m/s]	R [m]	Fr [-]	k [m/s]	v_e/k [-]	T [$°C$]
0	0	0.071	1.224	1.28E-05	0.036	1.5	4.65E-06	2.74	21
10	0.1	0.075	1.170	2.28E-05	0.037	1.4	4.65E-06	4.90	21
20	0.2	0.078	1.115	1.27E-05	0.038	1.3	4.65E-06	2.74	21
30	0.3	0.073	1.202	2.86E-05	0.036	1.4	4.65E-06	6.16	21
40	0.4	0.064	1.386	2.28E-05	0.034	1.8	4.65E-06	4.90	21
Average	-	0.072	1.219	1.99E-05	0.036	1.5	4.65E-06	4.29	21

Test 5

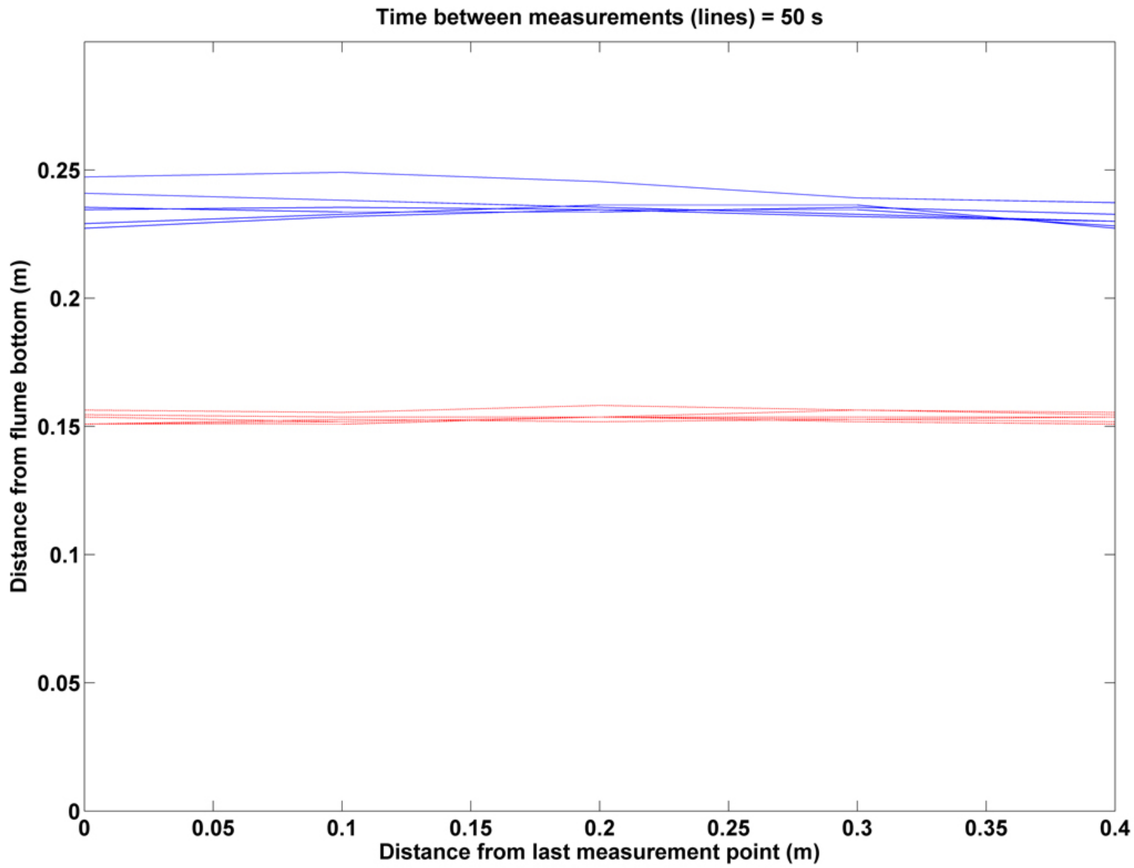

Figure D5: Water level (upper line) and bed level (lower line) measurements with an average discharge of 13.00 l/s.

Table D6: Test conditions and results of Run 5.

Point x	x [m]	h [m]	U [m/s]	v_e [m/s]	R [m]	Fr [-]	k [m/s]	v_e/k [-]	T [$^\circ C$]
0	0	0.078	1.157	2.18E-05	0.0375	1.3	8.09E-07	26.97	21
10	0.1	0.081	1.107	2.18E-05	0.0383	1.2	8.09E-07	26.97	21
20	0.2	0.083	1.087	2.55E-05	0.0386	1.2	8.09E-07	31.46	21
30	0.3	0.084	1.070	2.55E-05	0.0389	1.2	8.09E-07	31.46	21
40	0.4	0.083	1.088	4.36E-05	0.0387	1.2	8.09E-07	53.94	21
Average	-	0.082	1.102	2.76E-05	0.0384	1.2	8.09E-07	34.16	21

Test 6

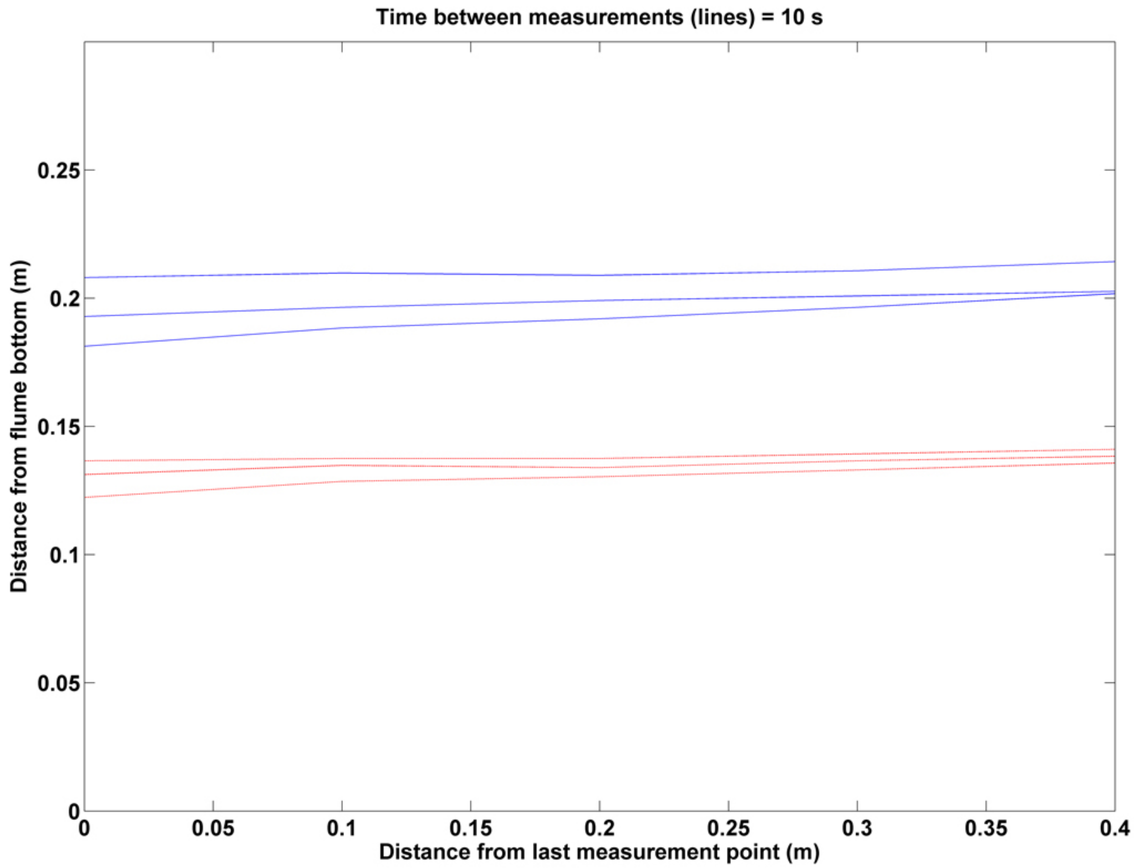

Figure D6: Water level (upper line) and bed level (lower line) measurements with an average discharge of 13.88 l/s.

Table D7: Test conditions and results of Run 6.

Point x	x [m]	h [m]	U [m/s]	v_e [m/s]	R [m]	Fr [-]	k [m/s]	v_e/k [-]	T [$^\circ C$]
0	0	0.069	1.415	2.68E-04	0.0354	1.7	9.88E-05	2.71	21
10	0.1	0.068	1.446	3.13E-04	0.0351	1.8	9.88E-05	3.16	21
20	0.2	0.067	1.454	3.57E-04	0.0349	1.8	9.88E-05	3.61	21
30	0.3	0.067	1.493	4.46E-04	0.0347	1.8	9.88E-05	4.52	21
40	0.4	0.064	1.506	7.14E-04	0.0341	1.9	9.88E-05	7.23	21
Average	-	0.067	1.463	4.20E-04	0.0348	1.8	9.88E-05	4.25	21

Test 7

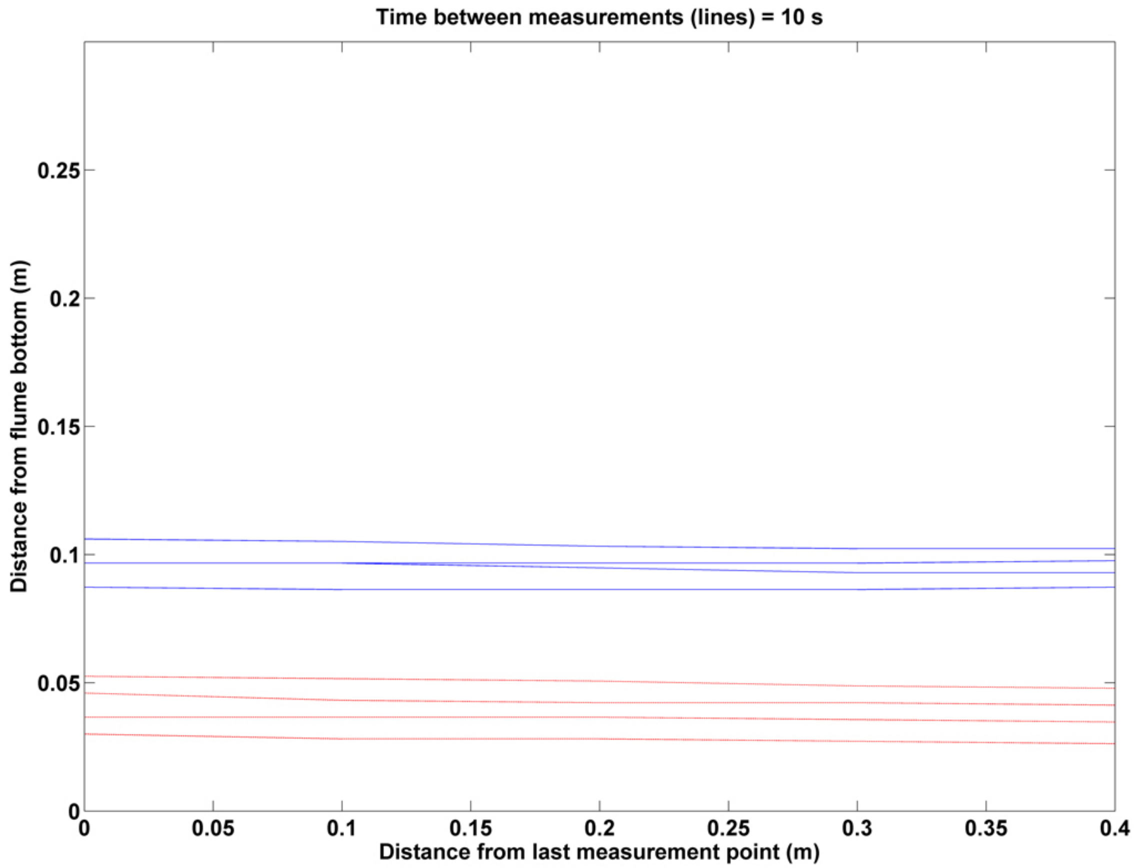

Figure D7: Water level (upper line) and bed level (lower line) measurements with an average discharge of 17.4 l/s.

Table D8: Test conditions and results of Run 7.

Point x	x [m]	h [m]	U [m/s]	v_e [m/s]	R [m]	Fr [-]	k [m/s]	v_e/k [-]	T [$°C$]
0	0	0.056	2.166	7.64E-04	0.0317	2.9	4.83E-04	1.58	21
10	0.1	0.056	2.148	7.18E-04	0.0317	2.9	4.83E-04	1.49	21
20	0.2	0.057	2.146	8.10E-04	0.0318	2.9	4.83E-04	1.68	21
30	0.3	0.056	2.183	8.10E-04	0.0315	3.0	4.83E-04	1.68	21
40	0.4	0.055	2.190	8.10E-04	0.0314	3.0	4.83E-04	1.68	21
Average	-	0.056	2.166	7.82E-04	0.0316	2.9	4.83E-04	1.62	21

Test 8

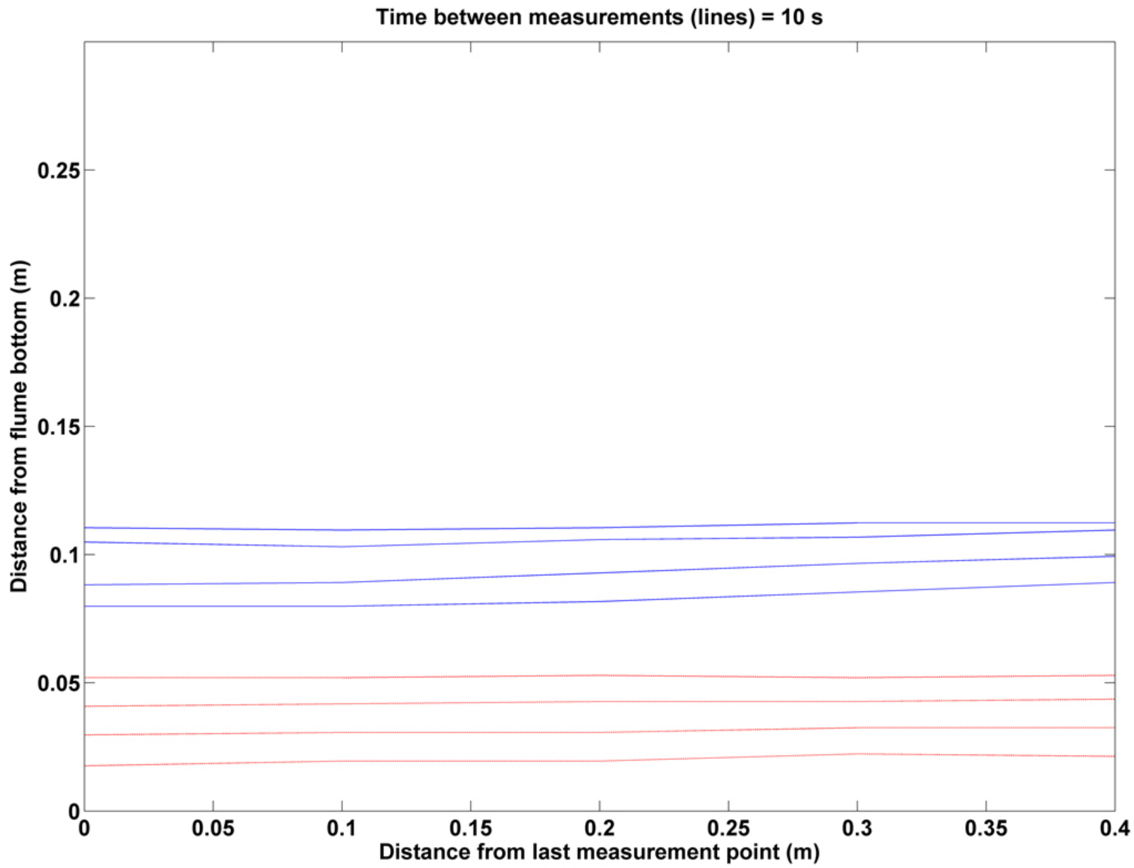

Figure D8: Water level (upper line) and bed level (lower line) measurements with an average discharge of 18.00 l/s.

Table D9: Test conditions and results of Run 8.

Point x	x [m]	h [m]	U [m/s]	v_e [m/s]	R [m]	Fr [-]	k [m/s]	v_e/k [-]	T [$°C$]
0	0	0.068	1.915	1.00E-03	0.0351	2.3	9.88E-05	10.12	21
10	0.1	0.070	1.974	1.00E-03	0.0355	2.4	9.88E-05	10.12	21
20	0.2	0.070	2.028	1.10E-03	0.0356	2.5	9.88E-05	11.13	21
30	0.3	0.070	2.090	1.10E-03	0.0356	2.5	9.88E-05	11.13	21
40	0.4	0.070	2.044	1.10E-03	0.0355	2.5	9.88E-05	11.13	21
Average	-	0.069	2.010	1.06E-03	0.0355	2.4	9.88E-05	10.73	21

Test 9

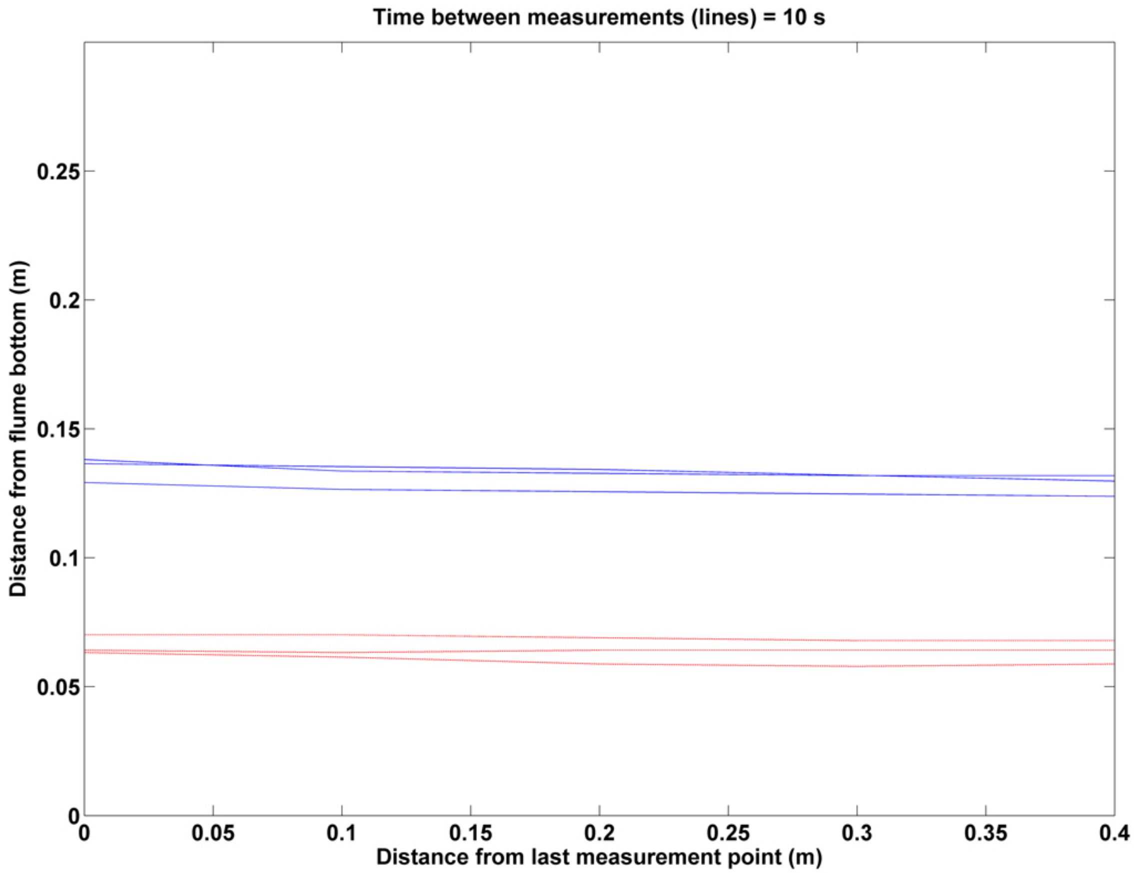

Figure D9: Water level (upper line) and bed level (lower line) measurements with an average discharge of 19.16 l/s.

Table D10: Test conditions and results of Run 9.

Point x	x [m]	h [m]	U [m/s]	v_e [m/s]	R [m]	Fr [-]	k [m/s]	v_e/k [-]	T [°C]
0	0	0.065	2.053	4.54E-04	0.0342	2.6	7.29E-05	6.23	21
10	0.1	0.066	2.010	4.99E-04	0.0347	2.5	7.29E-05	6.84	21
20	0.2	0.069	1.987	5.10E-04	0.0353	2.4	7.29E-05	7.00	21
30	0.3	0.066	1.982	4.33E-04	0.0344	2.5	7.29E-05	5.94	21
40	0.4	0.067	1.929	3.44E-04	0.0348	2.4	7.29E-05	4.71	21
Average	-	0.067	1.992	4.48E-04	0.0347	2.5	7.29E-05	6.14	21

Test 10

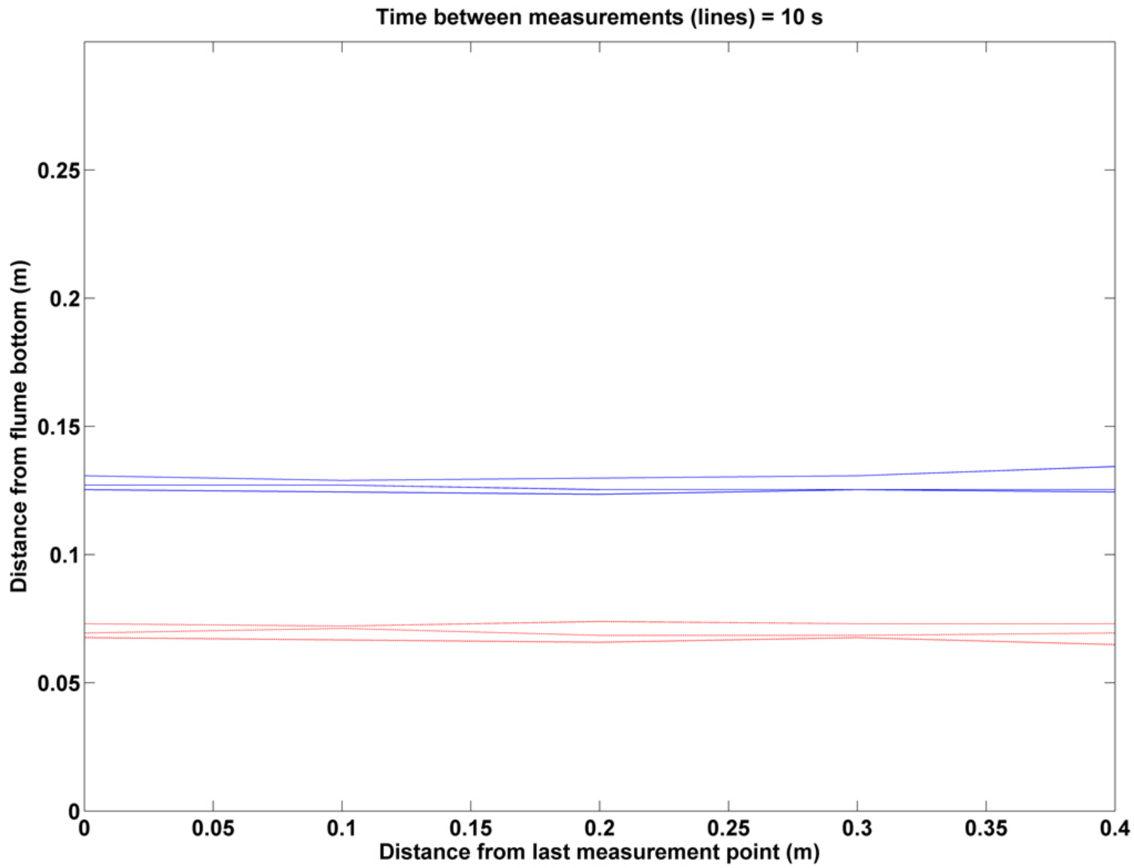

Figure D10: Water level (upper line) and bed level (lower line) measurements with an average discharge of 17.76 l/s.

Table D11: Test conditions and results of Run 10.

Point x	x [m]	h [m]	U [m/s]	v_e [m/s]	R [m]	Fr [-]	k [m/s]	v_e/k [-]	T [$^\circ C$]
0	0	0.059	2.113	4.06E-04	0.0325	2.8	3.23E-05	12.56	21
10	0.1	0.057	2.146	2.70E-04	0.0320	2.9	3.23E-05	8.36	21
20	0.2	0.057	2.174	4.06E-04	0.0319	2.9	3.23E-05	12.56	21
30	0.3	0.057	2.166	2.71E-04	0.0319	2.9	3.23E-05	8.37	21
40	0.4	0.058	2.132	2.71E-04	0.0321	2.8	3.23E-05	8.37	21
Average	-	0.058	2.146	3.25E-04	0.0321	2.9	3.23E-05	10.05	21

Test 11

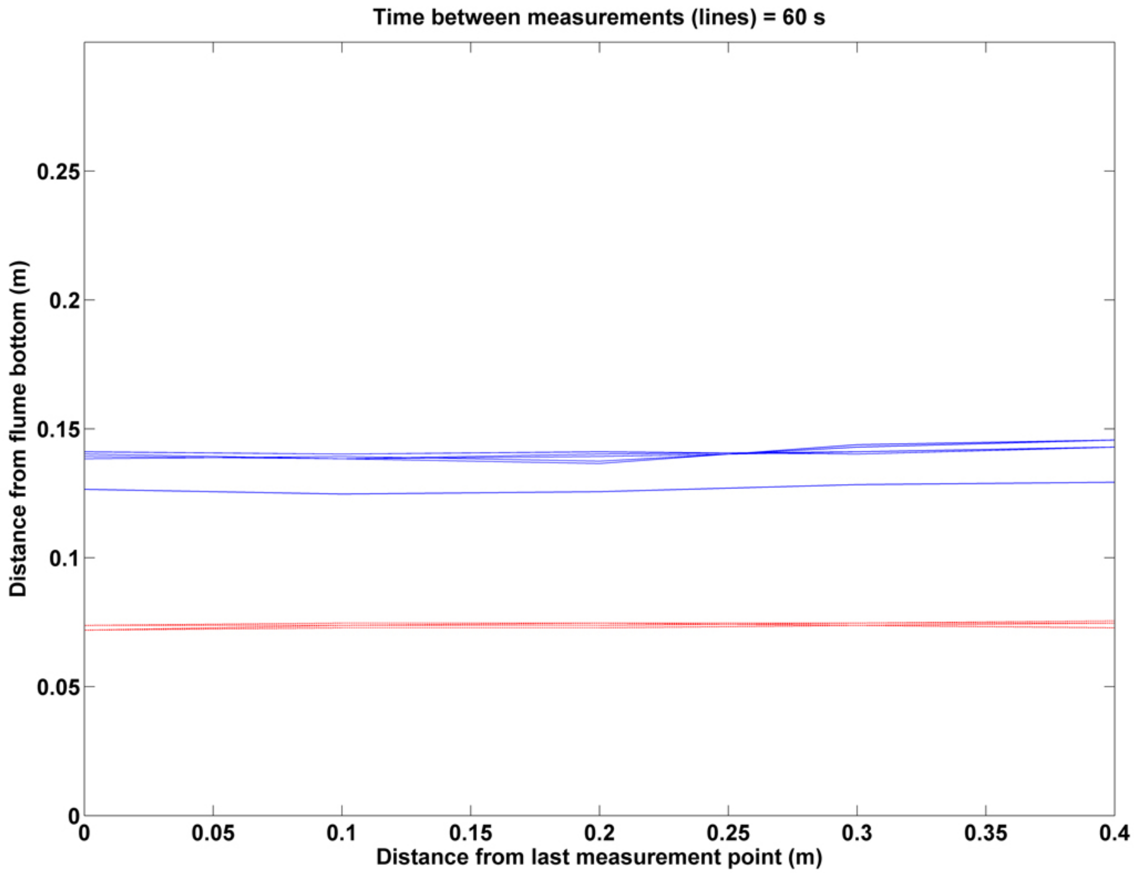

Figure D11: Water level (upper line) and bed level (lower line) measurements with an average discharge of 15.93 l/s.

Table D12: Test conditions and results of Run 11.

Point x	x [m]	h [m]	U [m/s]	v_e [m/s]	R [m]	Fr [-]	k [m/s]	v_e/k [-]	T [°C]
0	0	0.067	1.654	9.10E-06	0.0348	2.0	4.65E-06	1.96	21
10	0.1	0.065	1.696	9.10E-06	0.0343	2.1	4.65E-06	1.96	21
20	0.2	0.063	1.769	1.21E-05	0.0336	2.3	4.65E-06	2.61	21
30	0.3	0.063	1.766	6.07E-06	0.0337	2.2	4.65E-06	1.31	21
40	0.4	0.065	1.706	6.07E-06	0.0343	2.1	4.65E-06	1.31	21
Average	-	0.065	1.718	8.50E-06	0.0341	2.2	4.65E-06	1.83	21

Test 12

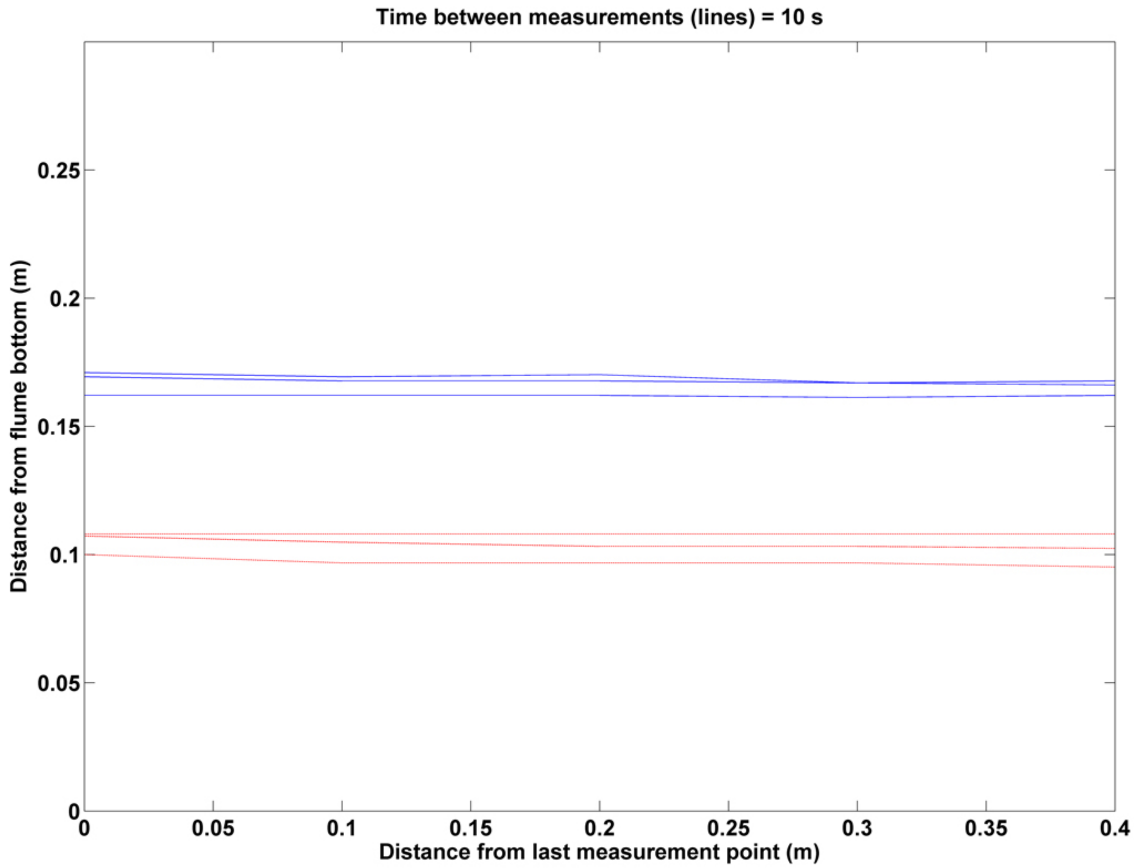

Figure D12: Water level (upper line) and bed level (lower line) measurements with an average discharge of 17.46 l/s.

Table D13: Test conditions and results of Run 12.

Point x	x [m]	h [m]	U [m/s]	v_e [m/s]	R [m]	Fr [-]	k [m/s]	v_e/k [-]	T [°C]
0	0	0.062	1.945	4.40E-04	0.0335	2.5	-	-	21
10	0.1	0.061	1.987	5.60E-04	0.0332	2.6	-	-	21
20	0.2	0.062	1.968	4.40E-04	0.0334	2.5	-	-	21
30	0.3	0.061	2.002	4.00E-04	0.0331	2.6	-	-	21
40	0.4	0.061	2.001	3.20E-04	0.0331	2.6	-	-	21
Average	-	0.061	1.980	4.32E-04	0.0333	2.6	-	-	21

Test 13

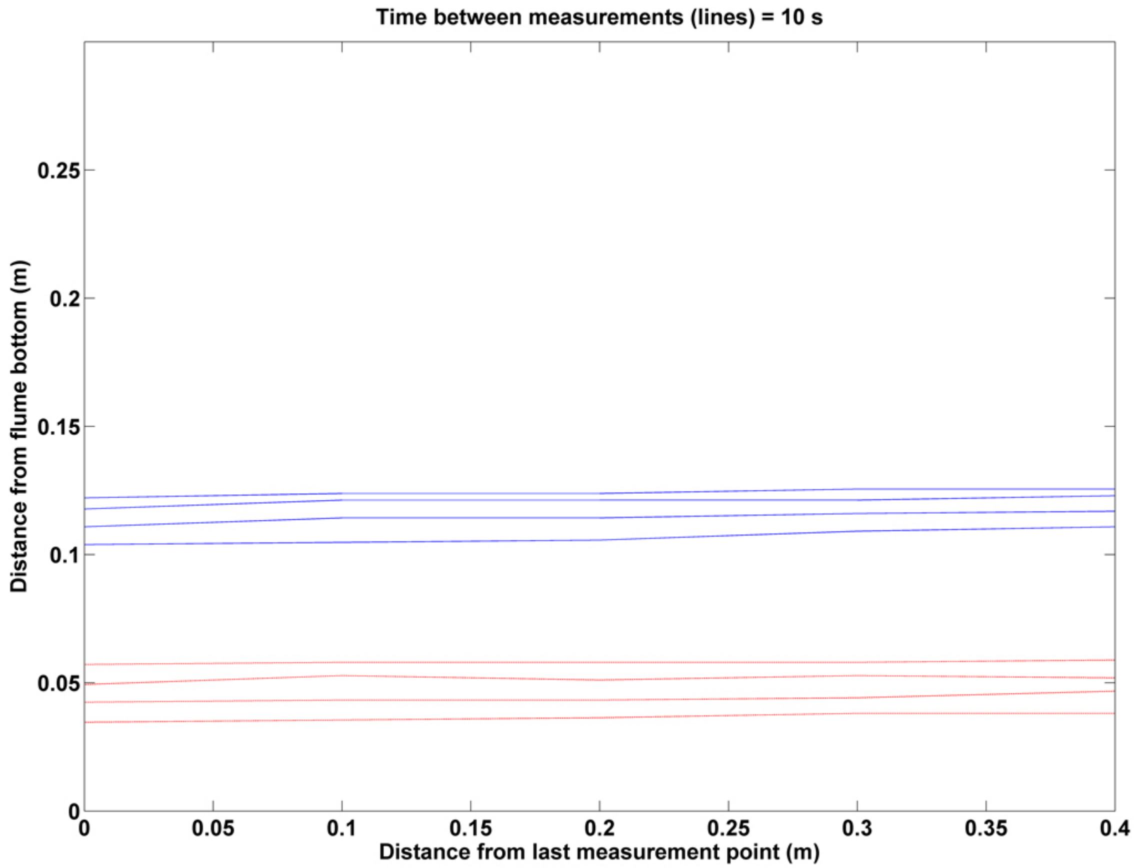

Figure D13: Water level (upper line) and bed level (lower line) measurements with an average discharge of 19.47 l/s.

Table D14: Test conditions and results of Run 13.

Point x	x [m]	h [m]	U [m/s]	v_e [m/s]	R [m]	Fr [-]	k [m/s]	v_e/k [-]	T [$^\circ C$]
0	0	0.070	1.916	6.93E-04	0.0357	2.3	4.83E-04	1.43	21
10	0.1	0.070	1.927	6.64E-04	0.0355	2.3	4.83E-04	1.37	21
20	0.2	0.069	1.946	7.22E-04	0.0354	2.4	4.83E-04	1.49	21
30	0.3	0.069	1.958	7.51E-04	0.0353	2.4	4.83E-04	1.55	21
40	0.4	0.068	1.983	7.51E-04	0.0350	2.4	4.83E-04	1.55	21
Average	-	0.069	1.946	7.16E-04	0.0354	2.4	4.83E-04	1.48	21

E | Clear water tests

This section elaborates on the clear water tests performed in the tilting flume in the Laboratory for Fluid Mechanics of the Delft University of Technology. The main goal of these tests was to get more insight into the flow velocity field within the flume. A secondary reason was the verification of reasonable uniform conditions in the area of interest. Two different test conditions were investigated. The first condition was with a smooth glass bottom (Fig. E1a). In the second condition 3 m of the bottom of the flume was covered with aluminium plates. The top of these aluminium plates were covered with sand with a D_{50} of 2 mm (Fig. E1b). The sand layer was glued to the plates in order to simulate a rough bottom.

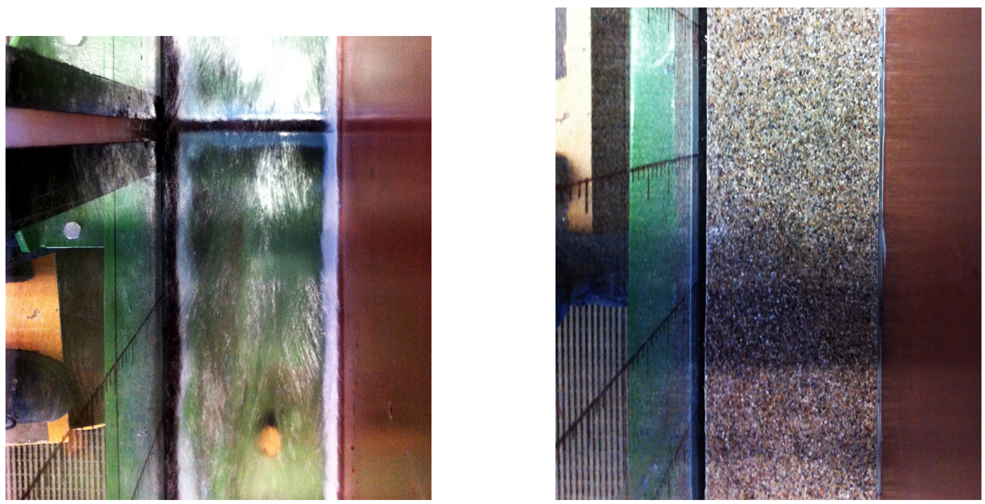

Figure E1: (a) Smooth glass bottom of the flume (b) Simulation of a rough bottom.

The water level measurements

The water level measurements were performed with an adjustable staff gauge as discussed in Section 5.1.2. Both the bottom level and the water surface level were measured. The water depth was calculated by subtracting the value of the bed level from the water surface level. Although the staff gauge could measure both levels with an accuracy of 1 mm, the slight water level fluctuation added another 2 mm of inaccuracy. The results of the smooth and rough bottom measurements are presented in Fig. E2 and Fig. E3.

In longitudinal direction, at three (rough bottom) or five (smooth bottom) locations, measurements were taken. The reference point (0 on the x-axis in Fig. E2 and Fig. E3) was positioned at the 50 cm line in the area of interest (see Fig. 22). Locations on the negative side of the x-axis are located upstream of the reference location and locations on the positive side of the x-axis more downstream. At each longitudinal postion, three measurements were taken in cross direction. Profile 1 represents the measurements closest to the glass wall (2,5 cm from the glass wall), profile 2 the measurements in the middle of the flume and profile 3 the measurements closest to the plywood wall (again 2,5 cm from the plywood wall).

Although the water level is slightly higher in the rough bottom case (with the same pump discharge) as opposed to the smooth bottom case, there is hardly any water level surface gradient present in both cases. The differences in cross direction are also negligible. Therefore, it is fair to assume that uniform conditions in the area of interest were indeed present.

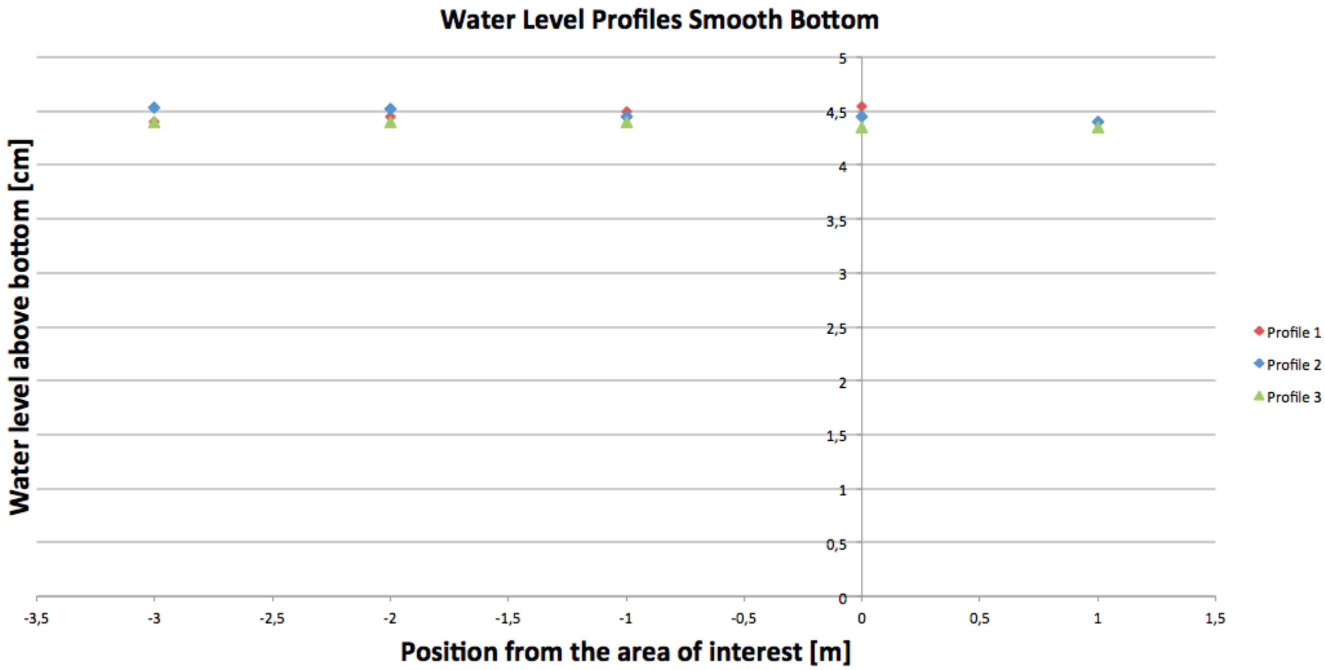

Figure E2: Water level measurements with a smooth bottom.

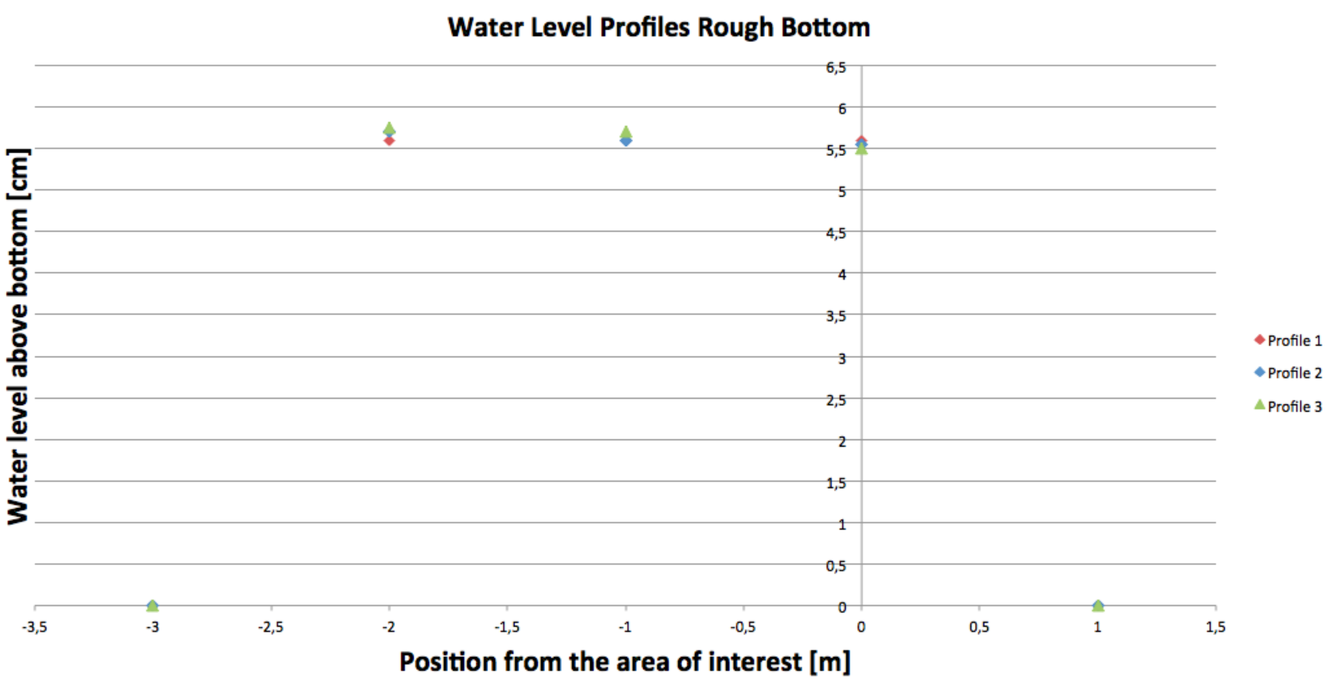

Figure E3: Water level measurements with a rough bottom.

The velocity field measurements
For the flow velocity measurements a electromagnetic flow velocity meter, as discussed in Section 5.1.2, was used. In total 50 measurements were recorded, 25 for the smooth bottom scenario and 25 for the rough bottom scenario. Only at one location in longitudinal direction measurements were recorded, namely at the 50 cm line in the area of interest (see Fig. 22). Every 2.5 cm in a total of five locations in cross direction measurements were taken. Profile 1 represents the measurements closest to the glass wall (2,5 cm from the glass wall), profile 2 the measurements

5.0 cm from the glass wall, profile 3 the measurements in the middle of the flume, profile 4 the measurements 5.0 cm from the plywood wall and profile 5 the measurements 2,5 cm from the plywood wall. In addition, 5 (smooth bottom) and 6 (rough bottom) measurements were taken in vertical direction. These measurements were taken at a height of 2, 6, 16, 26, 36 and (41) mm above the bed. The most upper measurement was taken as heigh up in the water column as possible, without being inaccurate. This was roughly 5 mm above the previous measurement point. The results of the smooth and rough bottom measurements are presented in Fig. E4 and Fig. E5.

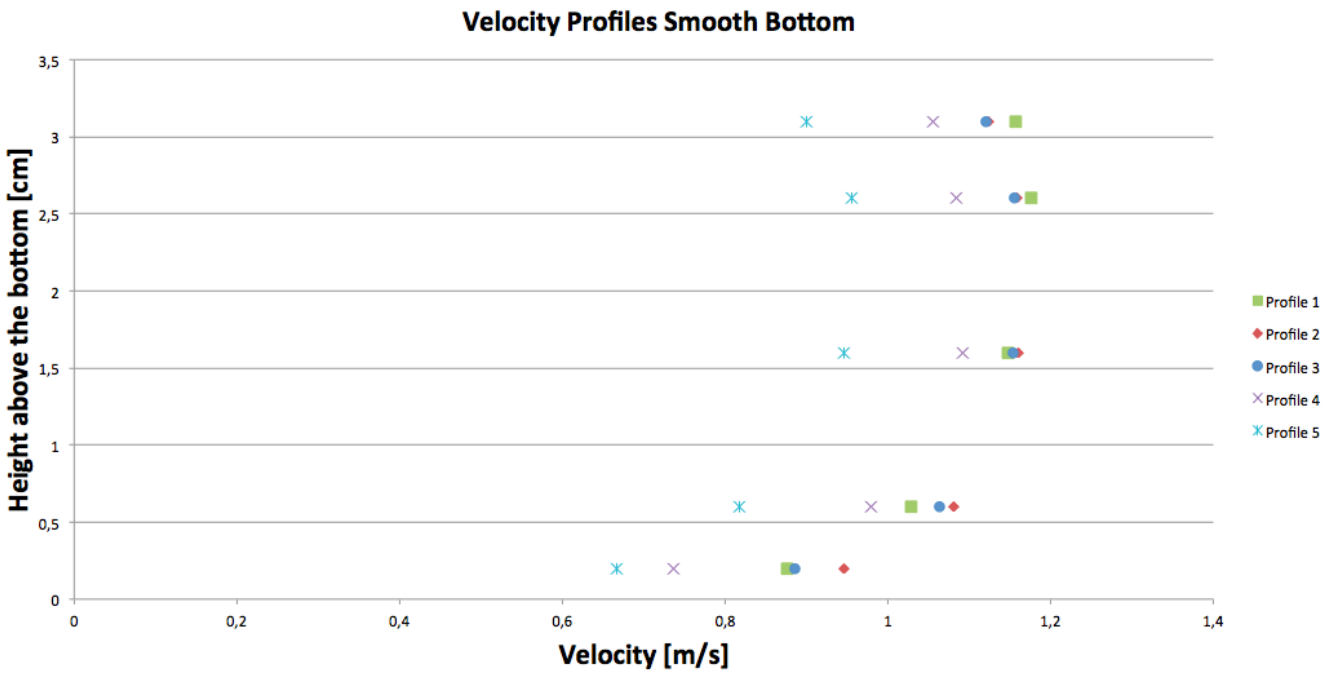

Figure E4: Velocity measurements with a smooth bottom.

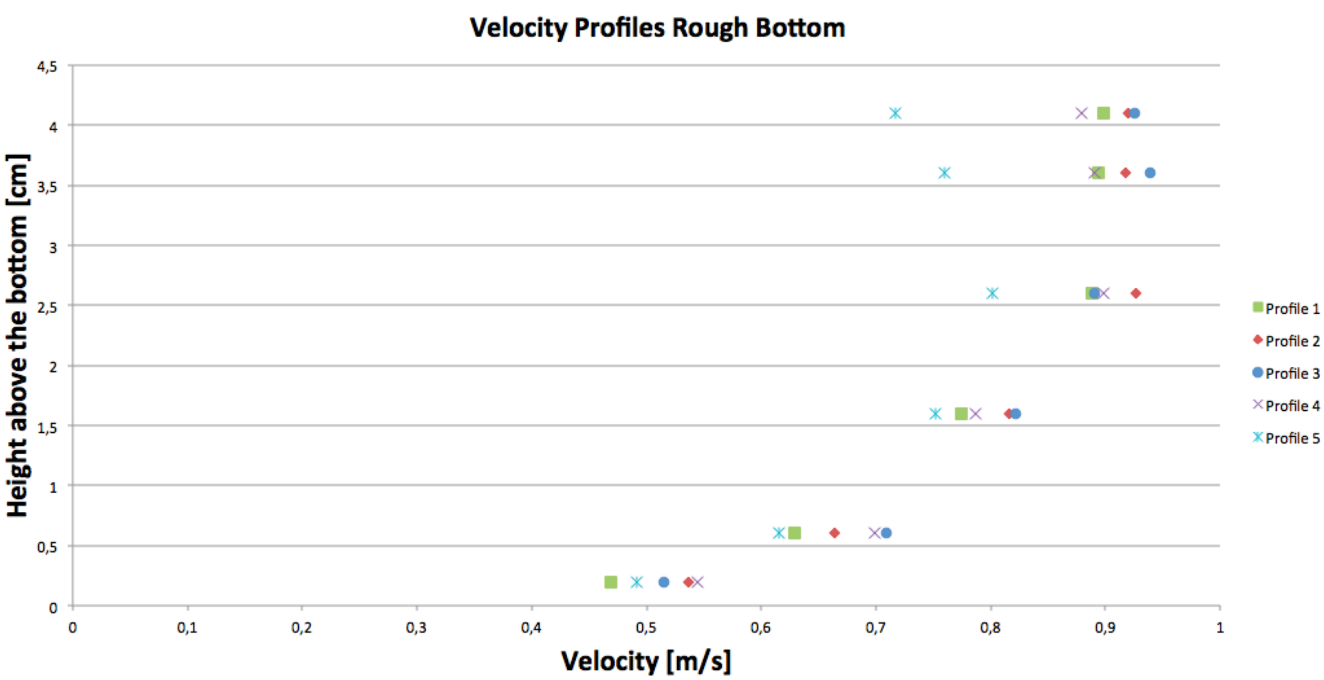

Figure E5: Velocity measurements with a rough bottom.

The measured flow velocity values in Fig. E4 and Fig. E5 show decreasing flow velocity values near the water surface, which were caused by both the presence of the measurement instrument and due to the boundary effects of the air layer above. The (logarithmic) shape of the vertical velocity profiles in both cases is fairly identical, with one exception. In the rough bottom case, the increased bottom friction is clearly visible (the profile is more stretched in horizontal direction). The most important observation however, is that there is a clear influence of the wall on the velocity profile. Based on these observations, the effect of the glass wall (profile 1 and 2) is almost not apparent, but the effect of the plywood wall (especially profile 5) is clearly affecting the velocity profile. This effect certainly has to be taken into account.

F | Data analyses

This section contains graphs of the results obtained in the tilting flume in the Laboratory for Fluid Mechanics of the Delft University of Technology. In addition, graphs of the data analysis of these results are presented. These graphs support the analysis of Section.6.1.

v_e/k **versus bed shear stress for different sand types.**

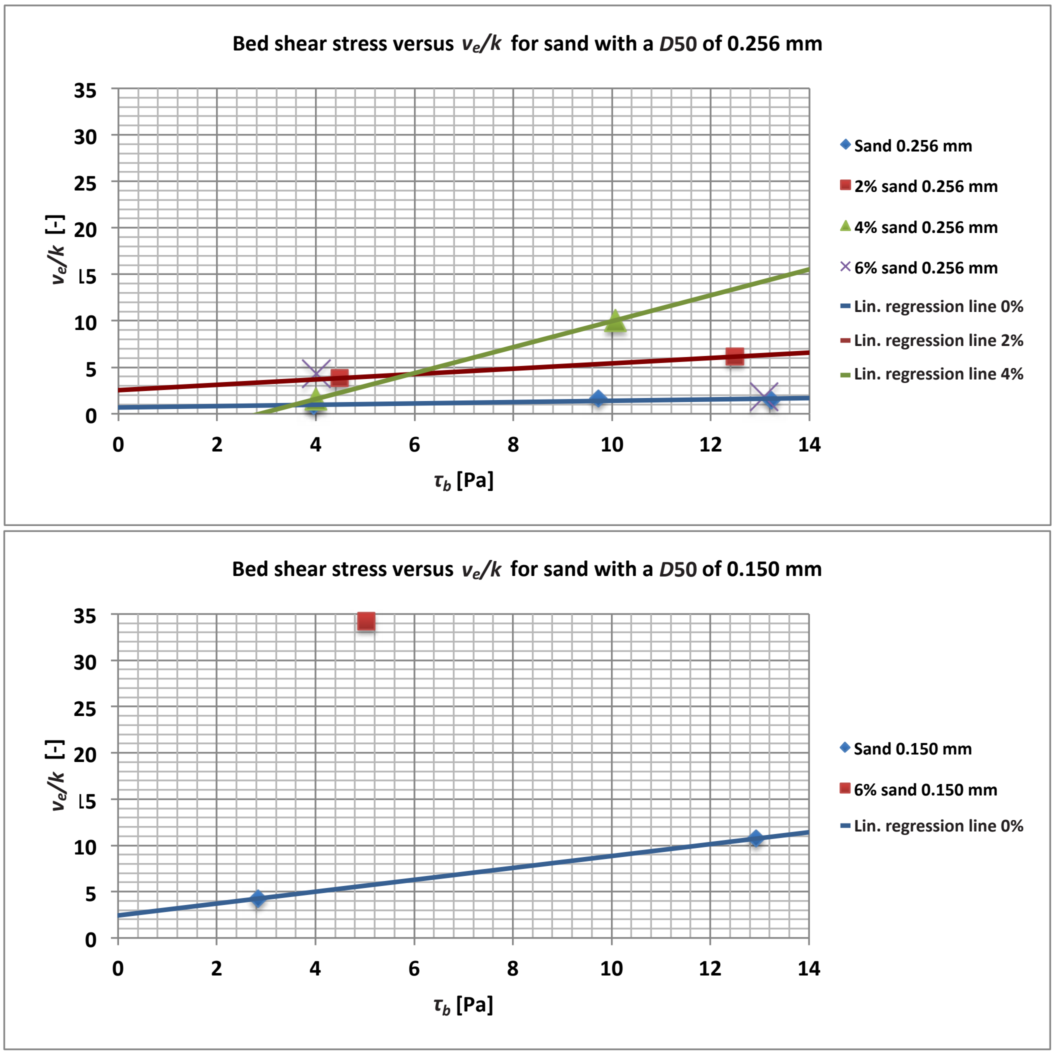

Figure F1: v_e/k versus bed shear stress for (a) sand mixtures with a D_{50} of 0.256 mm and (b) sand mixtures with a D_{50} of 0.150 mm.

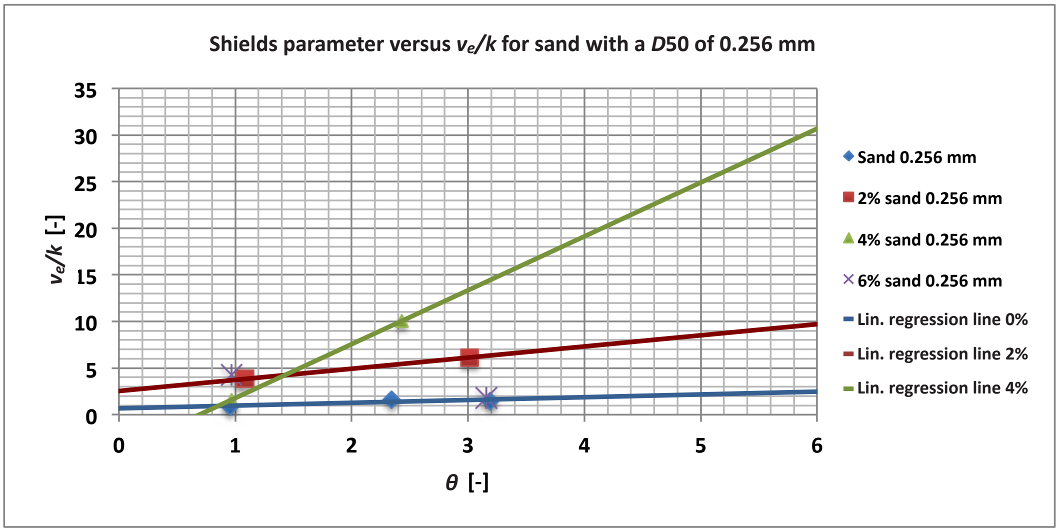

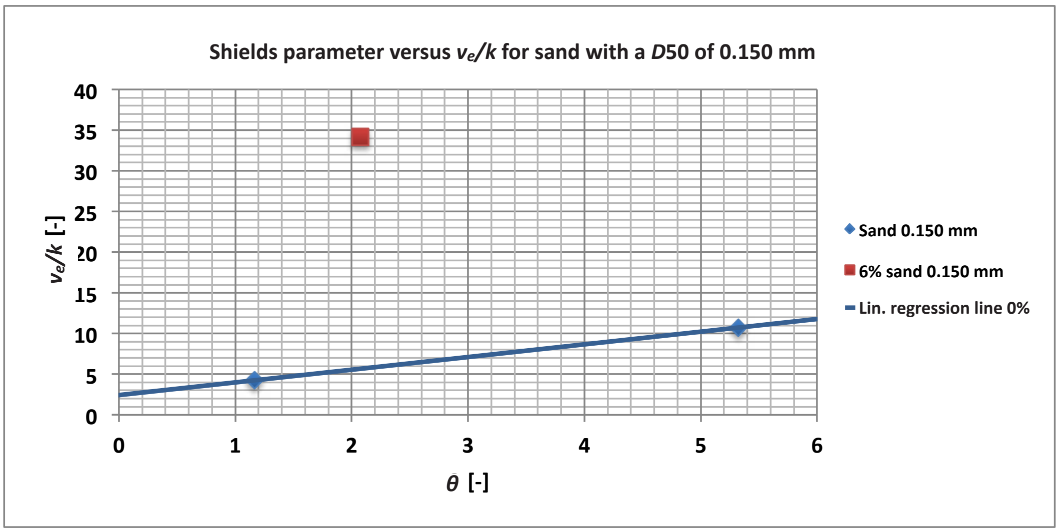

Figure F2: v_e/k versus the Shields parameter for (a) sand mixtures with a D_{50} of 0.256 mm and (b) sand mixtures with a D_{50} of 0.150 mm.

Averaged results of the erosion tests.

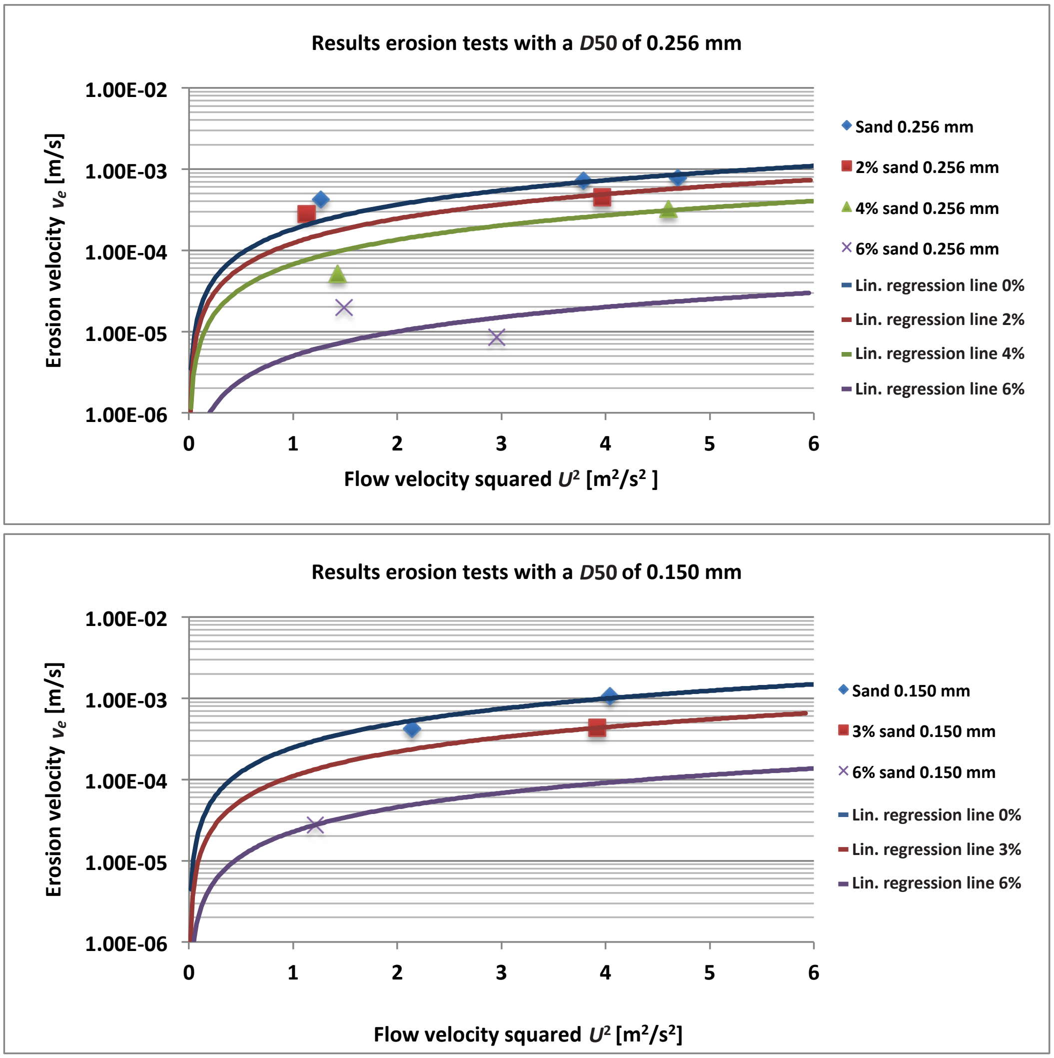

Figure F3: Averaged erosion velocity versus depth-average flow velocity squared for (a) sand with a D_{50} of 0.256 mm and (b) sand with a D_{50} of 0.150 mm.

Erosion velocity versus bed shear stresses.

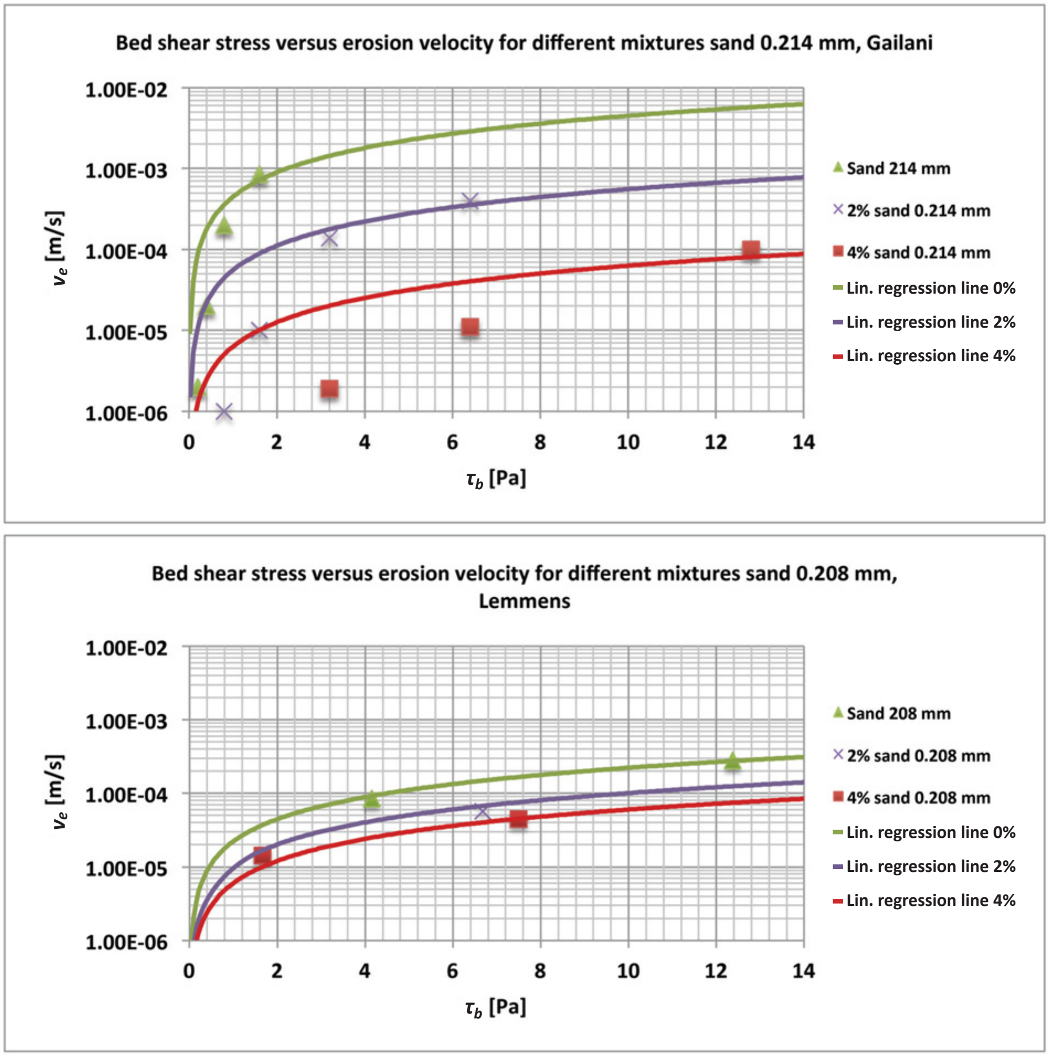

Figure F4: Erosion velocity versus bed shear stress versus velocity for (a) sand with a D_{50} of 0.214 mm from Lemmens Lemmens (2014) and (b) sand with a D_{50} of 0.208 mm from Gailani Gailani (2001).

Erosion velocity versus depth-averaged flow velocities squared with data from Lemmens

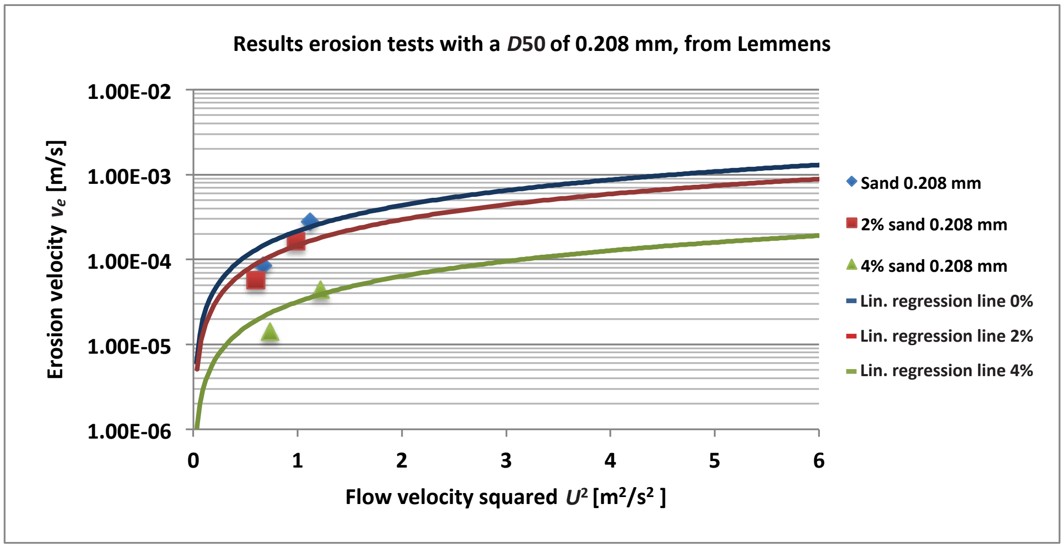

Figure F5: Reduction of the erosion velocity as function of the bentonite content from depth-averaged flow velocities squared, from Lemmens.

G | Additional data case study Borssele

This section contains graphs of the results for the runs of Scenario A and Scenario B with the largest initial breach height of 2 m. The water levels, in the graphs, are expressed as levels above NAP. NAP is the reference level in the Netherlands at about mean sea level.

Scenario A

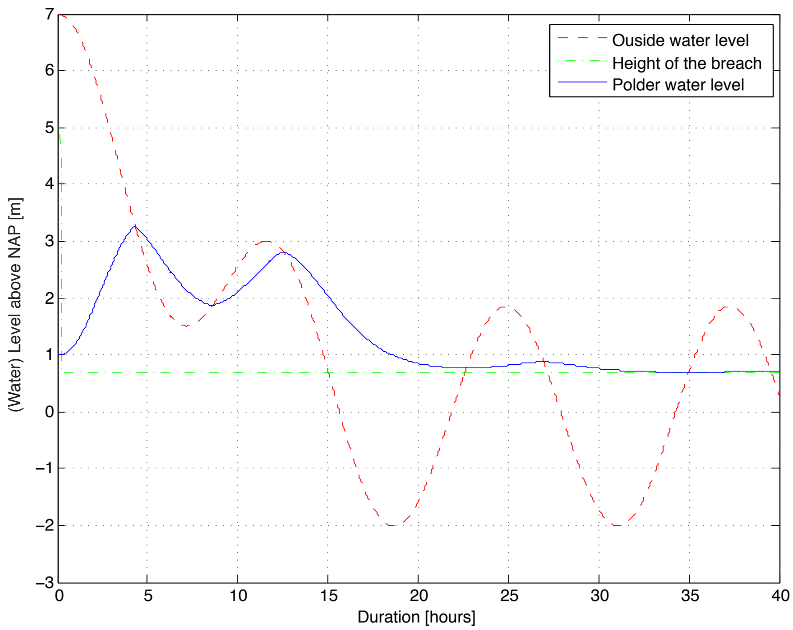

Figure G1: (Water) Levels of Scenario A-9.

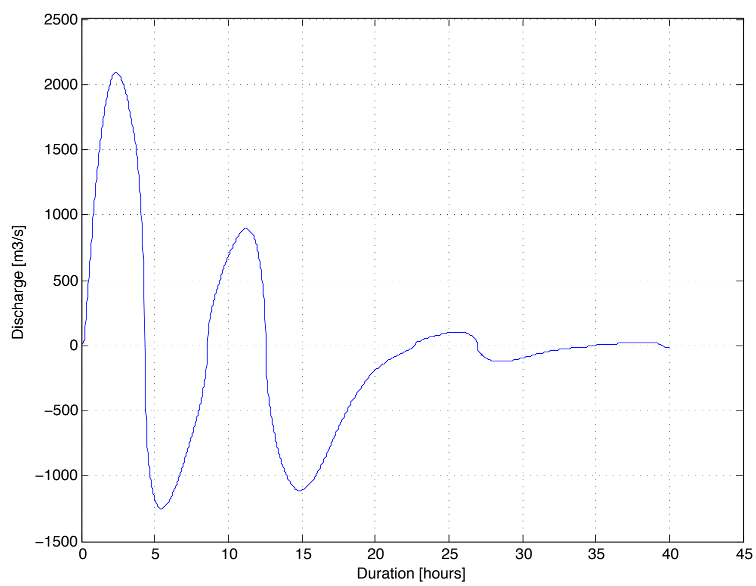

Figure G2: Discharge of Scenario A-9.

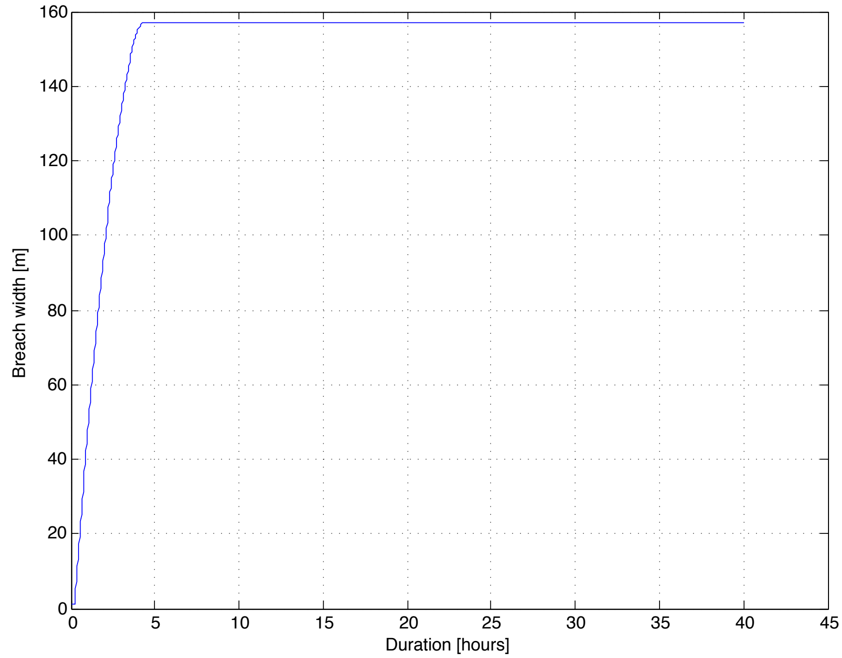

Figure G3: Development of the breach with in Scenario A-9.

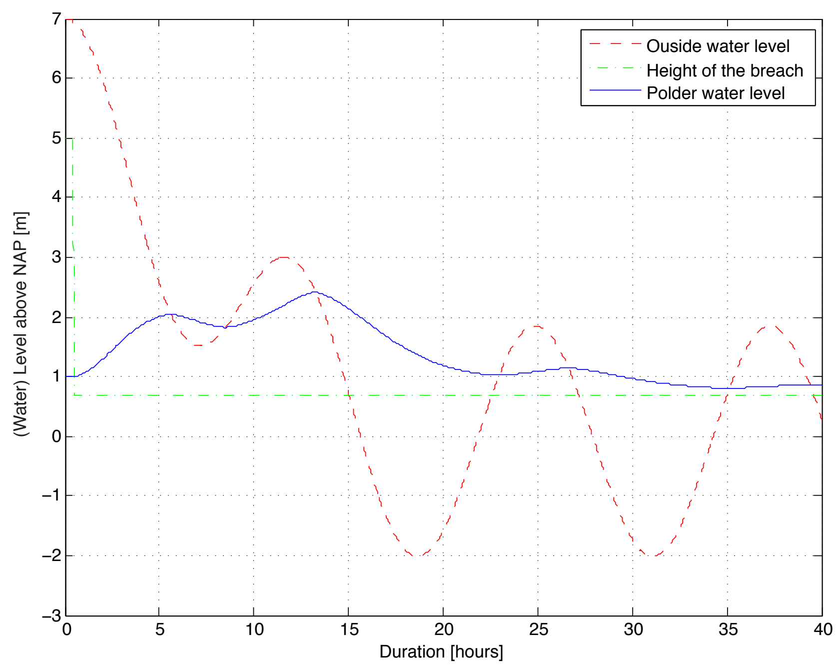

Figure G4: (Water) Levels of Scenario A-10.

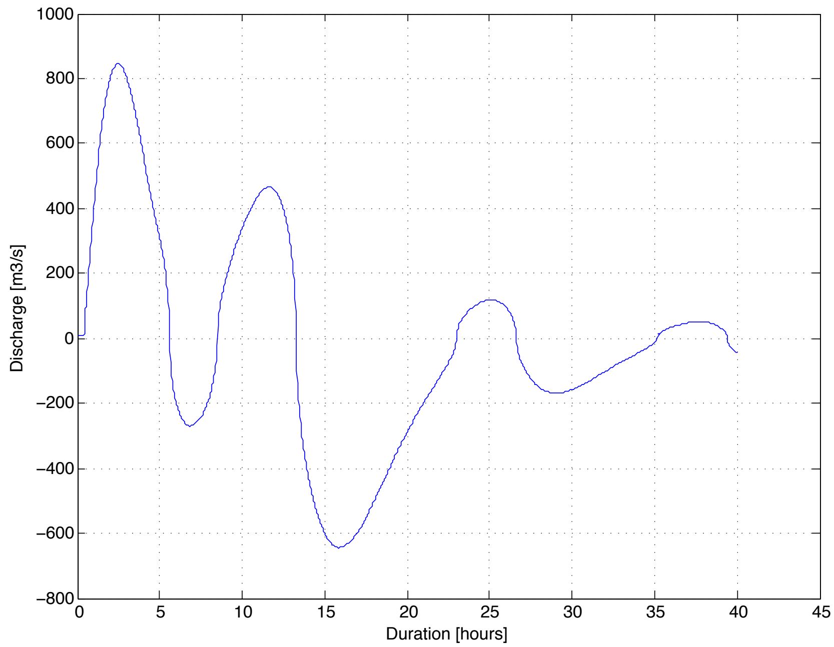

Figure G5: Discharge of Scenario A-10.

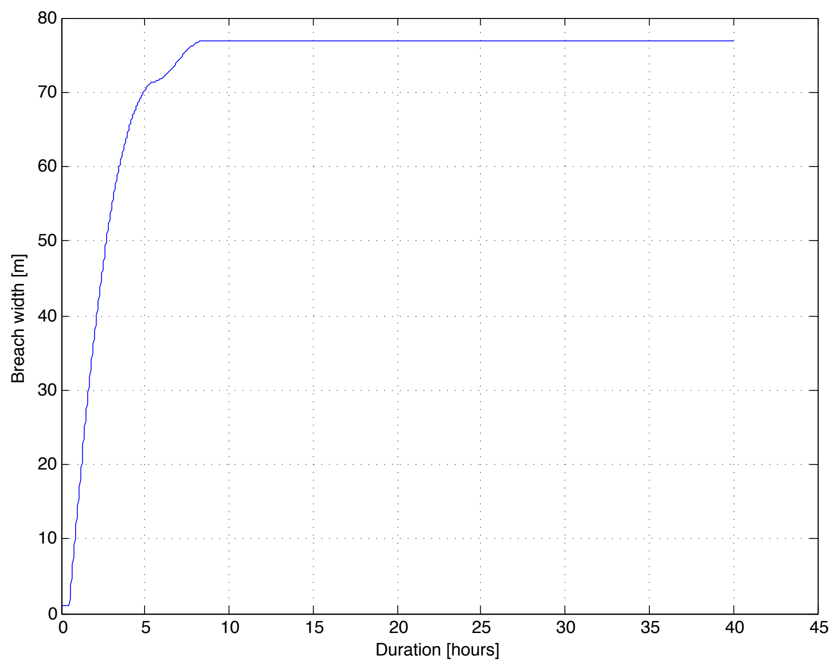

Figure G6: Development of the breach width in Scenario A-10.

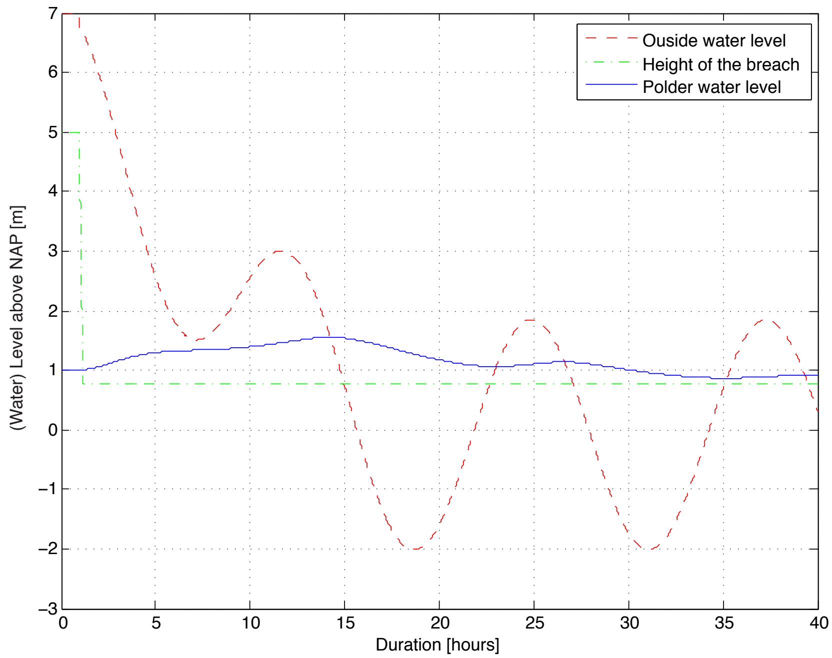

Figure G7: (Water) Levels of Scenario A-11.

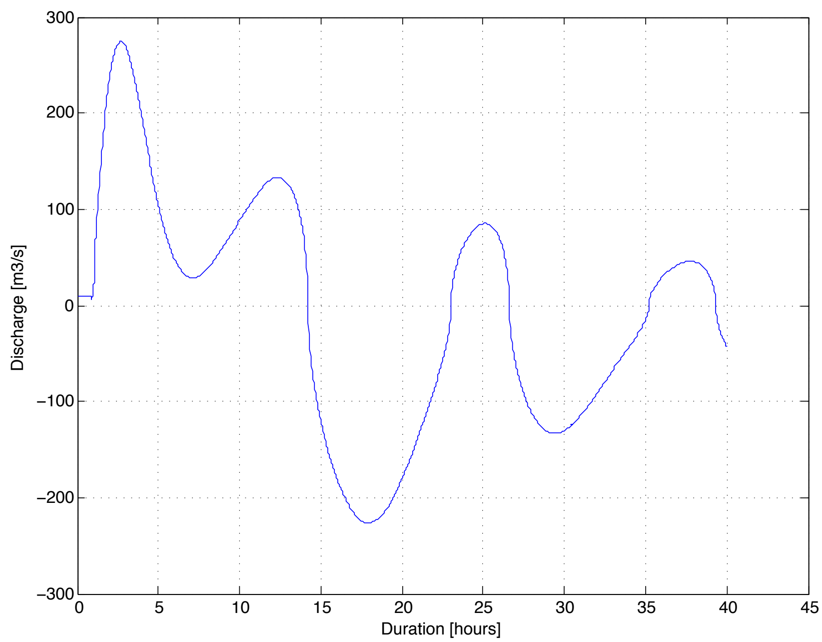

Figure G8: Discharge of Scenario A-11.

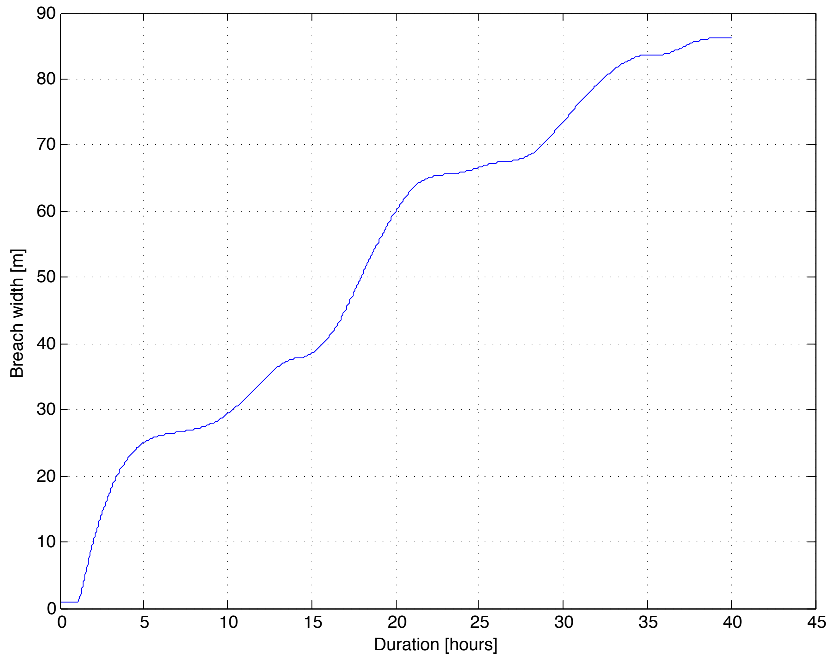

Figure G9: Development of the breach with in Scenario A-11.

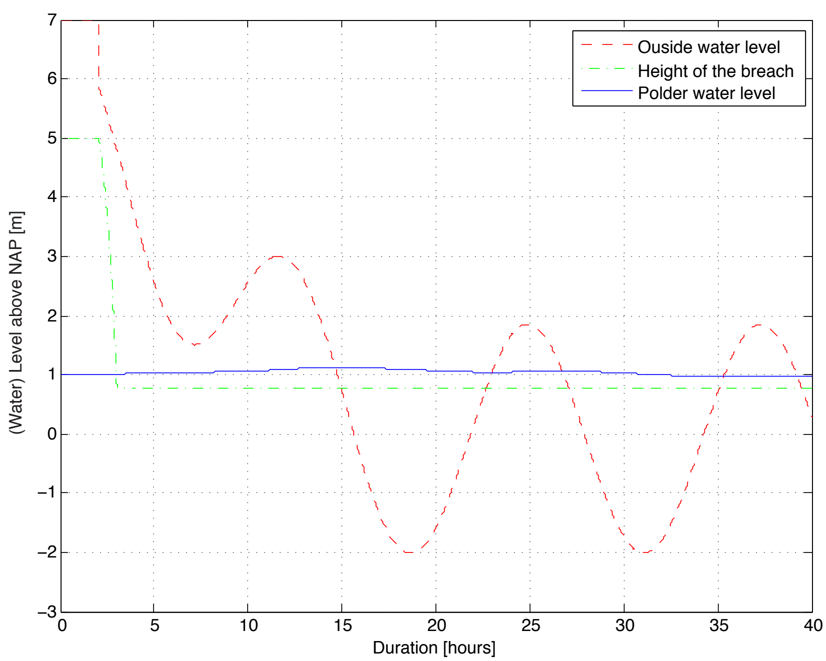

Figure G10: (Water) Levels of Scenario A-12.

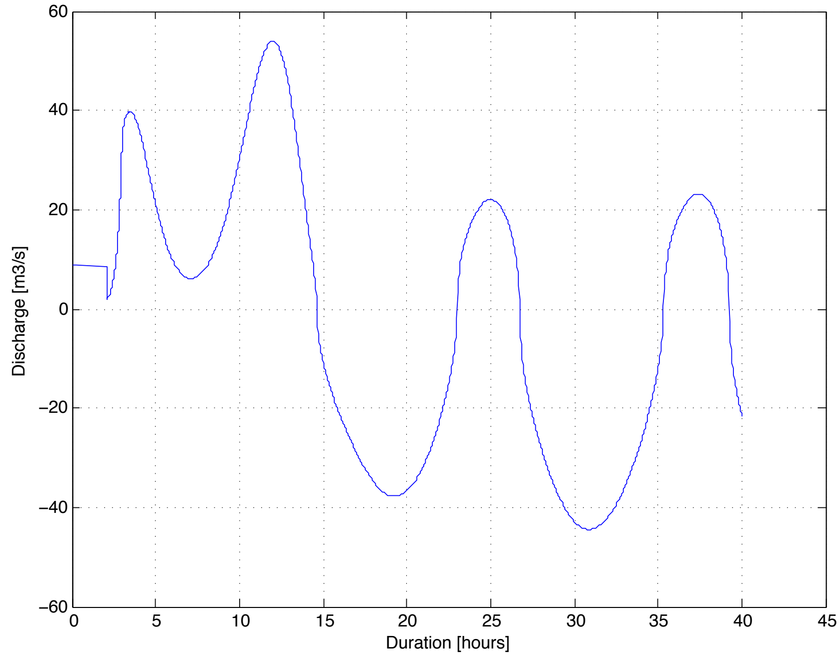

Figure G11: Discharge of Scenario A-12.

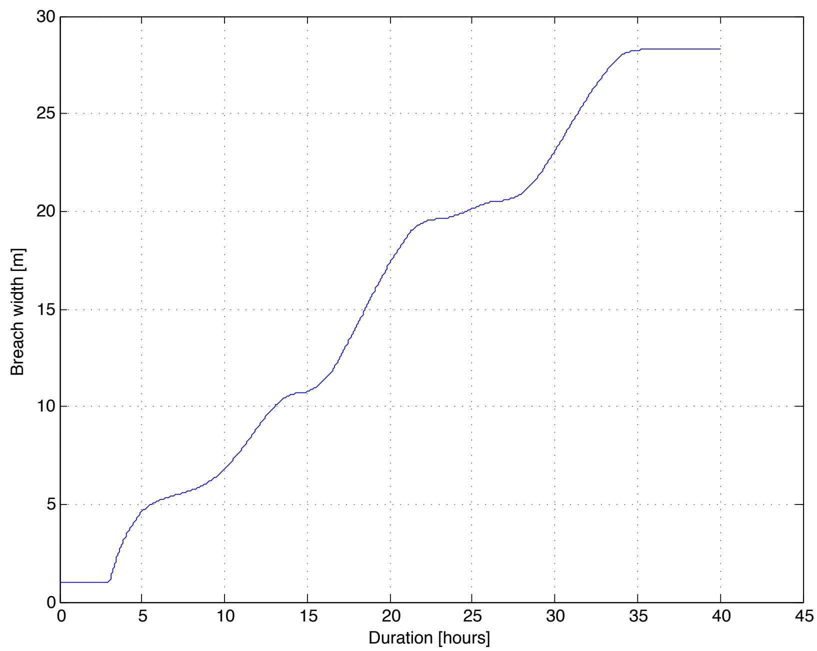

Figure G12: Development of the breach width in Scenario A-12.

Scenario B

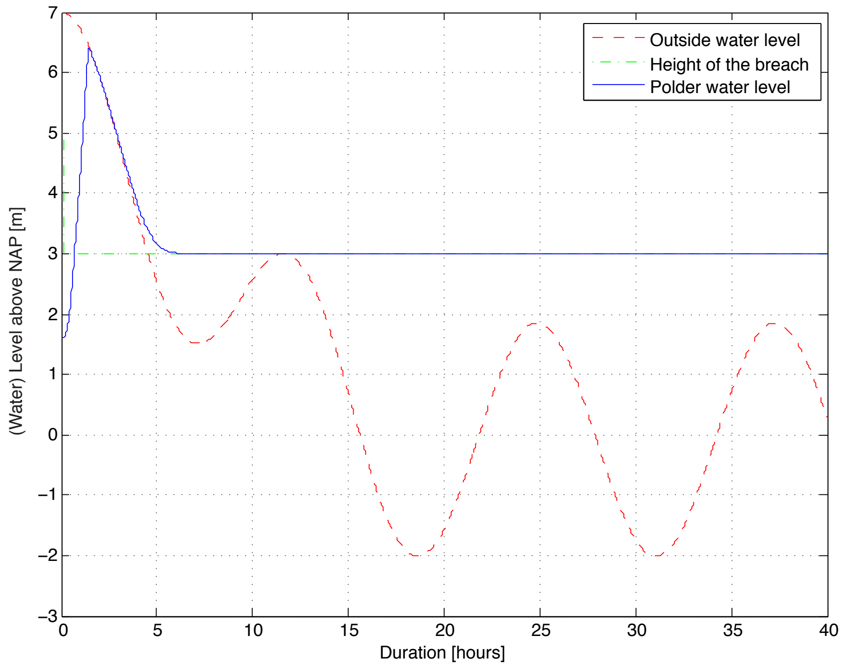

Figure G13: (Water) Levels of Scenario B-9.

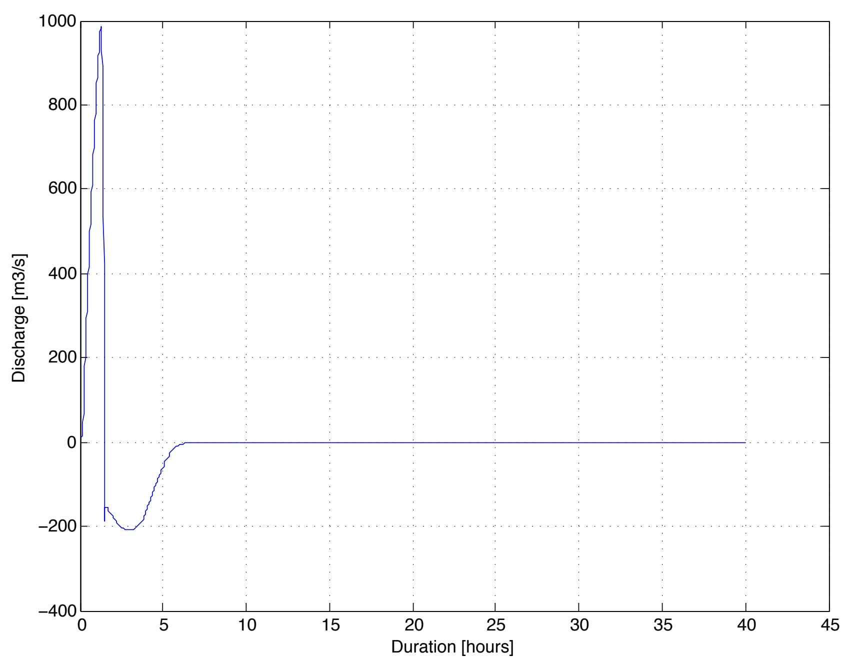

Figure G14: Discharge of Scenario B-9.

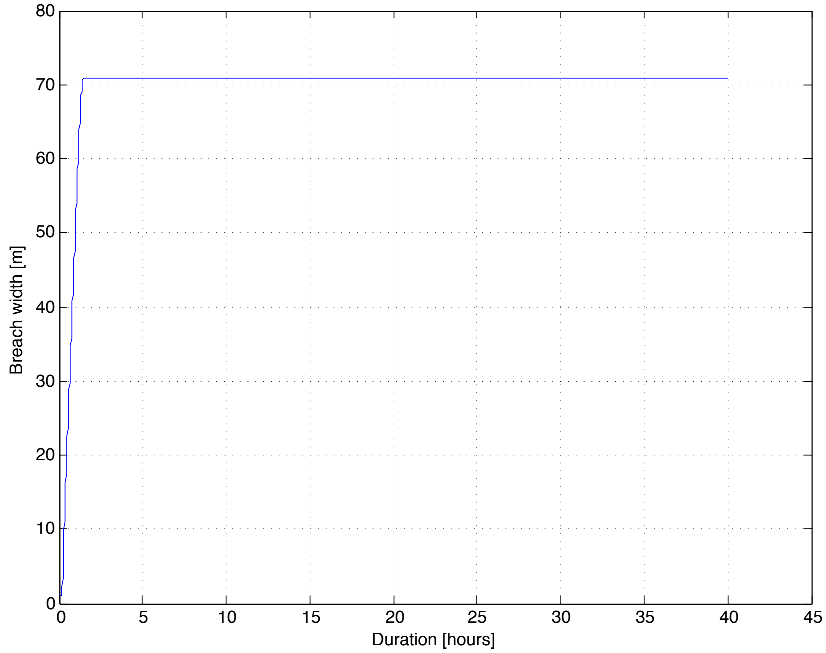

Figure G15: Development of the breach with in Scenario B-9.

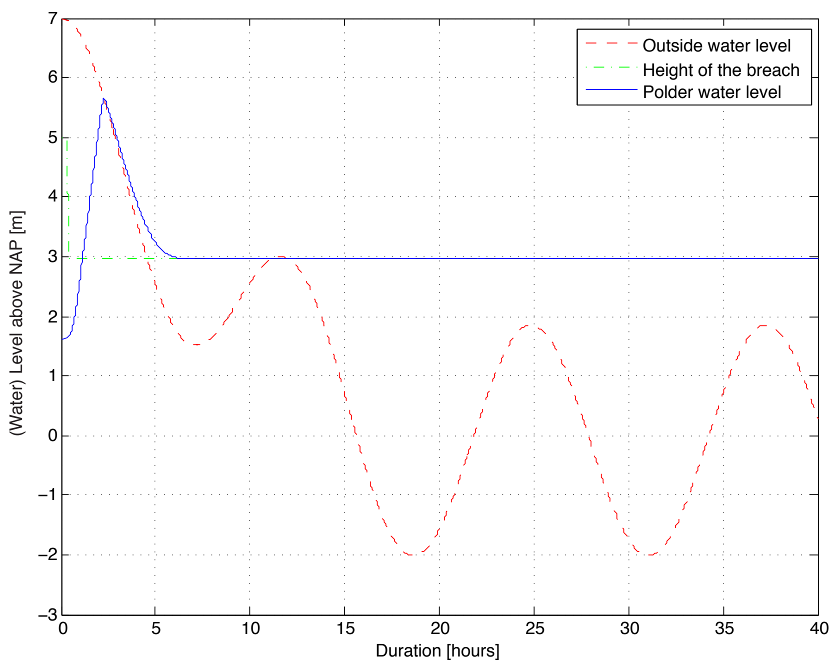

Figure G16: (Water) Levels of Scenario B-10.

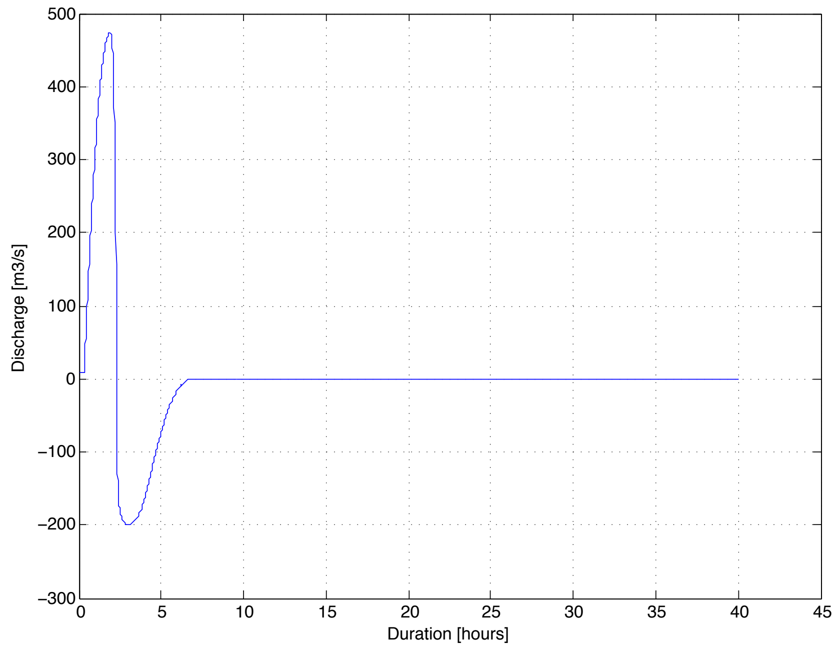

Figure G17: Discharge of Scenario B-10.

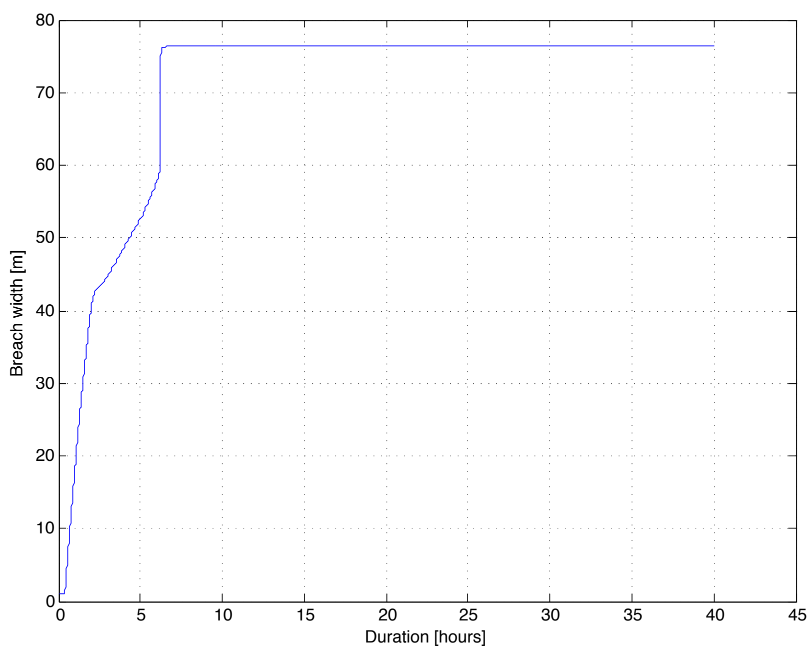

Figure G18: Development of the breach width in Scenario B-10.

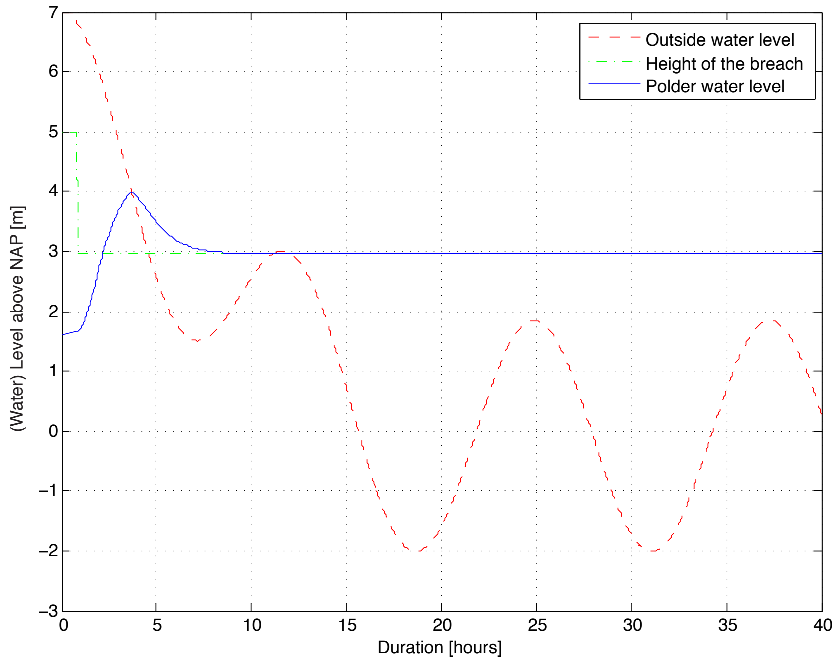

Figure G19: (Water) Levels of Scenario B-11.

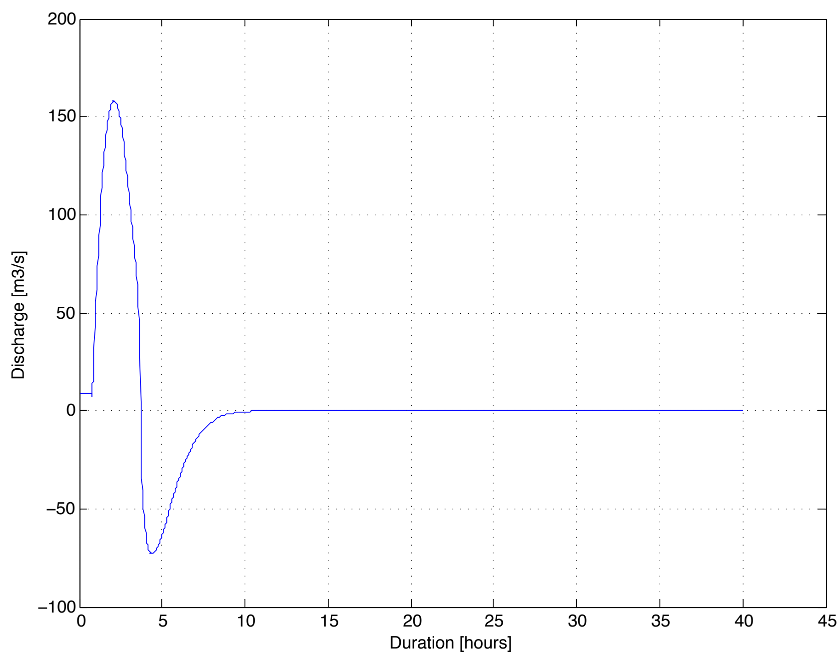

Figure G20: Discharge of Scenario B-11.

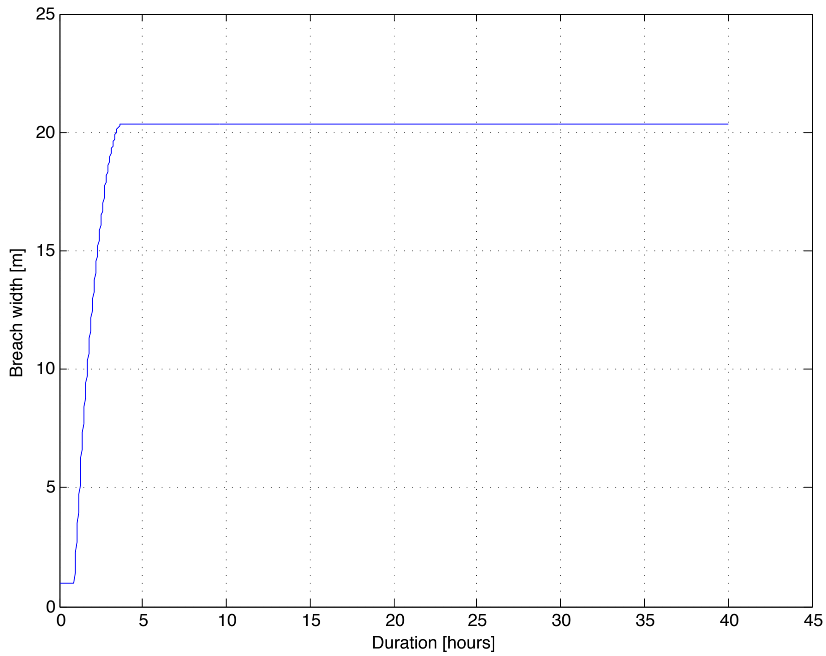

Figure G21: Development of the breach with in Scenario B-11.

H | Estimation of the near bed concentration

This appendix contains an estimation of the maximum near bed concentration and the minimum near bed concentration during the erosion experiments (Section H.1). In addition several graphs of theoretical vertical concentration profiles are provided. In Section H.2, the influence of the near bed concentration on the erosion behaviour is investigated.

H.1 Estimation of the near bed concentration

The Rouse profile represents a time-averaged vertical concentration profile for a given water depth, sediment diameter and shear stress. The concentration profile was originally derived from the diffusion equation and is given by:

$$\frac{c_z}{c_a} = \left[\left(\frac{h-z}{z}\right)\left(\frac{z_a}{h-z_a}\right)\right]^{\frac{w_s}{\kappa u_*}} \tag{H.1}$$

where c_z is the concentration at height z and c_a is the reference concentration at reference level z_a. Smith and McLean (1977) proposed the following equations for the reference concentration c_a and level of the reference concentration z_a:

$$c_a = \frac{c_{bed}\gamma_0 T}{1+\gamma_0 T} \tag{H.2}$$

$$z_a = \frac{26.3 \cdot (\tau_b - \tau_{b,cr})}{(\rho_s - \rho_w)g} + \frac{D_{50}}{12} \tag{H.3}$$

in which γ_0 is a constant (0.001 - 0.005), c_{bed} is the concentration of the initial bed, T is the dimensionless transport parameter and u_* is the bed shear velocity. The dimensionless transport parameter and the bed shear velocity are defined as follows:

$$T = \frac{\tau_b - \tau_{b,cr}}{\tau_{b,cr}} \tag{H.4}$$

$$u_* = \sqrt{\left(\frac{\tau_b}{\rho_w}\right)} \tag{H.5}$$

By using the (range of) values of Table H.1, the reference concentration c_a and level of the reference concentration z_a can be calculated with Eq.(H.2) and Eq.(H.3), respectively. The calculated values for the reference concentration are between 0.02 and 0.08. The values of the corresponding reference level are 4.4 mm and 21.6 mm, respectively. With these values and the hindered settling velocities - as calculated with the BRES model and ranging from 0.01 m/s to 0.34 m/s - the corresponding vertical concentrations profiles can be calculated with Eq.(H.1). The concentration profiles are shown in Fig. H1. The left side of Fig. H1 shows the vertical concentration profile for the lower shear stress and the right side of Fig. H1 shows the vertical concentration profile for the higher shear stress. By assuming that the near bed concentration is roughly located at a height of about 0.005 m to 0.01 m above the bed it can be concluded that the value of the near bed concentration c_b ranges from about 0.03 to 0.20 (see also Fig. H1).

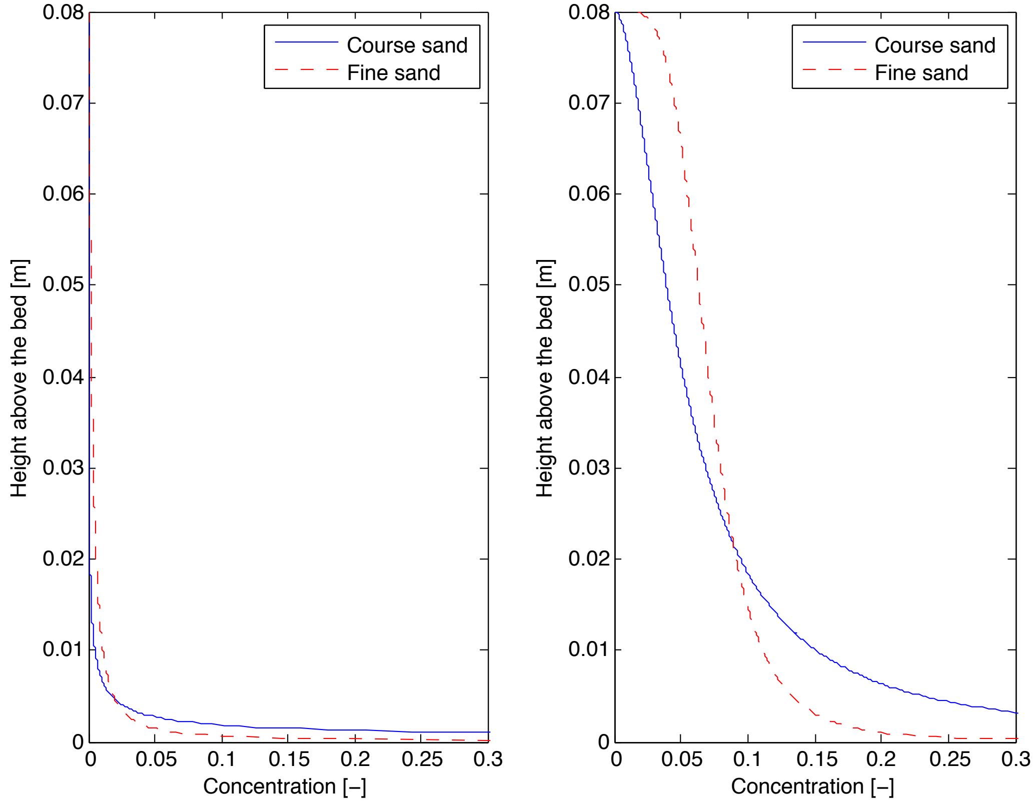

Figure H1: Vertical concentration profiles (a) with a relatively low bed shear stress and (b) with a relatively high bed shear stress.

Table H.1: Characteristic parameters of the.....

Parameter	Value
Bed shear stress τ_b in [Pa]	2.83 - 13.23
Critical bed shear stress $\tau_{b,cr}$ in [Pa]	0.15 - 0.17
Median sediment diameter D_{50} in [μm]	150 - 256
Initial bed concentration c_{bed} in [-]	0.60
An empirical constant γ_0 in [deg]	0.002
Von Karman constant κ in [-]	0.40
Density of the water ρ_w in [kg/m^3]	1025
Density of the sand ρ_s in [kg/m^3]	2650
Water depth h in [m]	0.08

H.2 Effect of the near bed concentration of the erosion behaviour

The erosion velocity, calculated with Eq.(59), depends on the near bed concentration. Hence, the near bed concentration is crucial for analyzing erosion behaviour. Both the erosion rate and the sedimentation rate ($w_s c_b$) depend on the near bed concentration (see Eq.(59)). In Section 8.2, 0.03 has been chosen as value for the near bed concentration. However, estimations of the near bed concentration, indicate that the value of the near bed concentration may be as high as 0.20 (see Section H.1). The influence of the near bed concentration on the erosion behaviour is shown in Fig. H2. In Fig. H2 results for three different near bed concentrations are shown. These are 0.03, 0.10 and 0.20, respectively.

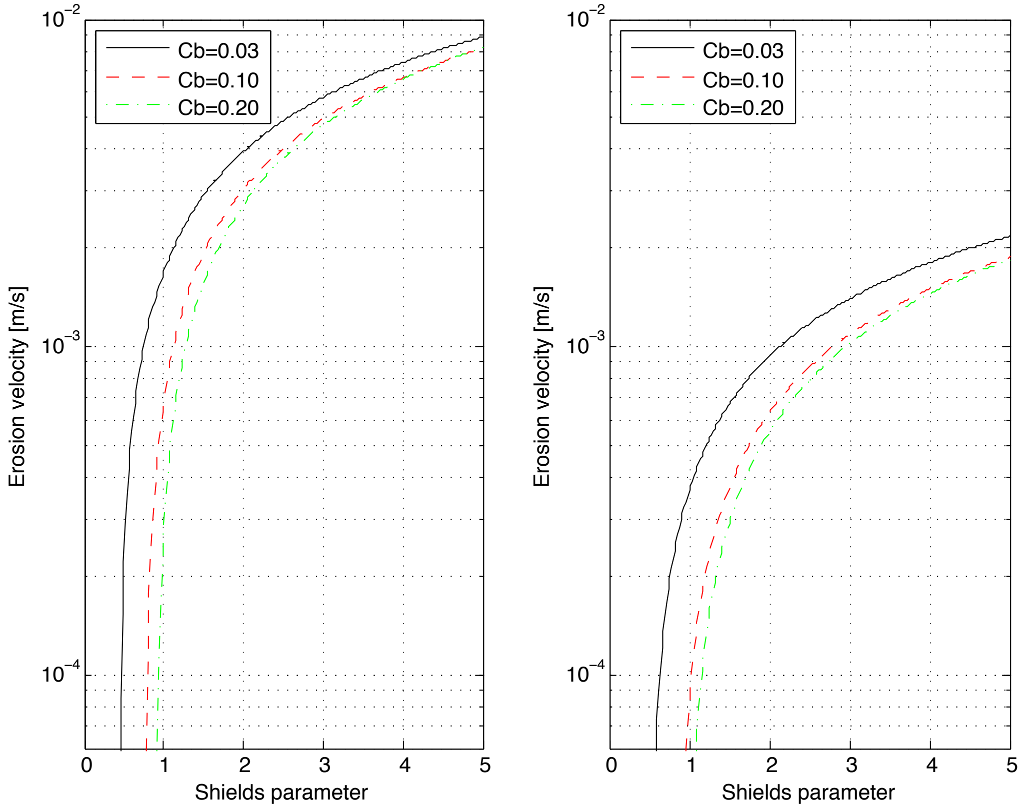

Figure H2: Influence of the near bed concentration on the erosion velocity (a) for the courser sand ($D_{50} = 0.256$ mm) and (b) for the finer sand ($D_{50} = 0.150$ mm).

From Fig. H2 it can be concluded that the erosion velocity v_e is lower for higher near bed concentrations c_b (for the same Shields parameters). This effect is visible for both the course sand and the fine sand. It also appears that the effect of the near bed concentration on the erosion velocity is less strong for higher Shields parameters (the lines are converging at higher Shields parameters). The difference in erosion velocity, between the near bed concentration of 0.03 and 0.20, at higher flow velocities (Shields parameter > 2) is less than a factor 2. From Fig. H2 it can also be concluded that the critical Shields parameter is slightly influenced by the near bed concentration. The higher the near bed concentration, the harder it becomes for a particle to start moving.